UNIVERSITÀ DEGLI STUDI DI MILANO

SCUOLA DI DOTTORATO IN INFORMATICA

DIPARTIMENTO DI INFORMATICA

DOTTORATO DI RICERCA IN INFORMATICA, XXV CICLO

Contactless Fingerprint Biometrics: Acquisition, Processing, and Privacy Protection

INF/01 INFORMATICA

TESI DI DOTTORATO DI RICERCA DI

Ruggero Donida Labati

RELATORE

Prof. Vincenzo Piuri

CORRELATORE

Dott. Fabio Scotti

DIRETTORE DELLA SCUOLA DI DOTTORATO

Prof. Ernesto Damiani

A.A. 2011/2012

Ai miei genitori

Ringraziamenti

Desidero innanzitutto ringraziare Fabio Scotti e Vincenzo Piuri per le opportunità che mi hanno offerto, il costante incoraggiamento, i preziosi consigli ed il tempo dedicatomi in questi anni. La loro guida è stata fondamentale per il raggiungimento di questo traguardo.

Ringrazio particolarmente Angelo Genovese per le proficue collaborazioni ed i quotidiani momenti di svago.

Ringrazio inoltre tutti coloro con cui ho collaborato durante questo lavoro, tra i quali Mauro Barni, Tiziano Bianchi, Dario Catalano, Mario di Raimondo, Pierluigi Failla, Dario Fiore, Riccardo Lazzeretti ed Alessandro Piva.

Un ringraziamento è rivolto a Giuseppe Livraga per l'apprezzata realizzazione di numerose componenti meccaniche necessarie alle attività sperimentali.

È inoltre doveroso ringraziare chi ha volontariamente partecipato alla raccolta dei dati biometrici utilizzati per la validazione dei sistemi realizzati in questa tesi.

Ringrazio anche tutti gli amici che hanno allietato questi anni di lavoro, in particolar modo Vincenzo Morandi, William Aiolfi, Paolo Francesconi, Angelo Bonomi, Alberto Bosio e Ravi Jahwar.

Il più sentito grazie è rivolto ai miei genitori, il cui appoggio è stato indispensabile durante questo percorso. Li ringrazio per avermi sempre sostenuto, dato fiducia ed incoraggiato. A loro dedico tutto il mio lavoro.

Ruggero Donida Labati

Table of Contents

List of Figures

List of Tables

Chapter 1

Introduction

Biometrics is defined by the International Organization for Standardization (ISO) as "the automated recognition of individuals based on their behavioral and biological characteristics" [1]. Examples of distinctive features evaluated by biometrics, called biometric traits, are behavioral characteristics like the signature, gait, voice, and keystroke, and biological characteristics like the fingerprint, face, iris, retina, hand geometry, palmprint, ear, and DNA.

The biometric recognition is the process that permits to establish the identity of a person, and can be performed in two modalities: verification, and identification. The verification modality evaluates if the identity declared by an individual corresponds to the acquired biometric data. Differently, in the identification modality, the recognition application has to determine a person's identity by comparing the acquired biometric data with the information related to a set of individuals.

Compared with traditional techniques used to establish the identity of a person, biometrics offers a greater confidence level that the authenticated individual is not impersonated by someone else. Traditional techniques, in fact, are based on surrogate representations of the identity, like tokens, smart cards, and passwords, which can easily be stolen or copied with respect to biometric traits. This characteristic permitted a wide diffusion of biometrics in different scenarios, like physical access control, government applications, forensic applications, logical access control to data, networks, and services.

Most of the biometric applications, also called biometric systems, require performing the acquisition process in a highly controlled and cooperative manner. In order to obtain good quality biometric samples, the acquisition procedures of these systems

need that the users perform deliberate actions, assume determinate poses, and stay still for a time period. Limitations regarding the applicative scenarios can also be present, for example the necessity of specific light and environmental conditions.

Examples of biometric technologies that traditionally require constrained acquisitions are based on the face, iris, fingerprint, and hand characteristics. Traditional face recognition systems need that the users take a neutral pose, and stay still for a time period. Moreover, the acquisitions are based on a frontal camera and performed in controlled light conditions. Iris acquisitions are usually performed at a distance of less than 30 cm from the camera, and require that the user assume a defined pose and stay still watching the camera. Moreover they use near infrared illumination techniques, which can be perceived as dangerous for the health. Fingerprint recognition systems and systems based on the hand characteristics require that the users touch the sensor surface applying a proper and uniform pressure. The contact with the sensor is often perceived as unhygienic and/or associated to a police procedure. This kind of constrained acquisition techniques can drastically reduce the usability and social acceptance of biometric technologies, therefore decreasing the number of possible applicative contexts in which biometric systems could be used.

In traditional fingerprint recognition systems, the usability and user acceptance are not the only negative aspects of the used acquisition procedures since the contact of the finger with the sensor platen introduces a security lack due to the release of a latent fingerprint on the touched surface, the presence of dirt on the surface of the finger can reduce the accuracy of the recognition process, and different pressures applied to the sensor platen can introduce non-linear distortions and low-contrast regions in the captured samples.

Other crucial aspects that influence the social acceptance of biometric systems are associated to the privacy and the risks related to misuses of biometric information acquired, stored and transmitted by the systems. One of the most important perceived risks is related to the fact that the persons consider the acquisition of biometric traits as an exact permanent filing of their activities and behaviors, and the idea that the biometric systems can guarantee recognition accuracy equal to 100% is very common. Other perceived risks consist in the use of the collected biometric data for malicious purposes, for tracing all the activities of the individuals, or for operating proscription lists.

In order to increase the usability and the social acceptance of biometric systems, researchers are studying less-constrained biometric recognition techniques based on different biometric traits, for example, face recognition systems in surveillance applications, iris recognition techniques based on images captured at a great distance and on the move, and contactless technologies based on the fingerprint and hand characteristics. Other recent studies aim to reduce the real and perceived privacy risks, and consequently increase the social acceptance of biometric technologies. In this context, many studies regard methods that perform the identity comparison in the encrypted domain in order to prevent possible thefts and misuses of biometric data.

The objective of this thesis is to research approaches able to increase the usability and social acceptance of biometric systems by performing less-constrained and highly accurate biometric recognitions in a privacy compliant manner. In particular, approaches designed for high security contexts are studied in order improve the existing technologies adopted in border controls, investigative, and governmental applications. Approaches based on low cost hardware configurations are also researched with the aim of increasing the number of possible applicative scenarios of biometric systems. The privacy compliancy is considered as a crucial aspect in all the studied applications.

Fingerprint is specifically considered in this thesis, since this biometric trait is characterized by high distinctivity and durability, is the most diffused trait in the literature, and is adopted in a wide range of applicative contexts. The studied contactless biometric systems are based on one or more CCD cameras, can use two-dimensional or three-dimensional samples, and include privacy protection methods. The main goal of these systems is to perform accurate and privacy compliant recognitions in less-constrained applicative contexts with respect to traditional fingerprint biometric systems. Other important goals are the use of a wider fingerprint area with respect to traditional techniques, compatibility with the existing databases, usability, social acceptance, and scalability.

The main contribution of this thesis consists in the realization of novel biometric systems based on contactless fingerprint acquisitions. In particular, different techniques for every step of the recognition process based on two-dimensional and three-dimensional samples have been researched. Novel techniques for the privacy protection of fingerprint data have also been designed. The studied approaches are multidisciplinary since

their design and realization involved optical acquisition systems, multiple view geometry, image processing, pattern recognition, computational intelligence, statistics, and cryptography.

The implemented biometric systems and algorithms have been applied to different biometric datasets describing a heterogeneous set of applicative scenarios. Results proved the feasibility of the studied approaches. In particular, the realized contactless biometric systems have been compared with traditional fingerprint recognition systems, obtaining positive results in terms of accuracy, usability, user acceptability, scalability, and security. Moreover, the developed techniques for the privacy protection of fingerprint biometric systems showed satisfactory performances in terms of security, accuracy, speed, and memory usage.

1.1 State of the art

In the literature, there are many studies on the fingerprint biometric trait, but most of them regard contact-based recognition systems.

There are only few studies on contactless fingerprint recognition techniques, which can be divided into two classes: methods based on two-dimensional samples, and methods based on three-dimensional samples. The first class of methods usually captures single fingerprint images using single CCD cameras. Differently, systems based on three-dimensional models require more complex hardware setups, but can provide a greater accuracy.

The fingerprint recognition process performed by contactless systems in the literature can be divided into three main steps: acquisition; computation of a contact-equivalent fingerprint image; feature extraction and matching. There are different contactless acquisition strategies, which are based on single CCD cameras, multiple view techniques, or structured light approaches. In systems based on two-dimensional samples, the computation of contact-equivalent fingerprint images is usually performed by applying enhancement algorithms and performing resolution normalization. Differently, systems based on three-dimensional samples perform an unwrapping step that aims to map the three-dimensional fingerprint models into a two-dimensional space. The obtained contact-equivalent images are then processed using traditional feature extraction and matching methods designed for contact-based fingerprint images.

Most of the contactless fingerprint recognition systems in the literature are based on complex and expansive hardware setups, use finger placement guides, and usually perform acquisitions at a distance to the cameras of less than 10 cm. Moreover, there are no works that report the recognition accuracy of contactless biometric systems based on three-dimensional samples, there are no feature extraction and matching techniques able to process characteristics directly extracted from three-dimensional models, and the existing techniques have been tested on small biometric datasets.

Another aspect that should be considered in contactless fingerprint recognition systems is the use of techniques for the privacy protection. There are different privacy protection techniques that could be applied to contactless fingerprint recognition systems, but most of these methods decrease the accuracy of biometric systems.

1.2 The performed research

The thesis presents innovative less-constrained biometric systems able to perform the identity recognition in privacy compliant and high accuracy applications.

The realized approaches include techniques for all the steps of contactless fingerprint recognition systems based on two-dimensional and three-dimensional samples. The first class of techniques is based on single fingerprint images and is designed to be adopted in mobile devices with integrated cameras. Differently, the techniques based on three-dimensional samples require more complex acquisition setups composed by two cameras and are able to obtain more accurate results.

Different techniques for contactless biometric systems based on two-dimensional samples have been researched: acquisition setups that do not require the use of finger placement guides and can capture biometric samples at a greater distance with respect to most of the techniques in the literature; a quality assessment method for contactless fingerprint images, which permits to select the best quality frames in frame sequences obtained representing less-constrained fingerprint acquisitions; techniques for the global analysis of contactless-images; methods that permit to compute contact-equivalent fingerprint images compatible with traditional feature extraction and matching algorithms designed for contact-based acquisitions.

The implemented fingerprint recognition techniques based on three-dimensional samples regard different acquisition setups based on multiple view techniques, three-

dimensional reconstruction approaches, feature extraction, and matching algorithms. In particular, they include two approaches for the identity recognition based on three-dimensional samples: the first approach extracts and compares features related to the three-dimensional coordinates of minutia points; the second approach computes contact-equivalent images and then applies biometric recognition algorithms designed for contact-based images, aiming to obtain fingerprint images compatible with the existing biometric databases.

In order to reduce the efforts necessary to collect the biometric data needed to design and test new algorithms and hardware setups, a technique for the computation of synthetic contactless samples has been studied.

The studied acquisition techniques and the three-dimensional reconstruction methods have also been applied to latent and ancient fingerprints in order to verify the feasibility of using these approaches also in forensic applications.

The performed research has also regarded a privacy protection approach capable to deal with distributed biometric applications, and which permits to perform the matching of biometric templates in the encrypted domain by exploiting the properties of homomorphic cryptosystems.

1.3 Results

The implemented methods have been analyzed using datasets captured in different applicative conditions and the obtained results have proved the feasibility of the proposed approaches in the considered applicative contexts. In particular, contactless recognition systems based on two-dimensional samples have obtained satisfactory performance in low-cost applications, and contactless systems based on three-dimensional samples achieved good accuracy in high security applications.

The realized fingerprint recognition approaches have also been compared with traditional contact-based systems by performing a multidisciplinary test that considers a set of important aspects of biometric systems: accuracy, speed, cost, scalability, interoperability, usability, social acceptance, security, and privacy. Results show that contactless biometric systems based on two-dimensional templates extracted from three-dimensional samples can obtain a comparable or enhanced accuracy with respect to traditional fingerprint recognition techniques. Moreover, the obtained results show that

contactless recognition techniques permit to increase the scalability, usability, social acceptance, and security of traditional fingerprint recognition systems.

The analysis of the performances obtained by the implemented feature extraction and matching techniques based on three-dimensional templates is also encouraging, and it proves that identity comparison techniques based on three-dimensional minutiae features can effectively use the supplementary information related to the finger shape to obtain accurate biometric recognitions.

Satisfactory results have also been obtained by applying the realized acquisition setups and three-dimensional reconstruction techniques to latent and ancient fingerprints.

Finally, results have proved that the implemented method for the privacy protection in fingerprint recognition systems can effectively be applied in client-server applications without decreasing the recognition accuracy, also obtaining satisfactory performance in terms of security, computational time, bandwidth, and memory usage.

1.4 Structure of the thesis

This thesis is structured as follows.

- Chapter 2 presents a brief description of different aspects of biometric systems: biometric traits, applications, evaluation techniques, privacy aspects, and research trends.
- Chapter 3 discusses recent studies on less-constrained biometric systems based on different traits. In particular, it describes recent researches on the face, iris, gait, ear, soft-biometric traits, and hand characteristics.
- Chapter 4 provides a literature review on fingerprint recognition systems. Well-known techniques in literature for all the steps of the biometric recognition process are fist analyzed, and recent studies on contactless recognition systems based on two-dimensional and three-dimensional samples are then discussed.
- Chapter 5 describes the performed research on contactless fingerprint recognition systems, detailing the implemented methods designed for two-dimensional samples, the studied approaches based on three-dimensional fingerprint samples, and a developed technique for the computation of synthetic contactless samples.

- Chapter 6 describes the experiments performed on the studied contactless fingerprint recognition approaches. In particular, this chapter analyzes the performance of every implemented technique, and presents a comparison between the realized contactless biometric systems with contact-based fingerprint recognition technologies.
- Chapter 7 discusses the application of contactless three-dimensional reconstruction techniques to latent and ancient fingerprints, reporting a case study on the authentication of a clay artwork.
- Chapter 8 describes different aspects of the studied approach for the privacy protection in fingerprint recognition systems and presents its experimental evaluation.
- Chapter 9 finally presents conclusions and future works.

Chapter 2

Biometric Systems

This chapter provides a brief overview on biometric systems in order to contextualize the researched biometric technologies.

A description of biometric systems, traits, and applications is first provided. The most common techniques and figures of merit in the literature used for the performance analysis of biometric systems are then analyzed. Privacy and security aspects in biometrics are also treated, with particular attention to methods in the literature for the protection of biometric data. Finally, the new research trends in biometrics are discussed.

2.1 Biometric recognition technologies

Traditional techniques used to establish the identity of a person are based on surrogate representations of his/her identity, such as passwords, keys, tokens, and identity cards. Biometric recognition systems, instead, are based on physiological or behavioral characteristics of the individual, which are univocally related to their owner, cannot be shared or misplaced, and are more difficult to be stolen. Systems based on physiological traits perform and analyze measurements of a part of the human body. Differently, systems based on behavioral traits evaluate actions taken by a person.

The choice of the most suitable recognition technology with respect to the applicative scenario should be performed by evaluating different factors. In the literature, there are studies on techniques and figures of merit for the evaluation of the characteristic aspects of biometric systems.

Important factors that should be considered are related to the security and privacy. In the literature, there are risk evaluation techniques, guidelines, and data protection methods designed to prevent possible thefts and misuses of biometric data.

The existing techniques for the privacy protection in biometrics, however, can increase the computational time of the recognition methods, and reduce their accuracy. In order to overcome these limitations, researchers are studying more efficient and robust methods. Other important research trends are the increasing of the accuracy of biometric systems, reduction of the hardware costs, and increasing of the usability and user acceptability.

In this chapter, the general characteristics of biometric systems and traits are first presented (Section 2.2). Then, the applicative contexts of biometric technologies are discussed (Section 2.3), and the most used techniques in the literature for the evaluation of biometric applications are described (Section 2.4). In Section 2.5, privacy and security aspects in biometrics are treated. Finally, Section 2.6 briefly presents the most important research trends.

2.2 Biometric traits

Biometric recognition or, simply, biometrics refers to the automatic recognition of the individuals based on their physiological and/or behavioral characteristics. By using biometrics, it is possible to confirm or establish an individual's identity based on "who she is", rather than by "what she possesses" (e.g., an ID card) or "what she remembers" (e.g., a password) [2]. Examples of physiological biometric traits are the fingerprint, hand geometry, iris, retina, and face. The distinctiveness of the signature and gait can be considered as behavioral biometric traits. Fig. 2.1 shows some examples of biometric traits.

A physiological or behavioral characteristic can be considered as a biometric trait only if it satisfies four conditions [2].

1. Universality: every person should possess the characteristic.

2. Distinctiveness: two persons should not own the same characteristic, or the probability of this event should be negligible. The differences between characteristics of different individuals should also be sufficient to discriminate their identities.

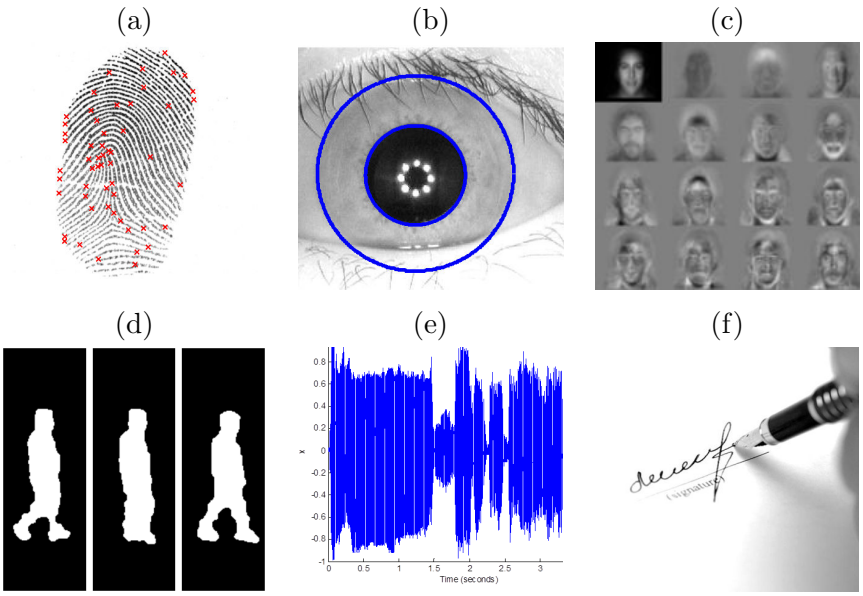

Figure 2.1: Examples of biometric traits. Physiological traits: (a) fingerprint; (b) iris; (c) face. Behavioral traits: (d) gait; (e) voice; (f) signature.

3. Permanence: the characteristic should be sufficiently invariant over a time period. The considered time period of time depends to the applicative context.

4. Collectability: the characteristic can be measured quantitatively.

Other important characteristics of the biometric traits are more related to the technologies adopted to perform the identity recognition:

1. Performance: accuracy, speed, and robustness of the considered technology.

2. Acceptability: the acceptation level of the biometric technology by the user.

3. Circumvention: robustness under fraudulent techniques.

A correct design of a biometric system should always take into account to obtain performances adequate to the applicative context, be accepted by the user set, and robust to fraudulent attacks.

In the literature, some of the most used physiological biometric traits are:

- fingerprint [3, 4];
- iris [5, 6];

- face [7];
- hand geometry [8];
- palmprint [9];
- palmvein [10];
- ear [11].

Some of the most used behavioral traits are:

- voice [12];
- signature [13];
- gait [14];
- keystroke [15].

Recently, soft biometric traits are also studied in order to increase the accuracy of biometric recognition systems or to perform uncooperative recognitions. Soft biometric traits are characteristics that provide some information about the individual, but lack the distinctiveness and permanence to sufficiently differentiate any two individuals [16]. Soft biometric traits can be continuous or discrete. Continuous traits are characteristics of the human body measured in a continuous scale, while discrete traits represent discrete classifications of distinctive characteristics. Examples of continuous characteristics are:

- height [17];
- weight [18];
- other measurements of body parts [19].

Examples of discrete soft biometric traits are:

- gender [20];
- race [20];
- eye color [21];
- clothes color [19].

2.3 Applications

In recognition applications, a biometric system can be considered a pattern recognition system that makes a personal recognition by determining the authenticity of a specific physiological or behavioral characteristic possessed by the user.

Biometric systems can work in two different modalities: verification and authentication.

The verification involves confirming or denying a person's claimed identity. The system compares the acquired biometric data with the stored information associated to the claimed identity, performing a one-to-one comparison. An individual who want to be recognized usually claims the identity via a personal identification number (PIN), a user name, or a smart card.

In the identification mode, the biometric system has to establish a person's identity by comparing the acquired biometric data with the information related to a set of individuals, performing a one-to-many comparison. The identification does not require that the user claims an identity. There are two classes of identifications: positive identification and negative identification. The first class answers the "Who am I?" question. Typically, the returned results are numerical identifiers or access permissions. The second class searches databases in the same fashion, comparing one template against many, while the negative identification systems are designed to ensure that a person is not present in a database. These systems are usually adopted for security controls in public buildings (e.g. stadiums, swimming pools, train stations).

The term recognition is generic and does not make a distinction between verification and identification.

Both the verification and identification modalities require a previous step in which the biometric data of the users are stored in biometric documents or in a database. This step is called enrollment and usually requires the presence of a certified authority. The schemas of the verification, identification, and enrollment modalities are shown in Fig. 2.2. These processes are based on common components: a biometric sensor, feature extractor, database, matcher, and decision module.

- The used acquisition sensor is related to the biometric trait. The acquired data are usually images, signals, or frame sequences. These data are called biometric samples.

(a)

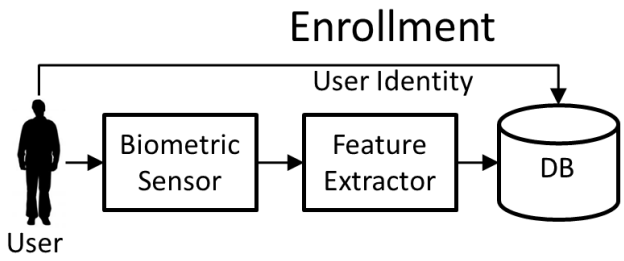

(b)

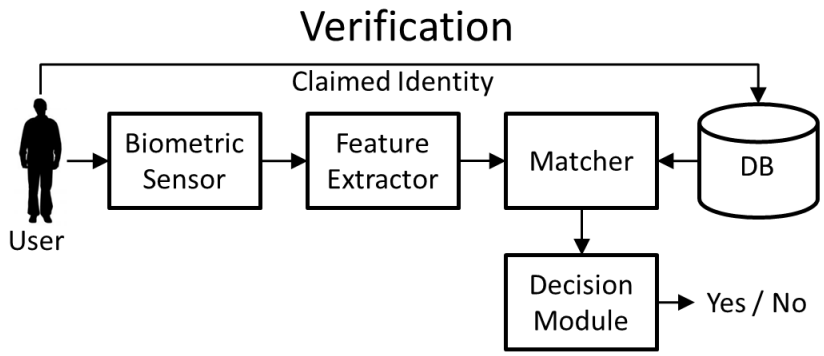

(c)

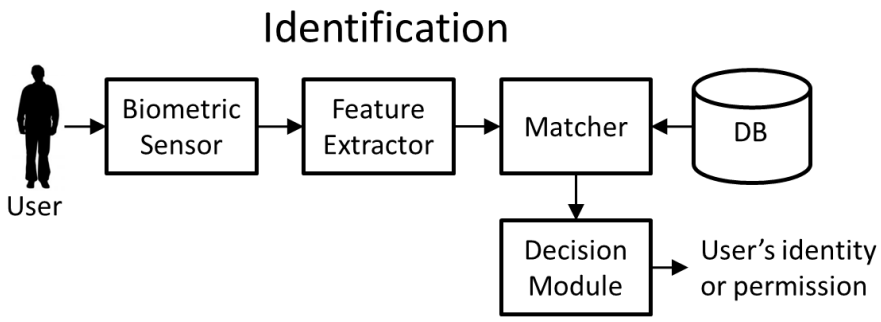

Figure 2.2: Modalities of biometric systems: (a) enrollment; (b) verification; (c) identification.

- The feature extraction module aims to extract an abstract and distinctive representation of the biometric sample, which is called template. The computed characteristics can be different also in systems based on the same biometric trait.

- The database contains the templates of the enrolled individuals. Many systems use centralized databases in order to perform verifications or identifications. In verification systems, it is also possible to use different storage supports, like smart cards, or USB devices.

- The matcher compares two or more biometric templates, obtaining a value called matching score. The template comparison can be based on different metrics and can return a similarity or dissimilarity index.

- The decision module uses the computed matching score to determine if a template appertains to an individual or not. The decision is obtained by applying a threshold on the matching score. The threshold value must be accurately tuned according to the applicative context because it determines the tradeoff between the false positives and false negatives.

Nowadays, the use of biometric systems is continuously increasing in different applicative scenarios [22]. The related market is showing a significant positive trend. In 2011, in fact, it reached the amount of 5 billion dollars and it is expected to reach 12 billion dollars by the end of 2015 [23].

Typical applicative scenarios are: physical access control (in critical areas, public buildings, sport arenas, bank caveau, transportations, etc.); surveillance (of private buildings, public areas, etc.); government applications (identity cards, passports, driving licenses, immigration control, health cards, access control to online government services, etc.); forensic applications (body identification, crime investigation, searching of disappeared children, kinship, intelligence, etc.); logical access control to data, networks and services (home banking, ATM, supermarkets, e-commerce, mobile phones, computers, etc.).

The most used biometric trait is the fingerprint [23]. This trait, in fact, is the first human characteristic used to perform biometric recognitions. Fingerprint recognition systems are also characterized by good performances in terms of accuracy and speed.

There are Automated Fingerprint Identification systems (AFIS) that are able to perform the recognition of millions of templates [24]. Most of the fingerprint recognition systems are based on the evaluation of the position and shape of particular local ridge patterns (minutiae), but there are also systems that use other features and correlation-based techniques [3].

Other diffused biometric systems are based on the face characteristics. These systems can obtain less accuracy then the fingerprint recognition techniques. However, they are characterized by a greater user acceptance because humans usually perform recognitions by evaluating the face characteristics. Moreover, the use of contactless acquisition systems is considered as less invasive. With respect to fingerprint recognition systems, face recognition techniques can also be used in different applicative contexts, like surveillance and entertainment applications. Biometric systems based on the face characteristics can use transformation-based techniques or attribute-based methods [7, 25].

Iris recognition systems are considered as the fastest and most accurate biometric techniques. For this reason, they are diffused in border controls and airports. The main problem of these systems is that they use constrained acquisition techniques, which can also be considered as invasive. For this reason, they are characterized by a low user acceptance. In order to overcome this limitation, researchers are studying systems that can work in less collaborative conditions [26, 27]. One of the most used recognition methods is based on a feature representation called Iriscode [6].

Other diffused biometric systems are based on hand characteristics, such as the hand geometry [8], or the palmprint and palmvein [9, 10]. Systems based on the hand geometry are usually adopted in applicative contexts in which it is not necessary a high security level. These systems, in fact, do not have a high accuracy, but are characterized by a high user acceptance and low hardware costs. Systems based on the palmprint and palmvein characteristics can obtain more accurate results.

Some promising systems based on other physical traits use the DNA [28], and ear shape [29]. The DNA is characterized by a high accuracy, but the recognition techniques based on this trait are expensive and require long evaluation times. Biometric systems based on the ear shape are researched because they can obtain sufficiently accurate results using contactless acquisitions performed at long distances.

Table 2.1: Properties of biometric systems related to the used biometric trait.

Trait	Univ.	Uniq.	Perm.	Coll.	Perf.	Acc.	Circ.
Face	H	L	M	H	L	H	L
Fingerprint	M	H	H	M	H	M	H
Hand geometry	M	M	M	H	M	M	M
Keystrokes	L	L	L	M	L	M	M
Hand vein	M	M	M	M	M	M	H
Iris	H	H	H	M	H	L	H
Retinal scan	H	H	M	L	H	L	H
Signature	L	L	L	H	L	H	L
Voice	M	L	L	M	L	H	L
Face thermograms	H	H	L	H	M	H	H
Odor	H	H	H	L	L	M	L
DNA	H	H	H	L	H	L	L
Gate	M	L	L	H	L	H	M
Ear	M	M	H	M	M	H	M

Notes: Univ. = Universality; Uniq. = Uniqueness; Perm. = Permanence; Coll.= Collectability; Perf. = Performance; Acc. = Acceptability; Circ. = Circumvention; H = High; M = Medium; L = Low.

Diffused systems based on behavioral traits consider the characteristics of the voice [12], signature [13], keystroke [15], and gait [14]. These systems are characterized by high user acceptability, but they are usually less accurate then systems based on physiological characteristics.

In the literature, there are also multimodal and multibiometric systems, which fuse the information obtained using different traits and/or recognition algorithms in order to increase the obtained recognition accuracy [30, 31, 32, 33, 34]. These systems are usually adopted in high security applicative contexts.

Other recognition applications use soft-biometrics. Soft biometrics traits are physical, behavioral, or adhered human characteristics, which usually do not permit to univocally recognize individuals [16]. Anyway, they can be used to perform unobtrusive identifications within a limited number of users, be used as a preliminary screening filter, or be combined in order to increase the recognition accuracy of biometric systems.

Table 2.1 reports the principal characteristics of biometric systems based on the most diffused biometric traits in the literature.

2.4 Evaluation of biometric systems

The evaluation of biometric systems is a complex multidisciplinary task. Systems used in different applicative contexts should be evaluated considering different aspects. It is also necessary to consider different characteristics of the system, regarding the accuracy, speed, cost, usability, acceptability, scalability, interoperability, security, and privacy. The accuracy is usually one of the most important aspects that should be considered during the design of biometric applications and should be evaluated using specific techniques and figures of merit.

2.4.1 Evaluation strategies

Biometric applications should be analyzed using different evaluation strategies in order to consider all the characteristics of the used technologies. It is possible to divide the evaluation strategies in three overlapped categories with increasing complexity in uncontrolled variables: technology, scenario, and operational [35].

The technology evaluation aims to measure the performances of biometric techniques. Typically, this category of evaluations is used to compare the performances of biometric algorithms on reference datasets. In order to compare the performances obtained by a biometric technique with the ones achieved by other algorithms in the literature, publically available datasets are usually adopted. An example of technology evaluation is the Fingerprint Verification Competition [36].

With respect to the technology evaluation, the scenario evaluation considers additional variables related to the applicative context. Its goal, in fact, is to measure the performance of different biometric systems in a particular application. An example of this evaluation is the comparison of the performances obtained by biometric systems based on different traits for the access control in a laboratory. Usually, every compared system captures the samples with different sensors. It is preferable to use data acquired from the same individuals. The creation of the testing datasets is usually a long process, which can require some weeks. This task, in fact, may obtain a statistically significant number of samples and may be based on different trials in order to ensure an adequate habituation of the users. Considering these factors, scenario evaluations are not always completely repeatable. The UK Biometric Product Testing is an example of big scale scenario evaluation [37].

The operational evaluation differs from the scenario evaluation because it is performed in the real applicative scenario. This evaluation can therefore be performed on all the effective users of the systems, on a randomly selected set of users, or on specifically selected users. For this reason, the performed test is difficult or impossible to repeat. The goal of this typology of test is not to measure the accuracy obtained by biometric systems, but it aims to determine the workflow impact determined by the addition of a biometric system in the considered applicative context. The operational evaluation can then permit to analyze the advantages obtained using the considered biometric system.

The described evaluation modalities are complementary and should be performed in sequence. First, the technology evaluation should be performed to analyze the performances of biometric methods in general conditions. Then, the scenario evaluation permits to select the best biometric technology for an applicative scenario. The operational evaluation should finally be performed in order to obtain solid business reports for potential installations.

2.4.2 Evaluation aspects

Biometric systems should be evaluated considering different viewpoints. As shown in Fig. 2.3, the main evaluative aspects can be quantized and plotted in a nine-dimensional space (e.g., in a spider diagram), where a specific application is represented by a point in this space.

- **Accuracy**: specific figures of merit should be adopted to measure the performances of the recognition systems. The evaluation procedures are discussed in Section 2.4.3.

- **Speed**: the time needed for every recognition is an important aspect that should be considered during the design of a biometric application. For example, identification systems require the use of faster algorithms with respect to verification systems. All the steps of the biometric recognition process should be distinctly considered: acquisition, feature extraction, and matching.

- **Cost**: systems based on expensive and accurate acquisition devices can usually obtain better performances with respect to systems based on low-cost hardware

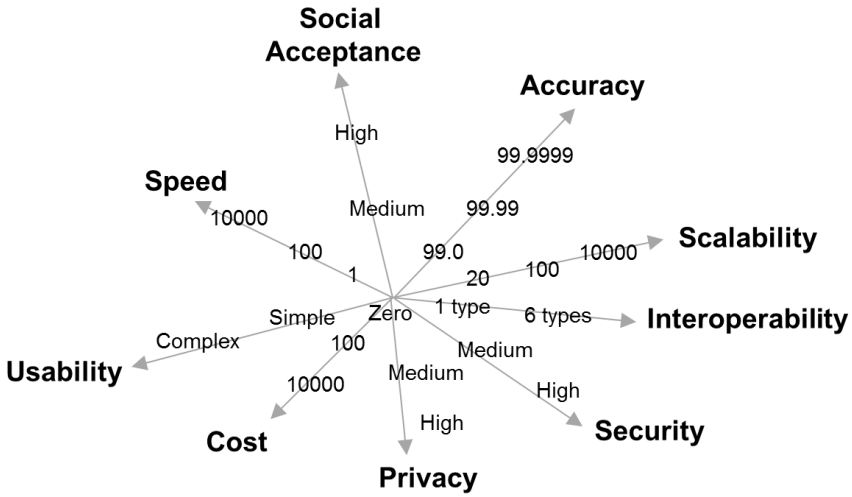

Figure 2.3: Evaluative aspects of biometric systems.

setups. The use of low-cost sensors, however, can permit a wider diffusion of a biometric technology. For this reason, a cost analysis should be performed to search the best biometric technique for the considered applicative context. This analysis also includes the costs of the design and software implementation.

- **Scalability**: is the ability of the system to work under an increased or expanding workload. In biometrics, this aspect should be evaluated by considering all the modules of the system: network architecture, availability of the used sensors, typology of the storing devices, performances of the recognition algorithms in terms of accuracy and speed.

- **Interoperability**: represents the level of compatibility between the evaluated system and the existing biometric technologies. The use of standards for the formats of templates and samples permits to obtain the compatibility between different systems based on the same trait [38].

- **Usability**: is the ease of use and learnability of the system. Low usability levels can reduce the social acceptance and system accuracy. In most of the cases, the usability is evaluated by analyzing the acquisition time, number of incorrectly captured samples, and results of questionnaires [39].

- **Social acceptance**: measures the users' perception, feelings and opinions regarding the system. It is a crucial factor for the diffusion of a biometric technology in different applicative contexts. The acceptance level can be different for every user and is influenced by different factors: cultural and religious aspects, usability, perceived privacy risks. The social acceptance can be measured by analyzing the results of questionnaires [40].

- **Security**: measures the robustness of the system to possible attacks. There are different kinds of attacks that can be performed to all the modules of biometric systems. More details are provided in Section 2.5.

- **Privacy**: measures the capability of the system to prevent possible thefts and misuses of biometric data. The evaluation of the privacy protection level is a complex task and should consider the risks perceived by the users and the real risks. Section 2.5 proposes a description of the privacy aspects in biometrics.

2.4.3 Accuracy evaluation

The accuracy evaluation methodologies described in this section permits to evaluate the results obtained by biometric techniques on sample datasets and can be applied to technologies based on symmetrical and asymmetrical matching functions.

The obtained results permit to compute the most common figures of merit in the literature. These accuracy indexes can then be used to compare the performances of existing biometric recognition techniques.

The accuracy indexes, however, express the performances of the evaluated biometric systems on limited sets of samples. For this reason, it is a good practice to estimate the confidence of the obtained measurements.

2.4.3.1 Methods for the accuracy evaluation

The used definition of accuracy presents differences with respect to the classical one used in metrology [41] but is generally accepted in biometric systems. Accuracy of measurements evaluates the agreement between the result of a measurement and the expected value, applying the system on a biometric database. As described in Section 2.4.1, the reported figures of merit can be used to perform technology evaluations and scenario evaluations.

The accuracy evaluation requires the use of a previously captured biometric database. Technology evaluations are usually performed on publically available datasets in order to compare the obtained results with the ones achieved by other methods in the literature. Usually, scenario evaluations do not use public datasets but require sets of biometric data specifically acquired in order to describe the evaluated scenario in an exhaustive manner.

In the literature, there are studies on the accuracy evaluation designed for symmetric matching functions [42]. Considering two biometric samples A and B, a matching function M is symmetric if $M(A, B) = M(B, A)$. The evaluation procedures reported here are the ones proposed in [43] and can be applied both to symmetric and asymmetric matching functions, in which $M(A, B) \neq M(B, A)$. The use of accuracy evaluation techniques that consider asymmetric matching functions is necessary in fingerprint biometrics since most of the recognition systems based on minutia features use asymmetric matching strategies.

We define B_{ij} as the jth sample of the ith individual; T_{ij} as the template computed from B_{ij}; n_i as the number of samples available for the ith individual; and N as the number of enrolled individuals. We then describe the steps to perform the accuracy evaluation using the most common figures of merit in the literature.

1. **Enrollment**

   During the enrollment step, the presence of errors is monitored by using an index named $\text{REJ}_{\text{ENROLL}}$. $\text{REJ}_{\text{ENROLL}}$ is the rejection ratio in the enrollment phase, due to fails (the algorithm declares that it cannot enroll the biometric data), timeouts (the enrollment exceeds the maximum allowed time), and crashes (the algorithm crashes during the biometric processing) situations. The templates $T_{ij}, i = 1, \ldots, N, j = 1, \ldots, n_i$, are computed from the corresponding B_{ij} and stored on the disk; if something wrong happens, the index $\text{REJ}_{\text{ENROLL}}$ has to be increased.

2. **A general matching score computation**

   The procedure to evaluate symmetric matching functions is reported: every biometric template T_{ij} successfully created in the previous step is matched against the templates $T_{ik} (j < k \leq n_i)$. The obtained matching scores are stored in a

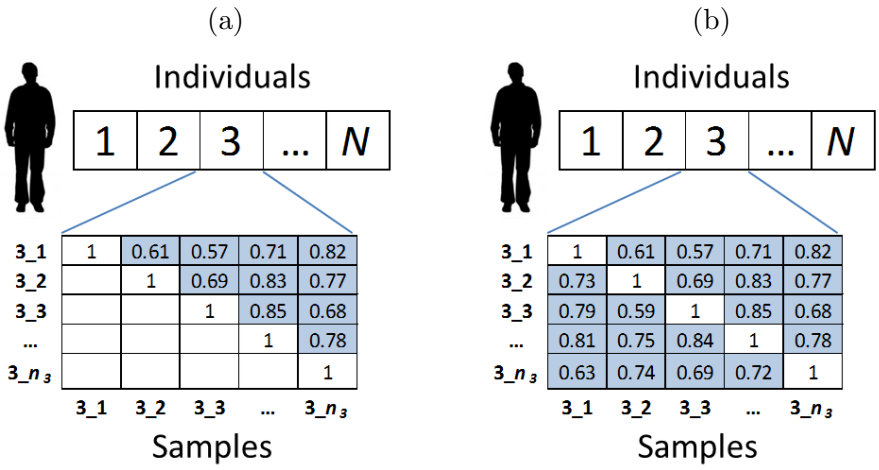

Figure 2.4: Accuracy evaluation: (a) gms for symmetric matching functions; (b) gms for asymmetric matching functions.

matrix called genuine matching scores gms_{ijk} (Fig. 2.4a). The term "genuine" refers to the fact that the matching is computed between samples of the same identity-certified individual. Since the matrix is symmetric by definition, only the upper triangular matrix is computed. Each individual has its squared gms matrix.

Differently, for asymmetric matching functions, every biometric template T_{ij} successfully created in the enrollment step is matched against the biometric templates $T_{ik}(j \leq n_i, k \neq i)$ and the corresponding genuine matching scores matrix gms_{ijk} is stored (Fig. 2.4a). The matrix is not symmetric but is still square.

Then, the number of matches, denoted as the number of genuine recognition attempts (NGRA), is given by

$$\text{NGRA}_{\text{symMatch}} = \frac{1}{2}\sum_{i=1}^{N} n_i\,(n_i - 1) \tag{2.1}$$

where, $\text{REJ}_{\text{ENROLL}} = 0$ for symmetric matching and

$$\text{NGRA}_{\text{asymMatch}} = \sum_{i=1}^{N} n_i\,(n_i - 1) \tag{2.2}$$

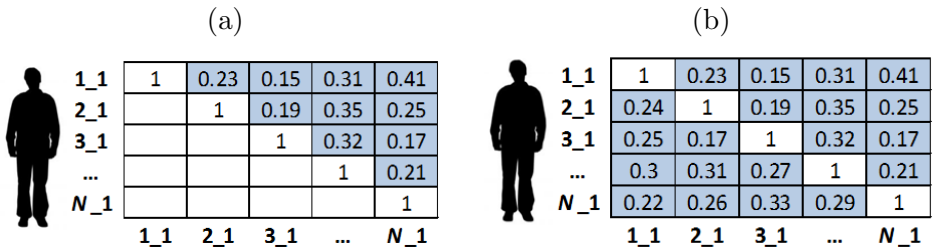

Figure 2.5: Accuracy evaluation: (a) ims for symmetric matching functions; (b) ims for asymmetric matching functions.

where $\text{REJ}_{\text{ENROLL}} = 0$ (asymmetric matching).

The matching scores of samples appertaining to different individuals (impostor matchings) have also to be considered. For symmetric matching functions, each biometric template $T_{i1}, i = 1 \ldots N$ is matched against the first biometric template of a different individual $T_{k1} (1 < k \leq N, k > i)$ and then the corresponding impostor matching score matrix is stored (Fig. 2.5a). The impostor matching in the case of asymmetric matching function is computed as follows: every biometric template $T_{i1}, i = 1 \ldots N$ is matched against the first biometric template of a different individual $T_{k1} (1 < k \leq N, k \neq i)$ and the corresponding impostor matching scores matrix is stored (Fig. 2.5b). The number of matches, denoted as the number of impostor recognition attempts (NIRA), is given by

$$\text{NIRA}_{\text{symMatch}} = \frac{1}{2} N (N - 1) \tag{2.3}$$

if $\text{REJ}_{\text{ENROLL}} = 0$ for symmetric matching, and

$$\text{NIRA}_{\text{asymMatch}} = N (N - 1) \tag{2.4}$$

if $\text{REJ}_{\text{ENROLL}} = 0$ for asymmetric matching.

Finally, in the determination of gms and ims matrixes, it is possible to consider the enrollment errors. These events are respectively accumulated into REJ_{NGRA} and REJ_{NIRA} counters. It follows that gms and ims matrixes can have missing values. Commonly, special values are stored, as "NULL" or out of range matching values.

2.4.3.2 Accuracy indexes

In this subsection, the most common figures of merit for the accuracy evaluation of biometric systems are briefly discussed.

Considering systems allowing multiple attempts for having multiple templates, a general definition expresses errors of the matching algorithms considering single comparisons of a submitted sample against a single enrolled template. Important metrics are the false match rate FMR(t) and false non-match rate FNMR(t). They are functions of the threshold value t used to compare the matching scores during the decision step.

The false match rate is the expected probability that a sample will be falsely declared to match a single randomly selected template (false positive). The false non-match rate is the expected probability that a sample will be falsely declared not to match a template of the same measure from the same user supplying the sample (false negative).

The FMR and FNMR curves are computed from the gms and ims distributions for t typically ranging from zero to one, and are defined as [3]:

$$\mathrm{FMR}(t) = \frac{\mathrm{card}\left\{\mathrm{ims}_{ik} | \mathrm{ims}_{ik} \geq t\right\}}{\mathrm{NIRA}}, \tag{2.5}$$

$$\mathrm{FMR}(t) = \frac{\mathrm{card}\left\{\mathrm{gms}_{ijk} | \mathrm{gms}_{ijk} < t\right\} + \mathrm{REJ}_{\mathrm{NGRA}}}{\mathrm{NGRA}}, \tag{2.6}$$

where card represents the cardinality.

The evaluation of the overall accuracy level of a biometric system is often performed by considering two error plots. The first is the receiving operating curve (ROC), which is a graphical plot of the fraction of true positives versus the fraction of false positives for a binary classification system as its discrimination threshold is varied. In biometrics, the axes are (1-FNMR) and FMR. The second graph is the plot of FNMR versus FMR, called the detection error tradeoff (DET) plot. Many works in the literature show these graphs plotted using logarithmic axes.

The ROC and DET curves can be used to directly compare biometric systems. In order to analyze the accuracy of different systems, the errors must be evaluated on the same dataset. Fig. 2.6 shows DET curves that compare the accuracy of four different systems [44]. The best system is the one that has its DET curve below all the other

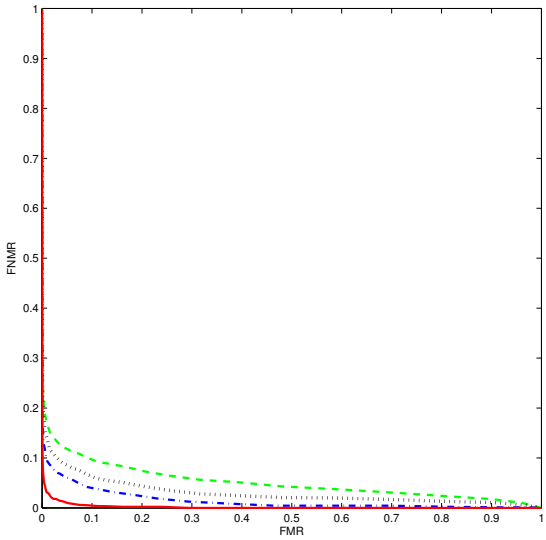

Figure 2.6: Examples of DET curves.

curves. It is common that a system outperforms the compared ones only in some regions determined by specific values of t.

In order to evaluate the peculiar behavior of a selected system in separating the genuine from the impostor attempts, the distributions of the matching scores obtained on the genuine population (gms_{ijk}) and of the impostor population (ims_{ik}) can be plotted. If there is not an overlap between the two curves, it means that there exists a threshold value t' that perfectly separates the genuine individuals from the impostors (ideal case). Fig. 2.7 shows an example of graph obtained by an iris recognition system [45] on a public dataset [46].

Another commonly used accuracy index is the equal error rate (EER), which is computed as the point where $\text{FMR}(t) = \text{FNMR}(t)$.

Others indexes measure the capability of the biometric system to acquire sample or to process and enroll templates: the failure to accept rate (FTAR) is the expected proportion of transactions for which the system is unable to capture or locate an image or signal with sufficient quality [3]; the failure to enroll rate (FER) represents the expected proportion of the population for whom the system is unable to generate repeatable templates [3].

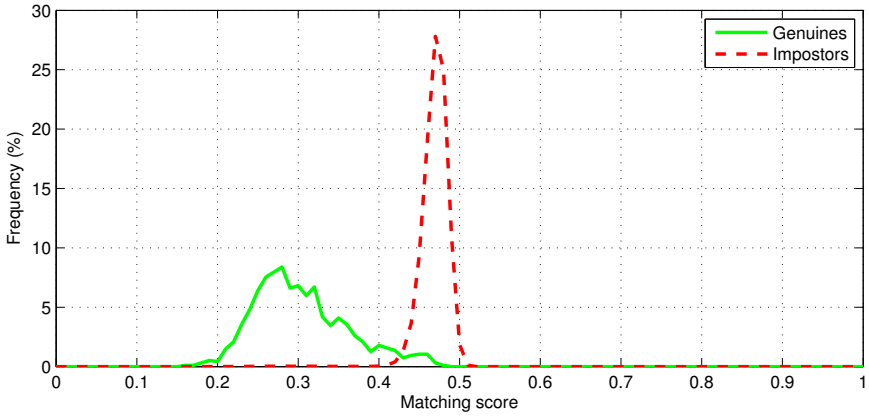

Figure 2.7: Examples of genuine and impostor distributions.

In the literature, there are many other indexes useful for testing the performances of biometric technologies. The choice of the used indexes depend on the system characteristics (identification/verification, fixed threshold, number of enrolled users, and number of templates per user) [3]. Common figures of merit are the false acceptance rate (FAR) and false reject rate (FRR). FAR represents the frequency that a non-authorized person (system user) is accepted as authorized. FRR is the frequency that an authorized person is erroneously rejected. Differently to FMR and FNMR, FAR and FRR are computed considering the number of incorrect acquisitions.

2.4.4 Confidence estimation

The accuracy evaluation of a biometric system is performed on limited sets of data. For this reason, it is useful to estimate the confidence of the performed measures.

The confidence of the accuracy indexes is strictly related to the testing dataset. As reported in [47], the datasets used to perform the evaluation should have a sufficient number of samples. Dimensioning the test size, two main rules can be followed: the Rule of 3 [48, 49], and Rule of 30 [50].

The Rule of 3 addresses the question: "What is the lowest error rate that can be statistically established with a given number N of comparisons?". This value is the error rate p for which the probability of zero errors in N trials is equal to a fixed value (typically 5%). The rule can be expressed as $p \approx 3/N$ for a 95% confidence level.

For example, a test without errors on a dataset composed by 300 independent samples suggests with 95% confidence that the biometric system has an error rate of 1% or less.

The Rule of 30 can be expressed as follows: "To be 90% confident that the true error rate is within ±30% of the observed error rate, there must be at least 30 errors". For example, 30 false non-match errors in 3000 independent genuine trials suggest with 90% confidence that the true error rate is between 0.7% and 1.3%. This rule has been derived from the binomial distribution assuming independent trials, and may be applied by considering the performance expectations for the evaluation.

With a sufficiently large number of samples, it is possible to evaluate the results using the central limit theorem [51], which implies that the observed error rates should follow an approximately normal distribution. Under the assumption of normality, $100(1-\alpha)\%$ confidence bounds on the observed error rates are given by the following formula:

$$\hat{p} \pm z\left(1-\frac{\alpha}{2}\right)\sqrt{\hat{V}\left(\hat{p}\right)}, \tag{2.7}$$

where $\hat{p}$ is the observed error rate, $\hat{V}\left(\hat{p}\right)$ is the estimated variance of the observed error rate [47], $z\left(.\right)$ is the inverse of the standard normal cumulative distribution. For 95% confidence limits, the value $z(0.975)$ is 1.96.

In the literature, there are also non-parametric methods, such as the bootstrap [52, 53]. This technique reduces the need to make assumptions about the underlying distribution of the observed error rates and the dependencies between attempts. The distributions and dependencies are inferred from the samples themselves. Bootstrap samples are computed by sampling with replacement from the original samples. Then, a large number of bootstrap samples are used to obtain the empirical distribution of the accuracy indexes, which can then be used to estimate the confidence intervals. The bootstrap values allow a direct approach for constructing $100(1-\alpha)\%$ confidence limits by choosing L (lower limit) and U (upper limit) such that only a fraction $\alpha/2$ of bootstrap values are lower than L, and $\alpha/2$ bootstrap values are higher than U. The work in [47] recommends using at least 1000 bootstrap samples for 95% limits, and at least 5000 bootstrap samples for 99% limits.

The approach proposed in [54] is based on the bootstrap technique, but also consider that the templates related to the same biometric traits and individuals are statistically

correlated. This approach samples with replacement from specifically determined subsets of the data. Every subset contains the templates obtained from a single biometric trait or individual.

Other works [55, 56] evaluate the robustness of bootstrap strategies in different applicative conditions.

In the literature, there are also studies on the confidence estimation of biometric systems based on different techniques. A semi-parametric approach based on multivariate copula models for correlated biometric acquisitions is proposed in [57]. Based on the same model, this work also propose a technique to determine the minimum number of samples required to achieve confidence bands of desired width for the ROC curve. Other studies regard multibiometric systems [58].

2.5 Privacy in biometrics

Compared with traditional techniques used to establish the identity of a person, biometric systems offer a greater confidence level that the authenticated individual is not impersonated by someone else. However, it is necessary to consider different privacy and security aspects in order to prevent possible thefts and misuses of biometric data. The effective protection of the privacy must encompass different aspects, such as the perceived and real risks pertaining to the users, the specificity of the application, the adoption of correct policies, and data protection methods as well [59, 60, 61, 62]. This section focuses on the most important privacy issues related to the use of biometrics, describes important aspects that should be considered for evaluating the privacy risks in biometric applications, presents actual guidelines for the implementation of privacy-protective biometric systems, and proposes a discussion of the methods for the protection of biometric data.

2.5.1 Privacy and security in biometric systems

Security and privacy aspects are important factors that should be considered in order to prevent possible thefts and misuses of biometric data. Security and privacy are two different concepts because the privacy protection is more restrictive than the security protection. The security ensures: verification, data integrity, confidentiality, and non-repudiation. Differently, the privacy requires also the data protection.

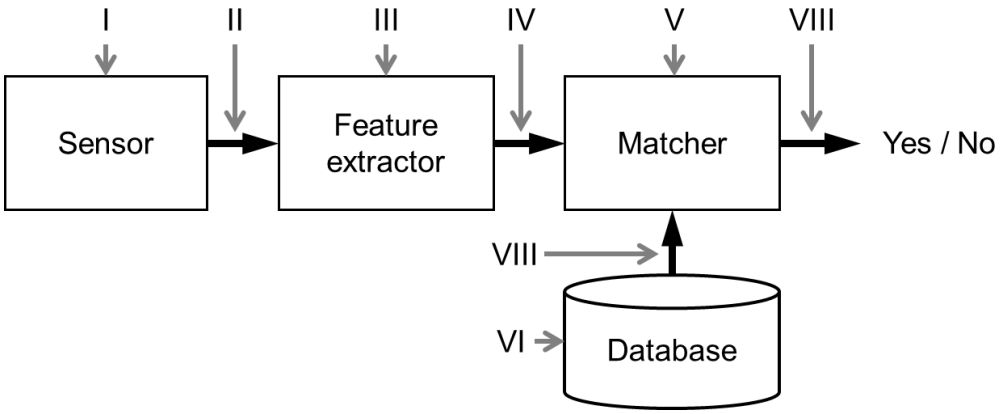

Figure 2.8: Points of attack in biometric systems.

The protection from privacy abuses is very important in biometric systems. For example, if the biometric data related to an individual are stolen, this person can be impersonated for a long time period and it is not easy to modify or substitute the compromised data. This is due to the fact that biometric traits are unique for every individual and strictly associated to their owner. Moreover, biometric traits are irrevocable, in the sense that the association cannot be changed during the human life.

In order to protect the privacy and security of the users, it is necessary to consider the possible attacks that can be performed to biometric systems. As shown in Fig. 2.8, it is possible to distinguish eight distinct classes of attacks to the different system modules [63, 64, 65]: (I) fake biometric at the sensor, (II) resubmission of old digitally stored biometric signals, (III) override the feature extractor, (IV) tampering with the feature representation; (V) override the matcher, (VI) tampering with stored templates, (VII) channel attack between stored templates and the matcher, (VIII) decision override.

There are different classes of techniques that should be used to protect the privacy of the users from possible attacks. Every component of the biometric system should in fact be protected by using properly methods. Important classes of techniques are: liveness detection methods, physical and cryptographic methods for the channel protection, secure code execution practices, template protection methods [66].

2.5.2 Evaluation of privacy risks

It is possible to distinguish three different perspectives about the privacy in biometrics. The first one is related to the risks perceived by the users and should be considered in order to evaluate the acceptability of the system itself. The second perspective regards the application context in which the biometric system should be exploited and permits to properly design privacy protection techniques. The last aspect that should be considered is the used biometric trait. Each biometric trait, in fact, presents different proprieties that influence privacy risks.

The evaluation of the risks perceived by the users is a complex task since the risk perception is different for every person. Generally speaking, one of the most important perceived risks is related to the fact that many people consider the acquisition of the biometric traits as an exact permanent filing of their activities and behaviors, and the idea that biometric systems can guarantee recognition accuracy equal to 100% is very common. Other perceived risks consist in the use of the collected biometric data for malicious purposes, for tracing all the activities of the individuals, or for operating proscription lists. Another important perceived risk is the fact that the acquisition of some biometric traits can be dangerous for the health. For example, the iris images are usually captured by using infrared illuminators, which can be erroneously considered as harmful. These psychological aspects should be taken into account during the deployment of biometric systems. During this process, it is very important to inform the users about the real risks for the health and for the privacy, as well as all the procedures designed and applied to protect biometric data.

The evaluation of the application context permits to determine some real risks of privacy invasiveness. Table 2.2 provides a qualitative representation of the privacy risks versus ten application features, according to the International Biometric Group [67]. Table 2.2 shows that the risk factors consist in the data storage strategies (data type, physical supports, owner of the information, storage period), used biometric traits (behavioral or physiological), and other important applicative conditions (environmental conditions, identification or verification modality, optional or mandatory use of the system).

In order to determine the real risks of privacy invasiveness, it is also necessary to consider the adopted biometric traits because they can introduce different kinds

Table 2.2: Applicative aspects concerning the privacy according to the IBG (Iternational Biometric Group).

Lower Risk	Question	Greater Risk
Overt	Is the system deployed overtly or covertly?	Covert
Optional	Is the system optional or mandatory?	Mandatory
Verification	Is the system used for Identification or Verification?	Identification
Fixed Period	Is the system deployed for a fixed period of time?	Indefinite
Private Sector	Is the system deployed in the private or public sector?	Public Sector
Individual/Customer	In what role is the user interacting with the system?	Employee/Citizen
Enrollee	Who owns the biometric information?	Institution
Personal storage	Where is the biometric data stored?	Database Storage
Behavioral	What type of biometric technology is being deployed?	Physiological
Templates	Does the system use templates, samples or both?	Sample/Images

of risks. Four important features related to the technologies associated to different biometric traits are presented in [67].

1. The first feature is the possibility to use the biometric trait in identification systems. In general, systems based on traits that can be used in identification are more invasive for the user's privacy.

2. The second feature is associated to the possibility of the trait to be used in covert systems. Covert systems present more privacy risks than overt systems.

3. The third feature evaluates the level in which biometric traits can be considered as physiological or behavioral. Behavioral traits are more privacy compliant because they can be modified by the users and are less permanent then physiological traits.

4. The forth feature is the database compatibility, which is related to the technology interoperability between different systems and considers the presence of numerous and/or large biometric databases. Traits characterized by low database compatibility can be considered as more privacy compliant.

Performing a weighted mean of these features, it is possible to classify the overall risk level related to the technologies based on a specific biometric trait. Examples of traits that present a high risk level are the face and fingerprint. A medium risk can be assigned to the iris and retina, and traits characterized by low privacy risks are the hand, voice, keystroke, and signature.

2.5.3 Design of privacy protective biometric systems

Considering the privacy aspect, it is possible to define four different classes of biometric applications: protective, sympathetic, neutral, invasive [67].

1. Privacy-protective applications use biometrics in order to protect personal information that might otherwise be compromised. Examples of privacy-protective applications are systems for the enterprise security and accountholder verification.

2. Privacy-sympathetic applications are designed to protect the biometric data from unauthorized access and usages. Most of the current applications can incorporate privacy-sympathetic elements.

3. Privacy-neutral applications use biometrics without considering privacy aspects. Examples of these applications are some access control technologies and verification systems for electronic devices (personal computers, mobile phones, etc.).

4. Privacy-invasive applications permit the use of personal data in a fashion that is contrary to privacy principles. Surveillance applications and some national ID services can be considered as privacy-invasive.

In order to design privacy-sympathetic and privacy-protective systems, it is necessary to follow a set of guidelines [67]. These guidelines are related to: scope and capabilities of the system; user control of the personal data; disclosure, auditing and accountability of the biometric system; data protection techniques:

1. The scope and capabilities of the system should be declared to the users and should not be extended during the life of the system. Moreover, biometric data should be deleted from the database after a period of time known by the users.

2. The user should have the control of her biometric data. The user should also have the possibilities to be unenrolled and to change or modify her data.

3. A disclosure regarding the biometric system should be provided. This document should regard the system purpose, enrollment modalities, matching modalities, optional or mandatory use of the biometric recognition, individuals who are responsible for the system, data protection system. Moreover, the owner of the biometric system and the operators should be able to provide a clear and effective process of auditing when required by the authorities.

4. The system should provide mechanisms for the protection of all the steps performed by the biometric recognition process from possible attacks. The result of every performed recognition should also be protected using proper techniques. Another important practice is to limit the access to the biometric data to a defined set of authorized operators.

2.5.4 Technologies for Biometric Privacy

In the literature, there are many methods for the protection of biometric templates. Ideally, a biometric template protection method should satisfy four properties [3, 66]:

1. **diversity**: the secure templates must not allow cross-matching across databases;
2. **revocability**: compromised templates can be revoked;
3. **security**: the estimation of the plain templates from the secure templates must be computationally hard;
4. **performance**: the accuracy of the biometric system must not be degraded by the biometric template protection method.

These four proprieties cannot be guaranteed by encrypting the templates with standard methods (e.g. RSA, AES, etc.). In fact, using these methods, the intraclass variability (biometric data captured from the same biometric trait look different from one another) does not allow performing the matching in the encrypted domain. Therefore, it is necessary to decrypt the templates during every recognition attempt. This approach is not secure and it is therefore necessary to adopt methods designed for the protection of biometric data.

In the literature, most of the biometric template protection methods are based on two classes of techniques: cancelable biometrics, and biometric cryptosystems [66, 68]. Recent researches also proposed other approaches based on cryptographically secure methods [69].

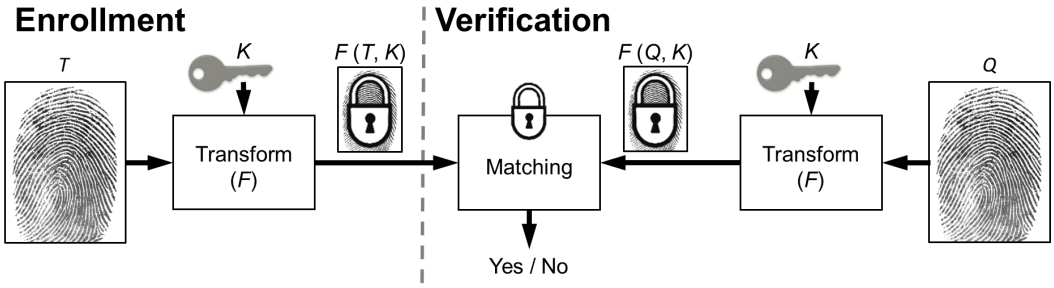

Figure 2.9: Cancelable biometrics: enrollment and verification.

2.5.4.1 Cancelable biometrics

Cancelable biometrics is based on intentional, repeatable distortions of biometric data. The used transformations permit to perform comparisons of biometric templates in the transformed domain [70]. During the enrollment phase, the biometric data T is modified by applying a transformation function F with parameters K obtained by a random key or a password. The transformed template $F(T, K)$ is then stored in the database. The verification step applies the same transformation to the query data Q and directly matches the transformed templates $F(Q, K)$ and $F(T, K)$. Fig. 2.9 schematizes the described process.

The main advantage of this technique is that, if a transformed template is compromised, cancelable biometrics permit to easily substitute the stored transformed template by changing the transformation parameters. The design of the transformation functions is particularly critical because it is necessary to adopt functions that are robust to intra-class variations in order to do not reduce the accuracy of the biometric system. Another aspect that should be considered is that the correlation of transformed templates should not reveal information about the transformation function. Transformation functions can be applied to biometric samples (e.g. face images [71]), processed signals (e.g. the iris pattern [72]), or templates (e.g. features extracted from a face image [73]). It is possible to distinguish two classes of methods: biometric salting, non-invertible transforms.

Usually, systems based on the biometric salting transform features using an invertible function defined by a user-specific key or password. Considering that the used transformation is invertible, the password must be securely stored by the user and presented during every verification. The principal advantage of the biometric salting is

that it is possible to use multiple templates for the same biometric trait because the keys are specified by the users. An important limitation of methods based on keys or passwords is that they are not usable in identification systems. Moreover, if the key is known, it is possible to obtain the original template. In the literature, one of the most used methods based on the biometric salting is the BioHashing [71, 74, 75]. This method is designed for the fingerprint trait and is divisible in two steps [76]: an invariant and discriminative transform of the biometric data, with a moderate degree offset tolerance; a discretization of the data. There are also methods designed for face recognition systems. One of these methods uses the Fisher discriminant analysis and then performs a transformation of the obtained vectors by using a randomly selected set of orthogonal directions [73]. Differently, the method proposed in [77] is based on minimum average correlation energy filters. Salting methods can also be applied to different biometric traits (e.g. iris [72] and dynamic handwriting [78]).

In the literature, many methods secure the templates by using non-invertible transformation functions. Non-invertible transformation refers to a one-way function that is computable in polynomial time and hard to invert. The main advantage of this class of methods is that the protection of the plain biometric template is more secure than the one offered by the methods appertaining to the salting class. In fact, if the key and/or the transformed template are known, the estimation of the plain template is a computationally hard task (considering a brute force attack). Another advantage of these methods is that diversity and revocability can be achieved by using different transformation functions. The main problem is that it is difficult to design transformation functions that satisfy both the discriminability and the non-invertibility. For example, a study on the measurement of the real non-invertibility of methods based on the fingerprint is presented in [79]. Another important aspect is that the transformation function depends on the biometric features to be used in a specific application. Moreover, similarly to the biometric salting, the adoption of keys obtained by passwords or tokens does not permit to use methods based on non-invertible transformation functions in identification systems. In the literature, there are methods based on non-invertible transformation functions designed for different biometric traits. For example, fingerprint [80], face [81, 82], and signature [83]. A general schema is proposed in [70] and is based on a non-invertible function designed to transform a point pattern by using high order polynomials. This method can be used in fingerprint recognition systems based

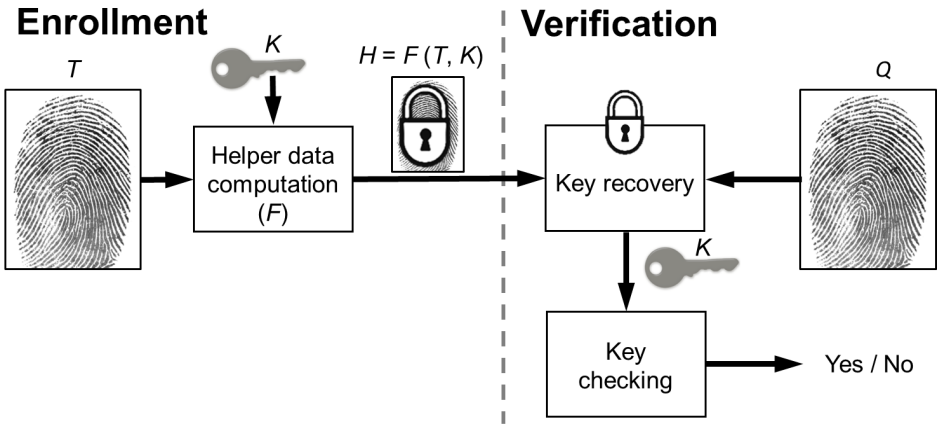

Figure 2.10: Key-binding biometric cryptosystems: enrollment and verification.

on minutiae features, and voice recognition systems. Also the approach proposed in [84] is designed for fingerprint recognition systems and proposes three different functions (Cartesian, Polar, and functional) in order to transform minutiae templates. A different schema, called Biotope, is proposed in [85, 86]. This schema transforms the original biometric data by using cryptographic primitives and supports a robust distance metric in order to perform the matching. The approach supports both transforms that are public-key cryptographically invertible and/or cryptographic one-way functions (such as MD5). The Biotope schema can be applied to different biometric traits, such as face [85] and fingerprint [86].

2.5.4.2 Biometric cryptosystems

Biometric cryptosystems were originally designed in order to secure cryptographic keys by using biometric information, or to directly compute cryptographic keys from biometric data [66]. Nowadays, these techniques are also used for the privacy protection of biometric templates. Biometric cryptosystems store public data regarding the biometric trait, called helper data. During the verification process, the helper data is used in order to extract a cryptographic key from the biometric query sample. The matching step checks the validity of the obtained key in order to verify the identity. It is possible to divide the biometric cryptosystems into two classes: key-binding biometric cryptosystems, and key-generating biometric cryptosystems.

Key-binding biometric cryptosystems store helper data by biding the template with a chosen cryptographic key. The binding process obtains a helper data considerable as a single entity that embeds both the key and the template without revealing information about them. In fact, it is computationally hard to estimate the key or the template without knowing the user's biometric data. The verification is performed by using the query template in order to retrieve the cryptographic key from the helper data. Usually, this task is based on error correction algorithms. If the obtained key corresponds to the correct cryptographic key, the result of the verification is a match value. Fig. 2.10 shows the general schema of the key-binding biometric cryptosystem. This class of methods has two main advantages. First, the helper data does not reveal much information about the key or the biometric data. Moreover, this approach is tolerant to intra-user variations. The main limitation consists in the degradation of the accuracy of the biometric system caused by the substitution of the original matching algorithms with error correction schemes. The second limitation is that these methods do not guarantee diversity and revocability. The firstly proposed key-binding biometric cryptosystems based on fingerprints are Mytec1 and Mytec2 [87], which are based on the correlation between filter functions and biometric images. Another well-known approach in the literature is the fuzzy commitment scheme [88]. This approach combines error correcting codes algorithms and cryptography techniques in order to achieve a cryptographic primitive called fuzzy commitment. During the enrollment, a biometric template x composed by a fixed length feature vector and a codeword w of an error correction schema C are bound. The helper data (fuzzy commitment) consists in $x - w$ and $h(w)$, where h is a hash function. The biometric matching tries to reconstruct w starting from a biometric query x'. First, the stored value $x - w$ is subtracted from x', obtaining $w' = w + \delta$, where $w' = x' - x$. If the value w is obtained by applying the error correction schema C to w', the result of the matching step is positive. The fuzzy vault [89] approach uses a set A to lock a secret key k, yielding a vault V_A. If the key k is reconstructed by using a set B that is sufficiently similar to A, the vault V_A is unlocked. This approach is based on polynomial encoding and error correction algorithms. Examples of other approaches appertaining to this class are the shielding functions [90] and distributed source coding [91]. In the literature, there are methods based on different biometric traits. For example, face [92], fingerprint [93], iris [94], and signature [95].

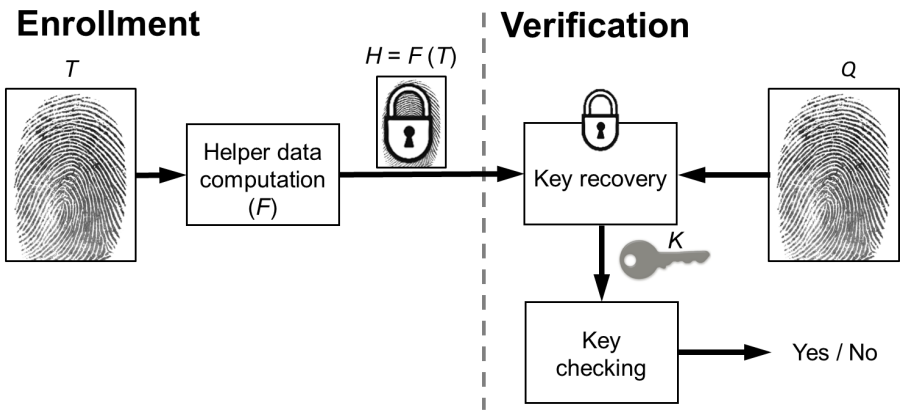

Figure 2.11: Key generating biometric cryptosystems: enrollment and verification.

Key generating biometric cryptosystems compute a cryptographic key directly from the biometric data. The recognition process performed by biometric systems based on key generating biometric cryptosystems is similar to the one executed by using key-binding biometric cryptosystems but do not requires external keys. The schema of this process is shown in Fig. 2.11. The main advantage of these methods is that the obtained cryptographic keys can be used in many applications. However, an important problem is that it is difficult to generate keys with high stability and entropy [96, 97]. Two well-known approaches are the secure sketch and fuzzy extractor [98]. Secure sketches solve the problem of error tolerance, enabling the computation of a public key P from a biometric reading r, such as from another reading r' sufficiently close to r, it is possible to reconstruct the original one. Fuzzy extractors address the problem of non-uniformity by associating a random uniform string R to the public string P still keeping all the properties of secure sketches. Indeed, fuzzy extractors can be built out of secure sketches and enable to recovering of the secret uniform random string R, from the knowledge of the public string P and a reading r' sufficiently close to r. A syndrome-based key-generating scheme called PinSketch is presented in [98]. Similarly to the fuzzy vault, this method is based on a polynomial interpolation. Compared with the fuzzy vault, the PinSketch scheme reduces the computational time, and length of the public key. During the enrollment phase, a syndrome based on polynomial interpolation is computed and stored as helper data. During the recognition phase, an error vector is computed from the query biometric sample and the helper data to recover the enrolled biometric data. An approach based on multiple biometric traits

is presented in [99]. This method is based on the fuzzy commitment scheme. During the enrollment phase, one biometric reading is xored with a random bit string obtained after a pseudo random permutation from the other biometric reading. Differently, during the verification phase, the process is inverted and the second biometric template is reconstructed in order to be used as preliminary check (by comparing the computed hash with the value stored into the identifier) and as input of the matching module. In the literature, there are also other types of key-binding biometric cryptosystem [95, 100] and techniques designed for multimodal and multibiometric systems [101].

2.5.4.3 Cryptographically secure methods

The recognition accuracy of systems based on cancelable biometrics can be decreased by the applied transformation functions. Similarly, in biometric cryptosystems, it is not possible to always adopt the best matching functions used in the plain domain and, as a consequence, the accuracy can be worsened. As a solution to this problem, in the literature there are template protection techniques specifically designed with the aim to perform the biometric recognition without applying transformations of the biometric data and without modifying the matching functions designed for the adopted templates. These methods can directly perform the matching using the encrypted data and are usually based on homomorphic cryptosystems.

In homomorphic cryptosystems, given a set M (resp., C) of the plaintexts (resp., ciphertexts), for any given encryption key k the encryption function E satisfies

$$\forall m_1, m_2 \in M, \quad E\left(m_1 \odot_M m_2\right) \leftarrow E\left(m_1\right) \odot_C E\left(m_2\right)$$

for some operators $\odot_M$ in M and $\odot_C$ in C, where $\leftarrow$ means "can be directly computed from", that is, without any intermediate decryption [102].

The main advantage of these systems is that the accuracy obtained by using the transformed templates is very similar to the accuracy obtained by using the plain data. Usually, a decreasing of the performance can be caused by an excessive quantization or data reduction [103]. The main disadvantage is that it is difficult to adopt homomorphic cryptosystems in biometric systems that require complex matching functions. Homomorphic cryptosystems are also computationally expensive.

A cryptographically secure method designed for distributed architectures described in [104, 105] and is designed for face recognition systems. In the literature, there are also approaches based on homomorphic encryption methods and designed for biometric systems that compute the matching score as the Hamming distance between feature vectors (e.g. Iriscode [6]): the system in [106] is based on the Blum-Goldwasser cryptosystem, the system in [107] on the Goldwasser-Micali scheme, the system in [108] on the homomorphic properties of Goldwasser-Micali and Paillier cryptosystems, the system in [109] on the ElGamal scheme and Garbled Circuits.

2.6 Research trends

The existing biometric systems present some problems and aspects that should be improved. For this reason, the international research community is very active in biometrics. It is possible to distinguish some major research fields.

- **Increasing of the accuracy**: many researches aim to improve the accuracy of biometric systems by using new software and hardware techniques.
- **Multimodal and multibiometric systems**: these systems use multiple biometric traits and/or multiple recognition algorithms in order to obtain a greater accuracy with respect to traditional biometric systems [30]. The information obtained from every biometric technology are fused using decisional techniques (e.g. computational intelligence methods [31]).
- **Reduction of the sensor costs**: many existing biometric systems are based on expansive sensors. For example, most of the iris recognition systems capture iris images using near infrared illuminators and cameras [6]. Systems based on images captured in natural light conditions can reduce the final costs. In this context, for example, there are different studies on the segmentation [27, 110, 111] and recognition [112] of iris images captured in natural light conditions.
- **Use of less-cooperative acquisition techniques**: the existing biometric methods usually require a high level of cooperation during the acquisition step. Technologies based on less-cooperative acquisition techniques permit to adopt biometric systems in different applicative scenarios, like surveillance applications [113].

- **Increasing of the usability and user's acceptance**: more usable systems and a greater user's acceptance can permit a wider diffusion of biometric systems. In the literature, there are studies on the usability of biometric systems [39] and techniques for the evaluation of the user's acceptance [40]. The use of less-cooperative contactless acquisition techniques can improve these aspects of biometric systems.

- **Increasing of the distances from the sensors**: biometric techniques based on samples captured at a greater distance with respect to the traditional systems can permit to reduce the acquisition time and to develop new biometric applications. As an example, the system described in [114] is based on iris images captured at a distance of three meters between the user and the sensor, and is designed to work in biometric portals.

- **Use of three-dimensional samples**: three-dimensional models of biometric traits do not present distortions due to the mapping of three-dimensional objects into a two-dimensional space. Moreover, they can increase the accuracy of traditional biometric techniques because they permit to use the additional information related to the z axis during the feature extraction and matching steps. In the literature, most of the studies on the use of three-dimensional samples are related to the face trait [115].

- **Security and privacy**: the protection of all the components of biometric systems and user's data are important factors for a wider diffusion of biometric technologies. As reported in Section 2.5, the existing techniques can reduce the performance of biometric systems in terms of accuracy and speed. Studies in the literature aim to overcome this limitation and to design more secure techniques.

- **Study of new biometric traits**: novel traits should permit the use of biometrics in new applicative contexts. For example, recent studies regard the ECG signals [116].

The main focus of this thesis is on less-constrained biometric systems and techniques for the privacy protection. The term less-constrained includes techniques that permit to increase the usability and user's acceptance, increase the distances from the sensors, and reduce the cooperation level needed during the biometric acquisitions.

2.7 Summary

Traditional techniques for the recognition of the individuals are based on surrogate representations of the identities, such as passwords, keys, tokens, and identity cards. In many situations, these representations cannot guarantee a sufficient level of security because they can be shared, misplaced or stolen. Biometric recognition systems, instead, are based on physiological or behavioral characteristics of the individuals, which are univocally related to their owner, cannot be shared or misplaced, and are more difficult to be stolen. Examples of physiological biometric traits are the face, fingerprint, iris, hand geometry, palmprint, and ear. Examples of behavioral characteristics are the voice, signature, gait, and keystroke. In the literature, there are also studies on recognition techniques based on less distinctive characteristics, called soft biometric traits. These characteristics can be used to increase the accuracy of existing biometric systems, or to perform recognitions in covert and uncooperative manners. Examples of soft biometric traits are the height, weight, gender, and race.

Biometric systems can perform the identity recognition in two different manners: verification, and identification. The verification compares the acquired biometric data with the stored information associated to the claimed identity. The identification establishes a person's identity by comparing the acquired biometric data with the information related to a set of individuals. Both verification and identification systems are based on common components: a biometric sensor, feature extractor, database, matcher, and decision module.

The use of biometric systems is continuously increasing in different applicative scenarios. Typical applicative scenarios are: physical access control, government applications, forensic applications, and logical access control to data, networks and services. The most used biometric trait is the fingerprint since fingerprint recognition systems are characterized by low costs and good performances in terms of accuracy and speed. Face recognition systems are also diffused because they have a greater user acceptance. Iris recognition systems are considered as the fastest and most accurate biometric techniques, but are based on complex acquisition procedures. For these reasons, they are principally used in high security applications, like border controls and airports. Other diffused biometric technologies are based on the hand characteristics or behavioral traits.

The choice of the most suitable biometric technology is strictly related to the applicative context and should be based on accurate analyses. The evaluation of a biometric system, in fact, is a complex and multidisciplinary task, which should be done considering different perspectives related to the recognition technique and applicative scenario. Some important aspects that should be considered are: accuracy, speed, cost, scalability, interoperability, social acceptance, usability, security, privacy. The system accuracy is usually one of the most important aspects that should be considered during the design of a biometric application and should be evaluated by using specific techniques and figures of merit. The obtained results, however, are related to limited sets of data. For this reason, it is a common practice to estimate the confidence of the obtained accuracy indexes.

Other important characteristics that should be evaluated are related to privacy and security aspects. Proper techniques for the privacy and security protection, in fact, should be adopted in order to prevent thefts and misuses of biometric data. In the literature, there are methods designed for the protection of all the modules of biometric systems from external attacks. The privacy protection strategies, anyway, should also consider other risk factors. Real privacy risks are usually different to the ones perceived by the users and are related to technological and applicative factors. For this reason, the design of privacy-protective biometric systems should consider appropriate guidelines. Another useful technique for the privacy protection is the use of methods for the protection of the biometric templates. In the literature, most of the biometric template protection methods are based on two classes of techniques: cancelable biometrics, and biometric cryptosystems. Recent researches also propose other approaches based on cryptographically secure methods. The privacy protection methods in the literature, however, can reduce the performances of biometric systems in terms of accuracy and computational time. In order to overcome this limitation, researchers are studying new privacy protection techniques.

Other important research trends are: the increasingof the accuracy of the existing techniques, study new biometric traits, design multimodal and multibiometric systems, reduction of the hardware costs, increasing of the usability and acceptability of biometric technologies, increasing of the distance between the user and the sensor, design of less-constrained acquisition techniques, and implementation of recognition techniques based on three-dimensional samples.

Chapter 3

Contactless and Less-Constrained Biometrics

In order to contextualize the research on less-constrained fingerprint recognition systems, this chapter presents a brief overview on recent studies regarding less-constrained technologies based on different biometric traits.

Studies on biometric technologies based on traits traditionally captured using CCD cameras (e.g. face, iris, gait, ear, and soft biometric traits) and researches on traits traditionally acquired with contact-based sensors (e.g. fingerprint and hand-characteristics) have different objectives. The goal of the studies on traits traditionally captured by contactless techniques is to design biometric systems able to work in covert applications, using samples captured in uncooperative scenarios, at a great distance, and in uncontrolled light conditions. Differently, the research on traits traditionally captured using contact-based sensors aims to perform accurate biometric recognitions using contactless acquisition procedures and without the need of guides for the placement of the interested body parts. These techniques, anyway, are the most diffused in the literature and can usually obtain a greater accuracy with respect to less-constrained biometric systems based on traits traditionally captured using CCD cameras.

3.1 Less-constrained biometric systems

Most of the biometric systems require performing the acquisition process in a highly controlled manner. In these constrained applications, the users take deliberate actions to cooperate with the system. Many systems, for example, require that the users touch a surface, take a defined pose, and stay still during the acquisition procedure.

In order to increase the usability and user acceptance of the recognition systems, researchers are studying techniques for the reduction of the constraints needed by the biometric acquisition procedures. Less-constrained technologies can also permit the use of biometrics in new applicative scenarios, like in mobile phones and surveillance applications.

The studies on less-constrained biometric systems are based on different biometric traits, and their principal goals are:

- the increasing of the distance between the user and the sensor;
- the reduction of the required level of user cooperation;
- the design of recognition methods able to work in uncontrolled light conditions;
- the design of highly usable adaptive acquisition systems;
- the design of preprocessing methods for the noise reduction and enhancement of data captured in less-constrained conditions;
- the development of new feature extraction and matching algorithms specifically designed to obtain accurate results with data captured in less-constrained conditions;
- the design of methods that permit to obtain data compatible with existing biometric technologies from samples captured in less-constrained applications.

Some studies on less-constrained biometric techniques are based on methods for the computation and processing of three-dimensional models, which can permit to obtain more information and less-distorted data with respect to two-dimensional acquisition techniques.

Many researches on less-constrained biometric systems are related to traits traditionally captured using CCD cameras (e.g. face and iris). These traits, in fact, are more

adapt to be used in uncooperative applications than traits that are usually captured by contact-based sensors (e.g. the fingerprint and hand characteristics). The goal of these studies is to use cameras placed at long distances to perform uncooperative recognitions. In many situations, however, the accuracy of less-constrained recognition systems based on traits traditionally captured by CCD cameras can be insufficient. Less-constrained face recognition systems, in fact, suffer from problems due to different light conditions, pose, and aging. Systems based on iris images captured in less-constrained scenarios present problems due to the low visibility of the distinctive pattern, reflections, occlusions, and gaze deviation. There are also researches regarding other biometric traits, like the gait and ear characteristics. Other studies aim to increase the recognition accuracy using soft biometric traits, which can also be adopted to perform continuous authentications and periodic re-authentications.

Biometric systems that use contact-based acquisition sensors are the most diffused in the literature. In order to reduce the constraints of the acquisition process, the main goal is to design contactless recognition techniques able to process images captured using CCD cameras. These traits do not permit to design completely unconstrained systems because the users should show their body parts to the acquisition sensors. However, they are characterized by a high distinctivity and can obtain accurate performance.

In this chapter, a brief literature review regarding less-constrained biometric systems based on traits captured by CCD cameras (face, iris, gait, ear, and soft biometric traits) is first proposed (Section 3.2). Finally, Section 3.3 presents contactless techniques designed for the analysis of biometric characteristics of the hand.

3.2 Contactless biometric traits

Biometric traits that are traditionally captured using contactless sensors are suitable to be used in uncooperative recognition systems. In the literature, there are many studies regarding the reduction of constraints in these systems. Two of the most researched technologies consist in less-constrained biometric systems based on the face and iris.

Biometric systems based on the face trait are characterized by high user acceptance and are based on CCD cameras that can be placed at long distances. For these reasons, many studies on less-constrained biometric technologies are based on this trait. Face

recognition systems, however, cannot provide sufficient accuracy in high security applications. Differently, the iris is usually considered as the most accurate biometric trait and can be captured using contactless techniques based on CCD cameras. The use of the iris in less constrained biometric applications, however, present problems due to the low visibility of the distinctive pattern, reflections, occlusions, and gaze deviation.

Other recent researches regard the gait and ear traits.

Recent studies also propose the use of soft biometric traits in order to increase the accuracy of less-constrained biometric applications. Moreover, soft-biometrics can be used to perform continuous authentications and periodical re-authentications.

3.2.1 Less-constrained face recognition

Traditional face recognition systems obtain satisfactory results under controlled conditions. Specifically, the used samples consist in face images captured by a frontal camera in controlled light conditions. Moreover, the users have to be cooperative to obtain good quality acquisitions. In order to overcome these limitations, researchers have recently started to investigate face recognition under unconstrained conditions.

The reduction of constraints can also permit to increase the number of possible applicative contexts of biometric technologies based on the face trait. Traditional biometric techniques, in fact, are usually adopted in security applications (like the access control to buildings, airports, border checkpoints, computer authentication, biometric documents). Less-constrained biometric techniques based on the face trait can also be used in new scenarios.

- Surveillance applications: biometric recognitions are performed from frame sequences captured by surveillance cameras, without the subjects' knowledge, and in uncontrolled scenarios. The used images present many non-idealities, such as, low resolution, shadows, reflections, occlusions, and pose and expression variations. Recent studies report encouraging results [113] and show that biometric recognitions can be performed at a distance of more than 15 m [117].

- Mobile devices: face recognition techniques can be integrated in mobile devices like mobile phones [118] . This kind of applications needs the use of fast algorithms robust to the noise.

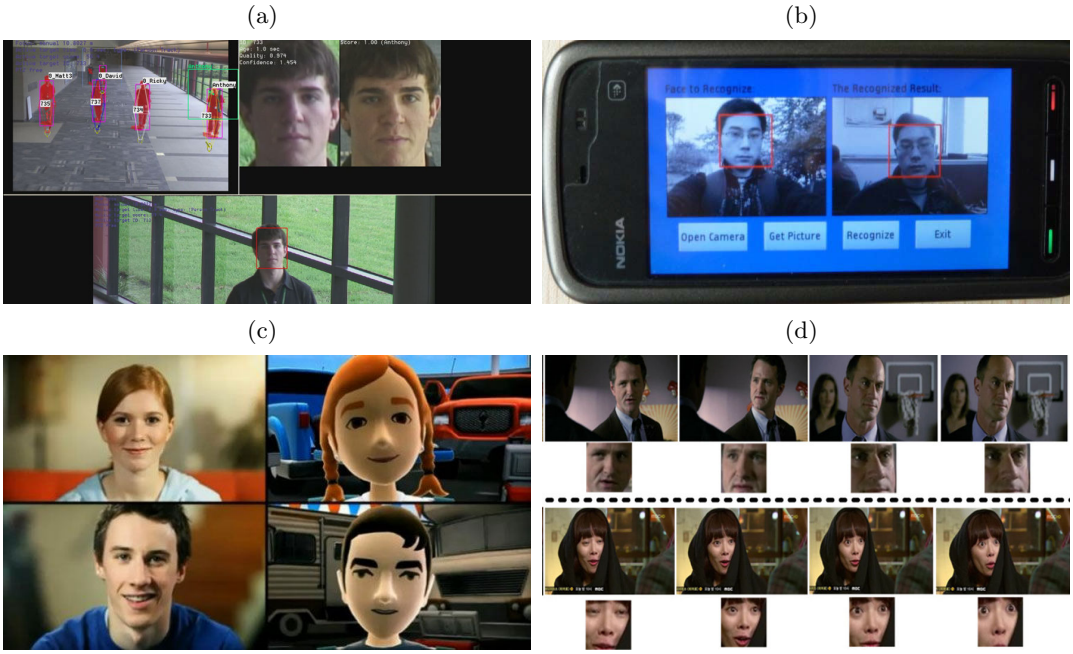

Figure 3.1: Examples of less-constrained face recognition applications: (a) surveillance [113]; (b) mobile phones [118]; (c) video games [120]; (d) video indexing [121].

- Multi-media environments with adaptive human-computer interfaces: the use of less-constrained acquisition techniques can permit to design new multi-media environments (e.g. behavior monitoring at childcare or care homes, and video games) [119, 120].

- Video indexing: biometric techniques are used to label faces in frame sequences captured in different environments and light conditions [121].

Fig. 3.1 shows examples of face recognition techniques applied in surveillance applications (Fig. 3.1a), mobile phones (Fig. 3.1 b), video games (Fig. 3.1 c), and video indexing (Fig. 3.1 d).

Less constrained face recognition systems, however, should overcome different non-idealities of the captured samples. As reported in [122], important aspects that have to be considered in the design of less-constrained face recognition systems are variations of the light conditions, pose, and aging.

- Illumination: in the literature, there are different techniques used to compensate illumination variations, which can be grouped in three principal classes: subspace

methods, reflectance-model methods, and methods based on three-dimensional models. Subspaces methods are very used in the literature and are able to capture the generic face space and thus recognize new samples not present in the training sets. There are studies on the robustness improvement of traditional subspace methods to variations under different light conditions. The work presented in [123], for example, reports that the Eigenface method is more robust to different illuminations if the first three eigenvectors are not considered. The second class of methods employs a Lambertian reflectance model with a varying albedo field. An example of reflectance-model methods is reported in [124]. Methods based on three-dimensional models are usually more robust to illumination variations, but require more complex data and algorithms. Examples of these methods are the Eigenhead [125], and the morphable model approach [126].

- Pose: traditional biometric systems can obtain poor results on face images captured with uncontrolled poses. For this reason, it is necessary to compensate the pose differences using dedicated methods. The pose compensation can be considered as a correspondence problem, because it aims to estimate the face position in the three-dimensional space [122]. In the literature, there are different methods for the compensation of pose variations in face recognition systems. Many methods aim to recover the face three-dimensional shape from two-dimensional images [122]. A literature review is proposed in [127].

- Aging: the aging effect is particularly important in unconstrained recognition systems that require long-time enrollments, like surveillance, investigative, and forensic applications. In the literature, there are different techniques for the aging compensation. Many methods simulate the aging effects [128], and other techniques use matching strategies specifically designed to be robust to age variations [129].

Some less-constrained face recognition systems in the literature use frame sequences and multiple views in order to increase the accuracy by evaluating the information related to the temporal continuity [130] and three-dimensional shape [131].

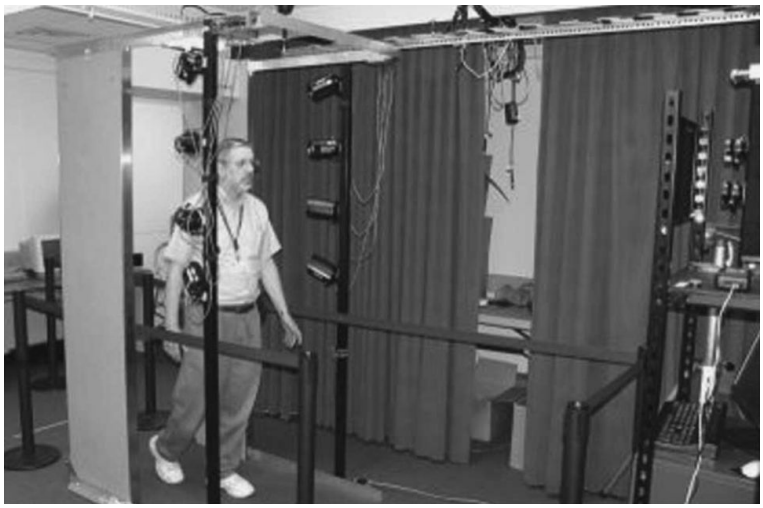

Figure 3.2: Example of iris recognition systems based on images captured at a distance on the move [132].

3.2.2 Less-constrained iris recognition

Iris recognition is considered as one of the most accurate biometric techniques. Iris recognition systems, however, are usually based on complex and expansive acquisition techniques. The acquisition process, indeed, has to deal with the fact that the iris region of the eye is a relatively small area, wet, and constantly in motion due to involuntary eye movements. Moreover, it can be occluded by eyelids, eyelashes, glasses, and reflections.

Most of the existing iris acquisition systems require that the users stay still watching a camera placed at a short distance from the eyes (usually less than 30 cm). The acquisition process is therefore time-consuming and can require some trials in order to obtain sufficient quality biometric samples. Moreover, the iris acquisition systems are usually based on near-infrared illumination techniques, which can be perceived as dangerous for the health. These aspects drastically influence the usability and user acceptance of iris recognition systems.

In order to overcome these problems, researchers are studying less-constrained iris recognition systems. The main goals are to increase the distance between the iris and the sensor, use images captured on the move, and use iris samples acquired in uncontrolled light conditions. An example of iris recognition systems based on images captured at a distance on the move is shown in Fig. 3.2.

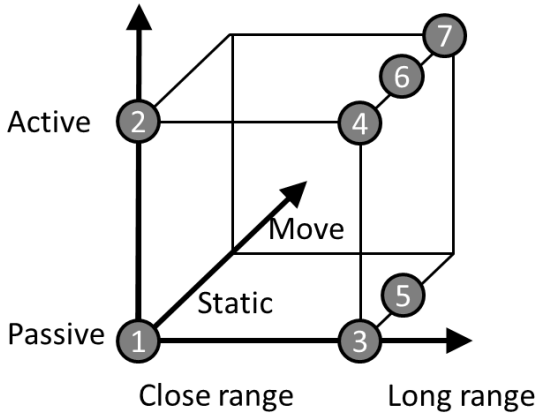

Figure 3.3: Classification of the less-constrained iris recognition systems [133].

In [133], iris recognition systems are classified in seven categories by considering three different characteristics: techniques used to search the iris region, distance between the eye and the sensor, required level of cooperation during the biometric acquisition. Fig. 3.3 shows a schema of the proposed classification.

1. Close-range iris recognition: this category of biometric systems is the most diffused in the literature. The eye has to be placed at a small distance from the camera, and the user has to stay still watching the camera during the acquisition process.

2. Active iris recognition: the iris images are captured at a small distance from the camera, but the user position is less constrained because active cameras reduce the required level of cooperation. The recognition systems, in fact, are able to automatically detect the iris position and align the camera with the iris. These systems usually capture a face image using a wide-angle camera, estimate the iris coordinates, and then move the iris camera towards the iris region [134].

3. Iris recognition at a distance: these systems use passive cameras, but are able to capture the iris images at a long distance. The users have to be cooperative and stay still during the biometric acquisitions. A study on techniques to perform the iris recognition at a distance is described in [132].

4. Active iris recognition at a distance: this category of iris recognitions systems permits to reduce the level of cooperation needed to obtain good quality samples with respect to the iris recognition at a distance. The users, however, have to stay still in a fixed position. An example of these systems is proposed in [135].

5. Passive iris recognition on the move: in these systems, the iris images are captured on the move. The use of passive cameras, however, requires predefined walking paths. An example of these systems is the biometric portal described in [114], which is based on multiple passive cameras.

6. Active iris recognition on the move: active cameras can search the irises of people walking in a defined direction, reducing constraints and costs with respect to the passive iris recognition on the move. There are no examples of these systems in the literature.

7. Iris recognition for surveillance: active iris camera networks can capture samples from multiple individuals. The acquisition process is completely unconstrained. In a future, this kind of biometric systems should be used in a wide range of applicative contexts that require accurate identification techniques (e.g. investigative and governmental applications).

Important research topics in the design of less-constrained iris recognition systems are the segmentation algorithms, recognition techniques, and gaze assessment methods.

- Segmentation: the task that locate and separate the iris pattern in the input face/eye image is called segmentation [136]. This task is particularly critical for less-constrained recognition systems because the captured images can present more reflections and occlusions with respect to traditional iris samples. Moreover, the correct detection of the iris boundaries and the removal of the occlusions are directly related to the accuracy of the iris recognition system. In the literature, there are different methods specifically designed for the estimation of the iris boundaries in iris images captured using less constrained techniques. They can be based on computational intelligence techniques [137], active contours algorithms [138], or incremental approaches [27]. Reflections and occlusions are then searched using statistical approaches [136] or more complex techniques [139, 140].

- Recognition techniques: images captured in less-constrained conditions present a lower visibility of the ridge pattern with respect to images captured by traditional iris acquisition systems. For this reason, it is necessary to use dedicated techniques for the enhancement, feature extraction, and matching. The method proposed in [141], for example, is specifically designed for frame sequences captured by a biometric portal, and uses super-resolution techniques to enhance the visibility of the ridge pattern. Results obtained by different matching methods on images captured at a distance, on the move, and in natural light conditions are reported in [112].

- Gaze assessment: iris images can present problems related to the gaze deviation with respect to the camera. Off-axis images can drastically reduce the recognition accuracy because they can affect the performances of the segmentation and feature extraction algorithms. The effect of this non-ideality can be reduced by using methods for the gaze assessment [142] or acquisition setups based on multiple cameras [143].

3.2.3 Soft biometrics

Soft biometric recognition techniques, while featuring a lack of distinctiveness, can use samples captured in an unobtrusive and unconstrained way, in uncooperative conditions [16, 19, 30], or with surveillance cameras placed at long distances [19]. Such recognition systems can be employed where it is difficult to adopt systems based on hard biometric traits (e.g. surveillance applications), the pool of users is small enough, or high accuracy is not required.

Soft biometric traits can be used in different applicative contexts. The method described in [20] computes categorical information about the individuals (e.g. gender and race) in order to filter large surveillance databases by limiting the number of entries to be searched for each biometric query. The approach proposed in [144] uses characteristics extracted from the face and the clothes in order to perform continuous authentications. A method based on color and height characteristics for the detection of the individuals throughout a sparse multi-camera network is presented in [17]. The technique described in [19] uses three part (head, torso, legs) height and color soft biometric models in order to perform the recognition of the individuals. Techniques for

the extraction of characteristics related to the gait, height, size, and gender are presented in [145]. The method described in [18] is designed for working in unconstrained conditions and it is able to estimate the weight of walking individuals from surveillance frame sequences. This technique can be particularly useful in forensic analyses because the weight is one of the few characteristics that can be inferred from the evaluation of a scene.

3.2.4 Other biometric traits

Examples of other biometric traits suitable for unconstrained recognition applications are the gait and ear shape.

The gait characteristics are estimated from frame sequences captured by CCD cameras [14]. Gait recognition systems can obtain a satisfactory accuracy and can work at great distances [146]. The gait, however, is a behavioral biometric trait and gait recognition systems can therefore obtain less accuracy with respect to biometric systems based on physiological characteristics.

Biometric systems based on the ear shape are recent technologies [11]. In the literature, there are studies on less-constrained recognition systems based on the ear trait [147, 148]. Less-constrained ear recognition systems, however, are less accurate with respect to more mature biometric recognition technologies.

3.3 Contact-based biometric traits

The most used biometric traits traditionally captured with contact-based sensors are the fingerprint and hand characteristics. Systems based on the hand can have different accuracy levels and can be based on different distinctive characteristics, like the hand shape [8], palmprint [9], palmvein [10], and multiple traits [149].

Most of the hand biometric systems use acquisition sensors composed by a flat-surface and pegs that guide the placement of the user's hand. Recent studies regard techniques for the reduction of the constraints imposed by the acquisition technologies. Considering the used acquisition techniques, hand recognition approaches available in the literature can be divided into three categories [150].

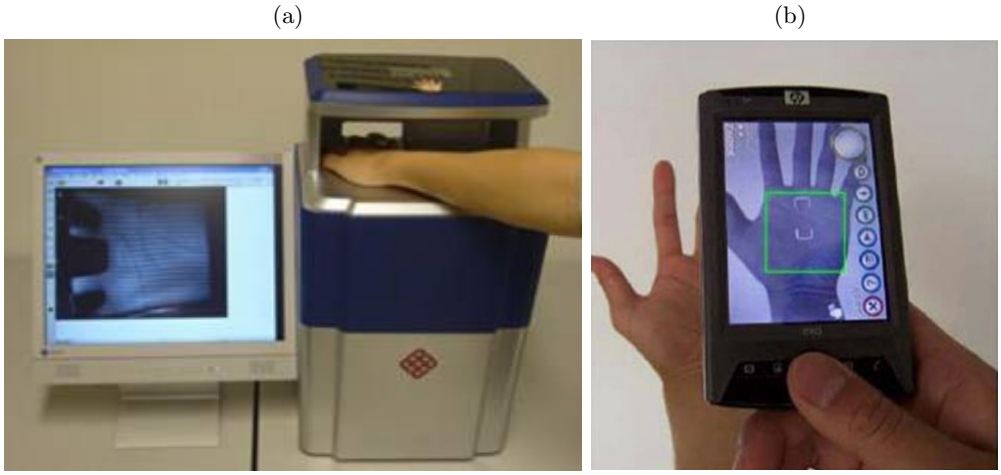

Figure 3.4: Examples of palmprint acquisition sensors: (a) constrained and contact-based system [158]; (b) unconstrained and contactless system [159].

- **Constrained and contact-based systems** use pegs or pins to constrain the position and posture of the hand.
- **Unconstrained and contact-based systems** do not use pegs and permit a less constrained placement of the hand on the acquisition sensor. They often require the users to place their hand on a flat surface [151] or a digital scanner [152]. These systems are characterized by more user acceptance with respect to constrained and contact-based systems. However, they require more complex strategies to perform the alignment of the samples [8].
- **Unconstrained and contactless systems** use CCD cameras to capture hand images. They do not require the contact of the hand on acquisition surfaces. Many systems in the literature are based on single images [153, 154], but there are also biometric systems that use three-dimensional models [150]. Most of the unconstrained and contactless systems are designed to work in controlled light and background conditions [155]. Other systems do not impose these constraints, using more complex segmentation strategies [156]. There are also studies on systems integrated in mobile devices [157].

Fig. 3.4 shows an example of constrained and contact-based system [158], and an unconstrained and contactless system [159].

3.4 Summary

The acquisition techniques traditionally adopted by biometric systems require that the users take deliberate actions to cooperate with the system, and impose constraints. Fingerprint recognition systems, for example, require that the users touch a surface, take a defined pose, and stay still during the acquisition procedure.

Researchers are studying techniques for the reduction of the acquisition constraints in biometrics systems based on the fingerprint and other biometric traits. The main goals of these studies are the increasing of the distance between the users and the system, design of recognition techniques able to work in uncontrolled light conditions, increasing of the usability and user acceptance of the systems, design of feature extraction and matching techniques robust to the noise, and implementation of techniques that guarantee the compatibility of the templates computed by less constrained systems with the existing biometric databases.

Biometric characteristics that are traditionally acquired using contactless techniques (e.g. face, iris, gait, ear, and soft biometric traits) are more suitable to be used in uncooperative applications with respect to traits traditionally captured with contact-based sensors (e.g. fingerprint and hand-characteristics). The main goal of the studies on less constrained biometric systems based on the first class of traits is the use of CCD cameras placed at long distances to perform uncooperative recognitions. Less-constrained face recognition systems can be applied in new applicative contexts, like surveillance applications, mobile devices, multimedia environments with adaptive human-computer interfaces, and video indexing. The design of less constrained face recognition techniques, however, has to consider important non-idealities, such as, uncontrolled illumination conditions, pose variations, and aging. Biometric systems based on the iris trait are typically more accurate than face recognition systems, but they are usually based on complex and expansive acquisition techniques. Recent studies in iris recognition systems aim to design techniques able to work on images capture at a long distance, on the move, and in uncontrolled light conditions. Important research topics in the design of less constrained iris recognition systems are the segmentation algorithms, recognition techniques, and gaze assessment methods. Other characteristics that can be acquired in unconstrained scenarios are soft biometric traits, which can also be used to perform

continuous authentications and periodic re-authentications. In the literature, there are also studies on less constrained biometric systems based on the gait and ear traits.

Biometric systems that traditionally use contact-based acquisition sensors are the most diffused in the literature and can obtain accurate results. Researchers are therefore studying less constrained recognition systems, with particular attentions to methods based on the hand characteristics. Considering the used acquisition techniques, hand recognition approaches available in the literature can be divided into three categories: constrained and contact-based systems, unconstrained and contact-based systems, unconstrained and contactless systems. The third category of methods performs acquisitions at a distance and can use two-dimensional or three-dimensional data.

Chapter 4

Fingerprint Biometrics

The fingerprint is one of the most used traits in biometric applications due to its high durability and distinctivity.

The analysis of fingerprint samples can be performed at three levels: global, thin, and ultra-thin. In the literature, there are many studies on techniques based on different analysis levels and designed to perform every step of the biometric recognition process. Usually, these steps are: acquisition, quality evaluation, enhancement, feature extraction, and matching. Other methods are proposed for the classification and indexing of fingerprint samples in identification applications, and for the computation of synthetic fingerprint images that can be used to design and test biometric algorithms.

Most of the fingerprint recognition systems use acquisition sensors that require the contact of the finger with a platen. These systems, however, suffer of problems due to the contact of the finger with the sensor surface (e.g. distortions in the captured images and latent fingerprints left on the sensor platen). In order to overcome these problems and to increase the user acceptability of the biometric recognition process, contactless recognition systems are researched. These systems are based on CCD cameras and can be divided into systems based on two-dimensional samples and systems based on three-dimensional samples. Most of these systems aim to guarantee the compatibility with the existing AFIS.

4.1 Fingerprint recognition

Among the possible biometric traits, the fingerprint is the most well-known and widely used physiological characteristic in recognition applications. Its use in police investigation can be traced back to the late 19th century, and the first automatic fingerprint recognition system was introduced in the '70s [160].

Fingerprint recognition systems are based on the analysis of the impression left by the friction ridges of the human finger. The evaluation of the ridge details can be performed with three levels of accuracy.

- Level 1: the overall global ridge flow pattern is considered.
- Level 2: the analysis is based on distinctive points of the ridges, called minutiae points.
- Level 3: ultra-thin details, such as pores and local peculiarities of the ridge edges, are studied.

These analysis levels can be used in different modules of biometric recognition systems. For example, Level 1 characteristics can be used to perform preliminary tasks like the quality evaluation of biometric samples and the enhancement of the ridge pattern visibility. More detailed analysis can then be used to perform identity comparisons.

In most of the cases, the acquisition of fingerprint samples is performed using contact-based techniques. These techniques can be based on different technologies and can be used in live recognition systems or in forensic analyses.

In general, fingerprint recognition systems can be divided into different modules: acquisition, quality evaluation, enhancement, feature extraction, and matching. Moreover, in identification systems, classification and indexing techniques can be used to reduce the number of identity comparisons performed for each biometric query. In the literature, there are many methods specifically designed for each step of the recognition process based on fingerprint images captured using contact-based techniques. There are also algorithms for the computation of synthetic fingerprint images, which can be used to reduce the efforts necessary to capture biometric samples during the design of recognition systems.

Contact-based fingerprint recognition systems can obtain a remarkable accuracy, but suffer of important problems, such as filth on the acquisition surface, distortions

in the captured images due to elastic skin deformations, and the possibility to obtain latent fingerprints from the surface of the sensors. Recent studies aim to overcome these problems by using contactless acquisition techniques. Contactless fingerprint recognition systems can be divided into two classes: systems based on two-dimensional samples, and systems based on three-dimensional samples. The first class of biometric systems usually captures single fingerprint images with CCD cameras. Systems based on three-dimensional models require more complex hardware setups, but can provide a greater accuracy.

In this chapter, the characteristics of the fingerprint biometric trait (Section 4.2) and its applicative contexts are first discussed (Section 4.3). The techniques designed for the analysis of fingerprint images at different levels are then treated in Section 4.4. Then, contact-based fingerprint recognition systems are reviewed (Section 4.5), considering the captured images, quality evaluation techniques, image enhancement algorithms, feature extraction and matching methods, classification and indexing approaches, and algorithms for the computation of synthetic fingerprint images. Section 4.6.1 presents a description of the recognition techniques based on contactless two-dimensional fingerprint samples. Finally, Section 4.6.2 analyzes the three-dimensional reconstruction techniques and recognition methods used by biometric systems based on contactless three-dimensional samples.

4.2 Characteristics of the fingerprint

The fingerprint is considered as one of the biometric traits with the higher durability [161]. The fingertip ridge structure, in fact, is fully formed at about the seventh month of the fetus development, and this pattern configuration does not change for all the life unless serious accidents or diseases [162]. Usually, cuts and bruises can only temporarily modify the fingerprint pattern. This property makes the fingerprint an attractive biometric trait, especially for applicative contexts that require long-term enrollments.

Another important propriety of the fingerprint is the uniqueness. In general, fingerprints are a part of an individual's phenotype and are different for each individual. Also the fingerprints of the same person are different, and even in the case of identical twins, the fingerprints are not equal [163, 164]. As an example, Fig. 4.1 shows four fingerprints acquired from two identical twins.

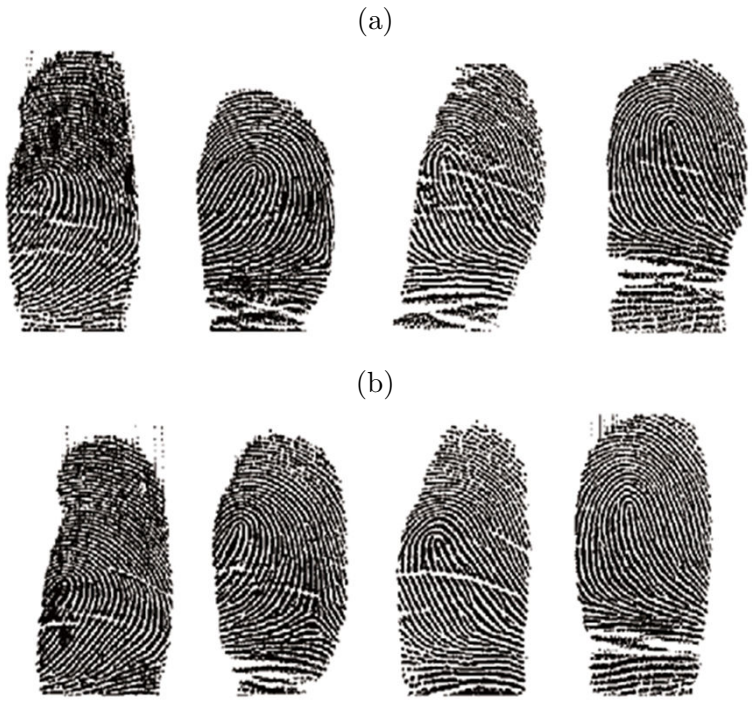

Figure 4.1: Examples of fingerprints appertaining to two identical twins: twins [164]: (a) individual A; (b) individual B. All the samples present differences in the ridge pattern.

However, the uniqueness is not an established fact but an empirical observation [3]. In the literature, there are studies on the amount of distinctive information of the fingerprint pattern. The work presented in [165] reports that the distinctiveness is proportional to the number of minutiae in the considered image, which is related to the size of the available fingerprint portion. Other studies compare the distinctiveness of different features extracted from the fingerprint pattern. For example, the work exposed in [166] compares Level 1, Level 2, and Level 3 features. The estimation of the fingerprint distinctiveness, however, is an open problem and is particularly important in legislative and forensic applications [167].

4.3 Applications

The fingerprint trait is the most used and known biometric characteristic [23].

The applications of fingerprint recognition technologies are heterogeneous and range from the public to the private sector. In the market, there are available fingerprint recognition systems with great differences in sizes of the sensors, costs, and accuracy [168]. For example, there are systems integrated in electronic devices (e.g., PDA and mobile phones [169]), on-card systems [170], systems based on a single personal computer, and large distributed systems, such as AFIS [24].

The main applicative contexts of fingerprint recognition systems are in forensics, governmental, and commercial sectors [3]. In the forensic sector, the fingerprint trait is used for the identification, search of lost persons, and general investigative activities. In the governmental sector, important applications are the border control and biometric documents (for example passports and IDs). Examples of applications in the commercial sector are authentication systems integrated in ATMs, terminal login, access control for on-line services (e.g. e-commerce and e-banking applications), protection of sensible data (e.g. in personal computers, PDA, mobile phones, and storage devices), and access control to restricted areas.

Fig. 4.2 shows some examples of applications based on the fingerprint trait.

4.4 Analysis of fingerprint samples

This section presents techniques in the literature for the analysis of contact-based and contactless fingerprint images.

4.4.1 Level 1 analysis

Techniques for the Level 1 analysis of fingerprint images evaluate the overall ridge flow. Examples of characteristics analyzed at Level 1 are the ridge orientation, local ridge frequency, singular regions, and ridge count.

The local ridge orientation is estimated as the angle of the ridges with respect to the horizontal axis. Usually, the orientation angle is considered as an unoriented direction lying in $[0^\circ \dots 180^\circ]$. The ridge orientation map can be computed by estimating the local ride orientation in areas centered in each pixel of the fingerprint image or by

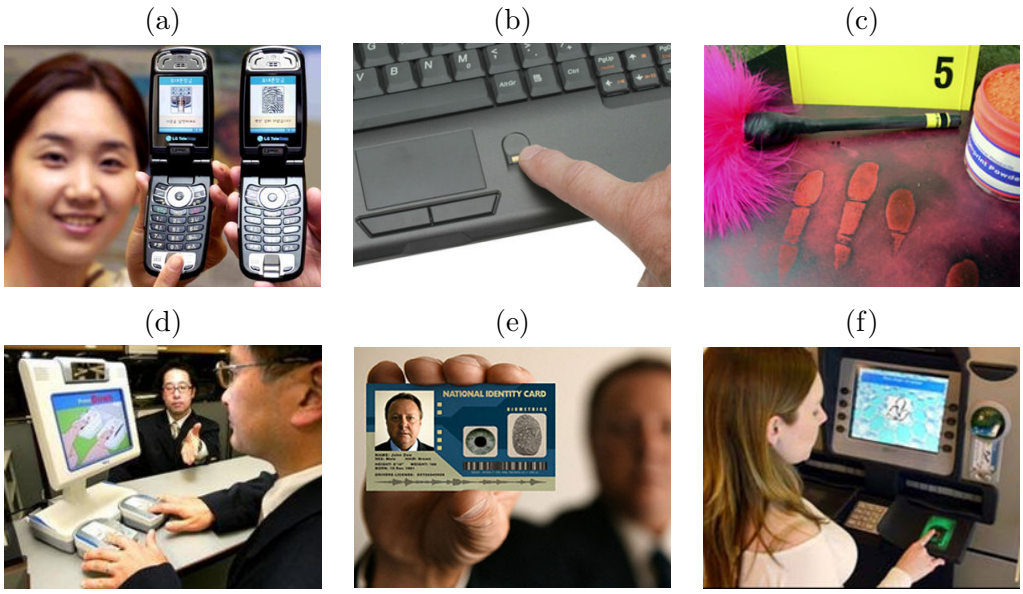

Figure 4.2: Examples of applications based on the fingerprint trait: (a) mobile phone; (b) laptop; (c) forensic analysis; (d) border control; (e) biometric document; (f) ATM.

using techniques based on global orientation models. Fig. 4.3 shows an example of ridge orientation map. In the literature, most of the methods for the computation of the ridge orientation are based on local analysis techniques [171]. These techniques are usually adopted by fingerprint enhancement methods. One of the most known local analysis technique is based on the evaluation of the gradient orientation in squared regions. For each local region, the ridge orientation is considered as the mean of the angular values of the pixels. This technique was first introduced in [172]. One of the main problems of this technique consists in the difficulty to perform robust means of the angular values. There are methods based on the gradient analysis that use different algorithms for the computation of the mean angle [173, 174]. Other local techniques are based on slit-based approaches [175], or on the frequency analysis of local regions of the fingerprint image [176, 177]. In the literature, there are also orientation regularization techniques designed to reduce artifacts due to the presence of noise or poor quality image regions [178, 179]. Global approaches are usually adopted during the enhancement of latent fingerprints or for the computation of synthetic fingerprint images. The method described in [180] is based on a mathematical model that estimates the local ridge orientation by considering the coordinates of core and delta points.

Figure 4.3: Example of ridge orientation map.

The local ridge frequency is the number of ridges per unit length along a segment orthogonal to the ridge orientation. Many methods in the literature assume that the ridge frequency of a fingerprint image can be represented using a single value. Other methods compute a ridge frequency map, which represents the local ridge frequency computed in each pixel of the fingerprint image. One of the most used algorithms in the literature designed for the estimation of the ridge frequency map is based on the computation of local oriented x-signatures [181]. This algorithm divides the image in local windows centered in every pixel, with fixed size, and orientation computed according to the ridge orientation map. The x-signature of every window is then obtained as a vector containing a cumulative function of the intensity values computed for each column x. The frequency if finally estimated as the inverse of the average distance between consecutive peaks of the image obtained by computing the x-signature. In the literature, other algorithms based on the concept of x-signature have been proposed in order to reduce the sensibility to the noise of the method [182, 183]. There are also methods for the estimation of the ridge frequency based on different techniques, for example, the Short Time Fourier Transform (STFT) [177] and the analysis of local curve regions [184].

Another important Level 1 analysis consists in the estimation of the singular regions. A singular region represents a portion of the finger pattern with a distinctive shape of

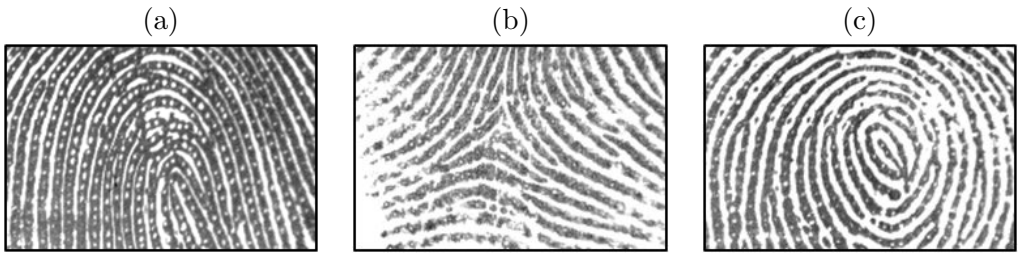

Figure 4.4: Examples of singular regions: (a) loop; (b) delta; (c) whorl.

the ridges. Commonly, three types of singular regions are considered: loop, delta, and whorl. The distinctive shapes of these regions are $\cap$, Δ, and O, respectively (Fig. 4.4). In the literature, the majority of the methods for the estimation of the singular regions use the Poincaré technique [185]. This technique computes the Poincaré index for each point of a ridge orientation map. This index represents the total rotation along the considered pixel. The value of the Poincaré index indicates the presence of a singular region: the value 180 corresponds to a loop, -180 represents a delta, and 360 is related to a whorl. The schema of this technique is shown in Fig. 4.5. Other methods are based on the analysis of the ridge orientation map, but use different analysis techniques. For example, the method proposed in [186] estimates the orientation of the ridges by an algorithm based on the Zero-Pole Model, and the method described in [187] is based on the analysis of the topological structure of the fingerprint image.

Many fingerprint recognition systems compare the sample images using a specific reference point called core point. This point is usually estimated by using Level 1 analysis techniques. A simple technique consists in the selection of the northern loop [3]. Many methods in the literature, anyway, use more complex techniques based on the search of singular regions [188]. Other methods use different strategies based on the analysis of the ridge orientation. In [189], the core is considered as the point in the middle of two center of gravity points obtained by computing the local axial symmetry of the image. In [190], the directional map of the ridges is quantized in four binary images related to the cardinal points. The reference point is then obtained by applying a set of rules and morphological operators. The method described in [191] is designed for fingerprint images that do not present singular regions. The local orientation of the ridges is computed, and the radial symmetry line is then estimated. The core consists in the point with the maximum value in the radial symmetry line.

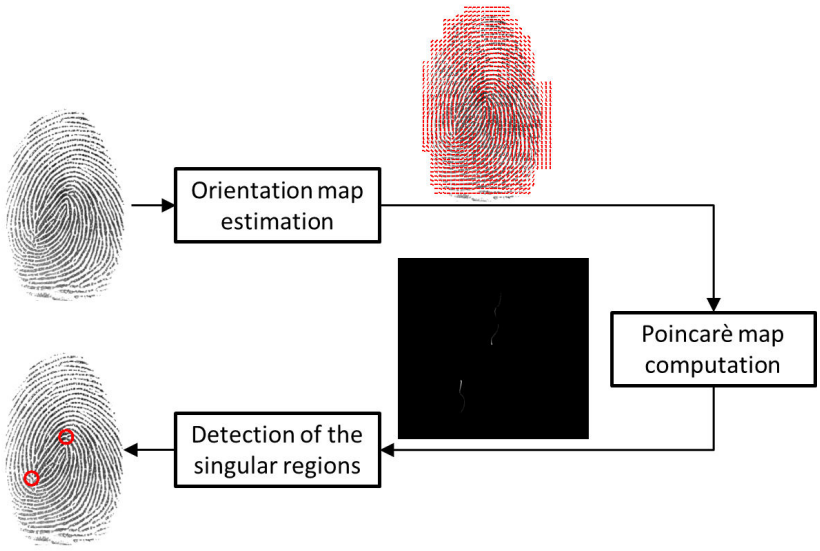

Figure 4.5: Schema of the Poincaré technique for the detection of singular regions in fingerprint images.

Other examples of Level 1 characteristics are the ridge count [192] and the global mapping information obtained by the application of Gabor filters to the input fingerprint images [193]. The ridge count is an abstract measurement of the distances between any two points in a fingerprint image. This characteristic is frequently used in forensic analyses performed by human operators. A typical measure performed by forensic experts, in fact, is the number of ridges between two singular regions. Differently, Gabor filters are used to extract the information related to the ridge frequency and orientation in local regions of the fingerprint images.

4.4.2 Level 2 analysis

Level 2 analysis methods evaluate specific ridge discontinuities called minutiae. It is possible to distinguish different classes of minutiae (Fig. 4.6), but most of the automatic biometric systems in the literature consider only terminations and bifurcations.

In the literature, there are many studies on techniques for the extraction of the minutia points [194]. These methods can be based on the computation of binary images of the ridge pattern or perform the minutiae extraction directly in gray-scale images. Moreover, the methods based on the computation of binary images can require the

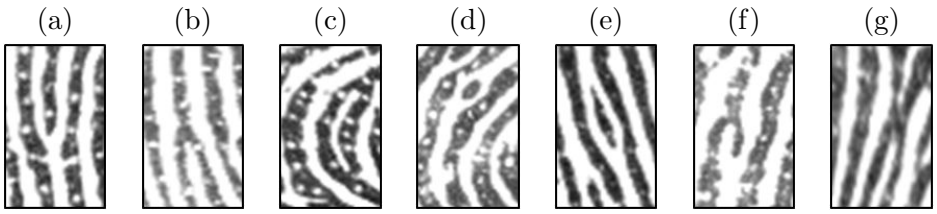

Figure 4.6: Examples of minutiae types: (a) termination; (b) bifurcation; (c) lake; (d) point or island; (d) independent ridge; (f) spur; (g) crossover.

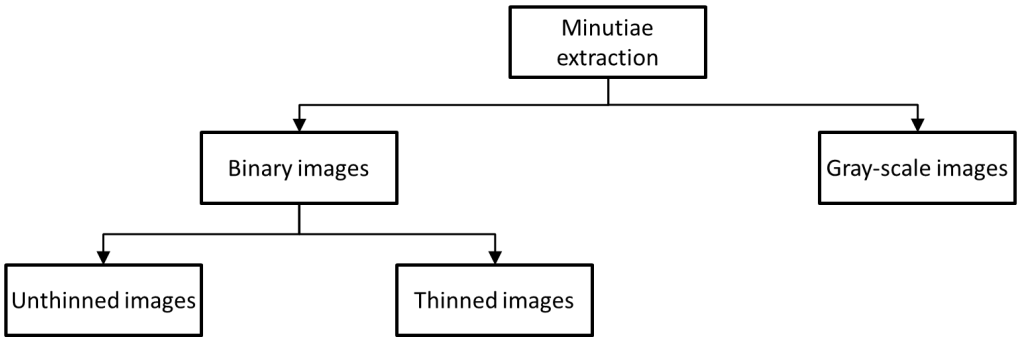

Figure 4.7: Classification of the minutiae extraction techniques.

processing of thinned images representing the skeleton of the ridges, or directly search the minutiae in the binary images. Fig. 4.7 shows a classification of the methods in the literature for the minutiae extraction [194].

The most diffused techniques extract the minutia points from thinned images. These techniques can be divided into four main steps [3]:

1. an adaptive binarization is applied in order to separate the ridges from the background of the fingerprint image;

2. a thinning operation is achieved in order to reduce the thickness of the ridges to one single pixel;

3. the coordinates of the minutiae are estimated by observing the specific local pattern of each single pixel of the ridges, typically in its 8-neighborhood;

4. a post-processing method is applied in order to reduce the number of false minutiae detected in the previous step.

Fig. 4.8 shows the schema of the described method.

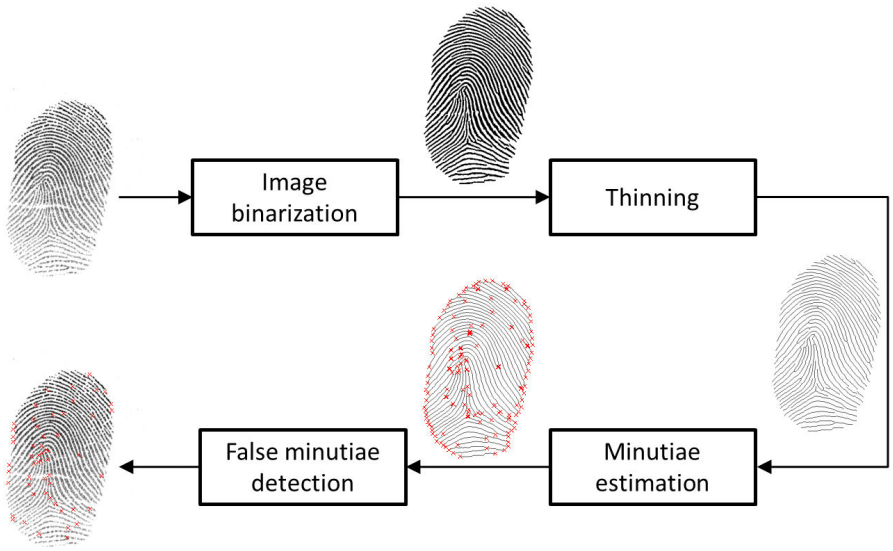

Figure 4.8: Schema of the most diffused minutiae extraction methods.

In the literature, there are many techniques designed for the binarization of fingerprint images. The simplest technique consists in the use of a global threshold [195]. The obtained results, however, can present artifacts and noisy regions due to different pressures of the finger to the sensor. Another simple technique used by the "FBI minutiae reader" is based on a local thresholding approach and on an algorithm that compares the pixel alignment along eight discrete directions [196]. Other techniques are based on different approaches, for example, fuzzy logic [197], directional filters tuned according to the ridge frequency [198], and iterative algorithms that follows the shape of the ridges [199].

The second step is the computation of the ridge skeleton. One of the most used techniques for the thinning of binary images representing the ridge pattern is based on morphological operators [195]. In order to limit problems due to artifacts introduced by morphological operators, there are techniques specifically designed for the analysis of the ridge skeleton and the removal of false ridges [200]. Other techniques are based on different approaches. For example, the one described in [201] uses pulse-coupled neural networks, and the algorithm presented in [202] is based on the analysis of the ridge orientation.

The coordinates of the minutia points are then estimated. A well-known algorithm for the detection of minutia points in thinned fingerprint images is based on the computation of the crossing number [203]. This value is computed by evaluating every pixel n_k in the 8-neighoboring of every point p:

$$CN(p) = \frac{1}{2}\sum_{k=1}^{8} \left| n_k - n_{((k+1) \mod 8)} \right|, \tag{4.1}$$

where $n_k \in \{0, 1\}$. Terminations are characterized by a crossing number $CN(p) = 1$, and bifurcations have a value $CN(p) = 3$. Other methods search the coordinates of the minutia points in thinned images by using different algorithms, like morphological operators [204].

The final step is the refinement of the obtained results, performed in order to remove the false minutiae. In the literature, there are techniques based on the analysis of the thinned fingerprint images and techniques that evaluate the shape of the ridges in gray-scale images. The first class of methods searches local patterns that describe false minutiae introduced by the thinning step [199, 205]. The methods based on the evaluation of gray scale images extract a set of features for each minutia point and then classify every minutia in valid or false. A method appertaining to this class and based on neural classifiers is proposed in [206].

In order to limit the presence of artifacts introduced by the thinning step, many algorithms search the minutia points in the binary image representing the ridge pattern without computing the ridge skeleton. The software NIST MINDTCT [199], for example, is based on the local search of all the binary patterns that define the presence of terminations and bifurcations. The method uses a set of 10 binary masks with size 3×2 pixel and scans the binary fingerprint image in the vertical and horizontal directions. Another method based on the local analysis of the ridge pattern is presented in [207] and is based on the evaluation of the intensity along squared paths of the image. There are also methods that use run-based algorithms [208], which search the minutiae by analyzing the graphs obtained by computing the horizontal and vertical run-length encoding of the binary fingerprint image. Another technique based on the analysis of binary images representing the ridge pattern searches the ridge by analyzing the chaincode obtained from the fingerprint image [209]. The chaincode is a reversible encoding technique for binary images. For each object in a binary image, the information related

to its boundary is stored in a vector. Starting from an initial position, the boundary is followed by a searching algorithm and the angles of the sequent pixels are stored. The minutiae are estimated by searching direction changes in the chaincode vectors.

In the literature, there are also approaches that search the coordinates of the minutiae points directly in gray-scale images. A well-known method based on a ridge-following technique is described in [210]. An iterative algorithm follows every ridge according to the angle described by the ridge orientation map. The algorithm stops when it detects a termination or a bifurcation. There are also variants of this method that consider the two valleys near to every ridge [211] or designed for low-cost hardware devices [212]. Other methods that search the minutiae in gray-scale images use different strategies. Neural network classifiers are used in [213], a local searching algorithm based on fuzzy logic is described in [214], and an approach based on the computation of the Linear Symmetry is proposed in [215].

Most of the techniques in the literature also estimate the orientation of the minutiae, which is usually considered as the value of the ridge orientation map in the minutia coordinates. Many techniques also estimate the correctness probability of every minutia as the local quality value of the fingerprint image [199].

4.4.3 Level 3 analysis

Level 3 analysis requires high-resolution acquisition devices (with at least 800 ppi [216]) and it is not commonly applied in commercial systems. Details that can be considered at this level of analysis are the pores, dots, and incipient ridges. Fig. 4.9 shows an example of Level 3 characteristics. Usually, the features extracted at this level of analysis by automatic algorithms consist in the spatial coordinates of the pores. Recent studies proved that the use of biometric recognition techniques based on Level 3 features can obtain a greater accuracy with respect to recognition techniques based on Level 1 and Level 2 features [217]. Level 3 features can also be used for the vitality detection during contact-based fingerprint acquisitions [218].

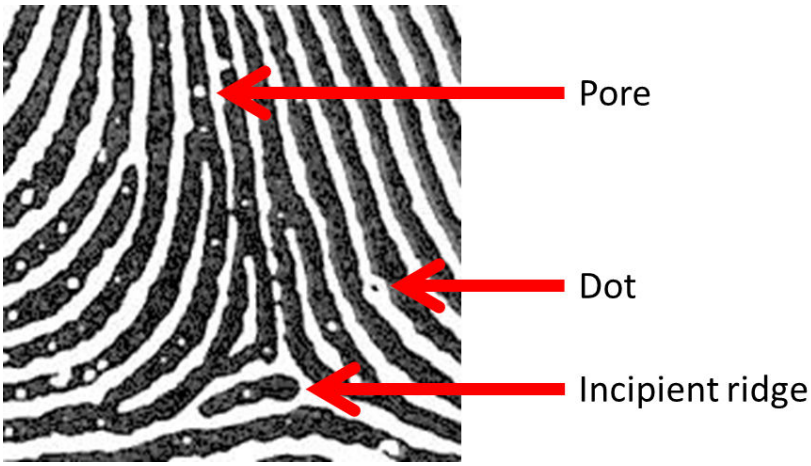

Figure 4.9: Example of fingerprint details considered in the analysis of Level 3 characteristics: pores, dots, and incipient ridges.

4.5 Contact-based fingerprint recognition

Biometric systems based on the fingerprint trait estimate the identity of an individual by extracting and comparing information related to the characteristics of the ridge pattern.

The schema of the biometric authentication process based on the fingerprint trait is shown in Fig. 4.10. The first step is the acquisition of the biometric sample. The sample consists in an image that can be captured using different kinds of sensors. In most of the fingerprint recognition systems, a quality evaluation of the captured image is then performed in order to discard samples with insufficient quality. Another step that is usually performed consists in the application of techniques for enhancing the visibility of the ridges. The next step is the feature extraction, which computes a biometric template from the captured fingerprint image. In the literature, there are recognition methods based on different characteristics of the ridge pattern. Then the matching step compares the obtained template with the stored data. The used algorithms are strictly dependent to the considered features. Finally, a decision is obtained by applying a threshold to the obtained matching score.

Moreover, many fingerprint recognition systems designed for the identification perform a classification or an indexing step in order to reduce the number of biometric queries.

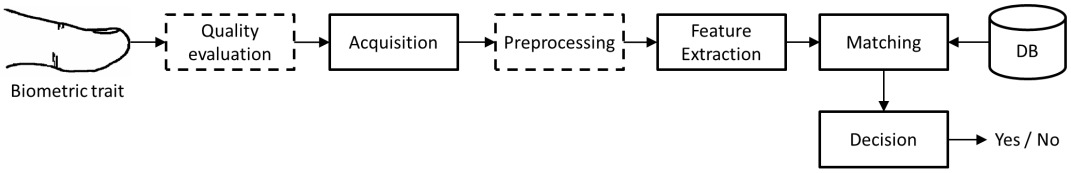

Figure 4.10: Schema of the biometric authentication process based on the fingerprint trait.

The design of fingerprint recognition systems requires the collection of large datasets of samples. This task is expensive and time consuming, and can also require the implementation of new hardware sensors. For this reason, there are methods in the literature specifically designed for the computation of realistic synthetic images, which can be used to test the envisioned methods and reduce the efforts necessary to collect a sufficient number of biometric samples.

This section proposes a literature review of the most important methods designed for the different steps of the biometric recognition process based on the fingerprint trait.

4.5.1 Acquisition and fingerprint images

Considering the used acquisition technique, it is possible to divide the obtained fingerprint images into three classes: latent fingerprints, inked fingerprints, and live-scan fingerprints. Fig. 4.11 shows an example of images obtained by the different fingerprint acquisition methods.

- **Latent** fingerprints are very important in forensics. This kind of fingerprints is produced by the transfer of the film of moisture and grease that is present on the finger surface when an object is touched. Usually, latent fingerprints are not visible to naked eye and forensic investigators use proper substances to enhance the visibility of the ridge pattern [219].

- **Inked** fingerprints are typically obtained with the following procedure. First, the user's finger is spread with black/blue ink and then rolled on a paper card; secondly the card is converted into a digital form by the means of a high-definition paper-scanner or by using a high-quality CCD camera [220].

- **Live-scan** fingerprints are obtained by impressing a finger on the acquisition surface of a device. There are sensors that can capture images of one or more

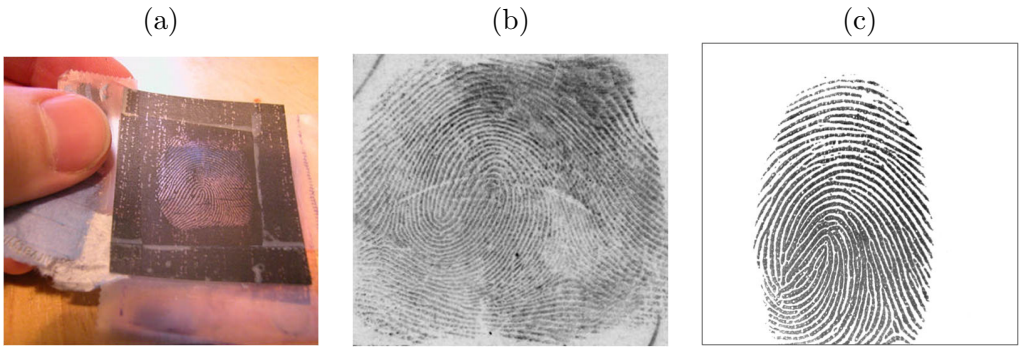

Figure 4.11: Examples of fingerprint images: (a) latent; (b) rolled and inked; (c) live-scan.

fingerprints. It is possible to distinguish two types of live-scan sensors: area scan sensors and swipe sensors [221]. The swipe sensors require that the user slides a finger vertically over the surface. These sensors are smaller and cheaper than the area scan sensors, but require previous user training and often fail to capture fingerprint samples. Examples of area scan sensors and swipe sensors are shown in Fig. 4.12. The first category of sensors permits to capture the fingerprint pattern in a single time instant. The sensors can be based on different technologies: optical, capacitive, thermal, piezoelectric, radio frequency, ultrasonic, microelectromechanical (MEMS), multispectral imaging [221].

Only good quality images have to be stored in order to achieve subsequently accurate biometric recognitions by automatic systems. For example, the Federal Bureau of Investigation (FBI) of the USA defined a set of main parameters characterizing the acquisition of a digital fingerprint image [222], which encompass the minimum resolution, minimum size of the captured area, minimum number of pixels, maximum geometry distortion of the acquisition device, minimum number of gray-levels, maximum gray-level uniformity, minimum spatial frequency response of the device, and minimum signal to noise ratio.

In many law enforcement and government applications that involve AFIS, the size of the fingerprint image database is typically very large. For example, the FBI fingerprint card archive contains over 200 million of identities [223]. In such cases, compressed formats are adopted to store the biometric samples. Most of the image compression algorithms in the literature obtain unsatisfactory results in the compression of fingerprint

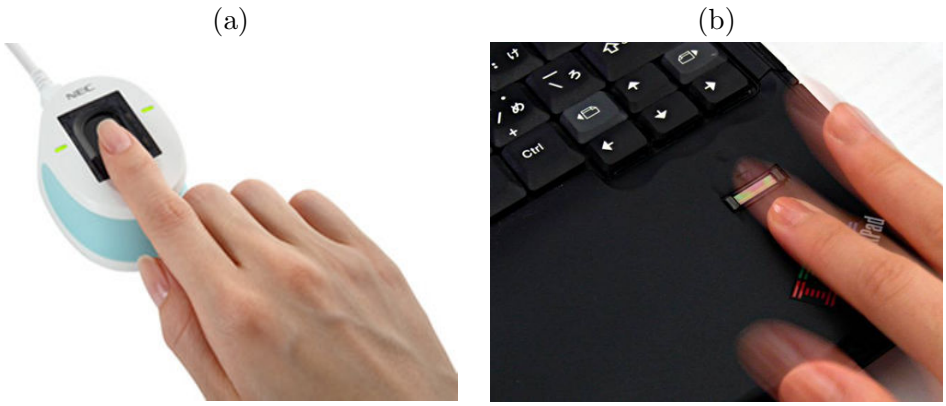

Figure 4.12: Examples of fingerprint acquisition sensors: (a) area scan sensor; (b) swipe sensor.

images. One of the most used compression atechniques had been proposed by the FBI and it is based on Wavelet Scalar Quantization (WSQ) [224]. This algorithm computes the scalar quantization of a 64-subband discrete wavelet transform decomposition of the image, followed by Huffman coding. Another diffused compression technique is JPEG 2000 [225], which is also adopted for different types of images. A comparison between the most used compression algorithms is proposed in [226].

4.5.2 Quality estimation of fingerprint samples

Fingerprint images can have very different quality levels. Low levels of fingerprint quality can compromise the recognition accuracy [43]. In order to control this factor, quality estimation methods are usually adopted [227]. Quality estimation is also useful to select unrecoverable image regions, and to properly weight the extracted features according to the local quality level of the input fingerprint image.

An example of a good quality fingerprint image and two images with low visibility of the ridge pattern due to different pressures of the finger on the sensor are shown in Fig. 4.13.

Many quality evaluation techniques designed for touch-based fingerprint images are based on the evaluation of local features. The method described in [228] evaluates the probability density function (PDF) of local regions. The technique presented in [229] computes the used features by applying a set of Gabor filters with different orientations to the local areas of the image. Other techniques are based on global characteristics.

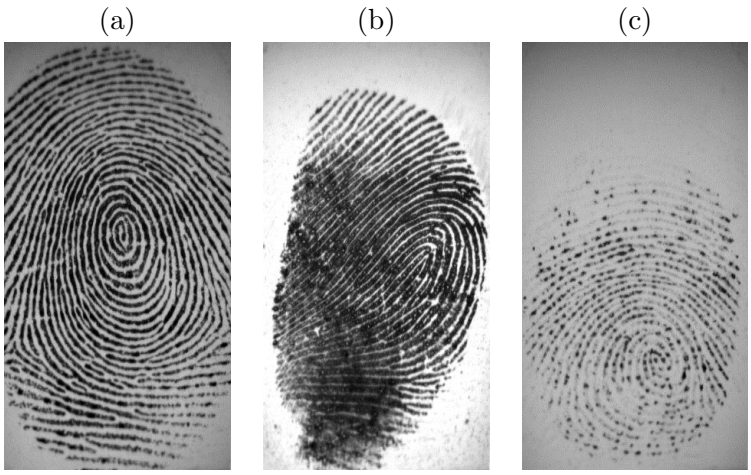

Figure 4.13: Examples of fingerprint images with different quality levels: (a) good quality image; (b) image with low visibility of the ridge pattern due to a high pressure of the finger on the sensor; (c) image with low visibility of the ridge pattern due to a low pressure of the finger on the sensor.

For example, the method described in [230] is based on the evaluation of the energy distribution rate in wavelet compressed fingerprint images. The technique proposed in [231] combines local and global features related to the frequency domain (a ring structure of DFT magnitude and directional Gabor features) and to the spatial domain (black pixel ratio of the central area). Also the method described in [232] combines local and global characteristics and is based on features related to the effective area, energy concentration, spatial consistency, and directional contrast.

One of the most used quality estimation techniques in the literature is described in [233]. This technique is specifically designed for working in fingerprint recognition systems based on identity comparison algorithms that use minutiae features, like the one presented in [199]. The method is based on neural networks and classifies five levels of quality, from poor to excellent. The used features are computed from the local quality map and the quality of the minutia points estimated using the software MINDTCT [199]. The local quality map is computed considering the ridge orientation map and detecting regions with low contrast, low ridge flow, and high curvature. The quality of every minutia is obtained by considering its coordinates and by computing statistics (mean and standard deviation) on the intensity values of the local image regions centered in the minutia coordinates.

4.5.3 Image enhancement

Another step that can be present in the fingerprint recognition process is the image enhancement. In the literature, there are different enhancement techniques for fingerprint images [3], which can be classified in pixel-wise enhancement, contextual filtering, and multi-resolution enhancement.

Pixel-wise enhancement techniques are based on image processing algorithms for the enhancement of the image intensity [195]. These techniques are usually adopteded as a preprocessing task during the enhancement of fingerprint images. Examples of these techniques are Wiener filtering [234] and the intensity normalization algorithm proposed in [181], which is one of the most used preprocessing techniques in the literature. This algorithm is based on the formula:

$$I'(x,y) = \begin{cases} \mu_0 + \sqrt{(I(x,y) - \mu)\,\sigma_0/\sigma} & \text{if} I(x,y) > \mu \\ \mu_0 - \sqrt{(I(x,y) - \mu)\,\sigma_0/\sigma} & \text{otherwise} \end{cases}, \tag{4.2}$$

where μ_0 and σ_0 are the desired mean and standard deviation of the normalized image I', and μ and σ are the mean and standard deviation of the image I.

The contextual filtering techniques are the most used in the literature. These techniques change the characteristics of the filter used for the enhancement of different fingerprint regions according to the local context. The used filters perform an averaging effect along the ridges in order to reduce the noise and enhance the contrast between ridges and valleys by performing a band-pass filtering according to the ridge orientation. The most used contextual filtering technique is based on Gabor filters tuned according to the local ridge characteristics [181]. This method computes two images that describe the local orientation O_R and the local frequency F_R of the ridges, and then it applies a convolution to the local areas of the original image with Gabor filters tuned according to the frequency and the orientation of the ridges. The schema of the enhancement process is shown in Fig. 4.14. The even-symmetric Gabor filter has the general form

$$\begin{gathered} h(x,y:\phi,f) = \exp\left\{-\tfrac{1}{2}\left[\frac{x_\phi^2}{\sigma_x^2} + \frac{y_\phi^2}{\sigma_y^2}\right]\right\}\cos(2\pi f x_\phi), \\ x_\phi = x\cos(\phi) + y\sin(\phi), \\ y_\phi = -x\cos(\phi) + y\sin(\phi), \end{gathered} \tag{4.3}$$

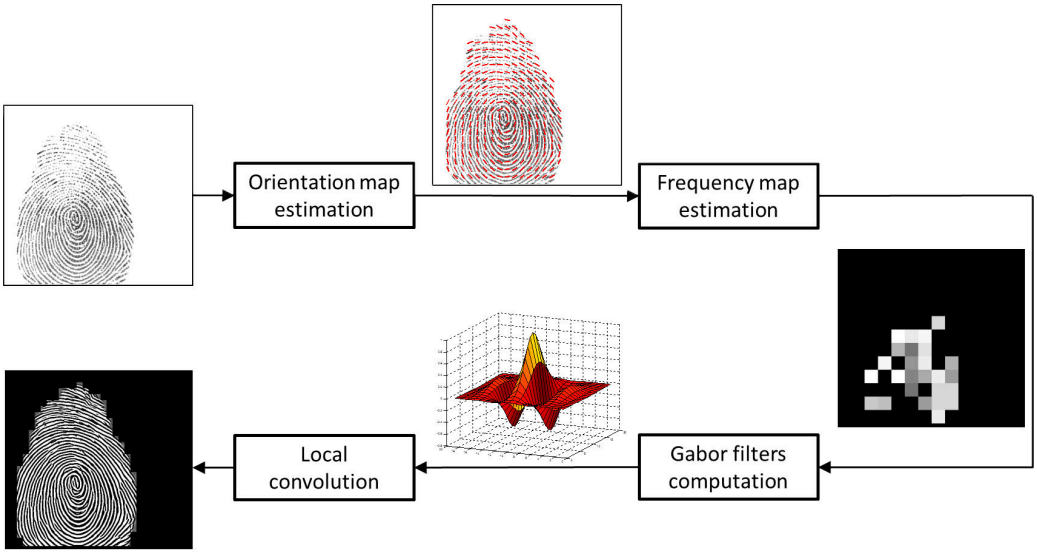

Figure 4.14: Schema of a fingerprint enhancement method based on a contextual filtering technique [181].

where ϕ is the orientation of the Gabor filter, f is the frequency of a sinusoidal plane wave, and σ_x and σ_y are the space constants of the Gaussian envelope along x and y axes, respectively. The parameters ϕ and f of the Gabor filter applied to the pixel (x, y) of the image I are selected accordingly to the $O_R(x, y)$ and $F_R(x, y)$ respectively. The parameters σ_x and σ_y are empirically tuned.

Other contextual filters are based on different masks. For example, the method described in [235] is based on bell-shaped filters, and the method proposed in [236] on log-Gabor filters. The method described in [177] performs the enhancement of local regions in the Fourier domain according to the maps describing the ridge orientation and frequency.

Enhancement methods based on multi-resolution techniques perform analyses at different scales (in the space domain or frequency domain) in order to enhance first the ridge structure and then the finest details. An example of these methods is described in [237] and is based on a Laplacian like image-scale pyramid.

In the literature, there are also techniques for the detection and compensation of creases in fingerprint images [238]. Creases, in fact, can produce artifacts in the enhanced images.

4.5.4 Feature extraction and matching

Fingerprint matching algorithms compute a similarity index called matching score between two fingerprints used in the verification/identification procedures. It is possible to divide the fingerprint matching algorithms into three classes: correlation-based techniques; minutiae-based methods; methods based on other features.

4.5.4.1 Correlation-based techniques

Correlation-based techniques compute the matching score between two fingerprint images. The images are usually scaled, translated, rotated, equalized, and finally, the matching score is obtained as a correlation measurement between the two images. A basic technique consists in the computation of the cross-correlation values [195]. There are also methods based on correlation techniques more robust to noise [239] and methods that perform the correlation between local regions [240]. The correlation-based approach is rather basic and not commonly present in automated fingerprint recognition systems. This approach, in fact, is not robust to distortions and intensity differences due to different pressures of the finger on the sensor.

4.5.4.2 Minutiae-based methods

The minutiae-based methods are the most studied and applied in the literature [241].

These methods compute the matching score between two templates T and T' by searching the corresponding minutiae in the considered feature sets. The templates usually consists in vectors of minutiae described as $m = (x, y, \theta)$. The minutia type is rarely considered because noise and different pressures of the finger on the sensor can easily transform a bifurcation in termination and vice versa. Two minutiae are considered as correspondent if their spatial distance s_d and direction difference d_d are less than fixed thresholds. The distances s_d and d_d are defined as:

$$\begin{aligned} s_d\left(m'_j, m_i\right) &= \sqrt{\left(x'_j - x_i\right)^2 + \left(y'_j - y_i\right)^2} \\ d_d\left(m'_j, m_i\right) &= \min\left(\left|\theta'_j - \theta_i\right|, \left(360 - \left|\theta'_j - \theta_i\right|\right)\right). \end{aligned} \tag{4.4}$$

In order to evaluate the number of corresponding minutiae points, it is necessary to perform a registration of the templates. The registration is essentially a point pattern matching problem, and aims to compensate rotations and translations of the templates

to align the minutia sets. The used algorithms, anyway, should be robust to different non idealities:

- the templates can contain false minutiae;
- some minutiae can be missed;
- the minutiae sets are affected by distortions due to the placement of the finger on the sensor;
- the number of minutiae appertaining to the template T can be different to the number of minutiae of T'.

After the registration step, the corresponding minutiae are searched and used to compute the matching score. In the literature, there are different techniques for the computation of the matching score between two minutia sets. One of the most diffused matching score formula is presented in [3]:

$$\text{matching score} = \frac{k}{(M+N)/2} \tag{4.5}$$

where k is the number of matched minutia pairs, M and N are the number of minutiae of the templates T and T' respectively.

Considering the used registration strategy and the technique adopted for searching the corresponding minutia pairs, it is possible to distinguish global and local minutiae matching algorithms. Global algorithms use all the minutiae points of the two fingerprint templates and search the best matching score by aligning the two minutia sets. Local algorithms consider sets of minutiae divided into sub-portions, for example by adopting auxiliary graph structures or additional information related to the local regions of the minutia points. Some algorithms are also specifically designed to compensate problems related to skin distortions.

In the literature, there are many different global minutiae matching algorithms. These algorithms can be based on the algebraic geometry [242], Hough transform [243], relaxation [244], energy minimization [245], etc. In order to reduce the time need by the matching step, some methods perform a pre-alignment of the query template with the corresponding one stored in the database [246].

The methods based on algebraic algorithms are the most diffused and perform the rectification of the considered templates by using heuristics based on geometrical

equations. A well-known software in the literature, NIST Bozorth3 [199], appertains to this class. The matching method can be divided into three steps.

1. Construct Intra-Fingerprint Minutia Comparison Tables: a table for the template T and a table for the template T' are computed. These tables describe a set of relative measurements from each minutia in a fingerprint to all other minutia in the same fingerprint.

2. Construct an Inter-Fingerprint Compatibility Table: the minutiae stored in the previously computed tables are compared and the obtained results are stored in a distinct table.

3. Traverse the Inter-Fingerprint Compatibility Table: the associations stored in the Inter-Fingerprint Compatibility Table represent single links in a compatibility graph. An iterative algorithm traverses the compatibility graph finding the longest path of linked compatibility associations. The matching score is then considered as the length of the longest path.

Local minutiae matching methods are based on the comparison between local characteristics of the fingerprint images that are invariant to rotations and translations. These characteristics can be used to directly compute a matching score value or to perform the registration between the considered templates. In the literature, there are many matching algorithms based on local characteristics. It is possible to distinguish methods that use nearest neighbor-based structures, fixed radius-based structures, minutiae triangles, and texture-based local structures. A well-known method that uses a nearest neighbor-based structure is presented in [247] and performs a local comparison by evaluating the characteristics (coordinates and orientation) of the nearest l minutiae. Methods that use fixed radius-based structures extract local features by considering local regions centered in every minutia point. An example of these techniques is proposed in [248]. For each minutia, this method computes a graph that represents a star obtained by connecting the considered minutia and the n nearest minutiae present in the evaluated local region. Methods based on minutiae triangles compute graphs that describe the connections between the nearest minutia points. Many recognition algorithms in the literature use this kind of templates to perform the template registration because the use of minutiae triangles permits to obtain accurate

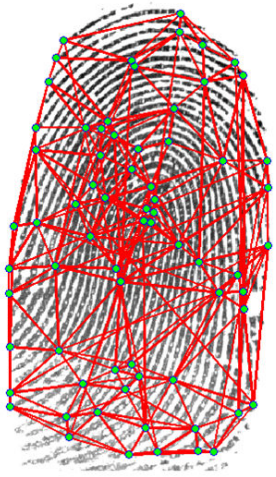

Figure 4.15: Visual example of the template used by local minutiae matching methods based on Delaunay graphs.

results and reduces the computational time. One of the most used techniques for the computation of these graphs is the Delaunay triangulation [249, 250, 251]. An example of the obtained results is shown in Fig. 4.15.

The techniques based on graphs obtained applying the Delaunay triangulation search the triangles corresponding in two templates by evaluating characteristics that are invariant to rotations and translations. Examples of these characteristics are the angles, lengths of the facets, and lengths of the bisectors of the triangles. The most important problem of these methods is that they are sensible to false minutiae and missed minutiae.

In the literature, there are also techniques specifically designed to compensate non-linear distortions due to different pressures of the finger on the sensor. A matching appertaining to this class is described in [252], and is based on a feature called Local Relative Location Error Descriptor. There are also methods based on multiple registrations [253], algorithms that estimates the mean distortion present in the considered data [254], and techniques for the estimation of the distortion models obtained by different placements of the finger on the sensor [255].

4.5.4.3 Methods based on other features

Other fingerprint matching methods can use features extracted at different levels as support information for processing a matching score based on the minutiae sets, or directly process features extracted at Level 1 or Level 3.

Most of these matching methods are based on the texture analysis performed at Level 1. A wll-known technique in the literature is based on the template called Fingercode [193]. Fig. 4.16 shows the schema of the Fingercode method. This method can be divided into the following steps.

- Estimation of the core point.
- Definition of the region of interest (ROI) as a ring with fixed size (height h).
- The ROI is partitioned in n_R rings and n_A arcs, obtaining $n_S = N_R \times n_A$ sectors S_i.
- A bank of n_F Gabor filters with different directions is applied to the image obtaining n_F filtered images $F_{i\theta}$.
- The Average Absolute Deviation (AAD) from the mean of gray values in individual sectors of filtered images is computed to define the feature vector that represent the biometric template. The value $V_{i\theta}$ of the template related to every sector of each filtered image is computed as:

$$V_{i\theta} = (1/n_i) \left(\sum_{1}^{n_i} |F_{i\theta}(x,y) - F_{i\theta}| \right) \tag{4.6}$$

  where n_i is the number of pixels in S_i and $P_{i\theta}$ is the mean of pixel values $P_{i\theta}$ of $F_{i\theta}(x,y)$ in the sector S_i.

The obtained feature vector is composed by $n_V = n_S \times n_F$ values (for example, in [193], n_V ranges from 640 to 896 according to the used fingerprint dataset). This method is not rotational invariant. For this reason, during the enroll phase, n_θ templates related to different rotations of the original image are computed. The matching score from two templates consists in the minimum Euclidean distance between the n_θ rotated templates and the live template. This step reduces the problem related to different placements of the finger on the sensor.

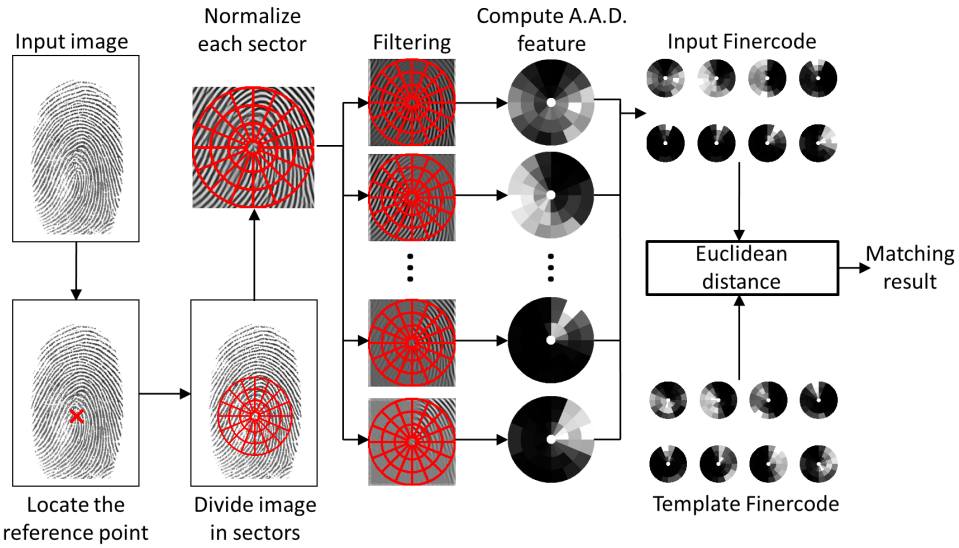

Figure 4.16: Schema of the biometric recognition method based on the template Fingercode.

Another well-known method is described in [256] and is based on templates obtained from the analysis of circular regions of the image spectrum. Other matching methods are based on different local and global characteristics, for example, the method described in [257] compares Scale-Invariant Features (SIFT) obtained from two fingerprint samples.

In the literature, there are also matching methods based on Level 1 analysis that computes features describing the shape of every ridge [258].

Methods based on Level 3 features are also researched. The recognition method described in [217] extracts the pore features using Gabor filters and wavelet transforms, and then it performs a local matching using the Iterative Closest Point (ICP) algorithm. Other matching methods based on Level 3 characteristics are described in [259, 260].

4.5.5 Fingerprint classification and indexing

The identification procedure requires comparing a biometric template with all the templates stored in a database. In the case of large databases, the computational time required for the evaluation of the full set of biometric templates can be unacceptable. A strategy used to reduce the required number of identity to be compared consists in the creation of partitions (called *bins*) containing only fingerprints of a defined class.

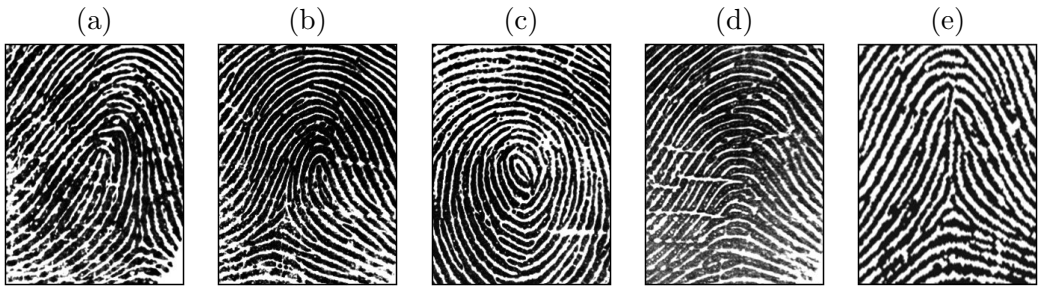

Figure 4.17: Galton-Henry classification scheme: (a) left loop; (b) right loop; (c) whorl; (d) arch; (e) tented arch.

Usually, fingerprints are classified by using the Galton-Henry classification scheme. This scheme is based on the analysis of Level 1 features and is composed by 5 classes (arch, tented-arch, left loop, right loop, and whorl). Fig. 4.17 shows an example of the considered classes. Fingerprint classification can be achieved by different approaches, such as neural networks classifiers, statistical methods, syntactic methods, rule-based methods, support vector machines [261]. Further strategies can be applied for reducing the number of identity comparisons, such as the use of a sub-classification [262], and the computation of continuous indexes related to different fingerprint features [251].

4.5.6 Computation of synthetic fingerprint images

The design of fingerprint recognition systems requires the collection of sample databases large enough to prove the validity of the envisioned method. This task is expensive and time consuming. Moreover, it can require the design and implementation of new acquisition sensors. In order to limit the efforts necessary to collect biometric data, it can be useful to perform tests on simulated samples.

The only works in the field of synthetic fingerprint computation are based on the simulation of two-dimensional images of fingerprints captured by contact-based sensors.

The method proposed in [263] is based on techniques for the computation of global and local features of the fingerprint. The global features are related to the orientation of the ridge pattern, which is modeled by using a limited set of coefficients describing a sampling of the two-dimensional function that represents the spatial direction of the ridges. A second-order model is then used to approximate the spatial orientation function. Local features are computed by first defining a set of points with a binary

mask, which is then iteratively refined using a stripe-shaped filter. The orientation of the filter is chosen according to the orientation field.

The method described in [264, 265] proposes a biologically-inspired mathematical model for the formation of the fingerprint ridge pattern, based on the idea that the ridge pattern is created by the differential growth of the skin basal layer, which is compressed by the adjacent skin layers. The compression that originates the fingerprint pattern is then modeled and reproduced to compute synthetic fingerprints.

An approach based on a genetic algorithm is introduced in [266]. This approach is designed for the computation of synthetic fingerprint samples from a limited set of real fingerprint images. The genetic algorithm is used to initialize and adapt a set of filters used to obtain the synthetic samples. The method is also able to adapt the process in order to produce synthetic samples that are similar to the ones appertaining to a specific set of real fingerprints.

The method described in [267] is based on the computation of different images describing the fingerprint area, the ridge orientation, the ridge frequency, and the ridge pattern. The fingerprint area is defined using a silhouette, while the orientation image is obtained starting from the position of the singular points (loops and deltas). A mathematical flow model is then applied to estimate a consistent orientation in the rest of the image. The frequency information image is obtained by using a heuristic criteria inferred from the visual inspection of real fingerprints. The ridge pattern and the minutiae are then computed by using a contextual iterative Gabor filtering technique. As a last step, the realism of the model is improved by simulating the displacement, rotation, distortion, skin condition, and acquisition noise.

An improved version of the method described in [267] is proposed in [268], and permits to compute synthetic fingerprints according to parameters such as gender, age, and race. The possibility to explicitly tune these parameters allows the creation of a database of fingerprints that realistically simulate specific applicative contexts.

4.6 Contactless fingerprint biometrics

Most of the fingerprint recognition systems use contact-based acquisition devices. However, these systems suffer from important intrinsic problems [269]:

- **Inconsistent contact** - the contact of the finger with the acquisition sensor causes distortions in the captured images due elastic deformations of the friction skin of the finger. For each acquisition, the introduced deformations can have different magnitude and directions.
- **Non-uniform contact** - different factors can introduce noise and reduce the contrast of the local regions of fingerprint images, such as: the dryness of the skin, shallow/worn-out ridges (due to aging or genetics), skin diseases, sweat, dirt, and humidity in the air.
- **Latent print** - each time a user places the finger on the sensor platen, a latent fingerprint is left on it. This fact represents a security lack of the system because latent fingerprints can be used to perform impostor accesses. During the acquisition process, moreover, the device can capture both the new fingerprint and portions of latent fingerprints, obtaining inconsistent samples.

Contactless fingerprint recognition systems are studied in order to overcome these problems. Contactless biometric systems, in fact, permit to obtain biometric samples without distortions due to the contact of the finger with the sensor, are more robust to dirt and different environmental conditions, and do not present latent fingerprints on the sensor surface.

Another important goal of contactless fingerprint recognition systems is to increase the user acceptability with respect to the contact-based techniques. Cultural factors and fears related to the transmission of skin diseases, in fact, can limit the acceptability of contact-based recognition systems. Moreover, the use of contactless acquisition techniques can permit to reduce the efforts necessary for the training of the users and to reduce the time needed for every biometric acquisition.

Contactless recognition systems are based on images captured by CCD cameras. These images are very different from the ones obtained by using contact-based acquisition sensors. An example of fingerprint images captured using a CCD camera and a

Figure 4.18: Examples of fingerprint images captured using a contact-based sensor and a CCD camera: (a) contact-based image; (b) contactless image. Contactless fingerprint images are more noisy and present a more complex background.

contact-based sensor are shown in Fig. 4.18. It is possible to observe that the contactless fingerprint images present more noise, reflections, and a more complex background with respect to contact-based images. Moreover, the skin can be considered as part of the background. Other problems that should be considered during the design of contactless recognition systems are related to inconstant resolutions and differences in the acquisition angle.

The biometric recognition process performed by most of the contactless systems in the literature can be divided into three main steps: acquisition; computation of a contact-equivalent fingerprint image; feature extraction and matching. The schema of the process is shown in Fig. 4.19.

In the literature, there are different contactless acquisition strategies, which can be based on single CCD cameras, multiple view techniques, or structured light approaches. The acquisition setups can also use specifically designed illumination systems.

The methods for the computation of contact-equivalent fingerprint images are strictly related to the used acquisition setup. The goal of these methods is to obtain fingerprint images that can be used by algorithms designed for contact-based recognition systems. In the case of systems based on single contactless fingerprint images, the contact-equivalent fingerprint images are obtained by applying specifically designed enhancement techniques and by performing a normalization of the image size to a

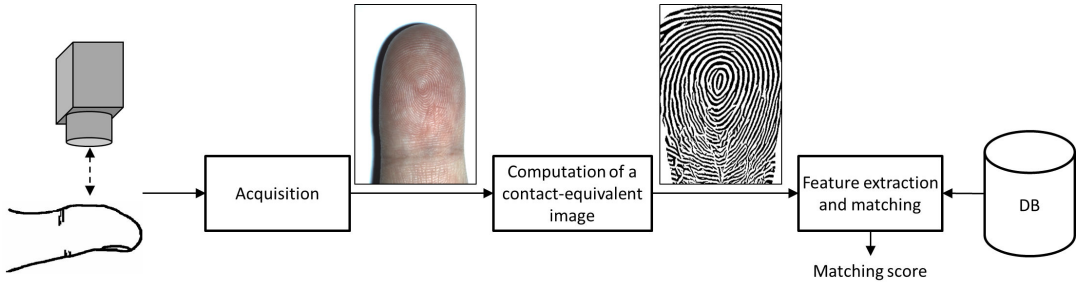

Figure 4.19: Schema of the contact-less fingerprint recognition systems.

standard resolution (usually equal to 500 or 1000ppi). Other systems compute a metric reconstruction of the fingertip and then apply techniques for mapping three-dimensional data into a two-dimensional space. The computation of three-dimensional models permits to obtain less-distorted samples, but require complex and expensive acquisition setups.

Feature extraction and matching techniques are finally applied in order to perform the biometric recognition. Most of the systems in the literature use methods designed for contact-based fingerprint images, but there are also algorithms specifically designed for contact-equivalent fingerprint images.

This section presents techniques in the literature for the acquisition and processing of contactless fingerprint samples. The described techniques are divided into two classes: methods based on two-dimensional samples, and methods based on three-dimensional samples.

4.6.1 Fingerprint recognition based on contactless two-dimensional samples

In the literature, there are contactless fingerprint recognition systems based on two-dimensional samples designed to be integrated in low-cost, and there are portable devices and systems that use more complex hardware setups in order to obtain higher recognition accuracy.

Contactless fingerprint recognition systems based on two-dimensional samples use CCD cameras to capture the details of the ridge pattern. Usually, they capture a single image and then process it in order to obtain a contact-equivalent fingerprint image. The biometric recognition is then performed by using well-known algorithms for the

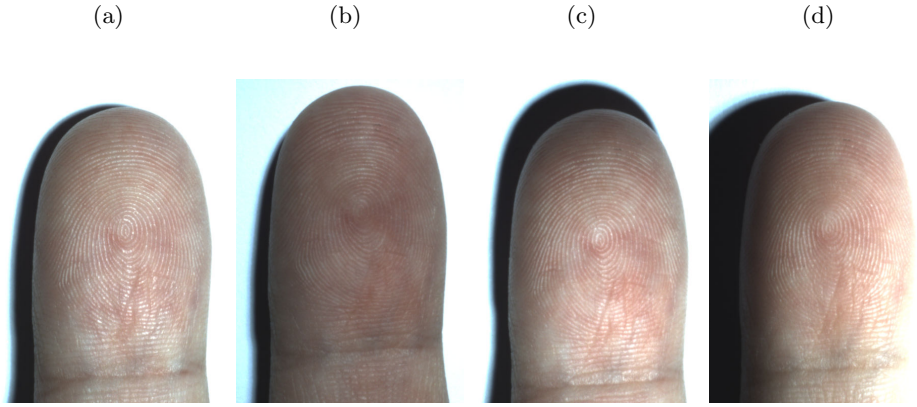

Figure 4.20: Fingerprint images captured contactless in different illumination conditions: (a) frontal illumination; (b) illumination from the left side; (c) illumination from the right side; (d) illumination from the top side.

feature extraction and matching of contact-based fingerprint images. There are also systems that use feature extraction and matching algorithms specifically designed for contactless two-dimensional samples. Some systems also use multiple view techniques or specifically designed optics in order to obtain contact-equivalent fingerprint images not affected by perspective deformations and out of focus problems.

4.6.1.1 Acquisition

The most important factors that characterize the acquisition setups used to capture contactless finger images are the use of supports for the finger placement, the adopted optical configuration, and the illumination technique. The obtained images, in fact, can present different characteristics and levels of noise. As an example, Fig. 4.20 shows some images obtained using the same point shaped light placed in different positions.

The simplest acquisition technique consists in the use of a low-cost CCD camera in uncontrolled light conditions. A biometric system that captures fingerprint images using a webcam in natural light conditions is presented in [270], and studies on the use of mobile phone cameras are described in [271, 272]. The images captured in uncontrolled light conditions, however, present poor contrast between ridges and valleys. For this reason, most of the contactless recognition systems in the literature use illumination techniques to improve the visibility of the fingerprint. A simple and low-cost illumination technique consists in the use of a point light source, like a lamp [273, 274, 275]. The main disadvantage of using point light sources is that they introduce shadows that

can reduce the visibility of the ridge pattern. Moreover, they do not permit to obtain a uniform illumination in the external regions of the fingerprint images. In order to overcome these problems and obtain a uniform illumination in all the regions of the images, other methods use ring illuminators [276].

In the literature, there are also studies on the light wavelengths that permit to enhance the visibility of the ridge pattern [269, 277]. These studies report that the white light does not bring the best contrast between ridges and valleys. Long wavelength rays, like white light and infrared, in fact, tend to penetrate the skin, and to be absorbed by the epidermis. Differently, a blue light with a wavelength of 500 nm permits to obtain the lower hemoglobin absorption and to enhance the details of the skin. For this reason, some contactless fingerprint acquisition systems use illumination techniques based on blue led lamps [278, 279]. The work presented in [277] compares illumination setups based on different light wavelengths, light positions, polarization, and diffusion techniques. The best quality images are obtained using a horizontally polarized blue light with a tilt angle of 45°, and treated with a scattering filter in order to obtain a uniform illumination in all the regions of the finger.

Other acquisition systems use transmission-based illumination techniques. The system described in [280] uses a red light source placed on the fingerprint side to focus the light transmitted through the finger onto a CCD. This method permits to capture images describing the shape of the ridges in the internal layers of the finger and is less sensible to problems related to bad skin conditions with respect to other illumination techniques. However, the acquisition setup requires that the finger is placed in fixed position, imposing constraints to the users.

Other important aspects of the contactless acquisition systems are that they have to guarantee a proper depth of focus and field of view in order to capture the details of all the regions of the fingertip. In order to obtain an appropriate field of view, most of the systems in the literature require that the distance between the finger and the camera is less than 10 cm. Considering the required magnification ratio and the cylindrical shape of the finger, standard lenses can obtain fingerprint images affected by out of focus problems in the lateral regions. In order to overcome this problem, some systems use multiple cameras [279, 281]. Another possibility to overcome this problem is to use curved lenses. These lenses, however, can produce distortions in the captured images and increase the costs of the hardware setups.

Other problems that should be addressed are related to the image resolution and motion blur. The use of supports for the finger placement permits to calibrate the acquisition setup in order to estimate the image resolution and to reduce the probability of finger movements. For these reasons, many systems use supports for the finger placement [269, 276, 281]. In the literature, there are also studies on less-constrained setups that do not require the use of supports [279].

Contactless fingerprint images captured by single cameras, however, do not present a constant resolution in the different fingerprint regions. In this kind of acquisition systems, in fact, the optical resolution decreases from the detector center to the detector side due to the finger curvature. This factor can also be influenced by the small focus field of single cameras with high magnification lenses.

In some governmental applications, the size of the fingerprint image database is typically very large. For this reason, compression algorithms are applied to the biometric samples. The work described in [282] evaluated the results obtained by different techniques for the compression of contactless fingerprint images. The best performance was obtained by the WSQ technique [224].

4.6.1.2 Computation of a contact-equivalent image

Usually, the samples captured by contactless sensors cannot be directly used by recognition methods designed for contact-based fingerprint images. In order to obtain the compatibility with these biometric algorithms and the existing AFIS, most of the contactless fingerprint recognition systems in the literature compute contact-equivalent fingerprint images, which represent the ridge pattern at a fixed resolution.

In [272], the performances obtained by a commercial fingerprint recognition software on contactless images are evaluated. The paper reports that sufficient results are obtained only on the best quality images.

In order to perform biometric recognitions based on well-known methods in the literature, the enhancement of the ridge pattern is usually computed. This task aims to obtain a gray-scale image representing only the fingerprint pattern and to reduce the noise present in the captured contactless image. An example of contactless fingerprint image and the corresponding contact-equivalent image are shown in Fig. 4.21.

Important goals of the computation of contact-equivalent fingerprint images are to increase the contrast between ridges and valley by removing the details of the finger

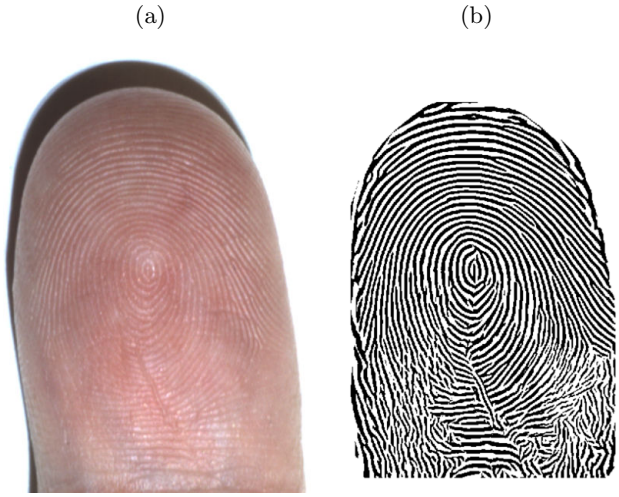

Figure 4.21: Example of results obtained by computing a contact-equivalent image from a contactless fingerprint image: (a) contactless image; (b) contact-equivalent image.

skin, to reduce out-of focus problems, to remove possible reflections, and to reduce the noise introduced by CCD cameras. In the literature, there are different techniques designed for the enhancement of contactless fingerprint images. The method described in [270] first performs a preprocessing task based on the Lucy-Richardson algorithm and on the deconvolution of the input image by a Wiener filter. This task aims to reduce out of focus problems and to decrease the presence of noise. Then, a background subtraction algorithm based on low-pass Gabor filters is applied. Finally, a cutoff filter tuned according to the mean ridge frequency is used in order to increase the contrast between ridges and valleys. Differently, the image enhancement method proposed in [273, 274, 275] is based on a contextual filtering technique. First, it estimates the fingerprint area by converting the captured color image in grayscale and by applying a segmentation technique based on an adaptive threshold and on morphological operators. Finally, the visibility of the contact-equivalent image is obtained by using the contextual filtering technique based on the STFT analysis described in [177]. Another enhancement method designed for contactless fingerprint images is described in [283]. Similarly to the technique presented in [181], this method applies Gabor filters tuned according to the local ridge frequency and orientation, but computes the ridge orientation map using an iterative regression algorithm designed to be more robust to the noise present in contactless fingerprint images.

In order to obtain contact-equivalent fingerprint images that can be used by matching techniques based on minutia features, it is also necessary to normalize the contactless images to a fixed resolution. Some contactless recognition systems that require the placement of the finger at a fixed position obtain this result by evaluating the information related to the focal length and the distance between the finger and the camera [269, 276]. Systems that do not impose constraints can only perform an approximated normalization. The method presented in [270] first computes an alignment of the fingerprint image by applying a rotation inverse to the angle of the major axis of the finger silhouette. The last task of the normalization is the registration of the minor axis of the image to the standard measure of 9/10 of the height of the final contact-equivalent image.

4.6.1.3 Contact-equivalent samples from multiple images

Contact-equivalent images obtained using single CCD cameras present problems related to perspective distortions and different resolutions in the local image regions. In order to overcome these problems, a two-dimensional contactless recognition system based on the mosaicing of fingerprint images obtained from three views is presented in [281]. The acquisition system is composed by a camera placed in front to the finger and two cold mirrors with a fixed tilt angle that are used both to obtain different views of the fingertip and to be a support for the finger placement. The contact-equivalent images are obtained by merging the information related to the different views. The schema of the acquisition setup is depicted in Fig. 4.22a, an example of captured images is shown in Fig. 4.22b, and the corresponding mosaiced image is reported in Fig. 4.22c. The first task is the image enhancement and is performed in order to increase the contrast between ridges and valleys in all the captured images. The enhancement method used by this biometric system is similar to the one presented in [283], but performs an adaptive histogram equalization task before applying the contextual filtering. The second task is the search of corresponding points in the captured fingerprint images. In order to reduce the number of corresponding candidate points, the images are first rectified by using the information obtained from a previously performed calibration of the multiple view setup. A first set of corresponding points in the frontal and lateral views are obtained by applying a minutiae matching technique. Starting from the obtained set of corresponding minutiae, a ridge following approach is used to search more

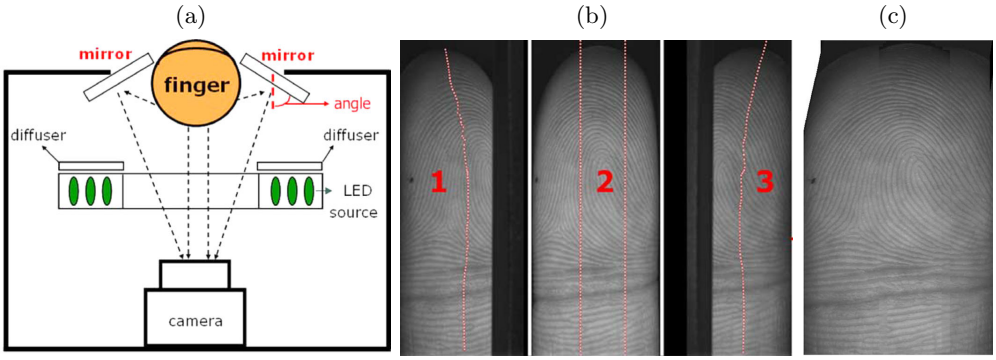

Figure 4.22: Multiple view technique for the computation of two-dimensional fingerprint samples [281]: (a) acquisition setup; (b) example of captured images; (c) mosaiced image.

corresponding points. The next step consists in the merging of the three-views. The regions of the lateral views that should be merged with the central region of the frontal view are selected by applying an iterative distance minimization technique to the set of corresponding points. The lateral views are then transformed accordingly to the results obtained by the distance minimization and then merged with the central region of the frontal view. Finally, the obtained contact-equivalent image is refined by smoothing the intensity values in the transitions between the merged regions. This system effectively reduce problems related to perspective distortions but it does not permit to properly overcome problems due to different resolutions of the local fingerprint regions because it does not compute a metric representation of the biometric samples like the contactless systems based on three-dimensional reconstruction techniques.

Another interesting system that considers the three-dimensional fingerprint shape in order to obtain a contact-equivalent fingerprint image is described in [284]. The acquisition setup is shown in Fig. 4.23 and is composed by a beveled ring mirror and a CCD camera. The acquisition process requires that the user moves the finger into the ring. During this process, the camera placed in front to the mirror captures a set of images that represent overlapped portions of the fingerprint. The captured circular regions are then mapped in rectangular areas by using a log-polar transformation. The obtained images are merged by using a correlation approach, obtaining an image describing the complete fingerprint area. Finally, the visibility of the ridge pattern is enhanced. A less expensive setup that can be used by this acquisition technique is also proposed in [284] and is based on a three-view configuration obtained using a line camera and

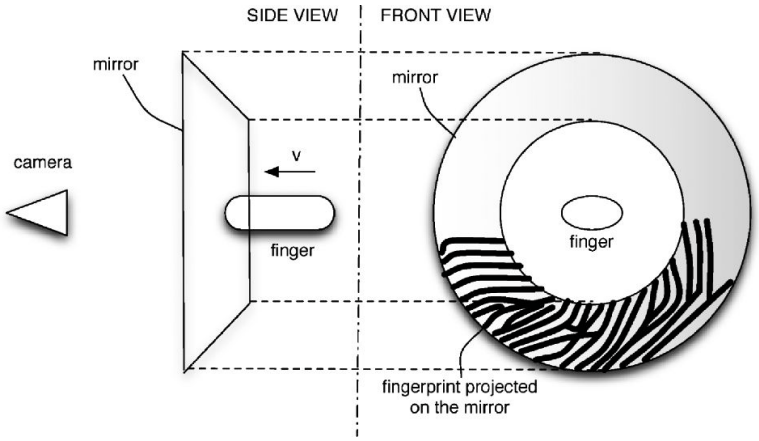

Figure 4.23: Schema of the contactless acquisition method based on a beveled ring mirror [284].

two mirrors. The main problem of this technique is that the speed and direction of the finger movement cannot be controlled and can introduce artifacts. Moreover, the system does not permit to obtain contact-equivalent images with a constant resolution in all the fingerprint regions because it assumes that the fingers have a fixed shape.

4.6.1.4 Feature extraction and matching

Similarly to contact-based fingerprint recognition systems, most of the biometric technologies based on contactless fingerprint images perform the recognition task using methods based on minutia features since they can obtain accurate results and require a limited computational time. These systems are usually based on matching techniques designed for contact-based images [269, 270, 281].

Matching algorithms based on minutia features require a constant resolution of the images in order to compute metric distances between the minutia points. For this reason, they can be used only if a proper resolution normalization is performed during the computation of the contact-equivalent images. This task can be performed with a sufficient accuracy only by adopting acquisition setups that use guides for the finger placement, since systems that impose fewer constraints on the finger placement can only infer the image resolution from characteristics of the image itself. In order to perform the recognition with sufficient accuracy also in systems based on this kind of acquisition setups, it is then useful to adopt matching methods based on adimensional features. The

matching technique proposed in [285] is specifically designed for contactless biometric systems that do not impose strong constraints on the placement of the finger during the acquisition task. This technique is based on a feature set similar to the Fingercode [193]. In order to overcome problems related to perspective distortions and noise, this method compares the fingerprint templates using computational intelligence techniques. The principal component analysis (PCA) is used to search the most distinctive features and support vector machines (SVM) are adopted to perform the template comparison.

A matching method specifically designed for low resolution contactless images (about 50 ppi) is presented in [286]. This method can use features computed by applying Gabor filters with different orientations and features based on the localized Radon transform (LRT).

In the literature, there are also multibiometric systems that fuse the information from the analysis of the ridge pattern of contactless images and the corresponding vein pattern. The vein pattern can also be used to check the vitality of the finger in contactless acquisitions. Contactless fingerprint acquisition systems that permit to capture images of the vein pattern are described in [279, 287].

4.6.2 Fingerprint recognition based on contactless three-dimensional samples

With respect to biometric systems based two-dimensional samples, the systems that compute three-dimensional fingerprint models can use more information and less distorted data. The used samples, in fact, consist in three-dimensional structures that are not affected by perspective deformations and represent a metric reconstruction of the fingertip. Moreover, the feature extraction and matching algorithms can use the additional information related to the z axis in order to improve the recognition accuracy. These systems, however, require more complex acquisition setups and are more expensive with respect to the ones based on single contactless images. Moreover, most of the methods in the literature require complex acquisition procedures.

The acquisition of three-dimensional biometric samples can be performed using different methods. This step requires specifically designed hardware setups and three-dimensional reconstruction algorithms. The three-dimensional fingerprint reconstruction techniques in the literature compute different kinds of samples. There are systems able to estimate the three-dimensional shape of ridges and valleys [284, 284, 288], and

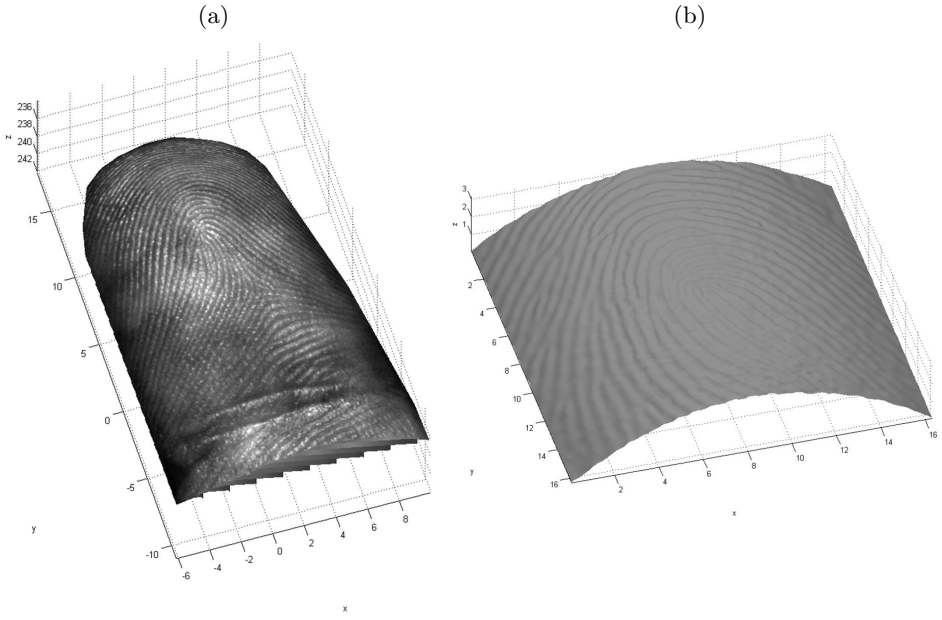

Figure 4.24: Example of three-dimensional samples obtained using different techniques: (a) finger volume with the texture of the ridge pattern; (b) portion of a three-dimensional model of ridges and valleys.

systems that represent the fingerprint as the three-dimensional volume of the finger with a superimposed texture that describe the ridge pattern [289, 290]. An example of a sample composed by the finger volume and the texture of the ridge pattern, and a portion of a sample describing the three-dimensional ridges are shown in Fig. 4.24.

Fingerprint three-dimensional models can be directly used by specifically designed feature extraction and matching techniques or converted in contact-equivalent fingerprint images. Dedicated techniques for the direct comparison of three-dimensional samples permit to use the additional information related to the height, in order to obtain more accurate recognitions. Differently, the computation of contact-equivalent images permits to use existing recognition techniques designed for contact-based fingerprint images. Moreover, using proper strategies, it can be possible to obtain fingerprint images compatible with the existing AFIS.

All the recognition systems in the literature based on three-dimensional fingerprint models perform the mapping of the three-dimensional samples into a two-dimensional space in order to obtain contact-equivalent images. This task is usually called unwrapping or unrolling.

4.6.2.1 Acquisition

It is possible to divide the methods for the computation of three-dimensional fingerprint models into two classes. The first class is composed by methods based on multiple view techniques. The reconstruction methods in the literature appertaining to this class are not able to estimate the three-dimensional shape of ridges and valleys. The obtained three-dimensional model consists in the finger volume with a superimposed texture representing the ridge pattern. The main advantage of these methods is that they can perform the three-dimensional reconstruction using data captured in a single time instant. The second class of methods for the computation of three-dimensional fingerprint samples is based on structured light techniques. The use of structured light patterns can permit to compute three-dimensional models of ridges and valleys. However, these methods require long acquisition times because they need to capture a relevant number of frames in order to reconstruct a three-dimensional model. For this reason, it is important that the users stay still during all the acquisition procedure in order to avoid motion blur problems in the captured frame sequences.

A system for the acquisition of three-dimensional fingerprint models based on a multiple view technique is presented in [284, 288, 291]. The acquisition setup uses five cameras located on a semicircle and pointing to its center, where the finger has to be placed during the biometric acquisition. The illumination system consists in a set of green leds placed around the semicircle. Fig. 4.25 shows the schema of the acquisition device. The three-dimensional reconstruction is performed using the information obtained from the calibration of the multiple view system, which is performed off-line. The first step is a rough estimation of the finger volume and is performed using a shape from silhouette technique. Then, the corresponding points in the images obtained from adjacent cameras are searched by using a correlation-based technique. Finally, the tree-dimensional shape is obtained by applying the triangulation algorithm [292], and the texture representing the ridge pattern is computed and superimposed to the three-dimensional model. The model is then composed by a depth map and a gray scale image. The ridge pattern computation is based on an image enhancement method that can be divided into two tasks. The first task is the enhancement of the ridge visibility and is performed by applying a Homomorphic filtering technique. The logarithm of the image is first computed, a high-pass filter is then applied, and the exponential of

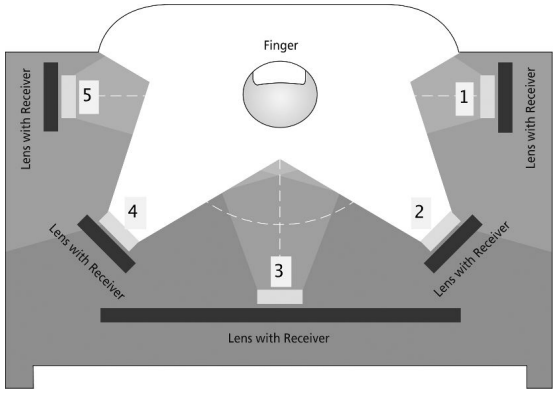

Figure 4.25: Multiple view setup for the computation of three-dimensional fingerprint models [284].

the obtained image is finally calculated. The second task consists in the ridge pattern enhancement and is performed by using the contextual filtering technique described in [181].

A system based on a structured light technique is presented in [289, 290]. This system is able to estimate both the three-dimensional shape of ridges and valleys and a texture of the ridge pattern obtained from the visual aspect of the finger. The acquisition setup is shown in Fig. 4.26 and is composed by a camera and a projector. The three-dimensional reconstruction of the ridge pattern is obtained by projecting a sine-wave pattern shifted several times. Every frequency pattern is used with 10 phase shift patterns. The frequency of 16 cycles per length of each pattern is used. Each acquisition therefore requires the capture of several frames. The three-dimensional shape is obtained by evaluating the phase shift of the projected pattern in every captured frame and by using the information related to a previous calibration of the acquisition system. In order to remove possible spikes, a median filter is finally applied to the obtained depth map. The texture of the ridge pattern is computed as the albedo image [293].

Another acquisition system based on a structured light technique is described in [294]. Differently from the device presented in [289, 290], this system does not estimate the three-dimensional shape of ridges and valleys, but only computes the finger volume and the texture describing the ridge pattern. The used three-dimensional reconstruction technique is based on the projection of a fringe pattern. The acquisition setup is composed by a camera and a blue led with a sinusoidal pattern. The finger volume is

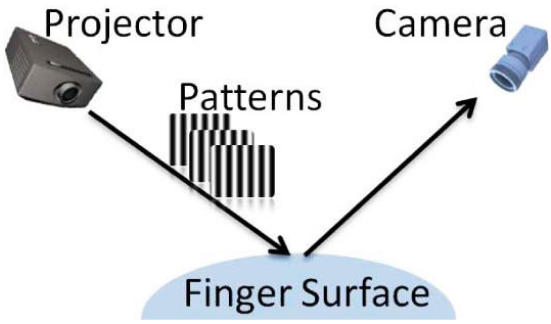

Figure 4.26: Structured light setup for the computation of three-dimensional fingerprint models [289].

obtained by computing the phase map of every pixel and by using the calibration data to estimate the depth of every point with the triangulation algorithm [292]. The texture describing the ridge map is considered as a contactless fingerprint image separately captured by the camera.

4.6.2.2 Computation of a contact-equivalent image

The computation of contact-equivalent images based on three-dimensional fingerprint models consists in the mapping of the three-dimensional shape into a two-dimensional space by using unwrapping techniques. The goal of this task is to obtain data compatible with the existing AFIS and recognition algorithms designed for contact-based fingerprint images. This task, in fact, permits to obtain fingerprint images similar to the ones captured by inked acquisitions. An example of obtained result is shown in Fig. 4.27. It is possible to observe that the contact-equivalent image does not present perspective distortions.

In the literature, there are different unwrapping techniques. These techniques can be divided into parametric methods and non-parametric methods. The first class of algorithms computes the projection of the three-dimensional fingerprint sample onto a parametric model (e.g. a cylindrical or a conic) and then unwraps this model in a two-dimensional space. Usually, these methods are computationally efficient. However, differences between the approximating model and the real shape can introduce distortions in the final image. Non parametric methods can be directly applied to the three-dimensional model without imposing constraints on its shape and are able to preserve local distances or angular relations. The mapping of a three-dimensional shape

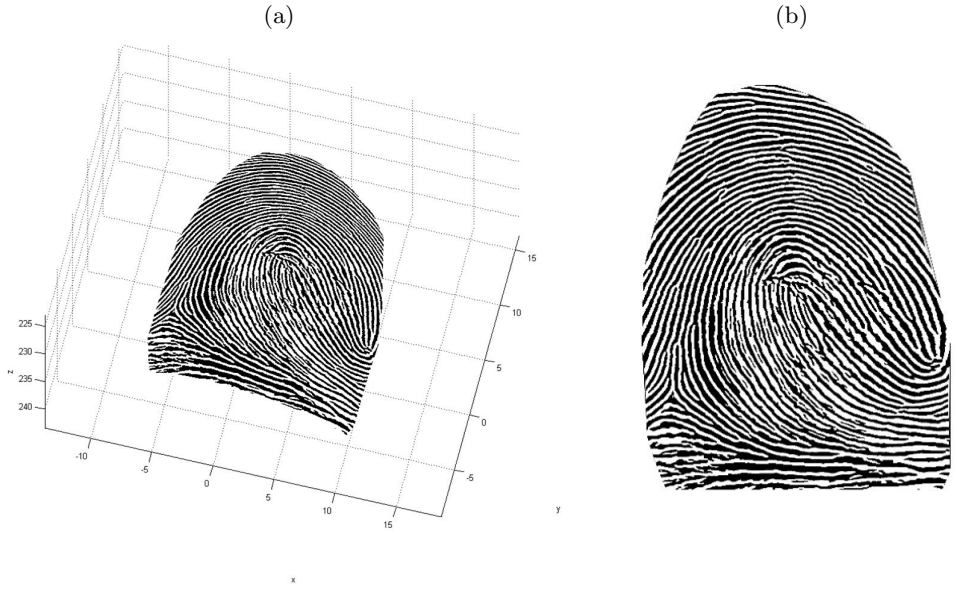

Figure 4.27: Computation of contact-equivalent fingerprint images by the unwrapping of three-dimensional models: (a) fingerprint model; (b) contact-equivalent image.

in a two-dimensional space, however, does not permit to maintain the original metric distances between all the points of the three-dimensional model.

A simple parametric method is based on the approximation of the finger shape to a cylindrical model [272]. The first step consists in the estimation of the center of rotation, which is considered as the minimum z and mean x of the finger model. Then, the coordinates of every three-dimensional point are converted in cylindrical coordinates. Finally, the texture image of the ridge pattern is mapped in the new space by using an interpolation technique. The main problem of this method is that the obtained images present important horizontal distortions. Moreover, it does not permit to obtain images with a fixed resolution in the horizontal axis.

A method proposed for reducing the distortion introduced by the approximation to a cylindrical model is described in [289]. The shape of the finger is first approximated as a set of rings with different radii and center coordinates. In order to reduce the noise present in the approximating model, a mobile averaging filter is then applied to the estimated radii. The approximating model can then be mapped into the two-dimensional space. If the three-dimensional map of the ridge pattern is available, this method applies an iterative algorithm in order to obtain an image representing the

three-dimensional ridge structure flattened on a plane. In this case, the best quality regions of the images representing the ridge pattern obtained from the three-dimensional model and texture image are fused, obtaining the contact-equivalent image.

Another parametric method is described in [295]. The first step consists in the estimation of a sphere that approximates the finger model. Then, a linear mapping into a two-dimensional space is performed and a distortion correction algorithm based on the analysis of the distance between adjacent points is applied. The obtained result consists in a nonlinear mapping of the points appertaining to the three-dimensional model, which is used to compute the contact-equivalent image.

The non-parametric unwrapping technique described in [272] is used by different systems in the literature [284, 288, 294]. The method aims to preserve the inter-point surface distances and scale to a maximum degree. First, the fingerprint model is divided into slices along the vertical direction. Each slice is then unfolded by a resampling algorithm that tries to preserve the distances between the points appertaining to the slice. The sampling algorithm starts from the center of the slice and estimates the new (x, y) coordinates of every point according to the distance from the nearest points of the slice.

A non-parametric method based on mechanical lows is presented in [296]. The first step consists in the estimation of the finger shape by removing the presence of ridges and valleys. This step is performed by using a weighted linear least square algorithm based on weights computed by a Gaussian function. The point cloud is then considered as a mechanical system, in which every point is connected to the 8-connected neighbors with virtual springs. An iterative algorithm searches the equilibrium position for each three-dimensional point and computes the contact-equivalent image according to the estimated positions.

All the three-dimensional fingerprint unwrapping methods in the literature, however, are not able to obtain images equal to the ones captured by contact-based sensors. In order to increase the similarity between contact-equivalent images and contact-based images and to consequently increase the compatibility of the contact-equivalent images with the existing AFIS, the method presented in [297] includes a simulation of the finger pressure on a contact-based sensor. This model assumes a higher pressure in the central region and a lower pressure in the lateral regions of the finger. The unwrapping method is based on the non-parametric technique described in [272], but it determines

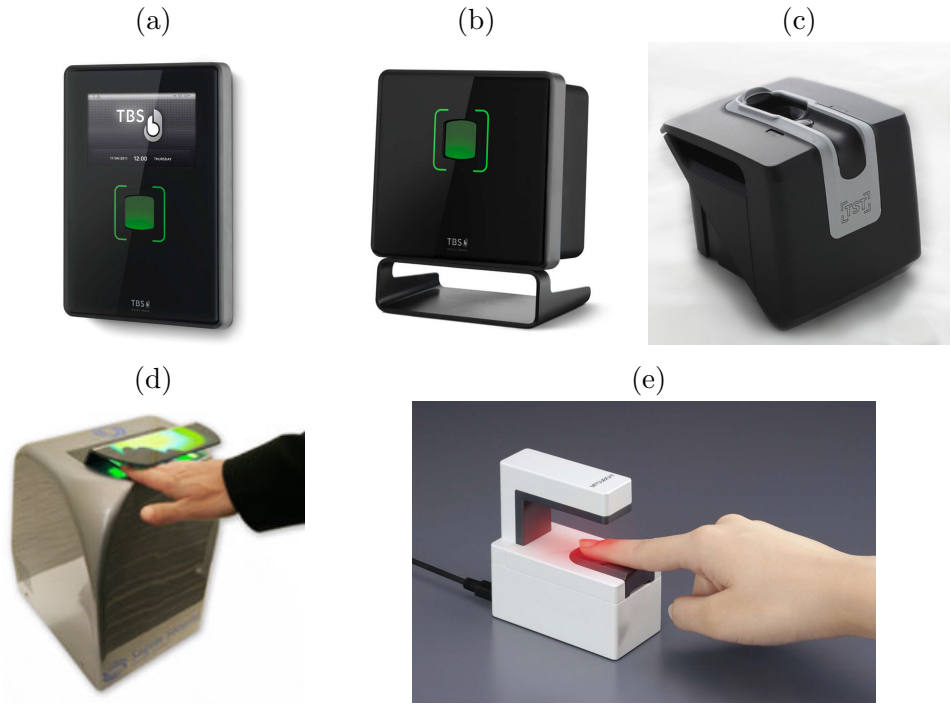

Figure 4.28: Commercial sensors for the contactless acquisition of fingerprint samples: (a) TBS 3D TERMINAL [298]; (b) TBS 3D ENROLL [298]; (c) TST BiRD 4 [299]; (d) Safran Morpho Finger on the Fly [300]; (e) Mitsubishi's Finger Identification Device By Penetrated Light [301].

a sampling interval for each point of the fingerprint according to its relative position with respect to the center of the ridge pattern. The obtained results show a greater compatibility with the existing contact-based biometric techniques compared to the contact-equivalent images obtained by other methods in the literature.

4.6.3 Applications of contactless fingerprint recognition techniques

The market analysis performed by the International Biometric Group (IGB) [23] reports that the majority of the existing biometric systems are based on the fingerprint trait.

Contactless fingerprint recognition systems are recent technologies. Most of the literature regarding these systems is related to prototypal studies, but there are also some commercial acquisition devices. Fig. 4.28 shows examples of these technologies. Most of the existing commercial systems are based on the computation of three-dimensional models [298, 299, 300]. Differently, the system proposed by Mitsubishi [301] captures

two-dimensional samples using a transmission-based illumination technique. All of these systems require that the finger is placed on dedicated supports.

Due to their recent introduction, the diffusion of contactless fingerprint technologies in real applicative scenarios is limited. Anyway, they should be adopted in all the applications that use live fingerprint acquisitions, introducing some advantages with respect to contact-based recognition systems. For example, contactless systems should be used in the governmental, commercial, and investigative sectors.

Important biometric applications in the governmental sector are the border controls. In this context, contactless techniques should permit to reduce the recognition time by using less constrained biometric acquisition procedures. Biometric documents should also be created using contactless acquisitions, which can reduce the costs of the enrollment and verification devices.

Examples of applications in the commercial sector are authentication systems integrated in ATMs, and terminal login. In this sector, the user satisfaction is a critical aspect for the diffusion of applications and services. Contactless fingerprint recognition systems should permit to increase the user acceptability of the biometric recognition process with respect to contact-based systems.

Other applications should be for investigative uses. Contactless acquisition techniques should permit to easily capture biometric samples from non-collaborative subjects with respect to contact-based acquisition systems. However, the compatibility of the contact-equivalent images obtained by contactless systems with the existing AFIS is a crucial aspect for the diffusion of contactless technologies in this applicative context. There are no studies on this aspect performed using large datasets of samples.

With respect to other biometric technologies, contactless fingerprint recognition systems should also increase the possibility to perform biometric authentications in web applications (e.g. e-banking, e-commerce, and e-government). Recognition techniques based on single fingerprint images, in fact, can obtain sufficiently accurate results using webcams or cameras integrated in mobile phones, without requiring dedicated biometric acquisition devices. Other biometric characteristics can be captured using the same devices (e.g. the face), but usually present less durability and accuracy.

The higher resolution of contactless images with respect to contact-based fingerprint images should also permit the design of new applications, like the network security protocol presented in [302].

4.7 Summary

Fingerprint biometrics is based on the analysis of the ridge pattern present on the human fingers, which is considered as one of the highly distinctive human characteristics. The fingertip ridge structure, moreover, is characterized by high durability since it is fully formed at about the seventh month of the fetus development, and it does not change for all the life unless serious accidents or diseases

Fingerprint recognition systems are the most well-known and widely used biometric technologies. The main applicative contexts of these systems are in forensics, governmental, and commercial sectors. Examples of applications in these sectors are the investigative analyses, search of lost persons, biometric documents, border controls, terminal login, and authentication systems integrated in ATMs.

The analysis of the fingerprint characteristics can be performed at three levels: global, thin, and ultra-thin. The first level evaluates the overall ridge flow. Examples of characteristics analyzed at Level 1 are the ridge orientation, local ridge frequency, singular regions, and ridge count. Level 2 analysis considers specific ridge discontinuities called minutiae. There are many different classes of minutiae, but, usually, only bifurcations and terminations are considered. In the literature, there are many studies on methods for the estimation of minutia points. The ultra-thin characteristics evaluated at Level 3 are related to small details like pores and incipient ridges. This level of analysis can only be performed on high resolution fingerprint images.

Usually, fingerprint recognition systems perform analyses of different levels in every step of the recognition process. In traditional fingerprint biometrics, this process can be divided into the sequent steps: acquisition, quality evaluation, enhancement, feature extraction, and matching. The acquisition process can produce three classes of images: latent fingerprints, inked fingerprints, and live-scan fingerprints. The quality of the captured image is then evaluated in order to discard samples that can produce erroneous recognitions. The visibility of the ridge pattern is then improved using enhancement techniques. The most used methods in the literature can be classified in pixelwise enhancement, contextual filtering, and multi-resolution enhancement. The next step is the feature extraction, which is usually based on minutia features. The final step is the matching between biometric templates. In systems based on minutia features, the matchers can consider local or global characteristics, and can use techniques designed

to overcome problems due the presence of distortions in the fingerprint images. There are also matching methods based on correlation techniques and Level 1 or Level 3 features. Identification systems can also use a supplementary classification or indexing step, which permits to reduce the number of identity comparisons. The most used fingerprint classification schema is based on five classes (arch, tented-arch, left loop, right loop, and whorl), which are estimated considering the characteristics of the ridge orientation. In the literature, there also methods for the computation of synthetic fingerprint images that can be used to design and evaluate new biometric algorithms.

Most of the fingerprint recognition systems use contact-based acquisition procedures. The obtained images, however, can present non-linear distortions and low contrast regions due to inconstant pressures of the finger on the sensor platen. In order to overcome this problem and to increase the usability and user acceptability of fingerprint biometrics, researchers are studying contactless recognition systems based on CCD cameras. Contactless fingerprint images, however, are very different from images captured by traditional sensors. Most of the contactless recognition systems therefore aim to compute contact-equivalent fingerprint images in order to use traditional feature extraction and matching algorithms and to obtain data compatible with the existing biometric databases. Contactless fingerprint recognition systems can be based on two-dimensional and three-dimensional samples. Systems based on two-dimensional samples can use different acquisition setups based on one or more cameras and dedicated illumination techniques. In these systems, the computation of contact-equivalent images is usually performed by applying image enhancement algorithms and methods for the resolution normalization. The obtained contact-equivalent images, however, usually present distortions due to perspective effects. The systems based on three-dimensional samples require more complex acquisition setups, but can generally achieve more accurate results. The samples can consist in three-dimensional models of the ridge pattern, or in models representing the finger volume with a superimposed texture representing the ridge pattern. The three-dimensional models can be obtained by using structured light approaches or multiple view techniques. In order to obtain contact-equivalent images, the three-dimensional models are mapped into a two-dimensional space by applying parametric or non-parametric unwrapping algorithms.

Contactless systems should be used in all the applicative contexts in which traditional fingerprint biometrics are applied, obtaining great advantages in terms of usability and user acceptability.

Chapter 5

Contactless Fingerprint Recognition

This chapter presents the researched methods for contactless fingerprint biometrics. An important characteristic of the studied approaches is that they do not use finger placement guides, reducing the acquisition constraints with respect to most of the contactless fingerprint recognition systems in the literature. Some implemented methods, in fact, do not use any support for the finger placement. Other realized techniques only require that the finger is placed on a desk with a fixed distance to the camera in order to control the lens focus. Using this hardware configuration, the finger can therefore be placed with uncontrolled yaw and roll orientations. Differently, most of the methods in the literature adopt finger support guides specifically designed to minimize the variability in the finger placement. Moreover, all the studied approaches are based on images captured in a single time instant in order to require a minimum level of user cooperation.

The researched approaches can be divided in methods based on two-dimensional samples and methods based on three-dimensional samples. The first class of techniques is designed for low-cost and portable applications. Differently, the methods based on three-dimensional samples permit to obtain more accurate results, but they are based on more complex hardware setups and algorithms.

The techniques described in this chapter regard different aspects of contactless biometric systems: acquisition, quality evaluation of biometric samples, computation of contact-equivalent images, matching algorithms, and computation of synthetic samples.

5.1 Contactless fingerprint recognition techniques

Methods for all the steps of the biometric recognition process based on two-dimensional and three-dimensional contactless fingerprint recognition systems have been researched. All the studied methods are designed to work in less-constrained conditions with respect to most of the contactless recognition technologies in the literature.

A schema of the researched biometric recognition techniques is shown in Fig. 5.1. Four approaches for contactless fingerprint recognition systems have been studied: approach based on two-dimensional samples; approach based on three-dimensional samples and contact-equivalent images; approach based on three-dimensional samples and three-dimensional templates; approach based on three-dimensional minutia points. Different techniques have been designed for all the steps of the biometric recognition process based on contactless fingerprint images: (I) acquisition and quality assessment; (II) computation of thee-dimensional samples; (III) computation of contact-equivalent fingerprint images; (IV) feature extraction; (V) matching.

Different acquisition setups for recognition systems based on two-dimensional and three-dimensional samples have been studied. These hardware setups do not require the use of finger placement guides, are based on one or two cameras, and are able to capture the information needed by the biometric recognition methods in a single time instant.

In order to perform biometric acquisitions in uncontrolled applications, a quality evaluation method able to estimate the best quality frames in frame sequences describing a finger that is moving toward the CCD camera have been realized.

Single contactless fingerprint images can then be directly used to compute contact-equivalent fingerprint images. The studied method for the computation of contact-equivalent images first performs an enhancement step in order to improve the visibility of the ridge pattern and to reduce the noise present in the contactless-image, and then it normalizes the image to a constant resolution. Two algorithms for the enhancement of contactless fingerprint images have been implemented. The first algorithm is designed to work in particularly noisy conditions, while the second one is more accurate ad computationally efficient. The studied resolution normalization technique is designed for fingerprint images captured at a fixed distance from the CCD camera.

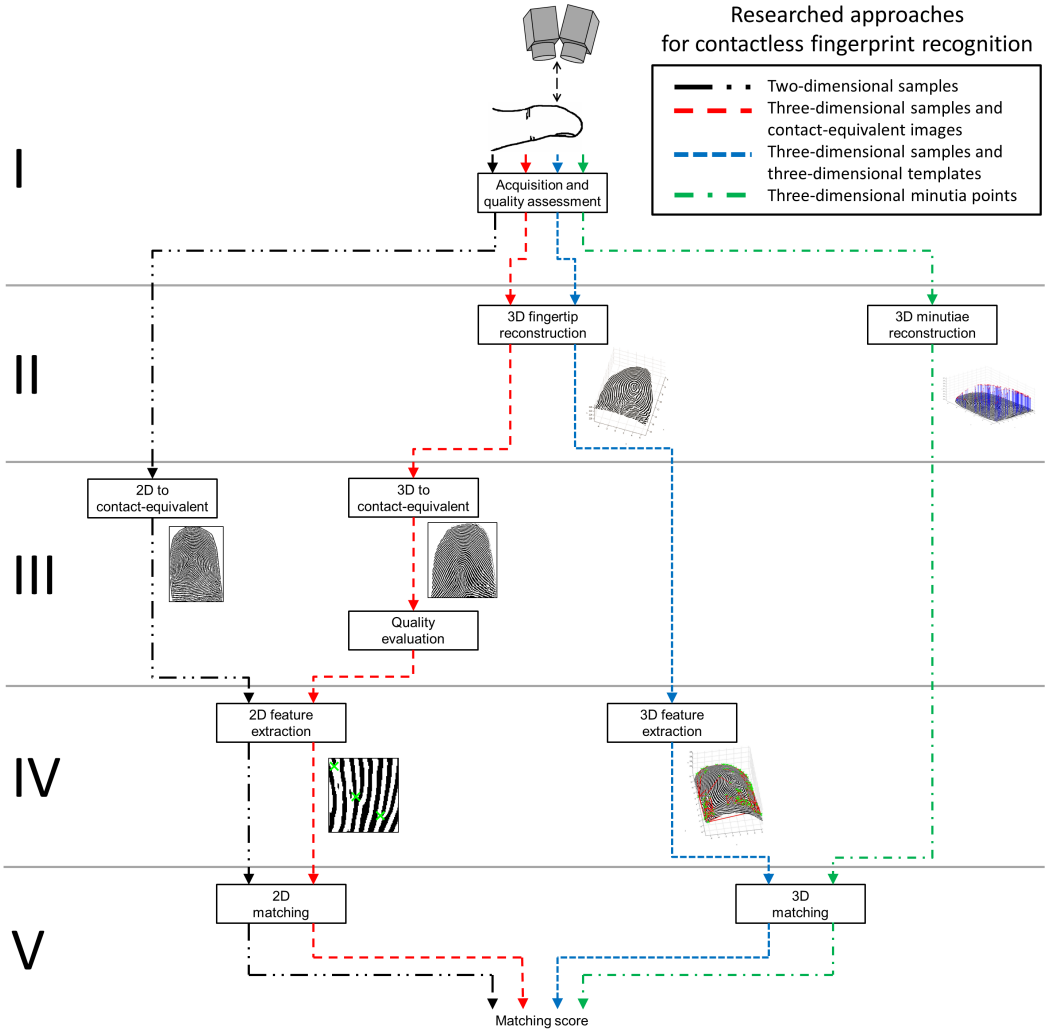

Figure 5.1: Schema of the researched approaches for contactless fingerprint recognition: approach based on two-dimensional samples; approach based on three-dimensional samples and contact-equivalent images; approach based on three-dimensional samples and three-dimensional templates; approach based on three-dimensional minutia points. Different techniques have been studied for all the steps of the biometric recognition process based on contactless fingerprint images: (I) acquisition and quality assessment; (II) computation of thee-dimensional samples; (III) computation of contact-equivalent fingerprint images; (IV) feature extraction; (V) matching.

The feature extraction and matching of contact-equivalent images obtained from two-dimensional samples is then performed by using well-known methods in the literature designed for the Level 2 analysis of contact-based fingerprint images. Differently, the evaluation of Level 1 characteristics require dedicated methods since contact-equivalent images obtained from two-dimensional contactless samples can present different non-idealities with respect to contact-based fingerprint images. An approach for the core estimation in contactless images which uses computational intelligence techniques to search the core in a list of candidate points has therefore been studied.

Different methods for the computation of three-dimensional fingerprint models have also been researched. The performed research include a method able to estimate the three-dimensional coordinates of the minutia points, and three different methods for the computation of three-dimensional models describing the complete finger surface. All the methods are based on multiple view acquisition setups. The first method can be used only to perform biometric recognitions based on matchers that consider three-dimensional features, and it is based on computational intelligence techniques. The methods for the computation of three-dimensional models describing the finger surface compute samples consisting in the three-dimensional fingerprint volume with a superimposed image representing the ridge pattern. These three-dimensional reconstruction techniques share a common computational schema: the enhancement of the ridge visibility is first performed; pairs of corresponding points are then extracted from the images obtained from the different views; a noise reduction technique is applied to the pairs of corresponding points; the three-dimensional finger volume is computed; the ridge pattern is finally estimated and superimposed to the three-dimensional model.

The matching of three-dimensional fingerprint models can be performed using algorithms that consider three-dimensional features, or applying unwrapping methods and then using techniques designed for contact-based fingerprint samples. Studies on both a matcher based on three-dimensional minutiae points, and an unwrapping technique have been performed. The three-dimensional matcher performs the comparison of Delaunay graphs computed from the three-dimensional coordinates of the minutia points. Differently, the unwrapping technique approximates the finger shape as a set of rings and then maps every ring into a two-dimensional space.

In order to improve the recognition accuracy by discarding insufficient quality samples, a quality estimation method specifically designed for contact-equivalent images

obtained from three-dimensional models have also been researched. This method is able to detect non-idealities introduced by the three-dimensional reconstruction step, and to estimate a discrete quality value by using computational intelligence classifiers.

The design and evaluation of biometric algorithms and acquisition setups require the use of big biometric databases. In order to reduce the efforts necessary to collect biometric samples, an approach for the computation of synthetic contactless fingerprint samples from contact-based images has also been studied. The method simulates three-dimensional fingerprint models obtained using different acquisition setups and illumination techniques.

This chapter is organized as follows. Section 5.2 presents the studied techniques for biometric systems based on contactless two-dimensional samples. It describes the acquisition setups, quality estimation techniques, and algorithms for the estimation of contact equivalent images. Section 5.3 discusses the researched techniques for the computation of three-dimensional models, three-dimensional matching, unwrapping of three-dimensional models, and quality estimation of contact-equivalent images obtained from the unwrapping of three-dimensional models. Finally, Section 5.4 presents the implemented approach for the computation of synthetic contactless fingerprint samples.

5.2 Methods based on two-dimensional samples

The studied approach for the acquisition and processing of contactless two-dimensional fingerprint samples is described. First, the acquisition setup is presented. Then, a quality assessment method for contactless images is analyzed. A technique for the computation of contact-equivalent images is then discussed. Finally, methods for the analysis of Level 1 and Level 2 features in contact-equivalent fingerprint images obtained from contactless two-dimensional samples are detailed.

5.2.1 Acquisition

The researched algorithms designed for contactless two-dimensional samples are based on fingerprint images captured using a single CCD camera. The acquisition setup is designed to be integrated in low-cost mobile applications. For this reason, it does not require the use of finger placement guides. Another important aspect consists in the used illumination technique. In the described applicative conditions, in fact, it is not

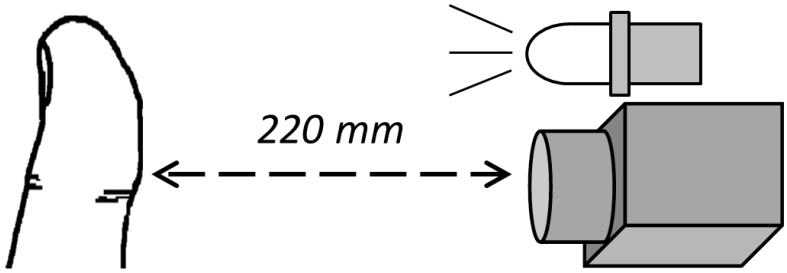

Figure 5.2: Schema of the realized hardware setup for the acquisition of contactless fingerprint images.

possible to use complex and expansive illumination systems in order to enhance the visibility of the ridge pattern. For this reason, the acquisition setup only uses a led light placed in front to the finger. Moreover, this setup is able to capture good-quality fingerprint images at a remarkable distance. All the contactless fingerprint acquisition systems in the literature require that the finger is placed at a distance of less than 100 mm from the sensor. Differently, the realized acquisition setup captures contactless fingerprint images at a distance of more than 200 mm. Fig. 5.2 shows a schema of the acquisition technique.

In order to control the lens focus and to perform metric measurements on the samples, the realized biometric recognition techniques require that the finger is placed on a desk with a fixed distance to the camera, permitting to place the finger with uncontrolled yaw and roll orientations.

In order to acquire the fingertip with a sufficient magnification/resolution, in fact, we obtained the best results with lenses with a focal of 25 mm. Unfortunately, this optical configuration permits to obtain a maximum depth of focus equal to 0.6 mm considering the pixel size of the used CCD. In acquisitions performed controlling the distance of the finger from the camera, this depth of focus is sufficient to capture good quality fingerprint samples since the blur gradually affects the ridge pattern in the lateral regions of the finger, without reducing the accuracy of the recognition process. Differently, improper placements of the finger can produce insufficient quality samples.

Anyway, the studied quality assessment technique permits to use fingerprint images captured without any restriction regarding the finger placement. In future works, it should therefore be possible to design recognition algorithms able the o work using

the best quality frames in frame sequences describing a finger moving toward the camera. The realized quality assessment technique should also permit to design autofocus methods for acquisition systems based on active cameras.

Moreover, the researched techniques for the evaluation of Level 1 features do not require particular techniques to control the distance between the finger and the camera because since they do not consider metric characteristics of the ridge pattern.

5.2.2 Quality assessment of contactless fingerprint images

Contactless fingertip acquisitions performed without finger placement guides and dedicated illumination techniques can produce poor quality images, which can cause recognition errors. Moreover, starting from hundreds of frames, only a limited number of images have sufficient quality to be effectively used in biometric systems. In order to perform this kind of biometric acquisitions in uncontrolled applications, it is therefore necessary to adopt quality assessment techniques able to discard insufficient quality images. A quality assessment approach able to search the best quality frames in frame sequences describing a finger moving toward the camera has been researched. This approach is described in [303].

A quality assessment technique for contactless fingerprint images should consider a set of non-idealities and aspects that influence the quality of the captured samples. Considered as noise effect, the environmental light can produce different shades along the fingertip due to its intrinsic convex shape. Also, blurring effects can be present due to errors in the focus of the lenses and the relative movements of the subject in front to the camera. Moreover, the electronic noise of the CCD sensor is always present and superimposed on the captured images. The quality of the captured fingerprint images is also related to the applicative context and the ability of the users.

Another important aspect is that the finger movement can cause four main non-idealities during every contactless biometric acquisition:

- the finger is too far from the capture system and the resulting ridge pattern is not clear or sufficiently detailed;
- the finger is too close to the capture system and the obtained image is blurred since the finger is out the focus range;

- the finger is placed in skewed positions with respect to the field of view of the capture system, hence the most important characteristics of the fingerprint are not visible;

- the finger is moving too fast with respect to the exposure time of the CCD, hence motion-blurred images are produced.

The goals of the studied approach are to process in real time each frame obtained by the capture system, and to produce in output a reliable estimation of the frame quality, hence permitting to the complete biometric system to select the best frame/frames from the input sequence. The quality of fingerprint images can be expressed with continuous values (e.g., ranging from 0 to 1) or with a set of discrete values that represent classes of quality. The latter technique has been proposed by the NIST [229] and encompasses 5 levels of quality, from poor to excellent. The researched quality estimation approach adopts a similar integer classification technique.

The studied approach includes two distinct methods, which are outlined in Fig. 5.3. For each captured frame, the first step of the methods is the ROI estimation. The Method QA performs an additional segmentation step, extracts a set of features, and then performs the quality classification by using computational intelligence techniques. Differently, the Method QB is based on the NIST NFIQ algorithm [233]. This algorithm, however, cannot be directly applied to contactless fingerprint images. Hence, the Method QB first computes the enhancement of the ridge pattern by applying a specific band-pass filter. The used enhancement algorithm does not permit to obtain accurate contact-equivalent images, but it permits to obtain sufficient details to perform a quality evaluation of contactless images in a computationally efficient manner. The use of computationally efficient algorithms is necessary for the integration of a quality estimation technique in real-time biometric acquisition systems.

5.2.2.1 Computation of the region of interest (ROI)

For each captured frame, the input fingerprint is processed by a method based on the local variance of the input image for detecting the presence of the ridges in the ROI of the input image. A method based on the local variance of the image divides the input image in M squared blocks $S_m(x_s, y_s)$ with fixed size. Then, the output image I_A is

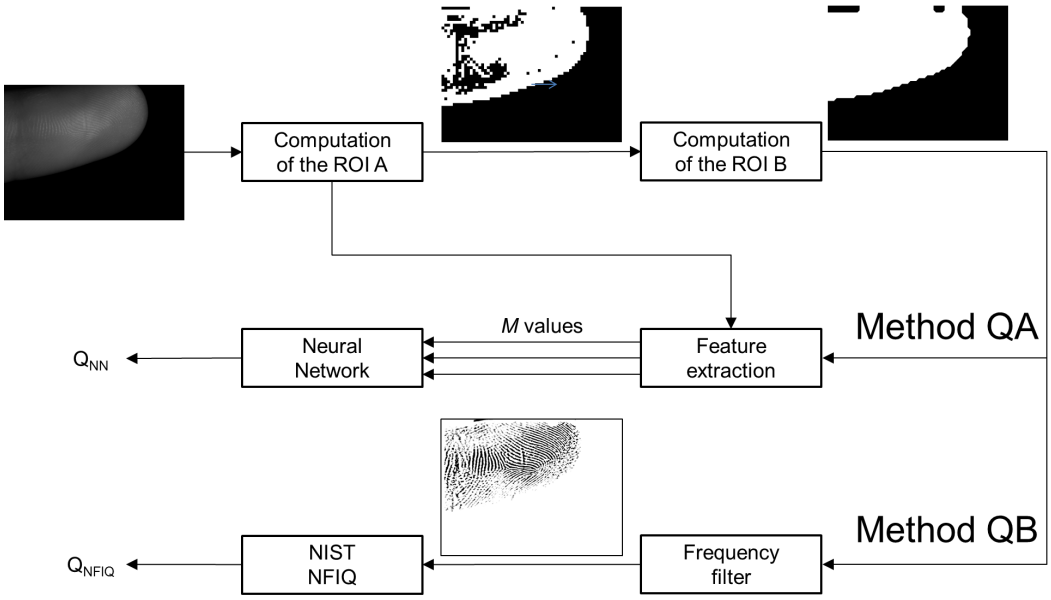

Figure 5.3: Schema of the studied methods for the quality estimation of contactless fingerprint images: the left branch of the schema describes the Method QA, the right branch of the schema describes the Method QB.

obtained by applying the following algorithm for all the M blocks

$$I_A(x,y)|_{x_s,y_s} = \begin{cases} S_b, & \text{if } \mathrm{var}(S(x_s,y_s) \leq t1), \\ 0, & \text{otherwise.} \end{cases} \tag{5.1}$$

where t_1 is a fixed threshold value, and x_s,y_s are the pixel coordinates in the selected block. In the following, we refer to ROI A as the binary image that describes $I_A(x,y) > 0$.

As a second step, the ROI A is regularized by the *flood-fill* and *open* morphological operators, obtaining the binary image I_M. The image I_B is computed by applying

$$I_B(x,y) = I_M(x,y) > 0 \tag{5.2}$$

The ROI B is equal to I_M.

5.2.2.2 Quality assessment based on computation intelligence classifiers (Method QA)

The studied quality assessment method based on computational intelligence classifiers (Method QA) first extracts a set of features from the input frames, and then it performs the quality estimation by using a neural classification system. First, a set of 45 features are computed for each frame, and then a feature selection technique is applied in order to estimate the best subset of features that maximize the classification accuracy. A brief description of the initial feature vector $F()$ is reported. We refer to I_A as the region of the image I appertaining to the ROI A, and to I_B as the region of the image I appertaining to the ROI B.

- $F(1)$: area of the ROI A;
- $F(2)$: area of the ROI B;
- $F(3)$: $F(1)/F(2)$;
- $F(4)$: standard deviation of I_A;
- $F(5)$: standard deviation of I_B;
- $F(6)$: standard deviation of the gradient phase of I_A;
- $F(7)$: standard deviation of the gradient module of I_A;
- $F(8)$: standard deviation of the gradient phase of I_B;
- $F(9)$: standard deviation of the gradient module of I_B;
- $F(10)$ - $F(11)$: coefficients of the first order polynomial that approximates the focus function $f_f()$. The focus function $f_f()$ estimates the focus level by observing the local gray-level gradient on set of candidate points placed on the edges or on the ridge points in the ROI B. This task is performed as follows:
  - the gradient module G_M and the gradient phase G_P of I_B are computed;
  - the histogram H_{GM} of G_M is computed;

- the cumulative frequency f_{cum} of H_{GM} is obtained by the formula

$$f(j) = H_{GM}(j) / \left(\sum_{i=0}^{255} H_{GM}(i) \right), \tag{5.3}$$

$$f_{cum} = \sum_{j=0}^{i} f(j); \tag{5.4}$$

- the threshold intensity t is computed as

$$t = \underset{0 \leq i \leq 255}{\operatorname{argmax}} \left(f_{cum}(i) \right); \tag{5.5}$$

- the set of candidate points C_M is created as

$$C_M(x, y) = G_M(x, y) \geq t; \tag{5.6}$$

- a random subset R_{CM} of the set C_M is computed;
- for each point (x, y) of R_{CM}, a segment s is computed with center in (x, y), fixed length, and angle normal to the value of the coordinates (x, y) in G_P;
- the histogram H_s of the intensity of the segments s_i in the image G_M is computed;
- the focus function $f_f()$ is estimated as

$$f_f() = \sum_{j=0}^{255} f(H(j)); \tag{5.7}$$

- $F(12)$ - $F(14)$: coefficients of the second order polynomial that approximates the focus function $f_f()$. The function $f_f()$ is computed in equal fashion to the features $F(10)$ and $F(11)$;

- $F(15)$ - $F(24)$: values obtained by computing the Fourier Discrete Transform of I_A. The computation of the Fourier feature can be divided into the sequent steps:
  - all the rows of I_A are concatenated in order to produce a linear vector V_C;
  - the discrete Fourier transformation V_F of V_C is computed;
  - the vector V_S is computed by shifting the zero-frequency component of V_F in the central position of the vector. The number of elements in V_F is called N_F;

– the Fourier feature is computed as

$$\text{Fourier feature} = \sum_{j=N_F-N}^{N_F-1} \left| V_S\left(j+1\right) - V_S\left(j\right) \right|, \tag{5.8}$$

where N is the number of the considered frequencies.

The used values of N are $[50, 100, 150, 200, 250, 300, 350, 400, 450, 500]$.

- $F\left(25\right)$ - $F\left(34\right)$: values obtained computing the Fourier feature of I_B, using N equal to $[50, 100, 150, 200, 250, 300, 350, 400, 450, 500]$ respectively. The Fourier feature is computed in equal fashion to computation of the features from $F\left(15\right)$ to $F\left(24\right)$;

- $F\left(35\right)$ normalized gray level differences in the image I, computed as follows

$$\Delta = \left(\max\left(I\right) - \min\left(I\right)\right) / \left(\max\left(I\right) + \min\left(I\right)\right); \tag{5.9}$$

- $F\left(36\right)$: modulation of the I_B;

- $F\left(37\right)$: Signal to Noise Ratio (SNR) of I_A computed as μ/σ, where μ and σ are the mean and the standard deviation of the image;

- $F\left(38\right)$: SNR of I_B;

- $F\left(39\right)$: Gabor feature of the I_A. Gabor filters with different angles can enhance the ridges that have similar angulations in the fingerprint images. When the ridges are not sufficiently visible, the response of Gabor filters is lower. The Gabor feature is computed as the mean of the standard deviation of the images obtained by applying 8 Gabor filters with different orientations to the ROI. The used angles are $[0, \pi/8, 1/4\pi, 3/8\pi, 1/2\pi, 5/8\pi, 3/2\pi, 7/8\pi]$;

- $F\left(40\right)$: Gabor feature of I_B. The Gabor feature is computed in equal fashion to the feature $F\left(39\right)$;

- $F\left(41\right)$: mean of the local entropy of I_A. For each pixel of an image I, the entropy is computed in a 9×9 neighborhood, obtaining the local entropy image L_E. The

local entropy is computed starting from the histogram $H_{(x,y)}$ of the local area centered in (x, y)

$$L_E(x,y) = -\sum_{i=0}^{255} H_{(x,y)}(i) \times \log_2\left(H_{(x,y)}(i)\right); \tag{5.10}$$

- $F(42)$: mean of the local entropy L_E of I_B;
- $F(43)$: standard deviation the local entropy L_E of I_A;
- $F(44)$: standard deviation the local entropy L_E of I_B;
- $F(45)$: global entropy of the normalized image I_{norm} obtained by mapping the intensity values of I_{norm} from 0 to 1.

The feature extraction step aims to show different parameters that can be used to estimate the focus level of the image. Depending on the available data/setup, different subsets of the proposed parameters should produce the best performance of the system in terms of accuracy and computational complexity.

Then, we discuss the methods designed to automatically search for the best subset of features with respect to the available data. We consider the approach based on wrapper algorithms [304, 305]. We use both classical greedy feature selection algorithms (like Sequential Forward Selection, Sequential Backward Selection) and a custom wrapper [306], obtaining remarkable accuracy improvements and reduction of the feature set complexity.

The exact relationship between the extracted features and the frame quality is not well known; hence it is not possible to directly produce an algorithm for a classification system. The capability of the neural classifiers to learn complex input-output relationships from examples can be here exploited to estimate the frame quality. Feedforward artificial neural networks are then applied to estimate frame quality and compared with some classical classification systems, such as k-Nearest-Neighbor (kNN) classifiers, and linear/quadratic discriminant classifiers.

5.2.2.3 Quality assessment based on literature techniques designed for contact-based samples (Method QB)

This method computes an enhanced image of the ridge pattern E starting from the input frame I, and then it evaluates the quality of this image by executing the NIST NFIQ algorithm [233]. The image E is obtained by computing the inverse Fourier transform of the product of the transformed image I and the frequency mask M:

$$E = \mathscr{F}^{-1}\left(\mathscr{F}\left(I_A\left(x,y\right)\cdot M\right)\right). \tag{5.11}$$

The mask $M\left(u,v\right)$ is computed as

$$M\left(u,v\right) = \exp\left\{\left(u^2+v^2\right)/r\right\} - \exp\left\{\left(u^2+v^2\right)/\alpha r\right\}, \tag{5.12}$$

where u and v are the x and y image spatial frequencies in the frequency spectrum, the parameter r is set according to the mean spatial frequency of the ridges in the images, and the parameter α is the spatial frequency bandwidth of the filter.

The final estimation of the frame quality is then given by analyzing the transformed image E with the algorithm NIST NFIQ [233]:

$$Q_{NFIQ} = \text{NIST NFIQ}\left(E\left(x,y\right)\right). \tag{5.13}$$

The filter in (5.11), (5.12) produces images where only the spatial wavelengths related to the ridge pattern are enhanced (Fig. 5.3, right branch). The obtained images are compatible with classical approaches for the quality estimation of contact-based fingerprint images. We decided to use the NFIQ method since it is a standard reference algorithm in the literature. This software returns five integer quality classes. The best image quality corresponds to the class 1. More details are reported in Section 4.5.

5.2.3 Computation of contact-equivalent images

The approach studied for the computation of contact-equivalent fingerprint images from contactless acquisitions can be divided into two steps: image enhancement, and resolution normalization.

The image enhancement is applied in order to obtain gray scale images representing only the ridge pattern, and to reduce the noise present in the contactless fingerprint images. Two image enhancement techniques designed for working in different applicative

contexts have been studied. These techniques only consider gray-scale images in order to be usable with a great variety of acquisition setups. Method EA is designed for particularly noisy images and permits to overcome many non-idealities due to uncontrolled acquisition conditions. Differently, Method EB is designed to be more computationally efficient with respect to Method EA. Moreover, Method EB can be applied in systems able to capture good quality contactless images, obtaining more accurate results with respect to Method EA.

The last step is the resolution normalization and permits to obtain a contact-equivalent image compatible with biometric algorithms designed for contact-based fingerprint images by normalizing the enhanced image to a resolution of about 500 ppi. This step assumes that the fingerprint images are captured at a constant distance to the camera.

5.2.3.1 Enhancement based on contextual filters (Method EA)

The realized enhancement technique based on contextual filters (Method EA) is designed to perform the enhancement of fingerprint images captured in uncontrolled applicative contexts, and can be divided into four distinct steps:

1. ROI estimation;
2. enhancement of the ridge visibility;
3. enhancement of the ridge pattern;
4. image binarization.

Fig. 5.4 shows the schema of the method.

The ROI estimation is performed by using an algorithm based on the local standard deviation of the image [181], and by removing the shadow of the finger by a threshold operation.

The second step of the method is the enhancement of the ridge visibility. First, the background image I_B is estimated by applying a morphological opening operation with a mask s to the image I. Then, the background is removed, obtaining the image I_R. In order to reduce the noise present in the images, we perform a nonlinear equalization by processing the logarithm of I_R. An image I_L is then computed as $I_L(x, y) = \log(I_R(x, y))$.

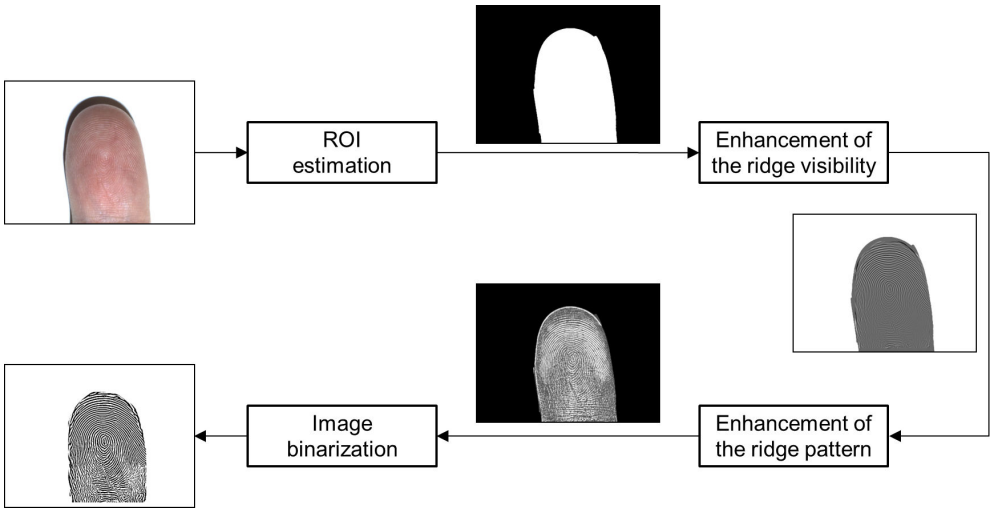

Figure 5.4: Schema of the studied method for the enhancement of contactless fingerprint images based on contextual filters (Method EA).

The third step is the enhancement of the ridge pattern. Similarly to the work proposed in [181], this algorithm estimates a ridge frequency map, a ridge orientation map, and applies a set of Gabor filters tuned according to the computed maps. The obtained result is the image I_E.

The last step consists in the image binarization. This step permits to reduce the noise present in the edges of the ridge pattern described in I_E, and to properly estimate the minutiae points. In order to obtain a uniform contrast between ridges and valleys, the logarithm of I_E is computed as $I_I(x,y) = \log\left(I_E(x,y)\right)$. Then, the histogram H of I_I is computed, and a binary image of the ridge pattern I_B is obtained as follows

$$I_B\left(x,y\right) = \begin{cases} 0 & \text{if } I_I\left(x,y\right) \leq \underset{i}{\operatorname{argmax}}\left(H\left(i\right)\right) \\ 1 & \text{otherwise} \end{cases} . \tag{5.14}$$

5.2.3.2 Enhancement based on the ridge following (Method EB)

The researched enhancement technique based on the ridge following approach (Method EB) is more computationally efficient and accurate with respect to Method EA. This method, however, can only be used in applications able to capture good quality contactless images.

The enhancement method can be divided into three steps:

1. ROI estimation;
2. enhancement of the ridge visibility;
3. enhancement and binarization of the ridge pattern.

The steps 1 and 2 are performed using the same algorithms adopted by Method A.

Differently, the third step performs the enhancement and binarization of the ridge pattern using the ridge following technique implemented by the NIST MINDTCT software [199]. This algorithm directly computes the binary image of the ridge pattern I_B by evaluating the shape of every ridge of the image I_L.

5.2.3.3 Resolution normalization

The studied resolution normalization technique assumes that the contactless fingerprint images are captured at a constant distance Δ_d from the camera.

This method first estimates the resolution of the captured images by evaluating the size of the plain captured at a distance Δ_L from the camera, and then it normalizes the contactless image to a resolution of 500 ppi.

Considering the plain perpendicular to the camera and distant Δ_L from the CCD, r_x inch along the horizontal diction of this plain correspond to i_x pixel along the horizontal diction of the captured images. The normalization factor is therefore estimated as

$$n_f = i_x / (r_x * 500) . \tag{5.15}$$

5.2.4 Analysis of Level 1 features in contactless fingerprint images

A Level 1 analysis technique able to estimate the position of the core point in contactless fingerprint images has been researched. The method is described in [307].

The accuracy of the core localization is a critical factor that strongly impacts on the overall accuracy of many biometric systems that require a common reference point to perform the fingerprint recognition. In these systems, all the subsequent processing steps are related to the position of the core point.

The researched approach selects the core from a list of singular regions obtained by the Poincaré method [185]. This task is particularly complex in contactless fingerprint

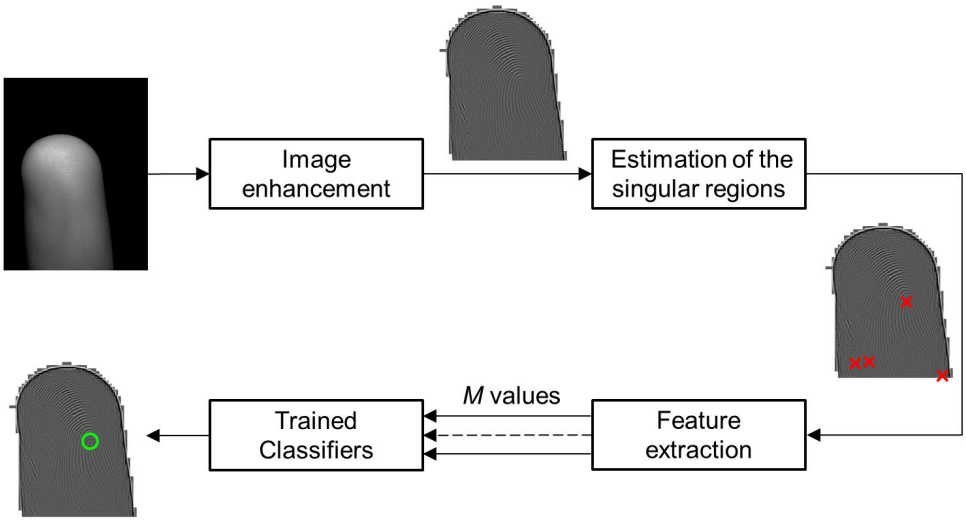

Figure 5.5: Schema of the researched core selection method.

images captured in uncontrolled conditions because the Poincaré method can return many false singularities. When there are not singular regions in the fingerprint image, the maximum curvature point of the image is selected. The researched approach consists in computational intelligence techniques capable to estimate the coordinates of the core point in fingerprint images that are captured using contactless technologies. The method can also be applied to contact-based fingerprint images with satisfactory results.

The schema of the method is shown in Fig. 5.5 and can be divided into four steps:

1. image enhancement;
2. estimation of the singular regions;
3. feature extraction;
4. core point estimation.

First, the image enhancement reduces the noise present in the contactless image and improves the contrast between ridges and valleys. This step is performed using the Method EA (Section 5.2.3.1).

Then, a list of the singular regions is obtained by a method based on the Poincaré algorithm. In the case of fingerprints that do not present singularities, the method returns the list of the maximum curvature points.

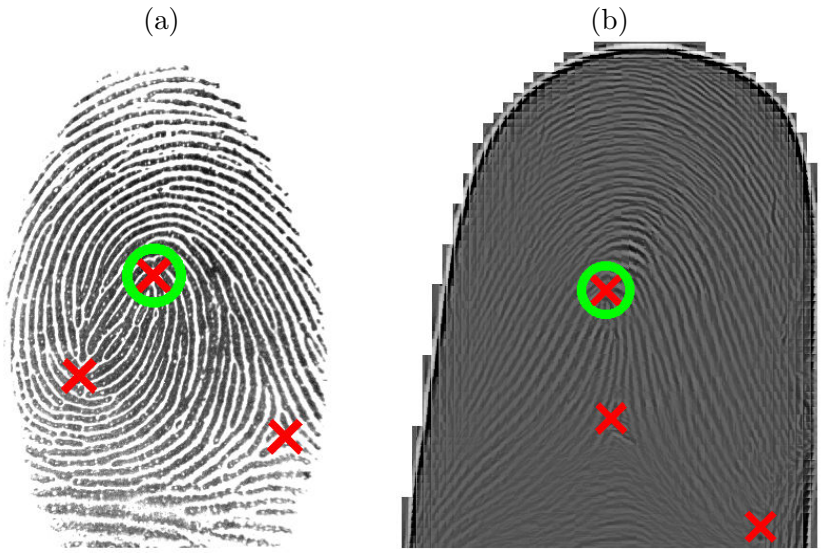

Figure 5.6: Application of the method for the core estimation on: (a) a fingerprint image captured using a contact-based sensor; (b) a fingerprint image captured using a contactless technique. The X markers represent the singular regions, and the O markers represent the core points.

The third step consists in the feature extraction. In this step, the fingerprint images are categorized with the software NIST PCASYS [199] into the classes of (1) arch, (2) left loop, (3) right loop, (4) scar, (5) tented arch, and (6) whorl. The fingerprint class is a very important information for the selection of the core point because it describes the global curvature of the ridges by using a single integer value. Other features consist in the position of the singular regions in different coordinate systems, and in a measure of the quantity of the information contained in the local region of the point.

Finally, the position of the core point is estimated by computational intelligence techniques. These methods extract the core from the list of the singular regions by processing the input features. Fig. 5.6 shows an application of the method on a contact-based fingerprint image and a contactless image.

5.2.4.1 Estimation of the singular regions

The following algorithm returns the list of the singular region coordinates and the type of every singularity. It is based on the Poincaré technique, and can be divided into the sequent steps.

- A ridge orientation map Ω is computed with the algorithm proposed in [185].
- The centroid $c_{ROI}(x, y)$ of the ROI is computed.
- The map of the Poincaré indexes P of the image I is computed.
- A binary image B_L of the candidate loop points is computed as:

$$B_L(x, y) = \begin{cases} 0 & \text{if } 180 - t_L < I_P(x, y) < 180 + t_L \\ 1 & \text{otherwise} \end{cases}, \tag{5.16}$$

  where t_L is an empirically threshold value.
- A binary image B_D of the candidate delta points is computed as:

$$B_D(x, y) = \begin{cases} 0 & \text{if } -180 - t_D < I_P(x, y) < -180 + t_D \\ 1 & \text{otherwise} \end{cases}, \tag{5.17}$$

  where t_D is an empirically threshold value.
- The vector of the loop points V_L is computed as the centroids of the 8-connected regions in B_L.
- The vector of the delta points V_D is computed as the centroids of the 8-connected regions in B_D.
- The final vector of the singular regions S is obtained by sorting V_L and V_D by the distance from $c_{ROI}(x, y)$, and merging them.
- If S is empty, the coordinates of the maximum value of P nearest to $c_{ROI}(x, y)$ are putted in S.

5.2.4.2 Feature extraction

Global and local features are computed from the input images. The first of them consists in the fingerprint class obtained by the software PCASYS [233] of the National Institute of Standard and Technologies (NIST). This information describes the global structure of the ridges. The software categorizes the fingerprint images in six classes: (1) arch, (2) left loop, (3) right loop, (4) scar, (5) tented arch, and (6) whorl. The method is based on a neural network classifier. The obtained results are ordered in a numeric vector by similarity in order to reduce the effect of the possible errors on the final system. We also use the returned probability of the classification as a feature.

For each image, we consider V_{SP} as the vector that contains all the singular points of the fingerprint. First, V_{SP} is sorted by type of singularity (loop and delta), and then the vector is sorted again by considering the proximity of the singular point from the centroid of the ROI. Only the first M singularities of the sorted vector V_{SP} are considered in the subsequent processing steps. As a consequence, if the algorithm estimates the presence of more singular regions far from the centroid, with high probability they can be considered as false positive and then discarded from further processing. For each of these points, we compute the following features.

- The point coordinates (x_O, y_O) in the original image.
- The point relative coordinates (x_R, y_R) expressed in percentage with respect to the maximum dimension of the ROI.
- The polar coordinates (ρ_O, θ_O) with respect to the centroid of the ROI.
- The angle θ_R of the SP relative to the orientation of the fingerprint α, as

$$\theta_R = \theta_O - \alpha; \tag{5.18}$$

  where α is computed as the angle from the ROI the y axis of the image.
- The mean and standard deviation of the pixels in the circle with radius r and center in the coordinates (x, y) of the singular point. These features permit to evaluate the presence of ridges in the local area of the singular region.
- The coordinates (x_c, y_c) of the centroid of the fingerprint and the angle α.

- The index of the singular region nearest to the top of the finger.
- The index of the singular region nearest to the centroid of the ROI.

The total number of the features computed for each image is $7 + 11 \times M$.

5.2.4.3 Estimation of the core using computational intelligence techniques

For each fingerprint image, the computed features are used as inputs of computational intelligence techniques, which estimate the index of the singularity corresponding to the core point. Different classifiers have been considered. More details are reported in the experimental result section (Section 6.2.3).

5.2.5 Analysis of level 2 features in contactless fingerprint images

As described in Chapter 4, most of the contact-based fingerprint recognition systems in the literature are based on the analysis of Level 2 features. Usually, these methods estimate the minutia coordinates and angles, and then perform the matching by searching the corresponding points in two or more templates. In most of the cases, this step is based on the analysis of the Euclidean distance between pairs of points.

Contactless biometric systems based on acquisition setups that do not use finger placement guides, however, can capture images with different magnifications due different placements of the finger during the acquisition step. Matching techniques based on the evaluation of the distances between minutia points should therefore be performed only after a resolution normalization step.

The studied approach for the evaluation of Level 2 features of contactless fingerprint images is based on well-known algorithms in the literature. Minutia features are first extracted from contact-equivalent images obtained by applying the method described in Section 5.2.3. The used minutia estimation technique is the software NIST MINDTCT [199]. The obtained templates are then compared using the software NIST BOZORTH3 [199]. Details about the algorithms NIST MINDTCT and NIST BOZORTH3 are provided in Chapter 4.

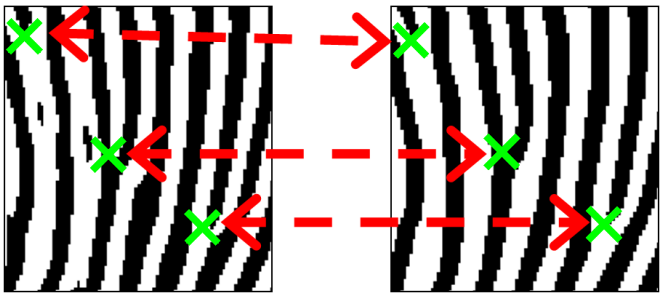

Figure 5.7: Example of minutiae pairs in different views of the same finger.

5.3 Methods based on three-dimensional models

This section presents the studied approaches for the acquisition and elaboration of contactless three-dimensional fingerprint samples. First, a method for the three-dimensional reconstruction of minutia points is detailed. Then, three different methods for the three-dimensional reconstruction of the finger surface are discussed. Feature extraction and matching techniques based on the three-dimensional coordinates of minutia points are then described. A method for the computation of contact-equivalent images by unwrapping fingerprint three-dimensional models and a technique for the quality evaluation of contact-equivalent images computed from three-dimensional models are finally described.

5.3.1 Three-dimensional reconstruction of minutia points

The realized method for the three-dimensional reconstruction of minutia points is presented in [308]. This method permits to search the corresponding minutia pairs in contactless fingerprint images and then estimate their three-dimensional coordinates. In particular, a new minutiae matcher based on neural networks and designed for contactless fingerprint images is described. This method is capable to identify two candidate sets of minutiae from two contactless images, and then select the final list of minutiae pairs. Fig. 5.7 shows an example of the input and output of the studied system, where the arrows show three identified pairs of minutiae, which can then be used to compute the corresponding three-dimensional points.

The researched approach can work with images related to the different views and captured simultaneously using N cameras, or with frame sequences captured using

a single camera at different viewpoints. The three-dimensional characteristics of the minutia points can then be directly used as a biometric template that fuses the information related to the different views at the feature level.

Considering two minutia points extracted from two fingerprint images, the studied approach is capable to estimate if these points belong to the same minutiae in the real finger. In this approach, the images captured by contactless sensors are first enhanced and segmented. Second, the minutiae positions are estimated using a well-known algorithm in the literature. Then, a set of features capable to describe the local discriminative intensity pattern are computed for each minutia. The final comparison is processed by using trained neural networks able to evaluate the differences between the local features of the candidate minutiae pairs. The obtained pairs of points are then used to compute a template representing the three-dimensional minutiae. A matcher able to compare three-dimensional features can then be used to compute the matching score within two templates. Fig. 5.8 shows the schema of the studied approach.

5.3.1.1 Acquisition

The schema of the used acquisition setup is shown in Fig. 5.9. The setup consists in two cameras placed at a distance Δ_H from the finger. The distance Δ_H is controlled by using a desk for the finger placement. Using this hardware configuration, the finger can therefore be placed with uncontrolled yaw and roll orientations. The parameter α is the tilt angle of the cameras. The values of Δ_H and α are empirically tuned for each performed experiment. The used illumination technique consists in a white led.

5.3.1.2 Image preprocessing

For each considered fingerprint image, the enhancement step is first performed. The used technique is the Method EA (Section 5.2.3.1), which permits to reduce the noise and increase the contrast of the ridge pattern.

5.3.1.3 Minutiae estimation

The minutia positions are estimated by the software NIST Mindtct [199]. For each minutia, the output of the method are the Cartesian coordinates, the angle θ of the ridge related to minutia, and the quality of the minutia points.

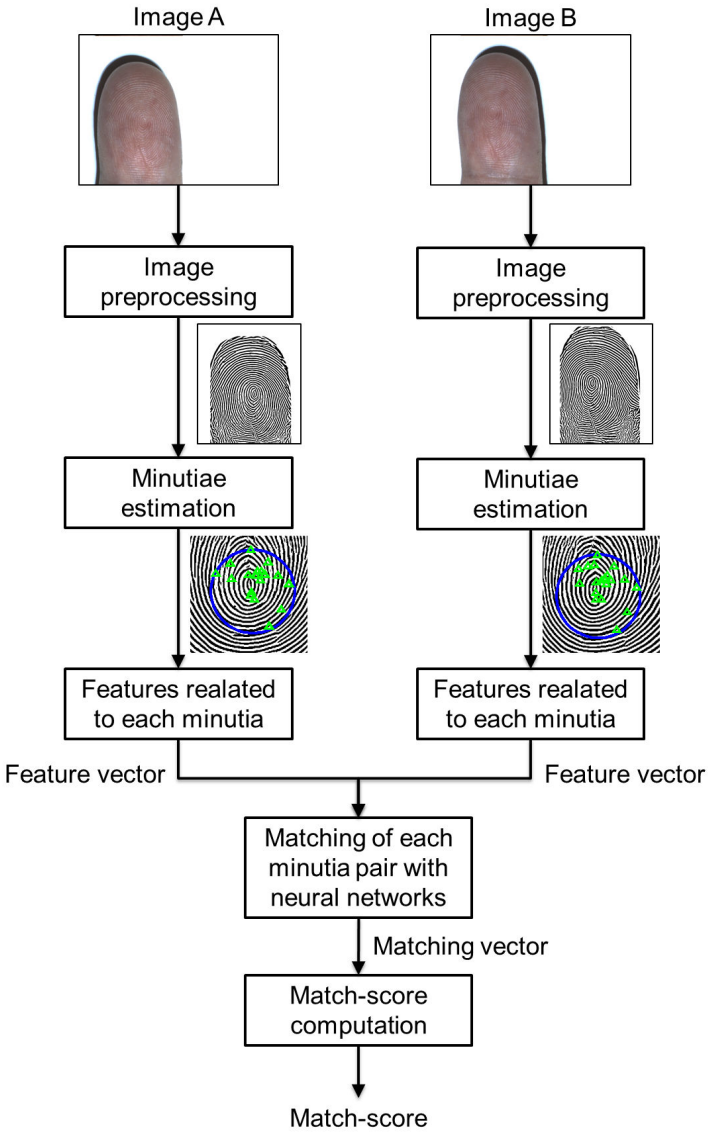

Figure 5.8: Schema of the realized method for the search of corresponding minutia points in contactless fingerprint images by using computational intelligence techniques.

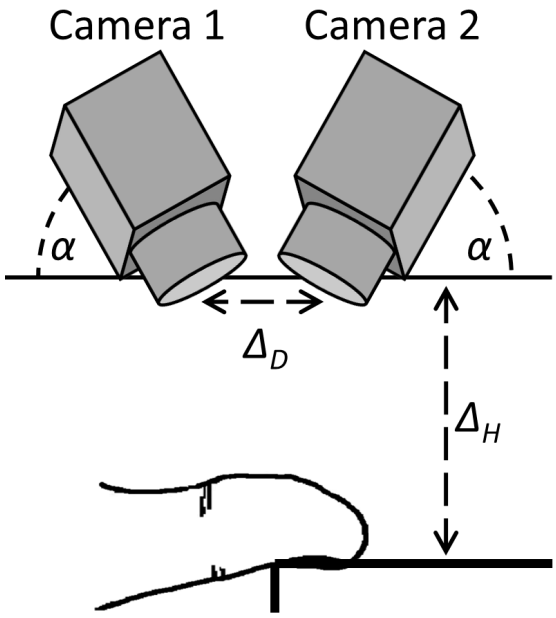

Figure 5.9: Schema of the realized acquisition setup for the computation of three-dimensional minutia points.

5.3.1.4 Computation of features related to each minutia

For a fingerprint image A, three different matrices of local feature (M_A, F_A, H_A) are computed. The values of these matrices are related to the local areas centered in every minutia point i.

The matrix M_A is related to the data obtained by the software Mindtct and is composed by the sequent elements.

- $M_A(i, 1)$: the x-coordinate of the point.
- $M_A(i, 2)$: the y-coordinate of the point.
- $M_A(i, 3)$: the minutia angle α normalized considering the median ridge orientation

$$\alpha = \beta + \theta, \tag{5.19}$$

  where β is the median value of the ridge orientation map computed from the fingerprint image.

- $M_A(i, 4)$: the estimated quality of the minutia.

The matrix F_A is composed by n_F elements obtained by the computation of the local Fingercode around each minutia point. This template is obtained by applying a method similar to the one described in [193] and is divisible in the sequent steps.

- A local ROI is defined as a circle with fixed size (height h) centered in the coordinates of the considered minutia point (x_i, y_i).
- The local ROI is tasseled in n_R rings and n_A arcs, obtaining $n_S = n_R \times n_A$ sectors S_i.
- A set of n_F Gabor filters with different directions are computed using (4.3), and then applied to the local area of the fingerprint image. The obtained result consists in n_F filtered images $T_{k\theta}$.
- A matrix of values $V(k, \theta)$ is obtained by computing the AAD (4.6) on each sector of the filtered images $T_{k\theta}$.

For each minutia, the obtained feature vector is composed by $n_F = n_S \times n_F$ values. Considering that the template Fingercode is not rotational-invariant, the feature matrix F_A is computed according the value of median ridge orientation β.

The matrix h_A is obtained by computing a set of Histogram of Oriented Gradients (HOG) features in a fixed size area ($n_p \times n_p$ pixels) around each minutia point i. The computation of the HOG features is performed by applying the method described in [309]. HOG features are gradient features designed for general object recognition. This method can be divided into the sequent steps.

- The gradient module image G_M and the gradient phase image G_P of the image I are computed.
- The images G_M and G_P are divided into $c_w \times c_h$ cells.
- At each cell, the orientation $\tilde{G}_p$ is quantized into c_b orientation bins, weighted by the magnitude G_M.
- The histogram with the c_b orientations is computed for each cell.

For each minutia i, $c_w \times c_h \times c_b$ features are obtained.

5.3.1.5 Classification of minutiae pairs

The pairs of minutiae estimated from the different views of the same finger are compared using computational intelligence techniques in order to estimate if they represent the same point of the fingertip. The obtained result consists in a binary classification ("corresponding points", "non-corresponding points"). More details are reported in the experimental results section (Section 6.3).

5.3.1.6 Three-dimensional reconstruction of minutiae pairs

Using a calibrated acquisition system, it is possible to compute a metric reconstruction of the three-dimensional coordinates of the minutiae pairs [292]. The depth coordinate of each three-dimensional point can therefore be estimated by using the triangulation formula:

$$z = \frac{fT}{x_A - x_B} \tag{5.20}$$

where f is the focal length of the two cameras, T is the baseline distance between the two cameras, and x_A and x_B are the two matched points.

5.3.2 Three-dimensional reconstruction of the finger surface

The methods in the literature for the computation of three-dimensional fingerprint samples use complex and constrained setups. They can be based on multiple cameras, special mirrors, and structured light illumination systems. All of them require that the finger is exactly placed and held still during the time needed to perform the acquisition.

A novel approach able to obtain a three-dimensional reconstruction of the fingertip in less constrained conditions than the ones proposed in the literature has been researched. This approach permits to obtain three-dimensional fingerprint samples without using finger placement guides and is based on multiple view images captured at a single time instant.

Three methods for the computation of three-dimensional fingerprint samples based on different acquisition setups have been realized.

- **3D Method A**: the three-dimensional reconstruction is based on a two-view acquisition system and on a static projected pattern. The use of the projected pattern aims to reduce the time needed for the computation of the three-dimensional models.

- **3D Method B**: the acquisition setup is composed by a two view-system and a white led light. This setup is designed to be integrated in low-cost applications.
- **3D Method C**: this method captures fingerprint images using a two-view acquisition technique and uses a diffused blue light in order to obtain images with a good quality ridge pattern.

The methods for the computation of three-dimensional fingerprint samples 3D Method A and 3D Method B are presented in [310].

The studied three-dimensional reconstruction methods present differences in the used algorithms and acquisition setups, but it is possible to define a common computational schema:

1. camera calibration;
2. image acquisition;
3. image preprocessing;
4. reference point extraction and matching;
5. matching of the corresponding pairs of points by cross-correlation;
6. refinement of the pairs of reference points:
7. three-dimensional surface estimation and image wrapping;
8. texture enhancement.

The schema of the studied three-dimensional reconstruction approach is shown in Fig. 5.10.

5.3.2.1 Camera calibration

The calibration step is performed off-line once, before the acquisition step, and uses the algorithms described in [311, 312] in order to compute the intrinsic and extrinsic parameters of the two-view setup. The used calibration object is a chessboard, which is captured in different positions. The obtained images are then processed by using a corner detection algorithm. The DLT method described in [292] is used to compute the homography matrix.

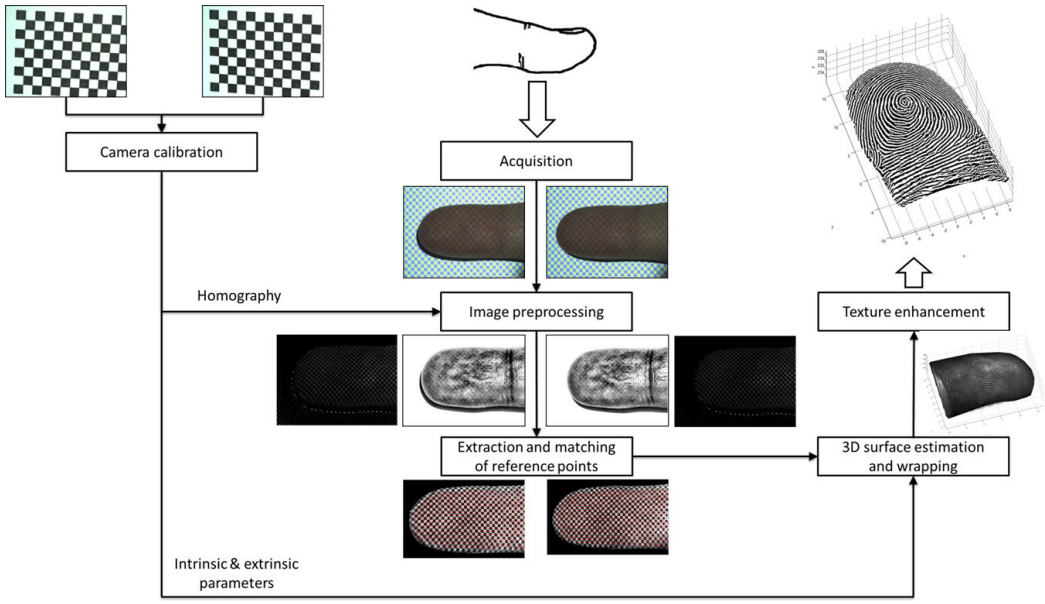

Figure 5.10: Schema of the studied approach for the three-dimensional reconstruction of the finger surface.

5.3.2.2 Image acquisition

The realized acquisition setups are shown in Fig. 5.11. These setups require that the finger is placed on a desk with a fixed distance to the cameras in order to control the lens focus. Using this hardware configuration, the finger can therefore be placed with uncontrolled yaw and roll orientations. The 3D Method A is based on a fixed projected pattern, which permits to perform fast three-dimensional reconstructions. The 3D Method B uses only a white led light to enhance the visibility of the ridge pattern in order to be used in low-cost applications. Differently, the 3D Method C uses a diffused blue light in order to better enhance the visibility of the ridge pattern.

- **3D Method A**

  An image of the projected pattern is shown in Fig. 5.12. The colors of the chessboard are computed starting from a uniform RGB image:

$$R(x,y) = G(x,y) = B(x,y) \quad \forall\,(x,y) \quad . \tag{5.21}$$

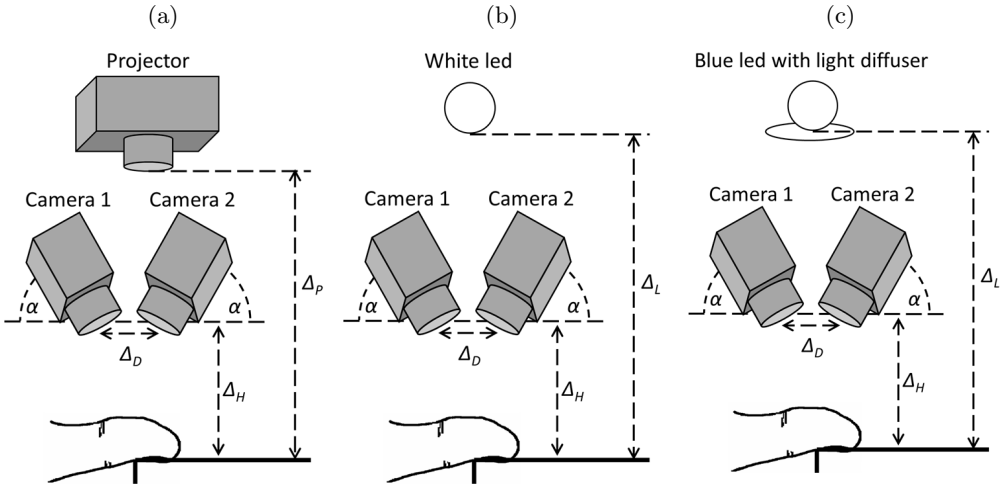

Figure 5.11: Schema of the acquisition setups used for the computation of three-dimensional fingerprint models: (a) 3D Method A; (b) 3D Method B; (c) 3D Method C.

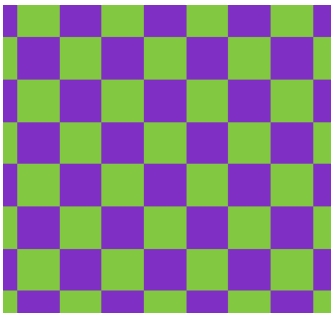

Figure 5.12: Portion of the projected pattern used by the 3D Method A.

The green and blue squares are obtained by summing and subtracting a constant value Δ_P to the G and B channels of the projected image:

$$\begin{cases} G_P(x,y) = G(x,y) + \Delta_P \\ B_P(x,y) = B(x,y) - \Delta_P \end{cases} \text{if } (x,y) \in \text{Green square}$$
$$\begin{cases} G_P(x,y) = G(x,y) - \Delta_P \\ B_P(x,y) = B(x,y) + \Delta_P \end{cases} \text{if } (x,y) \in \text{Blue square} \ , \tag{5.22}$$

where G and B are the green and blue channels of the image, G_P and B_P are the green and blue channels of the resulting chessboard pattern (Fig. 5.12). Fig. 5.13 shows an example of finger images obtained from the two cameras of the system by using the described projected pattern.

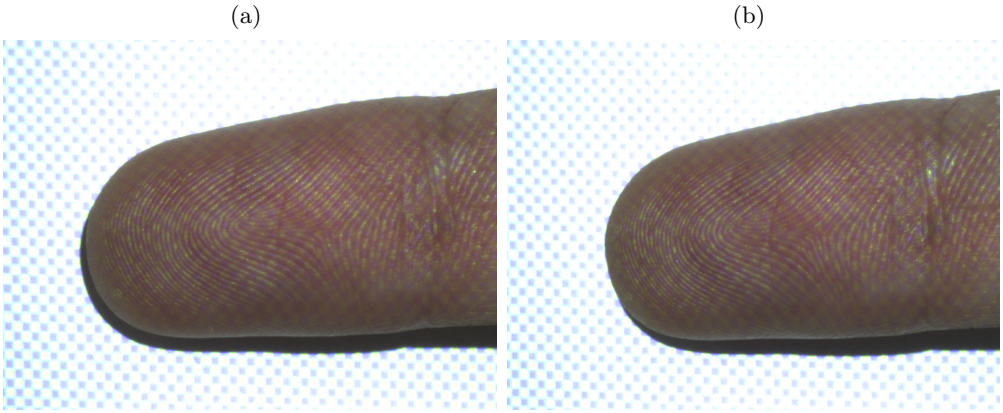

Figure 5.13: A two-view acquisition obtained using a static projected pattern (3D Method A).

Figure 5.14: A two-view acquisition obtained using a white led light (3D Method B).

- **3D Method B**

  The 3D Method B captures color images using a punctiform light source. The main advantage of this acquisition setup is the low-cost of the used illumination technique, which can permit to deploy the acquisition system in different applicative contexts. The captured images, however, present problems due to reflections and shadows. Fig. 5.14 shows an example of captured pairs of images.

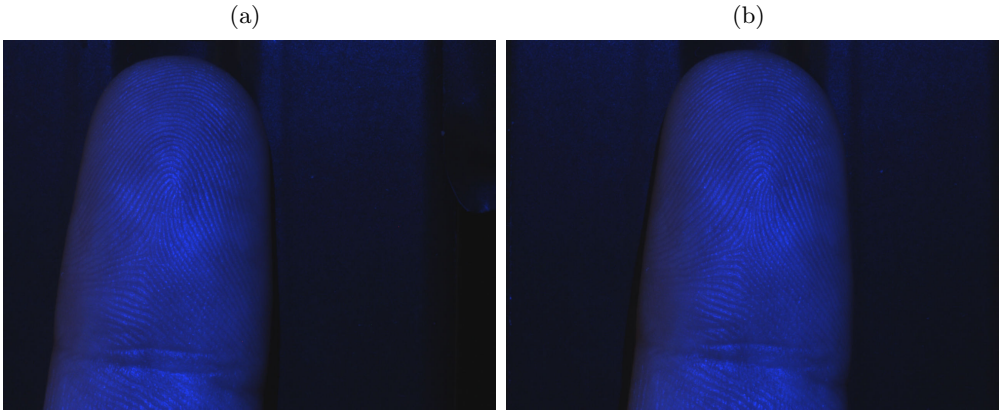

Figure 5.15: A two-view acquisition obtained using a diffused blue light (3D Method C).

- **3D Method C**

  The 3D Method C is based on a diffused blue light illumination. This kind of light permits to enhance the visibility of the ridge pattern, reducing problems related to reflections and shadows with respect to the 3D Method B. As described in Chapter 4, in fact, contactless fingerprint images captured using a diffused blue light usually present better quality with respect to images captured using a white light source. An example of a captured pair of images is shown in Fig. 5.15.

5.3.2.3 Image preprocessing

The image preprocessing step is different for the considered three-dimensional reconstruction methods. The images obtained by the 3D Method A, in fact, present additional information with respect to the images captured by 3D Method B and 3D Method C.

- **3D Method A**

  The images obtained by the 3D Method A are more complex with respect to the ones captured by the other methods, and require to separate the ridge pattern F from the square pattern P.

  The computation of the ridge pattern F is performed by using the following equation:

$$I_F(x, y) = G(x, y) + B(x, y) \ , \tag{5.23}$$

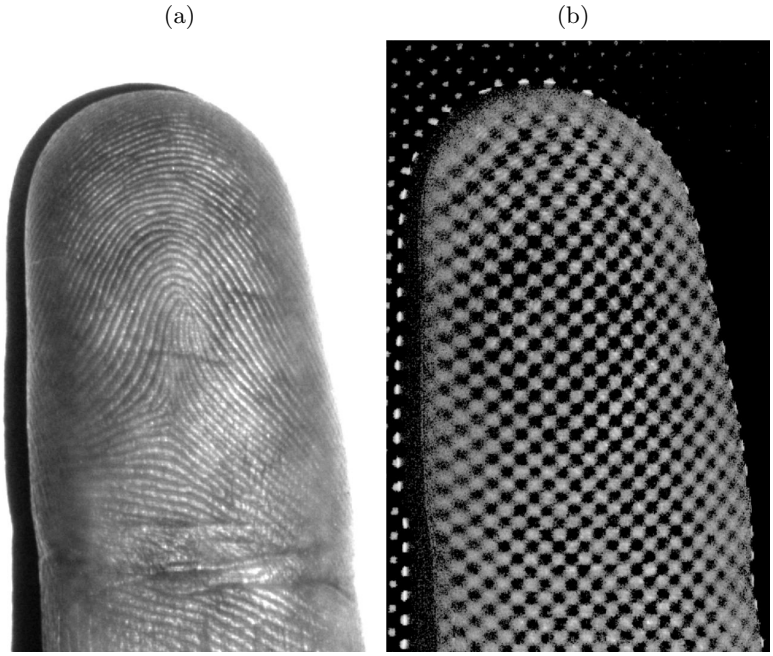

Figure 5.16: Separation of the finger details and structured light pattern in images captured using the 3D Method B: (a) finger details F; (b) enhanced structured light pattern P.

where G and B are the green and blue channels of the captured image. An example of ridge pattern image F is shown in Fig. 5.16 a.

A first approximation of the square pattern I_P is computed as:

$$I_P(x, y) = G(x, y) - B(x, y) \ . \tag{5.24}$$

In order to reduce the presence of noise, a histogram equalization is performed, and a logarithm image is then computed as:

$$P(x, y) = \log\left(1 - I_P(x, y)\right). \tag{5.25}$$

The resulting image representing the projected pattern P is shown in Fig. 5.16 b.

The next task is the fingerprint segmentation, which aims to remove both the background and shadows. The finger shape is estimated as:

$$I_s(x, y) = \begin{cases} 1 & t_l < F(x, y) < t_h \\ 0 & \text{otherwise} \end{cases} \ , \tag{5.26}$$

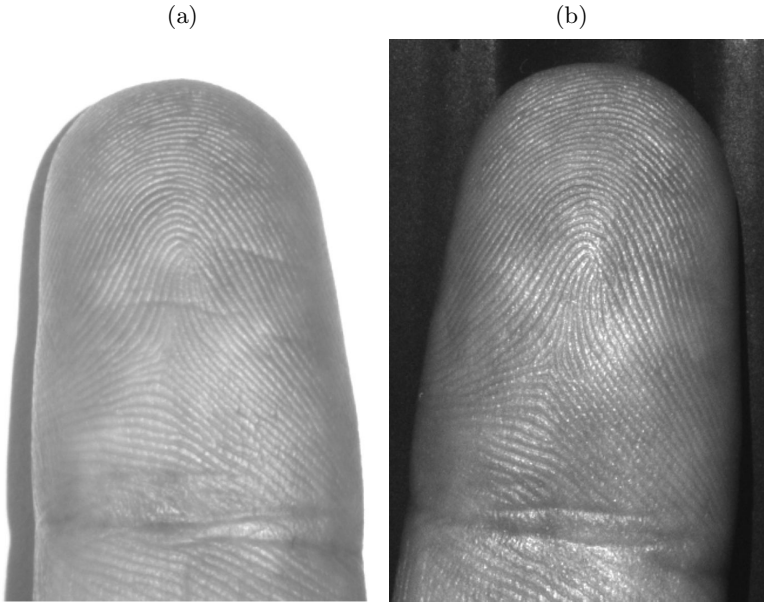

Figure 5.17: Examples of ridge pattern images obtained by using different acquisition and preprocessing techniques: (a) 3D Method B; (b) 3D Method C.

where t_l and t_h are two experimentally estimated threshold values. In order to assure that no points outside the finger boundary are considered in the sequent steps and to reduce possible errors caused by the presence of reflections of the skin, the binary mask is processed by using a morphological opening operator followed by a closing operator. These morphological operators are based on a circular structural element with an experimentally estimated radius value r_s. Since the pixels near to the boundary regions of the finger are often noisy, the ROI of each image is computed by eroding the segmentation mask. The used structural element is a circle with radius r_e.

- **3D Method B**

  The images captured by the 3D Method B represent only the finger skin illuminated by a white led light. The ridge pattern image F is therefore obtained by converting the captured image in gray-scale. Fig. 5.17a shows an example of the obtained results.

  The image segmentation is then performed by using the same algorithm adopted by the 3D Method A.

- **3D Method C**

  The images obtained by the 3D Method C represent the fingerprint illuminated by a punctiform white light. In these images, the details of the ridge pattern are particularly visible in the blue channel of the RGB colorspace. For this reason, the ridge pattern image F is considered as the channel B of the captured image. An example of the obtained results is shown in Fig. 5.17b.

  Differently from the images obtained by the 3D Method A and 3D Method B, the images captured by the 3D Method C present a dark background. For this reason, the segmentation step does not consider the presence of the finger shadows. First, the binary image I_S is computed as

$$I_s(x,y) = \begin{cases} 1 & F(x,y) > t_O \\ 0 & \text{otherwise} \end{cases} , \tag{5.27}$$

  where t_O is obtained by applying the Otsu's method [195]. The ROI is then obtained by eroding the image I_S . The used structural element is a circle with radius r_e.

5.3.2.4 Extraction and matching of the reference points

The method described in Section 5.3.1 permits to obtain pairs of corresponding points in multiple view images of contactless fingerprints. This method, however, is able to obtain a limited number of corresponding pairs of points because it only considers the minutiae present in the fingerprint images. Moreover, fingerprints do not present a fixed number of minutiae and the minutiae extraction algorithms can improperly estimate the coordinates of the feature points. The three-dimensional reconstruction of the finger shape based only on the corresponding minutia points can therefore obtain poor quality samples. In order to overcome these problems, two techniques able to estimate a greater number of corresponding points in contactless fingerprint images have been studied.

The first technique (F Correlation) can be applied in all the reconstruction methods since it only considers the fingerprint pattern image F. The second technique (P Correlation) can only be adopted by the 3D Method A since it uses the supplementary

information related to P in order to speed up the search of corresponding pairs of points.

The approaches are based on the cross-correlation. A cross-correlation coefficient r is computed according to the formula:

$$r = \frac{\sum_m \sum_n (A_{mn} - \bar{A})(B_{mn} - \bar{B})}{\sqrt{(\sum_m \sum_n (A_{mn} - \bar{A})^2)(\sum_m \sum_n (B_{mn} - \bar{B})^2)}} \ , \\ 1 < m < l, \ \ 1 < n < l \ , \tag{5.28}$$

where A and B are windows of size $l \times l$.

- **F Correlation**

  This method is designed for the images captured by the 3D Method B and 3D Method C, but can also work with images captured using the 3D Method A, since it considers only the images of the ridge pattern F_A and F_B obtained using a two view system.

  First, a set of regular spaced points is selected in the image F_A by downsampling the ROI with a step of s_d pixel. For each point (x_A, y_A) appertaining to F_A, the matching point in the image F_B is first estimated by using the homography matrix obtained from the calibration images:

  $$x_{BH} = H x_{AH} \ , \tag{5.29}$$

  where H is the 3×3 homography matrix, x_{AH} is the point (x_A, y_A) expressed in homogeneous coordinates, and x_{BH} is the candidate match point in the image I_B.

  The second step consists in the refinement of the matched pairs of points. This task is performed by searching the best cross-correlation between a $l \times l$ squared window centered in the coordinates (x_A, y_A) of the image F_A, and a $l \times l$ squared window sliding in a $h \times w$ rectangular search range centered in the Cartesian coordinates of x_{BH} of the image I_B. For each reference point of the image F_A, the corresponding point in the image F_B is considered as the pixel with the best value of r in the search range of the second view. Fig. 5.18 shows an example of areas considered during the cross-correlation task.

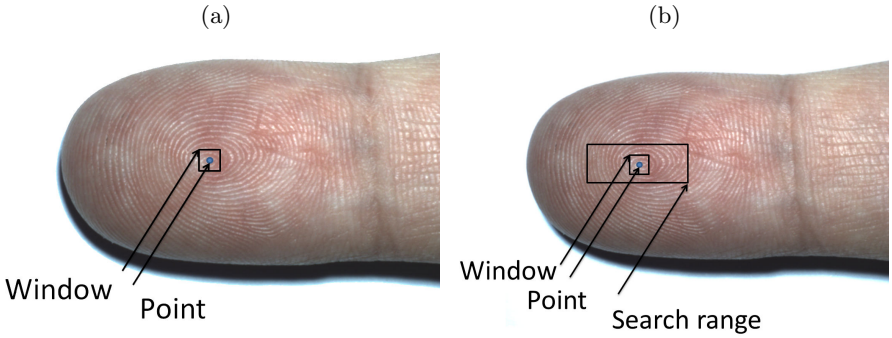

Figure 5.18: Representation of the F Correlation method for the estimation of corresponding pairs of points: (a) random-chosen point in the first image; (b) corresponding windows in the second image and bounded search range.

- **P Correlation**

  This method can only be applied to the images obtained by using the 3D Method A since it uses the information related to the projected pattern. In order to obtain a set of candidate matching points, the centroids of the black and white squares of the images B_A and B_B are estimated (Fig. 5.19).

  Similarly to the matching algorithm F Correlation, this method performs a first estimation of the corresponding points in the two images by using the homography matrix computed during the calibration step. For each reference point (x_A, y_A) appertaining to the first image F_A, the search for the matching point in the second image is performed by first using the homography matrix to define a preliminary match, obtaining a set of points (x'_B, y'_B). The matching is then refined by considering only the centroids related to the image B_N. For each reference point (x_A, y_A) in the first image, the corresponding point in the second image (x_B, y_B) is chosen as the centroid point with the maximum correlation coefficient computed on the F_A and F_B images. The correlations are performed considering $l \times l$ areas centered in the centroid points. Only the nearest points to (x'_B, y'_B) are considered.

  In order to limit possible errors, the described method is first applied to the centroids of the white squares, and then to the ones of the black squares.

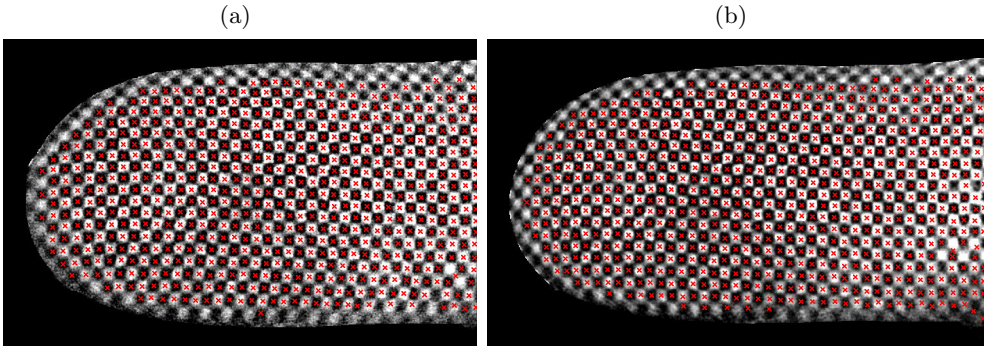

Figure 5.19: Reference points extracted by the P Correlation method for the estimation of corresponding pairs of points: (a) reference points in the first image, (b) reference points in the second image.

5.3.2.5 Refinement of the pairs of reference points

Before the computation of the three-dimensional model, the pairs of erroneously matched points are searched. Different strategies are adopted to remove the outliers.

- **3D Method A**

  A preliminary check for erroneously matched pairs of points is performed by using the Ransac algorithm to fit a homography between the pairs of matched points [313]. The Ransac algorithm discards values which do not fit in the homography estimation, according to an empirically estimated threshold.

  Then, a spike filter based on a statistical approach is applied. This algorithm is based on the evaluation of the Euclidean distance between corresponding points. The distance related to a pair of points is compared with the local mean and standard deviation of the distances computed for every pair of points:

  $$\bar{D}_S - \sigma_{DS} - t_s < d(x_A, y_A, x_B, y_B)_i < \bar{D}_S + \sigma_{DS} + t_s \qquad \forall 1 < i < N, \quad (5.30)$$

  where $\bar{D}_S$ and σ_{DS} are the weighted mean and the standard deviation of the Euclidean distance between each pair of points (x_A, y_A) and (x_B, y_B) in the local region S_A. The weights used to compute the weighted mean are the inverse of the Euclidean distances between (x_A, y_A) and each point of the region S_A.

- **3D Method B**

  First, an outlier removal task is performed. The pairs of matched points of V_x related to the same column of F_A are stored in a vector V_C. This vector is interpolated by a third order polynomial, obtaining the vector V_{CI}. For each element of the vector, $V_x(i)$ and $V_y(i)$ are removed if $|V_C(i) - V_{CI}(i)| < t_S$; where t_S is a fixed threshold.

  The values of D_X and D_Y are obtained by the linear interpolation of V_x and V_y in each point appertaining to the ROI of the image I_A. The coordinates of each point (x_B, y_B) corresponding to (x_A, y_A) are obtained as:

$$\begin{aligned} x_B &= x_A + D_x(x_A, y_A), \\ y_B &= y_A + D_y(x_A, y_A). \end{aligned} \tag{5.31}$$

  Then, the previously described spike filter (5.30) is adopted.

- **3D Method C**

  The filtering technique (5.30) is first applied.

  Similarly to methods in the in the literature for the estimation of non-linear deformations present in contact-based fingerprint images [254], a thin plate spline is then applied to the set of corresponding points. This task permits to obtain a smooth and accurate representation of the finger surface. The thin plate spline interpolation, however can obtain good results only on data with low level of noise.

5.3.2.6 Three-dimensional surface computation and image wrapping

This step estimates the dense three-dimensional shape of the finger. Considering the limited resolution of the used cameras, the method does not estimate the roughness of the fingertip, but computes a three-dimensional representation of the finger and wraps an image of the ridge pattern on the estimated model.

First, the two-dimensional point coordinates are normalized using a rectification procedure based on the calibration data and the matched reference points of the two images. The depth coordinate of every three-dimensional point is then estimated by using the triangulation formula (5.20).

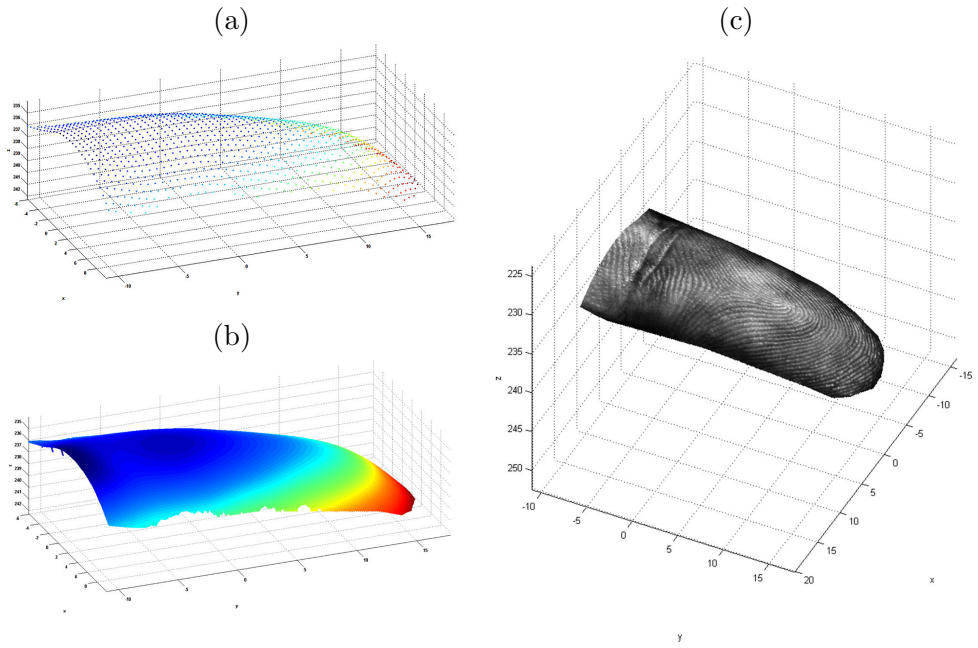

Figure 5.20: Three-dimensional model obtained by using the researched approach for the computation of the finger volume: (a) point cloud; (b) finger volume; (c) three-dimensional model with the wrapped texture.

A dense three-dimensional representation of the finger is then obtained by a linear interpolation of the estimated points with a constant step s_{interp}. This representation consists in three equispaced maps M_x, M_y, M_z, which describe the coordinates of the points of the finger. The texture of the three-dimensional model M_T is obtained by applying the same interpolation on the points of the image F_A. An example of a point cloud and its relative estimated surface are shown in Fig. 5.20.

5.3.2.7 Texture enhancement

Contactless fingerprint images captured by the realized two-view acquisition setups are affected by the same non-idealities that are present in contactless images captured by single CCD cameras. The images captured by the 3D Method A and 3D Method B, however, present more noise with respect to the images captured by the 3D Method C. For this reason, the 3D Method A and the 3D Method B perform the enhancement of the texture M_T by using the algorithm EA (Section 5.2.3.1). Differently the 3D Method C uses the algorithm EB (Section 5.2.3.2).

5.3.3 Feature extraction and matching based on three-dimensional templates

The researched method is able to compute the matching of three-dimensional fingertip models by using the information related to the three-dimensional characteristics of the minutiae points. In particular, the used template is composed by a description of the three-dimensional minutiae points included in a fixed area, and by the information related to the graph obtained by the Delaunay triangulation of the minutiae.

The representation of every minutia consists in a six-element vector (i, x, y, z, θ, q); where i is an identifier, (x, y, z) are the three-dimensional coordinates of the point, θ is the angle of the ridge in an ideal plain, and q is the quality of the minutia point. The estimation of the minutiae in the three-dimensional models first applies the NIST Bozorth3 software [199] on the enhanced fingertip texture map M_{TE}. This software estimates a matrix that describes every minutia by the characteristics (x_M, y_M, θ, q). The three-dimensional coordinates (x, y, z) of every minutia are then obtained as:

$$x = M_x(x_M, y_M); \quad y = M_y(x_M, y_M); \quad z = M_z(x_M, y_M). \tag{5.32}$$

Since the external areas of the fingertip models can be noisy, only the N_M minutiae with quality q greater than a fixed threshold t_q and with the minor distance to the centroid of the last finger bone are considered.

The graph that describes the minutiae is then computed by estimating the two-dimensional Delaunay triangulation of these points. The used template describes each triangle by a set of data (I, L, θ_{max}, C), where I is the vector that represent the indexes of the three vertices, L is the vector that contain the lengths of the facets sorted in decreasing order, θ_{max} is the maximum angle of the triangle in an ideal plane, and C represents the coordinates of the incenter in the three-dimensional space.

An example of the used template is shown in Fig. 5.21.

The matching method used to compare the three-dimensional templates can be divided into three steps:

1. searching of the triangle pairs;
2. minutiae alignment and matching;
3. matching score computation.

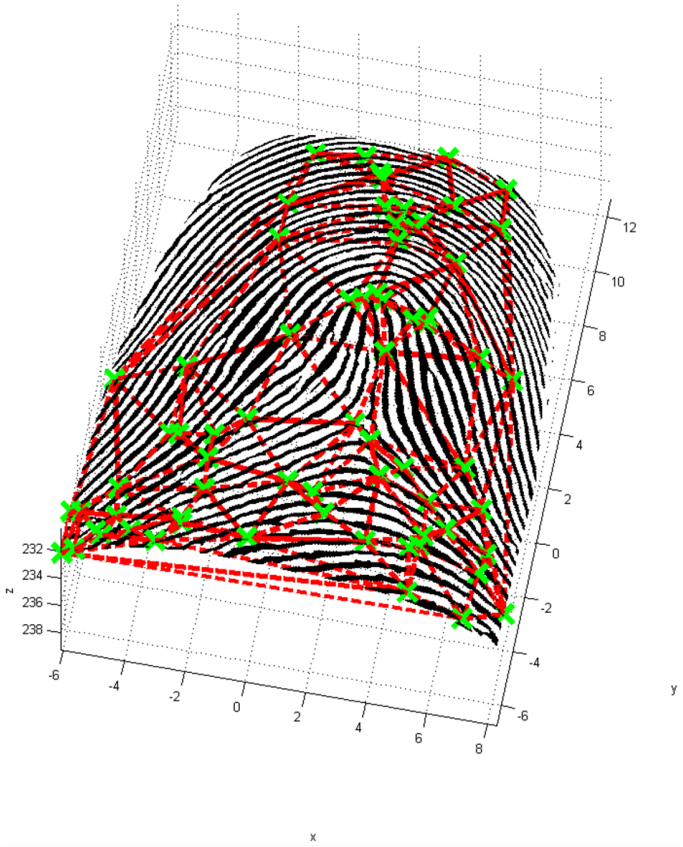

Figure 5.21: Graphical example of the template used by the studied matching algorithm based on three-dimensional fingerprint models. The X symbols represent the minutiae, and the lines represent the triangles of the Delaunay graph.

The goal of the first step is to find similar triangles in the templates T_A and T_B. This task permits to estimate the alignment between the templates. Two triangles are considered as similar if the following disequations are respected:

$$\begin{aligned} &|L_B(j) - L_A(i)| < s_L \ , \\ &\min\left(|\vartheta_B(j) - \vartheta_A(i)|, (360 - |\vartheta_B(i) - \vartheta_A(i)|)\right). \end{aligned} \tag{5.33}$$

where s_L and s_O are two empirically estimated threshold values.

The templates are then aligned by performing a roto-translation step based on the previously matched triangles. The aligned templates can then be used to search the corresponding minutiae. A roto-translation is performed for each pair of matched triangles. The rotation coefficient is defined as the average difference between the ori-

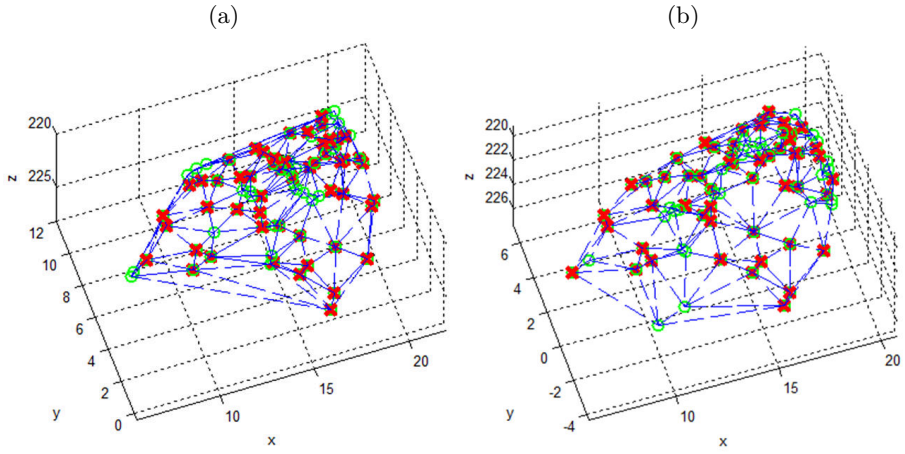

Figure 5.22: Example of matched three-dimensional minutiae points appertaining to templates of the same finger: (a) template A; (b) template B. The lines represent the graph obtained by applying the Delaunay triangulation, the O symbols represent the minutiae appertaining to the templates, and the X symbols represent the matched minutiae.

entations θ of the minutiae. The coefficients of the minutiae belonging to the template T_B are rotated in order to align the templates. The rotation is performed as:

$$\begin{bmatrix} X' \\ Y' \end{bmatrix} = \begin{bmatrix} \cos\Delta_\Theta & -\sin\Delta_\Theta \\ \sin\Delta_\Theta & \cos\Delta_\Theta \end{bmatrix} \begin{bmatrix} X \\ Y \end{bmatrix}, \tag{5.34}$$

where Δ_Θ is the rotation coefficient. The translation is performed according to the difference between the coordinates C_A and C_B of the incenter of the two matched triangles. For each roto-translation, the pairs of corresponding minutiae are searched. In order to match the corresponding points, the coordinates (x, y, z) and orientation ϑ are evaluated:

$$\sqrt{(x_A(i) - x_B(j))^2 + (y_A(i) - y_B(j))^2 + (z_A(i) - z_B(j))^2} < s_D,$$
$$\min\left(|\theta'_A - \theta_B|, (360 - |\theta'_A - \theta_V|)\right),$$

where s_D and s_ϑ are empirically estimated threshold values. Every minutia of the template A can match only a minutia of the template B. Fig. 5.22 shows an example of matched minutiae appertaining to two thee-dimensional templates of the same finger.

The maximum number of matched minutiae pairs N_m is then used to compute the matching score:

$$\text{matching score} = (2 \times N_m)/(N \times M), \tag{5.35}$$

where N and M are the numbers of minutiae appertaining to the templates T_A and T_B, respectively.

5.3.4 Unwrapping of three-dimensional models

A method for the computation of contact-equivalent images from three-dimensional fingerprint samples has been studied. The method is designed to obtain fingerprint images similar to rolled fingerprints and compatible with the existing matching algorithms designed for contact-based fingerprint images. This method is similar to the parametric unwrapping algorithm proposed in [289], and approximates the finger shape by using rings of different radii.

Starting from the depth map M_z and the matrices M_x, M_y, which describe the three-dimensional model, a circular approximation of the (x, z) values corresponding to each y coordinate of the model is performed by applying the Newton method, obtaining the vectors V_{x1} and V_{z1} representing the center coordinates of the circles.

Then, possible outliers are removed by searching the elements of V_{x1} and V_{z1} with a distance greater than the experimentally estimated thresholds t_x, t_z, with respect to the median values of these vectors. The vectors V_{x1}, V_{z1} are then approximated by a first order polynomial, obtaining V_x, V_z.

The vector V_r, which represents the radii of the circles, is then obtained by computing, for each y coordinate of the three-dimensional model, the average distance between the center of the approximating circle $(V_x(y), V_z(y))$ and the coordinates of all the three-dimensional points with said y coordinate, in the matrices M_x, M_y, and M_z. The shape approximation is completed by approximating the vector V_z to a third order polynomial.

The next step consists in the transformation of the fitted model into the two-dimensional space. For each column y, the pixel intensities of the texture map M_T are mapped into the approximating circle, obtaining an intensity vector I_y. A linear interpolation is then applied to merge all the obtained vectors in the unwrapped image I_U. A resolution of around 500 ppi along the y axis is obtained by using an interpolation step of 0.0508 mm. Similarly, a resolution of around 500 ppi along the y axis is obtained by sampling the approximating circles with an angular resolution equal to $(360/\text{perimiter}) \times 0.0508$.

Finally, the image I_U is segmented by using an algorithm based on the local standard deviation of the image [181].

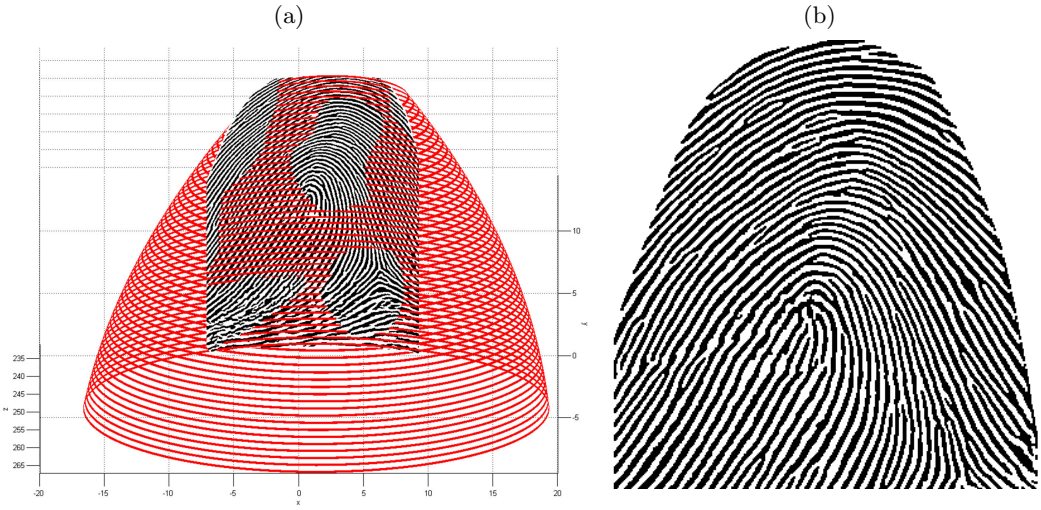

Figure 5.23: Example of results obtained by applying the studied three-dimensional unwrapping technique: (a) approximation of the three-dimensional fingerprint sample; (b) resulting contact-equivalent image.

Fig. 5.23 shows an example of approximation of the finger shape using the researched unwrapping technique, and the resulting contact-equivalent image.

Examples of contact-equivalent images obtained from three-dimensional models computed using the 3D Method A, 3D Method B, and 3D Method C on acquisitions of the same finger are shown in Fig. 5.24. It is possible to observe that all the contact-equivalent images present the same distances between the distinctive points of the minutia pattern. Anyway, the image obtained by using the 3D Method C is less affected by artifacts and represents a wider region of the fingertip.

5.3.5 Quality assessment of contact-equivalent fingerprint images obtained from three-dimensional models

An approach specifically designed for the quality evaluation of contact-equivalent fingerprint images obtained by unwrapping three-dimensional models has been researched. This approach is presented in [44].

The fingertip images captured using contactless sensors present different non-idealities compared to samples captured by contact-based sensors. Contactless images, in fact, present more noise, can be affected by strong reflections, and present a more complex background. In particularly unconstrained setups, there can also be present out of fo-

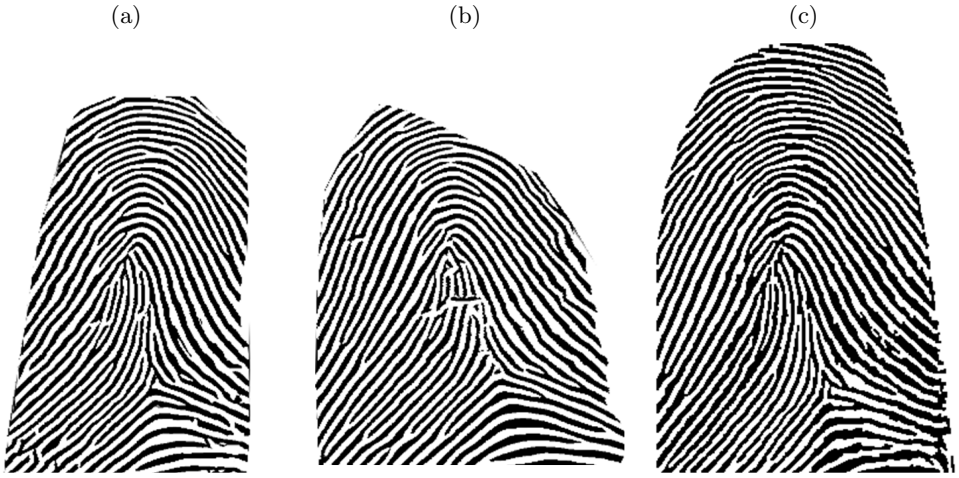

Figure 5.24: Results obtained by applying the studied three-dimensional unwrapping technique on three-dimensional samples of the same finger obtained by using different techniques: (a) 3D Method A; (b) 3D Method B; (c) 3D Method C.

cus and motion blur problems. Moreover, the quality of the obtained samples is strictly related to the applicative context and the user's ability. For these reasons, a correct biometric acquisition is more difficult to be performed in contactless systems.

Considering biometric systems that compute three-dimensional fingertip models, incorrect acquisitions can drastically reduce the visibility of the ridge pattern, causing problems during the three-dimensional reconstruction step. For example, biometric systems that compute three-dimensional models using N-view techniques reconstruct the finger surface by searching points that match in the images related to the different views. If the ridge pattern is not properly visible in the captured images, the estimation of the corresponding pairs of points can produce erroneously matched points, resulting in artifacts in the three-dimensional models. Consequently, the presence of artifacts can produce deformations in the contact-equivalent images.

The images obtained by the unwrapping of three-dimensional fingerprint models can present different problems:

1. deformations due to badly reconstructed regions of the three-dimensional model;
2. artifacts caused by the presence of spikes in the three-dimensional model;
3. areas with artifacts introduced during the enhancement of the fingerprint pattern and corresponding to low-contrast regions of the input images.

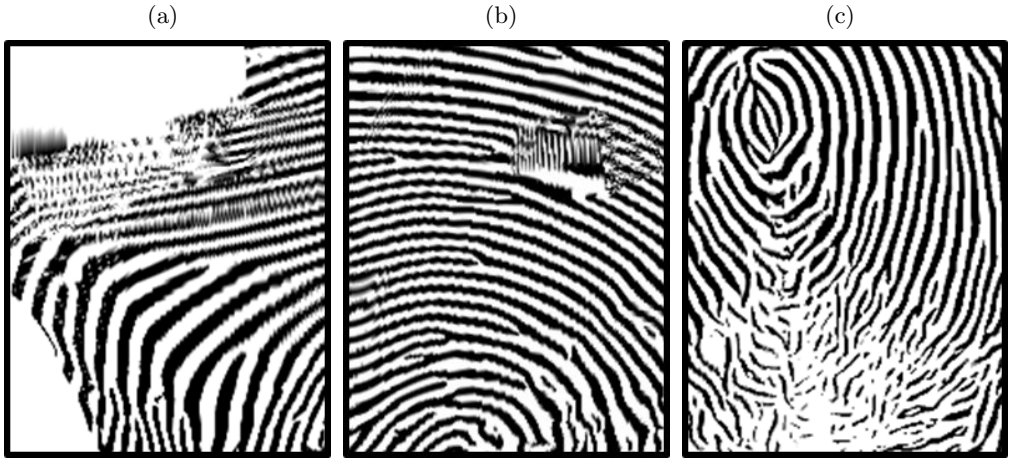

Figure 5.25: Examples of problems that can be present in unwrapped fingerprint images: (a) a deformation caused by a badly reconstructed portion of the three-dimensional model; (b) an artifact caused by the presence of a spike in the three-dimensional model; (c) an area with low visibility of the ridge pattern.

Fig. 5.25 shows an example of problems that can affect contact-equivalent fingerprint images obtained by unwrapping three-dimensional finger models.

Images affected by deformations and artifacts can drastically reduce the accuracy of the biometric system. For this reason, the use of quality estimation methods is necessary to improve the final accuracy and reliability of the whole system.

In the literature, there are no methods specifically designed for the evaluation of contact-equivalent images obtained by unwrapping three-dimensional models.

A novel approach for the quality evaluation of contact-equivalent fingerprint images obtained by unwrapping three-dimensional models has therefore been studied. This approach uses computational intelligence techniques to evaluate the presence of non-idealities in the ridge pattern. The quality can be expressed by using real or discrete values. In this approach, discrete classes are used in order to easily discard low quality biometric samples during the recognition process.

The approach can be divided into the sequent steps:

1. image segmentation;
2. feature extraction;
3. quality estimation using computational intelligence techniques.

5.3.5.1 Image segmentation

The image I_R representing the ROI is computed by applying an empirically estimated threshold t_s to local standard deviation values related to $l \times l$ squared regions.

5.3.5.2 Feature extraction

Different sets of features related to different image characteristics are extracted.

- *Features related to the minutiae* (F_M): the number of minutiae points, and the mean and standard deviation of their quality are computed. The method used for the extraction of the minutiae is the software NIST Bozorth3 [199].

- *Features related to the shape of the ROI* (F_S): this set is composed by 3 features that permit to evaluate the presence of deformations caused by errors in the estimation of the finger shape. These features are the length and width of the ROI, and the eccentricity of the ROI shape.

- *Gabor features* (F_G): this set is composed by $m_G \times n_G \times \theta_G$ values. Starting from the image I, θ_G images G_θ are computed by applying a set of θ_G Gabor filters (4.3) with different orientations. Each image G_θ is then divided into $m_G \times n_G$ local regions, and the AAD (4.6) of the intensity values is computed for each region.

- *Hog Features* (F_H): this set is composed by $c_w \times c_h \times c_b$ features. These values are obtained by computing a set of HOG features in the area of the image I appertaining to the ROI. Similarly to the method described in Section 5.2.2, these features are compute by applying the algorithm described in [309].

- *Standard deviation of Gabor features* ($F_{G\sigma}$): this set is composed by $m_G \times n_G$ features. Similarly to the Gabor features, θ_G images G_θ are obtained by applying a set of θ_G Gabor filters with different orientations to the image I. Each image G_θ is then divided into $m_G \times n_G$ local regions and the AAD of the intensity values of each region is computed. For each local region, the standard deviation of the values obtained by applying the θ_G Gabor filters is finally computed. These features permit to evaluate the presence of information in the local regions of the image, reducing the number of used values with respect to the Gabor features.

- *Standard deviation of HOG features* ($F_{H\sigma}$): this set is composed by $c_w \times c_h$ features. A set of HOG features are computed by dividing the image I in $c_w \times c_h$ local areas. For each local region, the standard deviation of the c_b obtained HOG values is finally computed. The size of this feature set is lower than the size of the set of HOG features F_H.

5.3.5.3 Quality estimation

The quality estimation aims to distinguish the contact-equivalent fingerprint images that can be properly used to perform an identity comparison and the images affected by artifacts due to the presence of noise in the corresponding three-dimensional models. In this approach, the quality estimation is considered as a classification problem. This task is performed by assigning two classes to the unwrapped fingerprint images: "sufficient" and "poor". The quality classes are obtained by evaluating the distributions of the matching scores obtained by genuine identity comparisons.

The used classifiers are based on feedforward neural networks.

More details and examples of classified images are reported in Subsection 6.3.3.

5.4 Computation of synthetic contactless samples

A technique for the simulation of three-dimensional fingerprint models able to simulate different acquisition setups has been studied. The simulated three-dimensional models can then be used to obtain three-dimensional and two-dimensional synthetic biometric samples. The researched technique aims to reduce the efforts necessary to collect biometric samples during the design and evaluation of biometric algorithms and acquisition setups. This technique is presented in [314].

The design of contactless fingerprint recognition systems requires the collection of sample databases large enough to prove the validity of the envisioned method. This task is expensive and time consuming. Moreover, it can require the design and implementation of new acquisition setups. In order to limit the effort necessary to collect biometric data, it can be useful to perform tests on simulated data. In the literature, some works have dealt with the creation of synthetic fingerprint images that realistically resemble the ones acquired using contact-based sensors. However, there are no works that deal with the computation of synthetic three-dimensional fingerprints. The

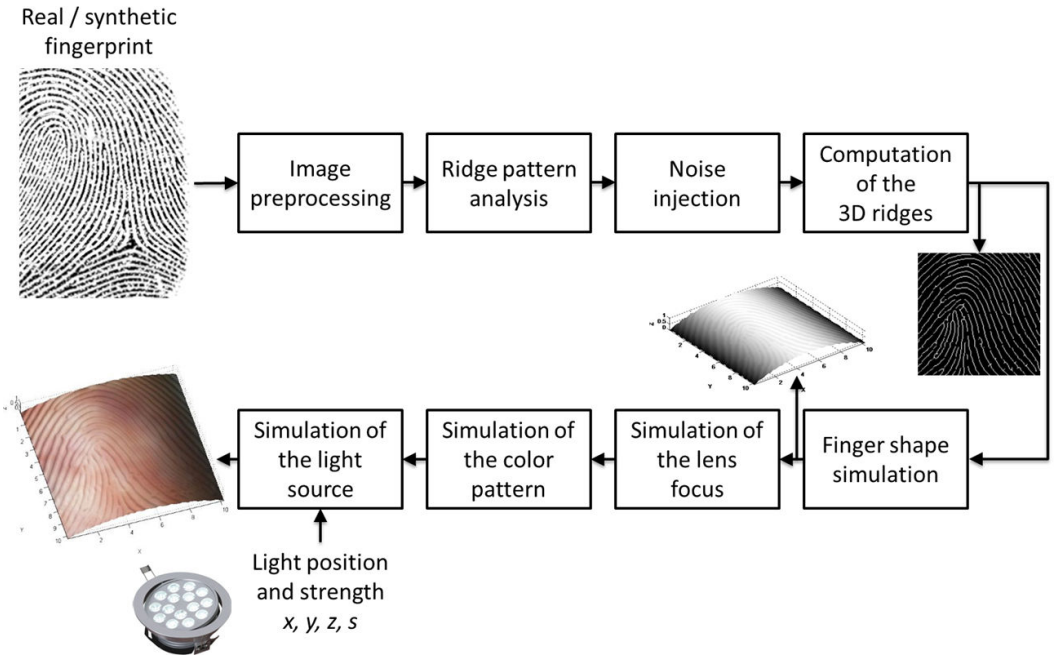

Figure 5.26: Schema of the studied method for the computation of three-dimensional synthetic fingerprints starting from contact-based fingerprint images.

realized method could therefore be a useful tool for research groups operating in biometrics and three-dimensional reconstruction techniques, allowing to easily simulate different acquisition setups. Moreover, the method can permit to compare the results of future algorithms with a ground truth of simulated samples.

The goal of the method is to simulate synthetic three-dimensional models of fingerprints, resembling contactless fingerprint images captured with different cameras and illumination conditions, using image processing techniques and well-known algorithms designed for fingerprint recognition systems. It focuses on modeling the central region of the fingerprint, since it is the region that contains the most discriminative part of the fingerprint information. The method takes in input a fingerprint image captured using a contact-based sensor, or obtained by applying techniques in the literature for the computation of synthetic fingerprint images. The information related to the ridge pattern is used to compute a realistic three-dimensional model of the fingerprtip. Realistic focus, color, and illumination details are then applied in order to increase the quality of the synthetic three-dimensional model.

The method can be divided into the following steps:

1. image preprocessing;
2. ridge pattern analysis;
3. noise injection;
4. computation of the three-dimensional ridges;
5. finger shape simulation;
6. simulation of the lens focus;
7. simulation of the color pattern;
8. simulation of the light source.

An outline of the method is shown in Fig. 5.26.

5.4.1 Image preprocessing

In the preprocessing step, the region of the contact-based fingerprint image describing the most discriminative area of the ridge pattern is selected, and then the image is normalized in order to enhance the visibility of the ridge pattern.

The used contact-based fingerprint images are acquired at a resolution of 500 ppi. The images are cropped and a central area of 100×100 pixel, approximately corresponding to an area of 5×5 mm of the finger skin, is extracted from the image.

The intensity of the cropped image I is then normalized using the formula (4.2) in order to obtain an image with 0 mean and standard deviation equal to 1.

5.4.2 Ridge pattern analysis

The analysis of the ridge pattern is performed in order to estimate a map image that represents the height of the ridges in a non-dimensional space. The used method assumes that the height of the ridge pattern is proportional to the result obtained by applying tuned Gabor filters to the contact-based fingerprint image. The use of Gabor filters permits to reduce the noise and to obtain ridges with smooth shapes.

This task is based on a well-known method in the literature for the enhancement of contact-based fingerprint images [181]. The first step is the computation of two images that describe the local orientation O_r and the local frequency F_r of the ridges. Then, a set of Gabor filters (4.3) tuned by using the estimated information are convolved to the fingerprint image.

In order to search the regions of the image G representing the ridges, a binary image B is computed as:

$$B(x,y) = \begin{cases} 0 & \text{if } G(x,y) < t_b \\ 1 & \text{otherwise} \end{cases}, \tag{5.36}$$

where t_b is an empirically estimated threshold.

A first approximation of the height of the ridges R and valleys V is computed as

$$\begin{aligned} R(x,y) &= \log\left(G(x,y) \times (\neg B(x,y))\right), \\ V(x,y) &= \log\left(1 - G(x,y) \times B(x,y)\right). \end{aligned} \tag{5.37}$$

The intensity values of the ridges R are then normalized in a range from $(1-\Delta_r)$ to 1, and the intensity values of the valleys V are then normalized in a range from 0 to Δ_r. The value of the constant Δ_r has been estimated by observing the shape of real three-dimensional fingerprint models.

Then, the image H describing the height of the ridge pattern in a non-dimensional space is computed as

$$H(x,y) = R(x,y) + V(x,y). \tag{5.38}$$

As a last task, an adaptive histogram equalization is applied to H.

5.4.3 Noise injection

This step has the purpose of simulating the presence of pores, incipient ridges, and acquisition noise.

A binary image B_n, composed by randomly distributed white dots, is first computed. A morphological dilation with a mask of $n_n \times n_n$ pixel is then applied to B_n. Finally, the image B_n is used to simulate pores and incipient ridges by applying the equation:

$$\begin{aligned} H_n(x,y) = \; & H(x,y) - \Delta_n \left(B_n(x,y)\left(\neg B(x,y)\right)\right) \\ & +\Delta_N \left(B_n(x,y)\, B(x,y)\right) \end{aligned}, \tag{5.39}$$

where $H_n(x,y)$ is the resulting image, and Δ_n is an empirically estimated value.

5.4.4 Computation of the three-dimensional ridges

In order to simulate the wear of the ridges, the height image H_n is smoothed using an approach based on an empirically estimated threshold t_w. The value of t_w corresponds to the p percentile of the histogram of H_n. The ridge shape is obtained as:

$$H_q(x,y) = \begin{cases} t_w & \text{if } H_n(x,y) > t_w \\ H_n(x,y) & \text{if } H_n(x,y) \leq t_w \end{cases} \quad . \tag{5.40}$$

The height of the ridges in the image H_q is then adjusted in order to have a mean value of 0.06 mm.

5.4.5 Finger shape simulation

A parametric finger shape model based on a cylinder is computed:

$$S(x,y) = \frac{-x^2 + f_n}{f_n} \quad , \tag{5.41}$$

where $S(x,y)$ is the three-dimensional surface based on the parametric model, and f_n is a normalization term used to compute a surface with a peak height of 1 mm. The peak height has been experimentally estimated on an area of 5×5 mm by considering the average curvature of the finger in its central area. The rendering of wider areas requires the usage of a more detailed model of the finger surface, which can be obtained, for example, by using multiple view three-dimensional systems or laser profilometers.

The normal vectors to each point of the surface $S(x,y)$ are then computed. The obtained result is a three-element vector (N_x, N_y, N_z). The parametric surface is then converted to a full three-dimensional point cloud (x_s, y_s, z_s), where $Z_s = S(x,y)$.

The ridges are superimposed on the surface according to the direction of the normal to the surface:

$$\begin{aligned} x_r &= x_s + N_x H_q(x,y), \\ y_r &= y_s + N_y H_q(x,y), \\ z_r &= z_s + N_z H_q(x,y), \end{aligned} \tag{5.42}$$

where H_q is the image describing the three-dimensional ridge structure. A surface approximation $S_r(x,y)$ is then computed from the point cloud (x_r, y_r, z_r) using a linear interpolation technique.

5.4.6 Simulation of the lens focus

Real contactless fingerprint images can present regions affected by out of focus problems. In most of the cases, in fact, the hardware setups use macro lenses in order to capture the details of the ridge pattern. A technique for the simulation of the lens focus is therefore used in order to improve the realism of the obtained three-dimensional models. This technique blurs every point of the ridge pattern proportionally to its height along the z axis.

The height of every point $Z_r(x, y)$ is normalized between two empirically estimated values b_{min} and b_{max}, obtaining the matrix B_s. For each point (x, y), a median filter with a mask of $B_s(x, y) \times B_s(x, y)$ pixels and centered in (x, y) is applied to $Z_r(x, y)$.

5.4.7 Simulation of the color pattern

The color pattern is acquired from a real contactless fingerprint image. The ridge pattern is then removed from the contactless fingerprint image using a Gaussian low-pass filter in order to extract only the underlying skin color and the vein pattern:

$$I_f = I_l * G_l \ , \tag{5.43}$$

where I_f is the resulting filtered image, I_l is the contactless image, G_l is a Gaussian $m \times m$ filter mask, with σ equal to an empirically estimated value σ_p.

In order to improve the realism of the color pattern, speckle noise is introduced by applying the equation:

$$I_p = I_f + n_s \times I_f * G_l \ , \tag{5.44}$$

where n_s is uniformly distributed random noise with 0 mean and variance v_s. The value of v_s is empirically estimated and is related to the simulated camera setup.

The image I_p is then superimposed on the surface $S_r(x, y)$ using a texture mapping procedure.

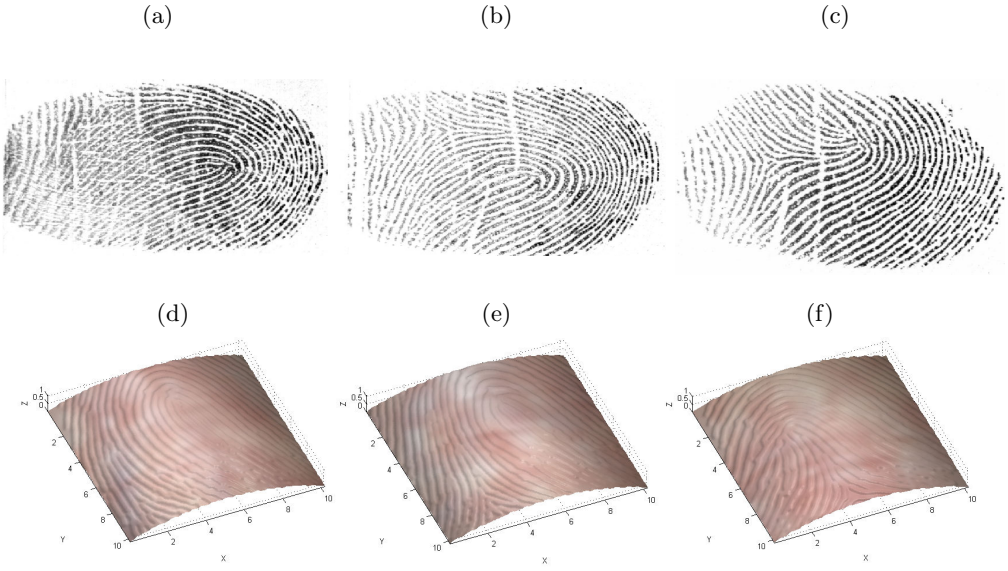

Figure 5.27: Examples of synthetic three-dimensional fingerprints: (a-c) contact-based acquisitions; (d-f) three-dimensional synthetic fingerprints.

5.4.8 Simulation of the light source

A point light source with strength s, radiating uniformly in all directions, is then positioned at coordinates (x_l, y_l, z_l) in order to simulate the illumination. The specular properties of the model are experimentally adjusted in order to meet the properties of the human skin. A Phong lighting algorithm is then used to compute the reflection model of the surface, but more complex rendering engines can be also applied [315].

Some examples of contact-based acquisitions and the resulting three-dimensional synthetic fingerprints are shown in Fig. 5.27.

5.5 Summary

Different methods for all the steps of contactless fingerprint recognition systems based on two-dimensional and three-dimensional samples have been presented. All the methods are based on acquisition setups that can be considered as less-constrained with respect to most of the systems in the literature since they do not use finger placement guides and are able to capture the samples in single time instants.

The researched techniques based on two-dimensional samples use acquisition setups based on single CCD cameras, which permit to capture fingerprint images at a distance of more than 200 mm from the sensor. Moreover, they do not require complex and expansive illumination techniques.

In order to evaluate the presence of noise and other non-idealities in the contactless images, a quality assessment technique specifically designed for contactless fingerprint images has been studied. This technique is based on neural classifiers and permits to discard insufficient quality samples.

A technique for the evaluation of Level 1 characteristics in contactless images has been implemented. This technique permits to estimate the coordinates of the core point by using neural networks.

Level 2 analysis techniques have also been studied. In particular a method for the computation of contact-equivalent images has been designed. The method can then be used to perform biometric recognitions based on techniques designed for the evaluation of minutia features in contact-based fingerprint images.

Biometric systems based on three-dimensional samples require more complex acquisition setups and recognition algorithms. Techniques for the estimation of the three-dimensional coordinates of minutia points and the three-dimensional reconstruction of the finger surface have been researched. These techniques are based on multiple view hardware setups and permit to perform biometric acquisitions in a less-constrained manner with respect to most of the systems in the literature.

Feature extraction and matching techniques based on three-dimensional templates have also been presented.

Moreover, an unwrapping method for the computation of contact-equivalent images from three-dimensional samples, and a technique for the quality assessment of the obtained fingerprint images have been studied.

In order to reduce the efforts necessary for the acquisition of the biometric samples required to test the researched approaches, a tool for the simulation of synthetic contactless fingerprint samples has also been realized.

Chapter 6

Experimental Results

This chapter describes the results obtained by evaluating the researched approaches for contactless fingerprint systems recognition based on two-dimensional and three-dimensional samples (Chapter 5).

The realized techniques have been evaluated considering different characteristics of biometric systems: accuracy, speed, cost, usability, acceptability, scalability, interoperability, security, and privacy. Particular attention has been given to the accuracy evaluation since it is usually considered as one of the most important aspects in the design of biometric applications. The used testing procedures and figures of merit are described in Section 2.4.

The reported results are related to the implemented techniques for biometric systems based on two-dimensional samples and three-dimensional fingerprint models. In this context, the performances of the researched techniques are compared with the ones obtained by traditional contact-based systems in a scenario evaluation.

The results obtained by the studied technique for the simulation of contactless fingerprint acquisitions are finally analyzed and compared with real data.

6.1 Performed experiments

This chapter describes the experiments performed for the validation of all the studied techniques described in Chapter 5.

First, a performance analysis of the studied techniques based on two-dimensional samples is described. In particular, the researched quality assessment method for con-

tactless fingerprint images (Section 5.2.2) is first evaluated, and the results obtained by the realized technique for the core point estimation in contactless fingerprint images are then provided (Section 5.2.4).

A quantitative accuracy evaluation of the researched three-dimensional reconstruction techniques (Section 5.3.1 and Section 5.3.2) is also reported. The accuracy of the method designed to reconstruct the three-dimensional coordinates of minutia points is first discussed. The results obtained by different techniques for the three-dimensional reconstruction of the finger surface are then compared.

A discussion of the results obtained by applying the implemented techniques for the computation of contact-equivalent images (Section 5.3.4), and the quality assessment of fingerprint images obtained by unwrapping three-dimensional finger models (Section 5.3.5) are then provided.

The realized biometric recognition techniques are then compared with contact-based recognition systems in a scenario evaluation. This comparison is based on the most common practices and figures of merit in the literature and include different aspects of biometric technologies: I accuracy; II speed; III cost; IV scalability; V interoperability; VI usability; VII social acceptance; VIII security; IX privacy.

Preliminary results obtained by the studied feature extraction and matching algorithms based on the three-dimensional coordinates of minutia points (Section 5.3.3) are discussed. The performed tests are related to biometric datasets acquired using different technologies.

Finally, the researched technique for the computation of synthetic contactless fingerprint samples (Section 5.4) is analyzed.

This chapter is organized as follow. Section 6.2 presents the experiments performed on the methods designed for the elaboration of contactless two-dimensional fingerprint samples. Section 6.3 describes a comparison between different three-dimensional reconstruction techniques, and provides results regarding the unwrapping of three-dimensional fingerprint models. A comparison of the researched contactless recognition techniques with contact-based fingerprint recognition systems is presented in Section 6.4. Section 6.5 discussed the preliminary results obtained by the methods for the feature extraction and matching based on three-dimensional templates. Finally, a discussion of the accuracy obtained by the studied approach for the computation of synthetic contactless samples is presented in Section 6.6.

6.2 Methods based on single contactless images

This section describes the performed evaluations on the researched methods for the acquisition and elaboration of two-dimensional fingerprint samples described in Section 5.2. In particular, the results obtained by the quality assessment method for contactless fingerprint images (Section 5.2.2) and core detection technique (Section 5.2.4) are provided.

6.2.1 Quality estimation of contactless fingerprint images

The studied quality assessment approach designed for contactless fingerprint images (Section 5.2.2) aims to search the best quality frames in frame sequences describing a finger moving toward the camera. We tested this approach on different biometric datasets collected in our laboratory, and compared the results of the Method QA and Method QB.

6.2.1.1 Creation of the training and test datasets

In the literature, there are no available any public datasets collecting contactless fingerprint images acquired in unconstrained conditions. We therefore created four different datasets to test the studied method in different operative conditions. The first dataset (Dataset Aq) is composed by 79 grayscale frame sequences describing different fingers, captured with a Sony XCD-V90 camera. The frame rate is 30 fps, the size of each frame is 1920×1024 pixel, the duration of each sequence is 6 s, the illumination is controlled by a led and the used focal is 25 mm. For each frame sequence, a user brings a finger near to the camera. The range of the movement is 20 mm. Each frame of the dataset had been evaluated by an experienced supervisor and labeled with its qualitative estimation in five different categories:

- Q = 5 (Poor): the ridges are not visible or the ROI is not present in the frame;
- Q = 4 (Fair): the visibility of the ridges is insufficient because the frame is blurred;
- Q = 3 (Good): the ridges are visible but some regions of the ROI are blurred;
- Q = 2 (Very good): the ridges are well visible;
- Q = 1 (Excellent): the ridges are clearly marked.

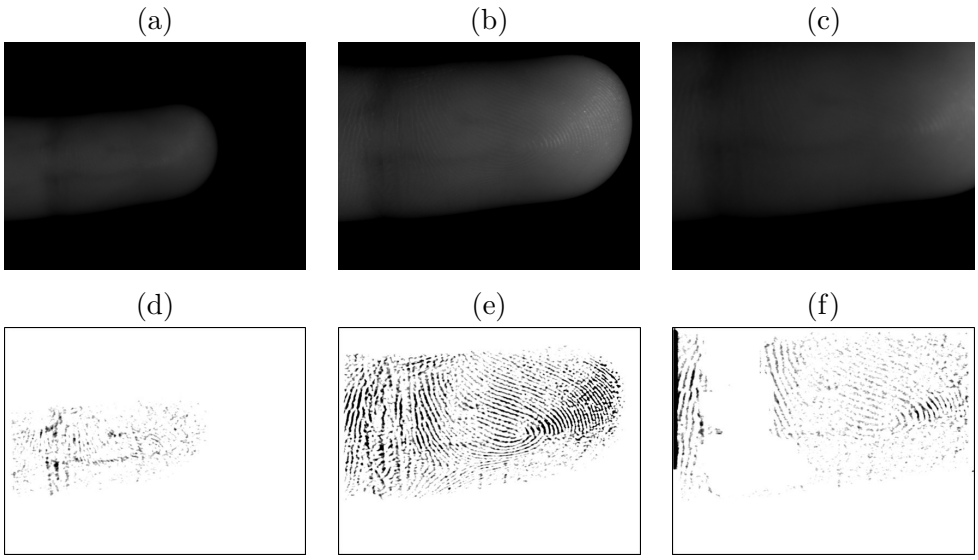

Figure 6.1: Method QB: Frame prefiltering. Subplots (a), (b) and (c) show examples of frames with different quality levels, while subplots (d), (e) and (f) show the output of the filter in the ROI region. The filtering algorithm tends to enhance only the ridges portion in focus, and it produces random-like patterns in the blurred regions. This behavior helps the subsequent NFIQ algorithm to properly estimate the quality of the frame.

This task is not simple due to facts that the defocusing effect is not linear with the finger distance to the optics, and the speed and direction of the finger movements are not constant.

We produced other three datasets by sub-sampling the Dataset Aq: the first one (Dataset Bq) is composed by 5 acquisitions of the same individual (993 frames); the second one (Dataset Cq) is composed by 5 frame sequences related to 5 different individuals (997 frames); the Dataset Dq is composed by 360 randomly selected frames captured in all the considered operative conditions. Each dataset has been created in a version labeled with 5 quality levels, and in a version with two quality levels (Good: quality level ≤ 1; Bad: quality level > 1). The rationale behind the two-class datasets is to produce a simplified classifier capable to directly identify the correct frames in the sequences. In the following, we refer to these datasets with the names Bq-5, Bq-2, Cq-5, Cq-2, Dq-5, and Dq-2, respectively.

6.2.1.2 Application of the Method QB

The results achievable with the Method QB are strictly related to the quality of the input images and to the capability of the filter (5.11) (5.12) to enhance only the ridge pattern in the image, minimizing all the remaining image components. Using the realized setup (Fig. 5.2), we qualitatively tuned the α filter parameter to a value equal to 10 and r equal to the height in pixel of the frame. Examples of results obtained by the studied filtering method are plotted in Fig. 6.1, where three frames with different quality levels are shown. The filtering algorithm tends to enhance only the ridges portion in focus, and it produces random-like patterns in the blurred regions. This behavior helps the subsequent algorithms to properly estimate the quality of the frames.

As a preliminary step, the application of the five-level approach proposed by the NIST is considered. Fig. 6.2 plots three examples of different quality frames extracted from a sequence of Dataset Aq. Fig. 6.2 a, Fig. 6.2 b, and Fig. 6.2 c show a far image, a good quality image, and an out of focus image, respectively. Fig. 6.2 d shows the output of the NFIQ algorithm used by the Method QB (dots) compared with the supervisor evaluation (dashed line) and the output of the Feature 7 of the Method QA.

The performed experiments show that Method QB is less robust to estimate the frame with the highest available quality estimated by the supervisor. Notably, the feature $F(7)$ shows a smooth pattern and it properly follows the real image quality during the sequence. This behavior is present in all the acquired sequences.

6.2.1.3 Application of the Method QA

The following parameter configuration of the Method QA was adopted: the size of the squares $S_m(x_s, y_s)$ in (5.1) is 20×20 pixel, the threshold value t_1 in (5.1) is 0.05, and the erosion structuring element S in (5.2) is fixed to a squared 30×30 matrix. These parameters were empirically tuned on the available images.

The produced main Dataset Aq has 14220 frames; hence it is almost impossible to manage such quantity of features vectors with the best wrapper algorithms available in the literature. For this reason, we used three subsampled datasets that describe different operative conditions of the acquisition setup. Experiments showed that the most effective feature selection method for the considered datasets is the forward selection

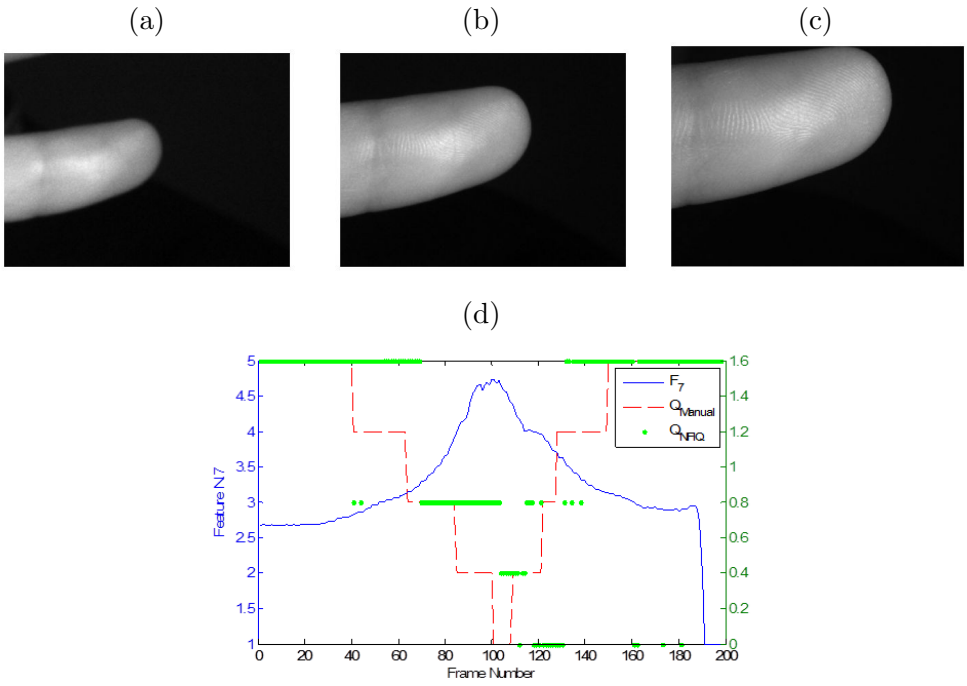

Figure 6.2: Examples of frames with different quality appertaining to a contactless fingerprint acquisition: (a) poor quality frame; (b) good quality frame; (c) excellent quality frame; (d) graph representing the quality levels related to the frame sequence. This graph shows the labels selected by the supervisor (dashed line), the pattern of the feature $F(7)$ of Method QA (continuous line), and the quality levels produced by Method QB (dotted line).

technique [316]. The feature selection phase produced the estimated best feature sets for the datasets Bq-5, Bq-2, Cq-5, Cq-2, Dq-5, and Dq-2.

In our experiments, we tested different classification paradigms in order to better study the complexity of the learning problem embedded in the six datasets. In particular, we adopted the following classifier families:

- the Linear Bayes Normal Classifier (LDC);
- the Quadratic Bayes Normal Classifier (QDC);
- the k-Nearest Neighbor classifier with odd values of the parameter $k\,(1, 3, 5)$;
- feedforward neural networks with different numbers of neurons in the hidden layer.

Table 6.1: Feature subsets obtained by the studied method for the quality assessment of contactless fingerprint images.

Dataset	Feature Subset
Bq-5	[1, 2, 6, 7, 35, 40, 41, 45]
Bq-2	[1, 3, 6, 7, 8, 31, 37, 38, 42]
Cq-5	[1, 6, 7, 41, 42, 43, 45]
Cq-2	[2, 3, 6, 7, 29, 31, 36, 45]
Dq-5	[6, 8, 35, 45]
Dq-2	[4, 6, 10, 11, 12, 13, 16, 27, 33, 44]

Notes. The datasets Bq-5, Cq-5 and Dq-5 are classified in five classes. The datasets Bq-2, Cq-2 and Dq-2 are classified in two classes.

In order to effectively estimate the generalization error of the trained neural networks, we adopted the N-fold cross validation technique with $N = 10$ [317]. The topology of the neural networks has been designed as follows: we used a linear node for the output layer of the neural networks, and we tested different numbers of nodes in the hidden layer. The selected topology for the nodes of this layer is log-sigmoidal. The algorithm used for training the neural networks is the back-propagation algorithm.

6.2.1.4 Final results and discussion

Table 6.1 reports the best subsets of features related to the six datasets obtained by the forward selection technique. Table 6.2 resumes the obtained results of the neural-based classification system compared with the classical inductive classification methods for all datasets, and with respect to the performance of Method QB. In particular, Table 6.2 reports only the best configurations found during the analysis (number of hidden layer for the neural networks, k-parameter for the kNN classifiers, and the best feature sets selected by the Sequential Forward Selection algorithm).

Table 6.2 shows that Method QA offers a remarkable accuracy compared with Method QB on the considered datasets. In addition, the neural-based classifier shows a very good accuracy compared with other classical inductive classification systems. The only classification family showing a similar accuracy (on the considered datasets) is the

Table 6.2: Classification error of the studied method for the quality assessment of contactless fingerprint images.

	Method QA								Method QB
Dataset	**Linear**		**FFNN-3**		**FFNN-5**		**kNN**		
	mean	**std**	**mean**	**std**	**mean**	**std**	**mean**	**std**	**mean**
Bq-5	0.191	0.002	0.046	0.004	0.065	0.004	0.042	0.004	0.478
Bq-2	0.083	0.000	0.013	0.000	0.017	0.004	0.011	0.001	0.140
Cq-5	0.239	0.004	0.066	0.008	0.065	0.001	0.068	0.000	0.358
Cq-2	0.049	0.001	0.013	0.002	0.016	0.001	0.015	0.003	0.150
Dq-5	0.354	0.006	0.275	0.008	0.286	0.012	0.278	0.016	0.469
Dq-2	0.047	0.000	0.064	0.024	0.047	0.000	0.050	0.000	0.180

Notes. Classification methods of Method QA: linear classifier (Linear); feedforeword neural networks with one hidden layer composed by 3 nodes (FFNN-3); feedforeword neural networks with a hidden layer composed by 5 nodes (FFNN-5); kNN with k=1 (kNN). The datasets Bq-5, Cq-5 and Dq-5 are classified in five classes. The datasets Bq-2, Cq-2 and Dq-2 are classified in two classes.

kNN classifiers, but the neural network approach offers a relevant gain in the computational complexity. Table 6.3 shows the computational gain of the neural networks compared to kNN classifiers. This gain depends on the number of samples stored in the k-NN classifier, compared to the number of neurons in the neural networks. Considering the datasets Bq-5, Bq-2, Cq-5, Cq-2, Dq-5 and Dq-2, the minimum found gain factor is equal to 36. Experiments showed that the Method QA applied with the neural-based quality classification technique is the most suitable for real-time applications.

The implemented methods have been written in Matlab language (Version 7.6) exploiting the available toolboxes on Intel Centrino 2.0Ghz working with Windows XP.

The computational time of the Method QA is different for each dataset/classifier.

The total computational time is also related to the feature extraction. The computation of the majority of the features requires less than 0.05 s. The features $F(39)$ and $F(40)$ require about 2.3 s and the feature $F(41)$, $F(42)$, $F(43)$ and $F(44)$ require about 4 s. The features $F(10)$ and $F(11)$ are computed at the same time and this step requires about 1.2 s. In a similar fashion, the computation of the features $F(12)$, $F(13)$ and $F(14)$ requires about 1.2 s. The feature selection step showed that these computational-heavy features are not strictly needed to guarantee the best accuracy of the system, and they can be replaced by subsets of relatively simple features.

Table 6.3: Computational Gain of neural networks with respect to traditional classifiers in the studied method for the quality assessment of contactless fingerprint images.

Dataset	Computational Gain
Bq-5	201.459
Bq-2	205.527
Cq-5	121.756
Cq-2	539.839
Dq-5	159.852
Dq-2	46.456

The computational gain is processed by the ratio of the computational time required by the most accurate traditional classifier to the computational time of the most accurate neural network. Accuracy values are reported in Table 6.2.

The bottleneck of the Method QA consists in the estimation of the ROIs. The implementations of the algorithms for the segmentation of the ROI A and ROI B are not suitably optimized and can require up to 1.5 s and 3.7 s, respectively. On the contrary, optimized versions can reduce the computational complexity by a factor of 100. This point is crucial to achieve the real-time goal.

The obtained results show that the researched method is achievable, and it offers suitable accuracy in real-time applications working on images captured at a distance of more than 0.2 m.

6.2.2 Comparison between image enhancement methods

The image enhancement methods described in Subsection 5.2.3 are designed for different applicative contexts. The researched method based on contextual filters (Method EA) permits to improve the visibility of the ridge pattern in noisy contactless fingerprint images. Differently, the method based on the ridge following (Method EB) is able to obtain images less affected by the presence of artifacts, but can properly process less noisy samples.

Results obtained by applying the two enhancement methods on images captured using a diffused blue light (image captured by the acquisition setup of the 3D Method C) are shown in Fig. 6.3. It is possible to observe that Method EA introduced some artifacts in the enhanced images, in particular in the core region of the finger.

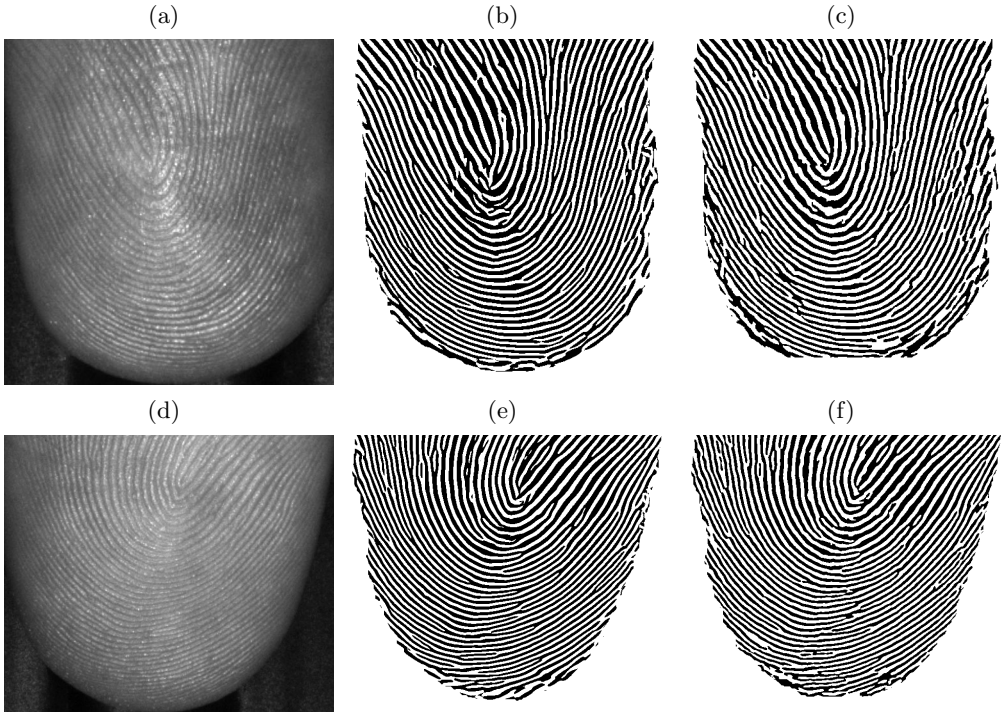

Figure 6.3: Example of results obtained by applying the researched enhancement techniques on contactless fingerprint images captured using a diffused blue light: (a, d) blue channel of the captured images; (b, c) results obtained by the Method EA; (d, e) results obtained by the Method EB.

Fig. 6.4 shows results obtained by applying the Method EA and Method EB on images captured using a projected static pattern as light source (image captured by the acquisition setup of the 3D Method A). In this case, the Method EA permitted to obtain wider regions of the ridge pattern with respect to the Method EB.

6.2.3 Analysis of Level 1 features in contactless fingerprint images

In this subsection, we describe the tests performed to evaluate the studied core detection method designed for contactless fingerprint images (Section 5.2.4). We depict the creation of the training and test datasets, and the results obtained by training the computational intelligence techniques for the estimation of the core point in contactless fingerprint images. The obtained results are then compared with the ones obtained by heuristic methods.

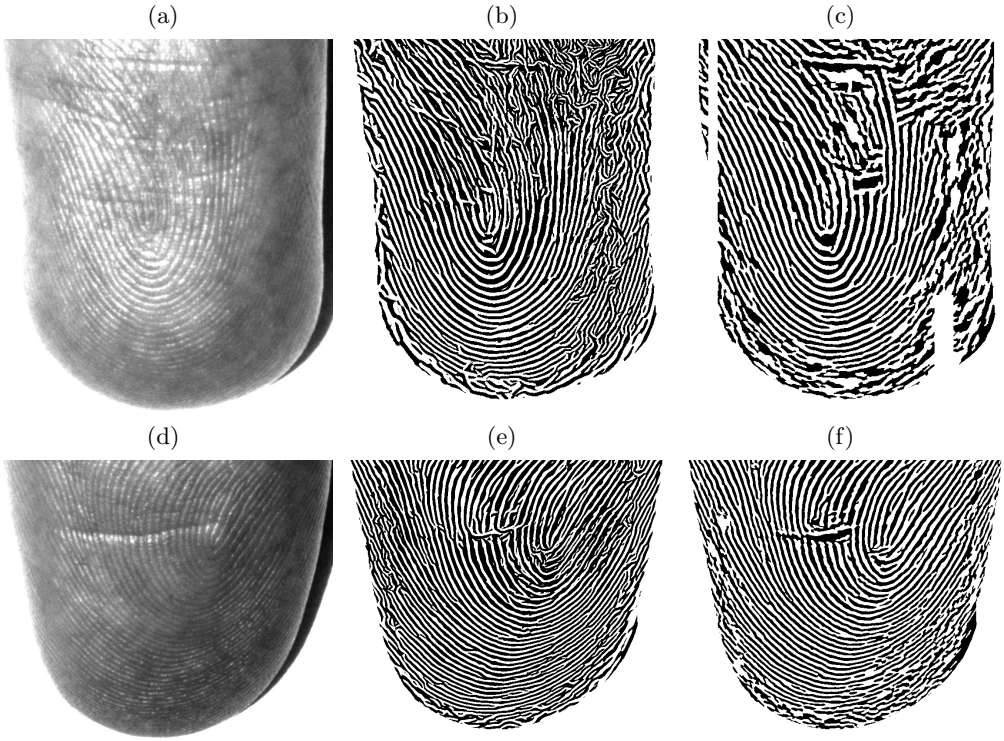

Figure 6.4: Example of results obtained by applying the researched enhancement techniques on contactless fingerprint images captured using a projected static pattern: (a, d) fingerprint images obtained after the removal of the projected pattern; (b, c) results obtained by the Method EA; (d, e) results obtained by the Method EB.

6.2.3.1 Creation of the training and test datasets

Two datasets of fingerprint images for the training and testing steps have been used. The first dataset (Dataset Ac) contains images captured using a contact-based sensor. Dataset Ac is composed by 498 contact-based fingerprint images acquired using a CrossMatch V300 sensor [318, 319]. There are 8 images for each individual. These images have a resolution equal to 500 ppi with the dimension of 512×480 pixel.

The second dataset (Dataset Bc) contains images captured with a contactless sensor. Dataset Bc is composed by 71 grayscale images related to different fingers, captured with a Sony XCD-V90 camera. The size of each image is 1920×1024 pixels, the illumination is controlled by a led, and the used focal is 25mm. The distance from the finger to the lens is about 220mm.

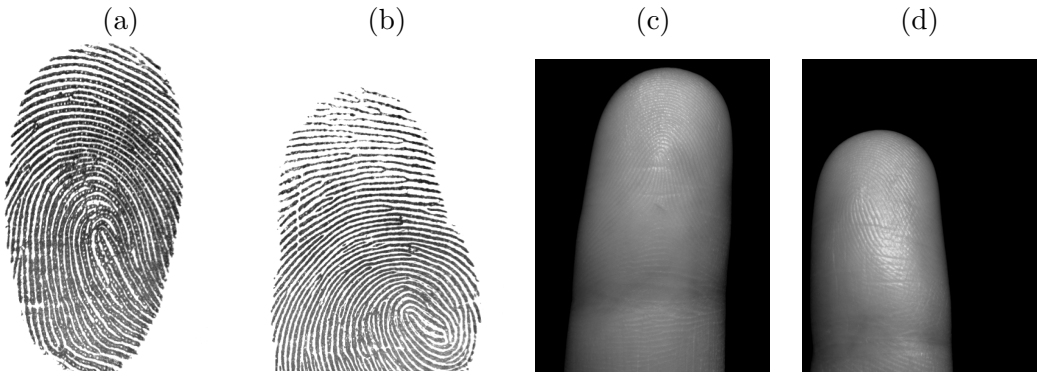

Figure 6.5: Examples of images used for the evaluation of the method for the estimation of the core point: (a,b) images obtained with a contact-based sensor; (c,d) images obtained with a contact-less sensors.

For each dataset, we have manually estimated the core position of every image by selecting the position of the best singular point from the list extracted by the algorithms described in section 5.2.4.1. Fig. 6.5 shows two examples of images of the Dataset Ac, and two examples of images of the Dataset Bc.

6.2.3.2 Computational intelligence techniques and obtained results

In the performed experiments, different classification paradigms have been tested in order to better enlighten the complexity of the learning problem embedded in the datasets. In particular, we adopted the k-Nearest Neighbor classifier with odd values of the parameter $k\,(1, 3, 5)$ and feedforward neural networks with different numbers of neurons in the hidden layer. The topology of the neural networks has been design as follows: we used a linear node for the output layer of the neural networks, and we tested different configurations for the hidden layer. In particular, we have tested one or two levels of nodes with different topologies: log-sigmoidal, and tan-sigmoidal. The algorithm used for the train of the neural networks is the back-propagation algorithm. Other classical inductive classification systems have been considered in our tests, such as the Fisher linear discriminant classifier, and quadratic classifiers with different pre-processing methods. As a reference, we also used two heuristic methods proposed in the literature: the method Heuristic 1 is based on the selection of the core point from the available list of singular regions by selecting the point nearest to the top of the

finger; the method Heuristic 2 considers the singular region nearest to the centroid of the ROI as the core.

In order to train the computational intelligence methods, we adopted the N-fold cross validation technique with $N = 10$ [317]. Table 6.4 reports the classification accuracy of the tested classifiers, and the relative standard deviation over the Dataset Ac and Dataset Bc.

Results show that the studied method offers a remarkable accuracy compared with the reference methods on all datasets. In fact, for the tested datasets, the use of trained classifiers produced better classification accuracy than the heuristic-based classification methods (the last two rows in Table 6.4).

In addition, in the classification of the Dataset Bc, the neural-based classifier showed a very good accuracy compared to the other classical inductive classification system.

The only classification family showing a similar accuracy (on the considered datasets) is the kNN classifiers, but the neural network approach offers a relevant gain in the computational complexity (up to a factor 10 in the classifier execution time on the evaluated datasets). Experiments showed that the neural-based quality classification system is the most suitable for real-time applications.

The obtained results suggest that researched method is general and it can be effectively applied to contact and contactless fingerprint images.

6.3 Methods based on three-dimensional models

This section describes the tests performed to evaluate the accuracy of the researched three-dimensional reconstruction techniques and methods for the computation of contact-equivalent images based on three-dimensional samples. First, the studied technique for the estimation of the three-dimensional coordinates of minutia points (Section 5.3.1) is treated. The three-dimensional reconstruction techniques 3D Method A and 3D Method B (Section 5.3.2) are then compared. Finally, the results obtained by the quality evaluation of contact-equivalent images obtained by unwrapping three-dimensional fingerprint samples (Section 5.3.4 and Section 5.3.5) are discussed.

Table 6.4: Classifiers evaluated for the researched method for the estimation of the core point in contactless fingerprint images.

	Dataset Ac		Dataset Bc	
Classifier	**Mean**	**Std**	**Mean**	**Std**
FFNN-1	0.078	0.032	0.014	0.045
FFNN-3	0.044	0.052	0.057	0.100
FFNN-5	0.048	0.025	0.029	0.060
FFNN-10	0.048	0.025	0.157	0.171
kNN-1	0.013	0.004	0.014	0.000
kNN-3	0.016	0.004	0.028	0.000
kNN-5	0.023	0.002	0.032	0.018
kNN-10	0.028	0.002	0.056	0.000
LDC	0.03	0.002	0.032	0.007
KL-LDC	0.038	0.006	0.039	0.013
PCA-LDC	0.035	0.007	0.028	0.000
Quadratic	0.049	0.006	0.944	0.000
Heuristic 1	0.065	0.248	0.113	0.318
Heuristic 2	0.156	0.364	0.127	0.335

Notes. Classification error obtained on the different datasets with the methods: feedforeword neural network with one hidden layer composed by 1 node (FFNN-1), 3 nodes (FFNN-3), 5 nodes (FFNN-5), 10 nodes (FFNN-10); k Nearest Neighbor with k = 1 (kNN-1), k = 3 (kNN-3), k = 5 (kNN-5), k = 10 (kNN-10); normal densities based linear classifier (ldc); linear classifier by KL expansion of common covariance matrix (KL-LDC); linear classifier by PCA expansion on the joint data (PCA-LDC); quadratic classifier (Quadratic); Heuristic 1; Heuristic 2.

6.3.1 Three-dimensional reconstruction of the minutia points

This subsection describes the experiments performed to evaluate the studied technique for the three-dimensional reconstruction of the minutia points described in Section 5.3.1.

The method has been written in Matlab language (Version 7.6) exploiting the available toolboxes on an Intel Centrino 2.0Ghz working with Windows XP Professional. The parameters used for the computation of the features related to the template Fingercode are: $n_R = 2$; $n_A = 4$; and $n_F = 4$. The parameters used to compute the HOG features are: $c_w = 3$; $c_h = 3$; $c_b = 9$.

6.3.1.1 Classification of minutiae pairs

In order to compare the effectiveness of the extracted feature set, we tested various families of classification systems, in particular, the Linear Bayes Normal Classifier (LDC), the family of the k-Nearest Neighbor classifier with odd values of the parameter k $(1, 3, 5)$, the Linear classifier by KL expansion of common covariance matrix (KLLDC), the Linear classifier by PCA expansion on the joint data (PCA-LDC), and feedforward neural networks with different number of neurons Nr in the hidden layer (FNN-Nr). In this context, we considered neural networks with a two-layered topology where the hidden nodes are log-sigmoidal and the output node is linear. The classical back-propagation algorithm had been used as the training method. All the tested classifiers had been validated with the N-fold cross validation technique with $N = 10$ [317].

We used images captured in our laboratory. The image dataset is composed by 120 color images related to two different fingers, captured by two Sony SX90CR CCD cameras with different angles and distances. The size of each image is 1280×960 pixel, the illumination are controlled by four white LEDs, and the used focal is 25 mm. We used three different acquisition setups characterized by different angles between the cameras and the reference plane (α), distances between the centers of the optics (Δ_D), and distances from the finger to the optics (Δ_H).

- Setup 05: $\alpha = 5°$, $\Delta_D = 45$mm, and $\Delta_H = 230$mm;
- Setup 10: $\alpha = 10°$, $\Delta_D = 75$mm, and $\Delta_H = 230$mm;
- Setup 15: $\alpha = 15°$, $\Delta_D = 125$mm, and $\Delta_H = 230$mm.

The schema of the used acquisition setup is shown is described in Section 5.3.1.

For each setup, we collected 10 pairs of images related to every finger.

We also collected a set of calibration images for each acquisition setup. We captured 15 pairs of chessboard images for each setup. The used calibration chessboard is composed by 12×9 squares of $2,8 \times 2.8$ mm. considering these images, we estimated a reconstruction error of the chessboards in the three-dimensional space equal to 0.03 mm. This error is computed by considering the Euclidean distance of the corner points of each image to equidistant points belonging to interpolated planes.

As a reference, we manually matched the minutiae present in a circle area with radius equal to 120 pixels around to the core point of the fingerprint images. We

considered a total of 24258 classified minutiae pairs, which are labeled as positive (real pairs) and negative (false pairs).

For each image acquisition setup, we considered six different feature sets, obtaining 24 datasets. For each minutiae pair (i, j) of two fingerprint images A and B, these datasets contain the following values.

- Feature set A: the Euclidean distance between $F_A(i)$ and $F_B(j)$;
- Feature set B: the Euclidean distance between $H_A(i)$ and $H_B(j)$;
- Feature set C: $M_A(i)$ - $M_B(j)$, and the Euclidean distance between $F_A(i)$ and $F_B(j)$;
- Feature set D: $M_A(i)$ - $M_B(j)$, and the Euclidean distance between $H_A(i)$ and $H_B(j)$;
- Feature set E: $M_A(i)$ - $M_B(j)$, and $F_A(i)$ - $F_B(j)$;
- Feature set F: $M_A(i)$ - $M_B(j)$, and $H_A(i)$ - $H_B(j)$.

The studied method showed a remarkable accuracy, especially when neural networks had been adopted as the final classifiers of the system. Experiments showed the possibility to suitable train neural networks in order to produce a proper behavior with different setup configurations. Remarkably, neural networks achieved a similar (or better) accuracy with respect to the best traditional inductive methods among the set we considered in our tests, and, most of the time, with a minor computational complexity.

In particular, Table 6.5 shows the results of different compositions of features for the Setup 05. The studied method achieved a good accuracy especially using features related to the Euclidean distance between the features processed by Gabor filters (Dataset 05-C) with a classification mean error equal to 0.9%. A similar situation is present in the experiments related to the Setup 10 and Setup 15. In particular, Table 6.6 reports that neural networks obtained the best accuracy with a classification error of 1.5% in the Setup 15 by using the Dataset 15-A and Dataset 05-C. The only classification family showing a similar accuracy (on the considered datasets) is the kNN classifiers, but the neural network approach offers a relevant gain in the computational complexity. Within the presented experiments, the minimum gain factor found is more than 100.

Table 6.5: Results obtained by the studied method for the search of corresponding minutia points using neural networks on the 05° datasets

Method	Dataset 05-A		Dataset 05-B		Dataset 05-C		Dataset 05-D		Dataset 05-E		Dataset 05-F	
	Mean	Std	Mean	Std	Mean	Std	Mean	Std	Mean	Std	Mean	Std
linear	0.010	0.000	0.017	0.000	0.009	0.001	0.015	0.000	0.037	0.000	0.038	0.000
quadratic	0.010	0.000	0.018	0.000	0.008	0.000	0.008	0.000	0.012	0.001	0.036	0.001
pcldc	0.010	0.000	0.017	0.000	0.009	0.000	0.015	0.001	0.037	0.000	0.038	0.001
klldc	0.010	0.000	0.017	0.000	0.009	0.000	0.015	0.000	0.037	0.000	0.038	0.000
kNN-1	0.018	0.001	0.031	0.001	0.011	0.001	0.016	0.001	0.013	0.001	0.016	0.001
kNN-3	0.012	0.000	0.022	0.001	0.010	0.001	0.014	0.001	0.014	0.001	0.015	0.001
kNN-5	0.011	0.001	0.021	0.001	0.010	0.000	0.013	0.001	0.015	0.000	0.014	0.000
kNN-10	0.011	0.001	0.020	0.001	0.009	0.001	0.015	0.000	0.020	0.000	0.015	0.000
FNN-1	0.015	0.016	0.026	0.015	0.008	0.004	0.014	0.006	0.040	0.016	0.065	0.020
FNN-3	0.010	0.006	0.018	0.010	0.007	0.003	0.015	0.010	0.049	0.016	0.063	0.014
FNN-5	0.0100	0.005	0.019	0.007	0.010	0.003	0.013	0.008	0.042	0.025	0.056	0.026
FNN-10	0.010	0.006	0.020	0.009	0.014	0.012	0.008	0.006	0.030	0.018	0.049	0.020

Notes. Classification methods: linear classifier (linear); quadratic classifier (quadratic); linear classifier using PC expansion (pcldc); linear classifier using KL expansion (klldc); kNN with k=1 (kNN-1); kNN with k=3 (kNN-3); kNN with k=5 (kNN-5); kNN with k=10 (kNN-10); feedforeword neural network with one hidden layer composed by 1 nodes (NN-1); feedforeword neural network with one hidden layer composed by 3 nodes (NN-3); feedforeword neural network with one hidden layer composed by 5 nodes (NN-5); feedforeword neural network with one hidden layer composed by 10 nodes (NN-10).

Experiments showed that the used feature sets permit to properly classify the minutiae pairs with an interesting accuracy and that the neural-based system is probably the most suitable model for real-time applications.

A quality analysis of the obtained three-dimensional minutiae sets for each image shows the effectiveness of the studied reconstruction technique. The calibration procedure of the system, obtained by 2.8×2.8 mm chessboards, showed a remarkable three-dimensional reconstruction accuracy with localization errors of few less than one tenth of millimeters. Fig. 6.6 plots an example of the reconstructed three-dimensional minutiae above the corresponding left input image. Vertical segments show the correspondences between the identified three-dimensional points and the relative position of the minutiae in the left image.

Classification errors produce mismatches in the minutiae pairs, hence, as a consequence, the resulting three-dimensional points tend to be quite far from the finger surface. This kind of points can be further post-processed and deleted from the minutiae list by using a three-dimensional spike filter.

Table 6.6: Results obtained by the studied method for the search of corresponding minutia points using neural networks on the 15° datasets

Method	Dataset 15-A		Dataset 15-B		Dataset 15-C		Dataset 15-D		Dataset 15-E		Dataset 15-F	
	Mean	Std	Mean	Std	Mean	Std	Mean	Std	Mean	Std	Mean	Std
linear	0.016	0.001	0.018	0.000	0.020	0.000	0.018	0.001	0.044	0.001	0.052	0.002
quadratic	0.020	0.000	0.017	0.000	0.018	0.000	0.015	0.001	0.040	0.001	0.146	0.007
pcldc	0.016	0.001	0.018	0.001	0.020	0.000	0.017	0.001	0.043	0.000	0.052	0.002
klldc	0.016	0.001	0.017	0.000	0.020	0.000	0.018	0.001	0.044	0.000	0.052	0.002
kNN-1	0.023	0.001	0.031	0.002	0.027	0.002	0.020	0.002	0.017	0.000	0.019	0.001
kNN-3	0.021	0.002	0.020	0.002	0.021	0.001	0.017	0.001	0.022	0.002	0.020	0.002
kNN-5	0.018	0.002	0.017	0.001	0.015	0.001	0.020	0.001	0.027	0.003	0.019	0.002
kNN-10	0.014	0.000	0.015	0.001	0.015	0.001	0.019	0.000	0.030	0.002	0.018	0.001
FNN-1	0.024	0.020	0.024	0.022	0.020	0.015	0.020	0.017	0.059	0.024	0.065	0.015
FNN-3	0.016	0.013	0.016	0.009	0.019	0.009	0.022	0.018	0.067	0.022	0.069	0.029
FNN-5	0.015	0.012	0.017	0.009	0.015	0.012	0.018	0.011	0.078	0.037	0.050	0.017
FNN-10	0.015	0.014	0.019	0.017	0.026	0.015	0.023	0.023	0.044	0.034	0.096	0.126

Notes. Classification methods: linear classifier (linear); quadratic classifier (quadratic); linear classifier using PC expansion (pcldc); linear classifier using KL expansion (klldc); kNN with k=1 (kNN-1); kNN with k=3 (kNN-3); kNN with k=5 (kNN-5); kNN with k=10 (kNN-10); feedforeword neural network with one hidden layer composed by 1 nodes (NN-1); feedforeword neural network with one hidden layer composed by 3 nodes (NN-3); feedforeword neural network with one hidden layer composed by 5 nodes (NN-5); feedforeword neural network with one hidden layer composed by 10 nodes (NN-10).

The results obtained on three-dimensional minutiae captured from stereoscopic contactless images show that the final accuracy can be improved with respect to the use of single contactless images.

6.3.2 Three-dimensional reconstruction of the finger surface

This subsection compares the performances obtained by the 3D Method A and 3D Method B of the researched approach for the reconstruction of the finger volume (Section 5.3.2). This comparison is first performed by evaluating the quality of the contact-equivalent images obtained by the two methods.

6.3.2.1 The used datasets

The performances obtained the 3D Method A and 3D Method B have been compared on biometric samples captured in our laboratory.

The used setup consists of two Sony XCD-SX90CR CCD color cameras synchronized by using a trigger mechanism. The angle of the cameras with respect to the horizontal

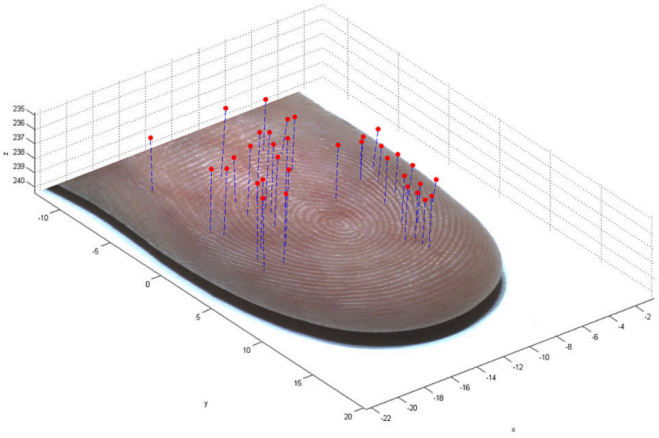

Figure 6.6: Example of three-dimensional minutiae reconstructed by the studied method for the search of corresponding minutia points using neural networks. Vertical segments show the correspondence between the identified three-dimensional points and the relative position of the minutiae of the left image. The distances are related to the reference view.

support is $\alpha = 85°$, with a baseline distance between the cameras $\Delta_D = 45$ mm (from the centers of the CCDs). The projector is placed at a distance of $\Delta_P = 460$ mm and with an inclination angle $\beta = 15°$ with respect to the surface. The distance between the led light and the surface is $\Delta_L = 290$ mm. The distance from the finger to the cameras is $\Delta_H = 235$ mm. This distance is controlled by using a wooden panel in order to correctly place the finger. The setup configurations are shown Fig. 5.11.

We captured two datasets of images by using the structured light and non-structured light configurations. The two datasets are obtained by capturing 36 different fingers with the realized two-view acquisition systems. For each finger, 10 pairs of images were captured, for a total of 360 pairs of images. We refer to the dataset captured using the acquisition setup of the 3D Method A as Dataset A3d, and to the dataset captured using the 3D Method B as Dataset B3d.

The data used to perform the calibration consit in 15 pairs of images describing a chessboard acquired in different positions. The calibration chessboard is composed by 12×9 squares of 2.8×2.8 mm. From these images, we computed a reconstruction error of 0.03 mm. This error had been obtained by triangulating the two-dimensional coordinates of the chessboard corners, extracted by the calibration algorithm, and computing the interpolating plane of the three-dimensional corner positions. We assumed as an error measure the standard deviation of the Euclidean distance between the triangulated corners and the plane, with an approach similar to the one described in [320].

6.3.2.2 Parameters of the evaluated methods

The parameters of the studied methods have been empirically tuned on the used datasets. The value Δ_P used for the computation of the projected pattern is equal to 80; the parameters of the segmentation algorithm are $t_h = 0.9$, $t_l = 0.15$, $r_s = 20$, and $r_p = 40$; the values used by the method for the matching of the reference points are $l = 21$, $\Delta_x = 130$, $\Delta_y = 5$, $w = 130$, and $h = 7$; the parameters used by the three-dimensional estimation algorithm are $t_s = 8$, and $n_p = 8$; the values used by the unwrapping technique are $t_y = 8$, and $t_z = 8$.

6.3.2.3 Comparison between three-dimensional reconstruction methods

Three-dimensional models have been computed from the images appertaining to the considered datasets by using both the 3D Method A and 3D Method B, and the quality of the resulting unwrapped three-dimensional models was then evaluated. One important quality measure consists in the evaluation of the ridge pattern visibility and distortion after the unwrapping step. In fact, low quality ridge patterns can drastically reduce the accuracy of biometric recognition systems. This analysis is particularly important in the studied system because an incorrect projected pattern would drastically decrease the visibility of the ridges. Fig. 6.7 shows two examples of enhanced fingertip images after the unwrapping of the three-dimensional models, computed by using the 3D Method A and 3D Method B. It is possible to observe that the use of the structured light does not affect the quality of the resulting textures.

Another important quality measure is the number of outliers present in the three-dimensional models. These points, in fact, can produce distortions of the finger shape, introducing errors in the subsequent unwrapping step. Using the 3D Method A, the number of spikes is smaller. It is therefore possible to use simpler and faster filtering techniques and to obtain more accurate three-dimensional reconstructions. Fig. 6.8 shows a comparison between the filtered and unfiltered point clouds, and the respective surface estimations. It is possible to observe that, with the aid of the structured light, the small number of outliers does not affect the surface estimation.

In order to numerically evaluate the quality of the reconstructed three-dimensional models, we tested the contact-equivalent images related to each reconstructed three-dimensional fingertip sample by using the NIST NFIQ software. The quality of the

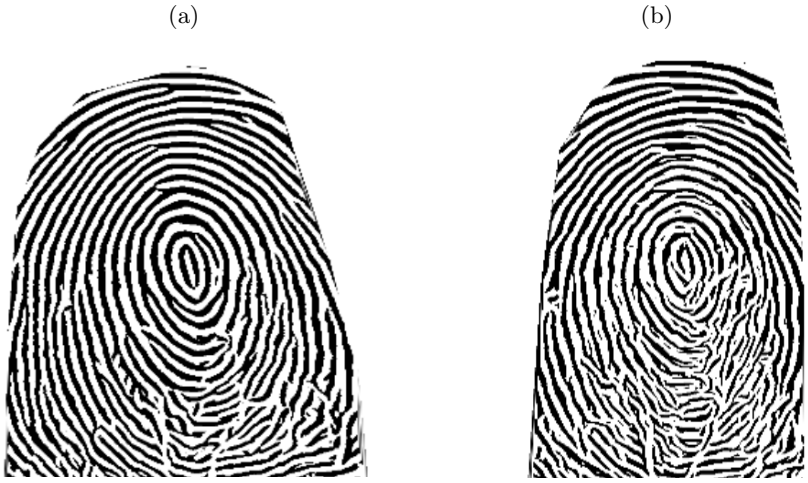

Figure 6.7: Enhanced images obtained by unwrapping the three dimensional models computed by using the structured light and non-structured light approaches: (a) image obtained by using the 3D Method A; (b) image obtained by using the 3D Method B. The usage of the structured light can speed-up the creation of the 3D templates up to 90%.

Table 6.7: Numerical evaluation of the unwrapped fingerprint images obtained from three-dimensional samples representing the finger volume.

3D Method A		**3D Method B**	
Mean	**Std**	**Mean**	**Std**
1.380	0.840	1.890	1.120

contact-equivalent images, in fact, is strictly related to the presence of spikes and to the correctness of the ridge pattern. The obtained results are summarized in Table 6.7.

Table 6.7 shows that the 3D Method A permitted to obtain contact-equivalent images with better quality levels. This result is related to the fact that the presence of spikes influences the quality of the images obtained by the studied unwrapping method.

We also compared the computational time needed by the three-dimensional reconstruction methods. The use of the projected pattern allowed to drastically reduce the time needed by the point matching method. In the 3D Method A, the search of every matching point is performed by considering a subset of 60 points adjacent to the candidate point. In the 3D Method B, we defined the minimum size of the search range as equal to 910 pixel. For this reason, the average time needed to reconstruct a three-dimensional point cloud using the projected pattern is decreased by 90%.

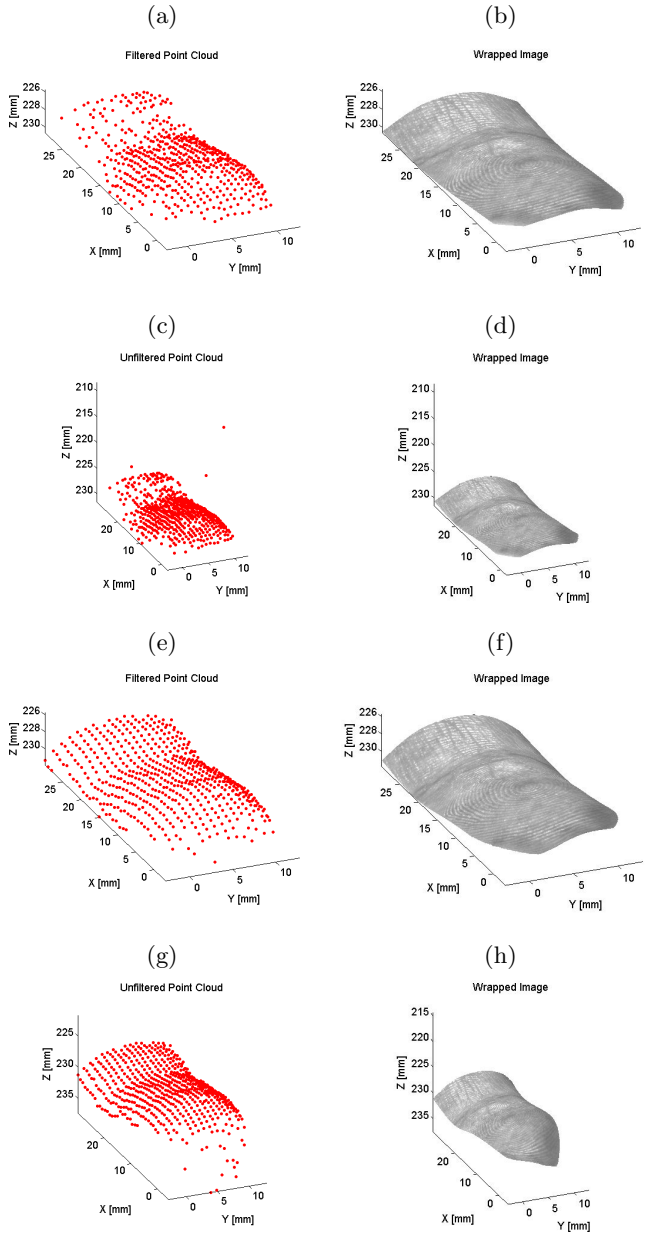

Figure 6.8: Three-dimensional point clouds, filtered and unfiltered, computed using the 3D Method A and 3D Method B: (a,b): filtered point cloud and surface mapping using the 3D Method A; (c,d): unfiltered point cloud and surface mapping using the 3D Method A; (e,f): filtered point cloud and surface mapping using the 3D Method B; (g,h): unfiltered point cloud and surface mapping using the 3D Method B.

6.3.3 Quality assessment of unwrapped fingerprint images

The researched approach for the quality estimation of contact-equivalent fingerprint images obtained by unwrapping three-dimensional models (Section 5.3.5) has been tested by using a set of 300 images with a resolution of about 500 ppi. These images are captured from 30 individuals (10 images per individual). The contact-equivalent fingerprint images are related to the three-dimensional models computed by using the 3D Method A described in Section 5.3.2, and unwrapped using the method described in Section 5.3.4. The input pairs of images captured by the two-view acquisition system are affected by different kinds of problems: reflections, out of focus, and dirty fingers. These problems compromised the correctness of some reconstructed three-dimensional models and, consequently, the quality of the corresponding contact-equivalent images. The obtained contact-equivalent images can present deformations, artifacts, and areas with low visibility of the ridge pattern. The researched method aims to detect the presence of the mentioned problems in order to provide a qualitative measure of the contact-equivalent fingerprint images, which can be used to improve the accuracy of the biometric recognition process.

The acquisition setup is composed by two synchronized Sony XCD-SX90CR CCD color camera, and a DLP projector. The hardware configuration is the one used by the 3D Method B. The parameters of the setup are: $\alpha = 85°$, $\Delta_D = 45$ mm, $\Delta_P = 460$ mm, $\Delta_H = 205$ mm. The two-view system is calibrated by using the technique described in [311, 312], with 15 pairs of chessboard images captured in different positions. The used calibration chessboard is composed by 12×9 squares of 2.8×2.8 mm.

We assigned a quality value for each contact-equivalent fingerprint image. Similarly to the approach described in [229], this value is a predictor of a matcher's performance. The first step of the quality estimation consists in the computation of the distribution of genuines and impostors by using the identity comparison software NIST Bozorth3 [199]. Considering the obtained results, we defined a metric called normalized matching score in order to evaluate the capability of a sample to be properly matched with other samples of the same individual. This measure permits to evaluate if the biometric sample contains sufficient information, and is defined as

$$o\left(x_i\right) = s_m\left(x_{ii}\right) + \left(\mu\left(s_m\left(x_{ij}\right)\right) - s_m\left(x_{ii}\right)\right) / \sigma\left(s_m\left(x_{ij}\right)\right), \tag{6.1}$$

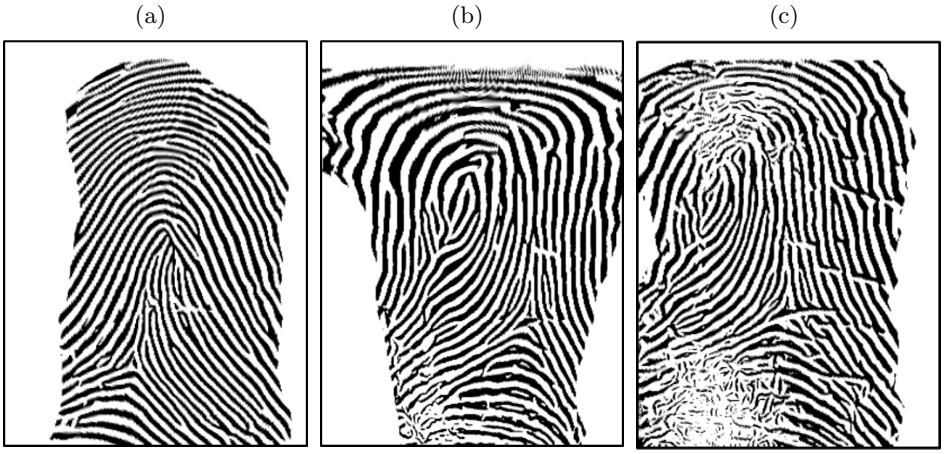

Figure 6.9: Examples of classified contact-equivalent fingerprint images: (a) sufficient quality image; (b) poor quality image with shape deformations; (c) poor quality image affected by the presence of artifacts.

where x_i is the considered sample, $s_m(x_{ii})$ is the matching score obtained by comparing the sample x_i with x_i itself, $\mu(s_m(x_{ij}))$ and $\sigma(s_m(x_{ij}))$ are the mean and standard deviation of the matching scores obtained by comparing the sample x_i with the other samples appertaining to the same individual. In order to maximize the distance between genuines and impostors, we defined the class of each sample x_i as

$$q(x_i) = \begin{cases} +1 & \text{if } o(x_i) > 96 \\ -1 & \text{otherwise} \end{cases} . \tag{6.2}$$

The value $+1$ corresponds to the class "sufficient", and -1 to the class "poor". The resulting number of "sufficient" images is 244, and the number of "poor" images is 56.

Fig. 6.9 shows an example of a contact-equivalent fingerprint image with sufficient quality, and two examples of poor quality images. The image in Fig. 6.9 b suffers of deformations related to the presence of improperly reconstructed regions of the corresponding three-dimensional model. Differently, Fig. 6.9 c presents artifacts caused by out of focus regions in the pair of images captured by the two-view acquisition system.

An example of minutia templates extracted from a sufficient quality image and a poor quality sample of the same finger are shown in Fig. 6.10. It is possible to observe that the minutia coordinates of the poor quality image (Fig. 6.10 b) do not correspond to the ones of the sufficient quality image (Fig. 6.10 a). An identity comparison between the two considered templates can therefore obtain a low similarity value.

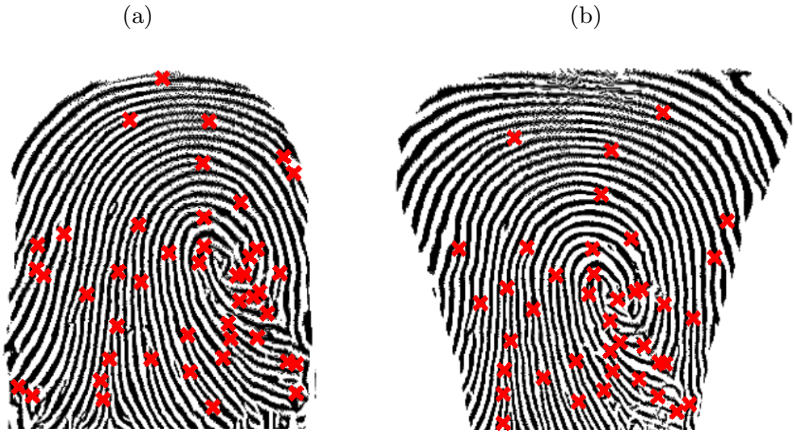

Figure 6.10: Example of minutia templates extracted from fingerprint images with different quality levels: (a) sufficient quality image; (b) poor quality image with shape deformations.

6.3.3.1 Classification results

Different values of the parameters used by the feature extraction algorithm have been experimentally evaluated. In order to compute the Gabor features, we used three sets of angles θ:

- $\Theta_a = (0°, 90°)$,
- $\Theta_b = (-45°, 45°)$,
- $\Theta_c = (-45°, 0°, 45°, 90°)$.

We also evaluated values from 1 to 6 for the parameters m_G and n_G. Similiarly, we considered values from 1 to 6 for the parameters c_w and c_h describing the number of local regions used during the computation of the HOG features, and values from 3 to 12 for the parameters c_b, which define the number of considered orientation bins.

Considering different combinations of features, we created 24 feature sets, which are summarized in Table 6.8.

The quality evaluation of the feature sets is performed by using classifiers based on feedforward neural networks. The topology of the neural networks had been designed as follows: we used a linear node as output layer for the neural networks and we tested different numbers of nodes in the hidden layer. The nodes of the hidden layer are

Table 6.8: Feature datasets tested for the evaluation of the researched approach for the quality assessment of contact-equivalent fingerprint images.

Feature Set Name	**Feature Set Composition**							
	Minutiae	ROI	F_G, Θ_a	F_G, Θ_b	F_G, Θ_c	F_H	$F_{G\sigma}$ Θ_c	$F_{H\sigma}$
Gabor-a1			√					
Gabor-a2	√		√					
Gabor-a3		√	√					
Gabor-a4	√	√	√					
Gabor-b1				√				
Gabor-b2	√			√				
Gabor-b3		√		√				
Gabor-b4	√	√		√				
Gabor-c1					√			
Gabor-c2	√				√			
Gabor-c3		√			√			
Gabor-c4	√	√			√			
HOG-1						√		
HOG-2	√					√		
HOG-3		√				√		
HOG-4	√	√				√		
Gabor-std-1							√	
Gabor-std-2	√						√	
Gabor-std-3		√					√	
Gabor-std-4	√	√					√	
HOG-std-1								√
HOG-std-2	√							√
HOG-std-3		√						√
HOG-std-4	√	√						√

tan-sigmoidal. The method used for the training of the neural networks is the back-propagation algorithm. In order to properly estimate the generalization capability of the trained neural networks, we used the N-fold cross validation technique with N = 10 [317].

Table 6.9 reports the results obtained by the neural classifiers on the evaluated feature sets. This table shows only the best configurations found during the analysis, describing the parameters used by the feature extraction algorithms, the number of considered features, and the number of nodes of the hidden layer. Table 6.9 shows that the studied method obtained a remarkable accuracy with all the evaluated feature sets. Moreover, the best configurations obtained a total classification error equal to 1%. It is also possible to observe that the features computed by using Gabor Filters (F_G and $F_{G\sigma}$) are the most discriminative ones. Another interesting observation is that the accuracy obtained by using the feature sets F_G and F_H is very similar to the accuracy obtained by using $F_{G\sigma}$ and $F_{G\sigma}$.

We compared the results obtained by different classifiers on the best feature set. Table 6.10 shows the results obtained by applying feedforward neural networks, k Nearest Neighbor, linear, and quadratic classifiers on the feature set Gabor-std-1 (with $m_G = 6$, $n_G = 6$, and $\theta_G = 4$).

Table 6.10 shows that simple classifiers do not obtain sufficient results on the evaluated dataset. Differently, classifiers able to approximate more complex functions, like neural networks with a large number of nodes in the hidden layer, can obtain a significant reduction of the classification error. For example, in our experiments, with 45 hidden nodes, the mean error had been reduced by a factor of 10 with respect to different kinds of simpler classifiers.

6.3.4 Comparison with literature methods

The results obtained by applying the reference software NIST NFIQ for the quality classification of fingerprint images [199, 233] to the studied dataset of contact-equivalent fingerprint images is reported in Fig. 6.11. This software returns five integer quality classes and the best image quality corresponds to the class 1. More details are reported in Section 4.5.2.

Table 6.9: Accuracy of neural classifiers on different feature sets obtained by the studied method for the quality estimation of contact-equivalent fingerprint images.

Feature Set	Parameters	Feat. #	Hidden	TP (%)	FN (%)	FP (%)	TN (%)	Tot. (%)
Gabor-a1	$m_G = 3$, $n_G = 3$, $\theta_G = 2$	18	60	18.00	0.67	2.33	79.00	3.00
Gabor-a2	$m_G = 5$, $n_G = 5$, $\theta_G = 2$	55	35	18.00	0.67	0.67	80.67	1.33
Gabor-a3	$m_G = 4$, $n_G = 4$, $\theta_G = 2$	36	45	17.67	1.00	1.00	80.33	2.00
Gabor-a4	$m_G = 4$, $n_G = 4$, $\theta_G = 2$	39	75	17.67	1.00	1.00	80.33	2.00
Gabor-b1	$m_G = 4$, $n_G = 4$, $\theta_G = 2$	32	70	17.00	1.67	0.67	80.67	2.33
Gabor-b2	$m_G = 5$, $n_G = 5$, $\theta_G = 2$	55	55	17.67	1.00	0.33	81.00	1.33
Gabor-b3	$m_G = 4$, $n_G = 4$, $\theta_G = 2$	36	70	17.67	1.00	2.00	79.33	3.00
Gabor-b4	$m_G = 5$, $n_G = 5$, $\theta_G = 2$	57	75	17.33	1.33	1.00	80.33	2.33
Gabor-c1	$m_G = 3$, $n_G = 3$, $\theta_G = 4$	36	50	16.67	2.00	0.33	81.00	2.33
Gabor-c2	$m_G = 5$, $n_G = 5$, $\theta_G = 4$	67	75	18.33	0.33	0.67	80.67	1.00
Gabor-c3	$m_G = 4$, $n_G = 4$, $\theta_G = 4$	68	55	16.33	2.33	0.67	80.67	3.00
Gabor-c4	$m_G = 4$, $n_G = 4$, $\theta_G = 4$	71	30	17.67	1.00	0.33	81.00	1.33
HOG-1	$c_w = 3$, $c_h = 3$, $c_b = 12$	108	55	16.67	2.00	1.00	80.33	3.00
HOG-2	$c_w = 3$, $c_h = 3$, $c_b = 9$	86	35	17.00	1.67	0.33	81.00	2.00
HOG-3	$c_w = 3$, $c_h = 3$, $c_b = 9$	85	55	16.00	2.67	0.33	81.00	3.00
HOG-4	$c_w = 3$, $c_h = 3$, $c_b = 9$	88	50	17.33	1.33	1.00	80.33	2.33
Gabor-std-1	$m_G = 6$, $n_G = 6$, $\theta_G = 4$	36	45	18.00	0.67	0.33	81.00	1.00
Gabor-std-2	$m_G = 4$, $n_G = 4$, $\theta_G = 4$	20	65	17.00	1.67	0.33	81.00	2.00
Gabor-std-3	$m_G = 6$, $n_G = 6$, $\theta_G = 4$	39	40	17.33	1.33	0.33	81.00	1.67
Gabor-std-4	$m_G = 5$, $n_G = 5$, $\theta_G = 4$	32	60	17.00	1.67	0.00	81.33	1.67
HOG-std-1	$c_w = 3$, $c_h = 3$, $c_b = 9$	9	55	14.67	4.00	0.33	81.00	4.33
HOG-std-2	$c_w = 3$, $c_h = 3$, $c_b = 9$	13	55	17.33	1.33	2.00	79.33	3.33
HOG-std-3	$c_w = 3$, $c_h = 3$, $c_b = 9$	12	80	18.00	0.67	2.00	79.33	2.67
HOG-std-4	$c_w = 3$, $c_h = 3$, $c_b = 9$	16	70	16.33	2.33	1.33	80.00	3.67

Notes: Feat. # = number of features; Hidden = number of hidden layer nodes of the feedforward neural networks; TP = true positives; FN = false negatives; FP = false positives; TN = true negatives; Tot. = total classification error.

Table 6.10: Results of different classifiers on the best feature set (Gabor-std-1) for the classification of contact-equivalent fingerprint images.

Classifier	Total	Std
FNN-45	0.01	0.04
ldc	0.18	0.013
klldc	0.18	0.011
pcldc	0.18	0.006
quad	0.17	0.002
kNN-1	0.16	0.007
kNN-3	0.16	0.003
kNN-5	0.15	0.007
kNN-10	0.16	0.002

Notes: Total = total classification error; Std = standard deviation of the classification error; NN-45 = feedforward neural networks with one hidden layer composed by 45 nodes; lin = linear classifier; klldc = linear classifier using KL expansion; pcldc = linear classifier using PC expansion; quad = quadratic classifier; kNN = k Nearest Neighbor, where k stands for the number of first neighbors.

Table 6.11: Effects on the EER of the application of different quality classifiers for the studied dataset of contact-equivalent fingerprint images.

Data	Used samples	Discarded samples	EER (%)
Original dataset	300	0	9.56
$q_{NFIQ} = 1$	238	62	5.76
$q_{NFIQ} <= 2$	288	12	7.45
Studied method	244	56	1.97

It is worth noting that the software NFIQ is designed for the quality classification of fingerprint images captured using contact-based sensors and its application in the context of contactless fingerprint images produces sufficient results.

In order to compare the performances of the two methods, we performed an identification test by using the identity comparison method NIST Bozorth3 [199], and by discarding the images classified as insufficient by applying the two considered methods. Table 6.11 reports the number of discarded samples and the obtained EER. Fig. 6.12 shows the obtained DET curves.

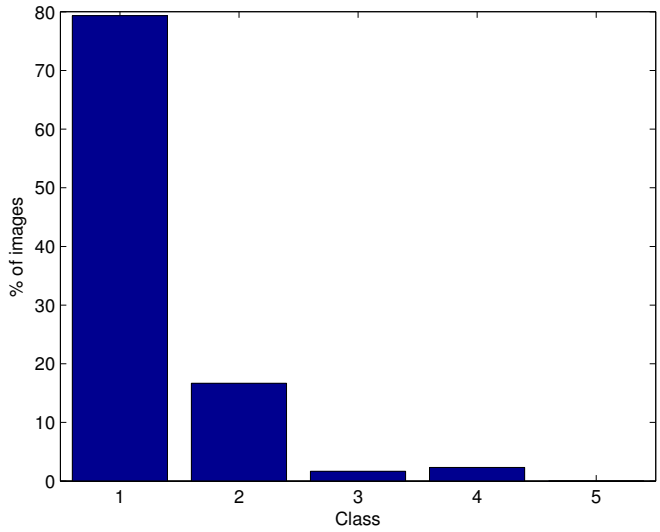

Figure 6.11: Class distribution of the reference software NIST NFIQ on the studied dataset of contact-equivalent fingerprint images. The best image quality corresponds to the class 1.

Table 6.11 and Fig. 6.12 show that the researched method effectively improved the accuracy of the biometric system on the evaluated dataset. In fact, the EER obtained without using this approach is equal to 9.56%, and the EER obtained by discarding the "poor" quality images estimated by the researched approach is 1.97%. The results obtained on the test dataset by the researched approach are also better than the ones obtained by the method NIST NFIQ. The studied approach, in fact, excluded a minor number of samples (56 v.s. 62) and obtained a better EER (1.97% v.s. 5.76 %). Moreover, experiments show that the recognition accuracy is enhanced with respect to the reference methods for almost all the DET curve plot. This fact can be explained by considering that the kind of problems which can affect fingerprint images captured by contact-based sensors are different from the ones that can affect fingerprint images obtained by unwrapping three-dimensional finger models. Notably, the fact that the overall accuracy of the biometric system can be considered as lower than the state-of-the-art systems based on contact-based sensors can be related to the particularly noisy biometric samples that we used for testing the researched approach.

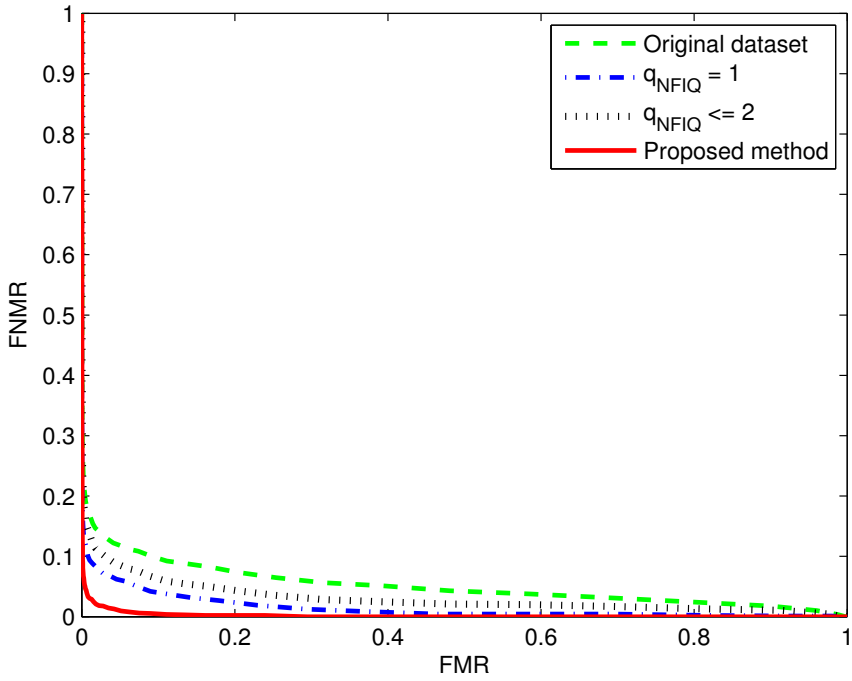

Figure 6.12: Effects on the DET curves of the application of the studied quality assessment method and the software NIST NFIQ on the test dataset composed by 300 contact-equivalent images of fingertip three-dimensional models.

6.4 Comparison between biometric recognition methods

In order to compare the studied contactless fingerprint recognition techniques with traditional biometric systems that require contact-based acquisitions, we performed a scenario evaluation.

The performed comparison considers all the evaluation aspects described in Section 2.4.2: I accuracy; II speed; III cost; IV scalability; V interoperability; VI usability; VII social acceptance; VIII security; IX privacy.

First, the used datasets and applicative conditions are described. Then, the parameters of the implemented methods are reported. Finally, the evaluated aspects of the considered biometric systems are analyzed.

6.4.1 The used datasets

A scenario evaluation have been performed by analyzing the performances of different biometric technologies for the access control in a laboratory.

We captured two datasets of fingerprint samples by using contactless and contact-based sensors. The samples appertaining to Dataset C3d were acquired using the 3D Method C described in Section 6.3.2. The fingerprint images appertaining to the Dataset Ct were acquired using a Crossmatch V300 [318, 319].

The samples appertaining to Dataset C3d and Dataset Ct were captured during a single session of one week. Dataset C3d is composed by 1040 pairs of synchronously captured pairs of contactless fingerprint images, and Dataset Ct is composed by 1040 contact-based fingerprint images. These datasets contain samples captured from the same fingers. Biometric data were captured from a set of 13 volunteers, both men and women. The volunteers range from 24 to 63 years old, and include graduate students, workers, pensioner, etc. For both the databases, each volunteer contributed 80 acquisitions of the ten fingers (left and right hands). Each finger was acquired 8 times.

The acquisition setup used to create Dataset C3d is composed by two synchronized Sony XCD-SX90CR CCD color camera, and a blue led with a diffuser lens (Section 6.3.2). The parameters of the setup are: $\alpha = 85°$, $\Delta_D = 45\,\text{mm}$, $\Delta_L = 90\,\text{mm}$, $\Delta_H = 240\,\text{mm}$. The two-view system is calibrated by using the technique described in [311, 312], with 12 pairs of chessboard images captured in different positions. The used calibration chessboard is composed by 12×9 squares of $2.8 \times 2.8\,\text{mm}$.

6.4.2 Parameters used by contactless techniques

The parameters of the researched methods have been empirically tuned on the used dataset. The values used by the 3D Method C for the matching of the reference points are $l = 21$, $\Delta_x = 70$, $\Delta_y = 3$; the parameter used by the three-dimensional estimation algorithm are $t_S = 8$, and $n_p = 8$; the values used by the unwrapping technique are $t_y = 8$, and $t_z = 8$.

6.4.3 Accuracy

The accuracy of the researched contactless fingerprint recognition techniques based on two-dimensional and tree-dimensional samples is compared with the one achieved by traditional biometric systems that adopt contact-based acquisition methods.

We first describe the results obtained by the studied contactless recognition methods based on two-dimensional and three-dimensional samples. Then, the best obtained results are compared with the ones achieved using a contact-based recognition system based on well-known algorithms in the literature.

6.4.3.1 Accuracy of the approach based on two-dimensional samples

The accuracy of the implemented biometric recognition technique based on the analysis of Level 2 features of contactless two-dimensional samples (Section 5.2) has been evaluated. This method computes contact-equivalent images from fingerprint acquisitions obtained by single cameras, and then it performs the feature extraction and matching steps by using well-known algorithms in the literature designed for contact-based fingerprint images.

This method was tested on the images captured by the single views of Dataset C3d. The dataset was then divided into Dataset C3d-1 and Dataset C3d-2. The first subset contains the images captured by the camera A, and the second subset contains the images captured by the camera B. Examples of contact-equivalent images related to the two views of the acquisition system are shown in Fig. 6.13. It is possible to observe that these images present differences due to perspective distortions.

The DET curves obtained by the minutiae based recognition technique on Dataset C3d-1 and Dataset C3d-2 are shown in Fig. 6.14. The obtained EER values on the evaluated datasets are 3.52% and 1.32%. The level of accuracy obtained by the studied technique based on single cameras can therefore be sufficient for low cost applications. For example, this technique can be used in mobile devices with integrated cameras.

Another interesting result is that the researched method obtained better results on Dataset C3d-2 with respect to Dataset C3d-1. This fact can be due to perspective deformations of the images captured by the Camera A.

We also evaluated a multimodal biometric system that fuses the matching scores obtained by applying the studied approach based on contactless two-dimensional sam-

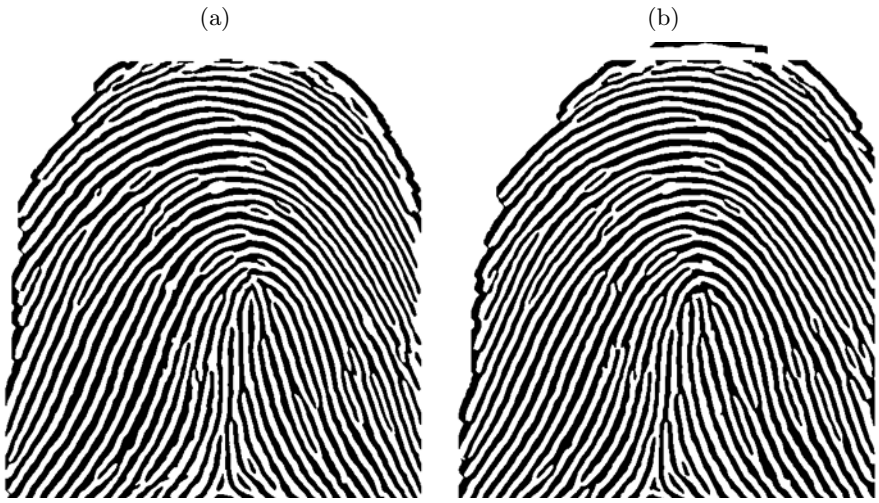

Figure 6.13: Examples of contact-equivalent images related to the two views of the acquisition system: (a) Camera A; (b) Camera B.

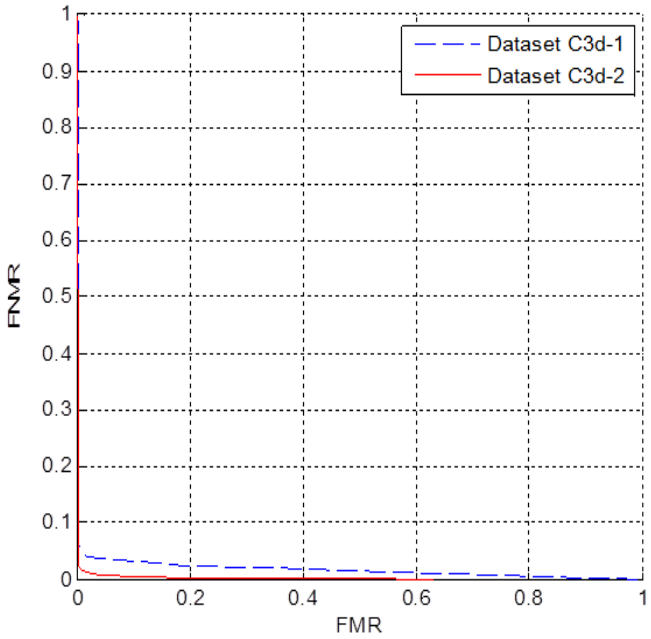

Figure 6.14: DET curves obtained by the studied recognition technique designed for two-dimensional samples on Dataset C3d-1 and Dataset C3d-2.

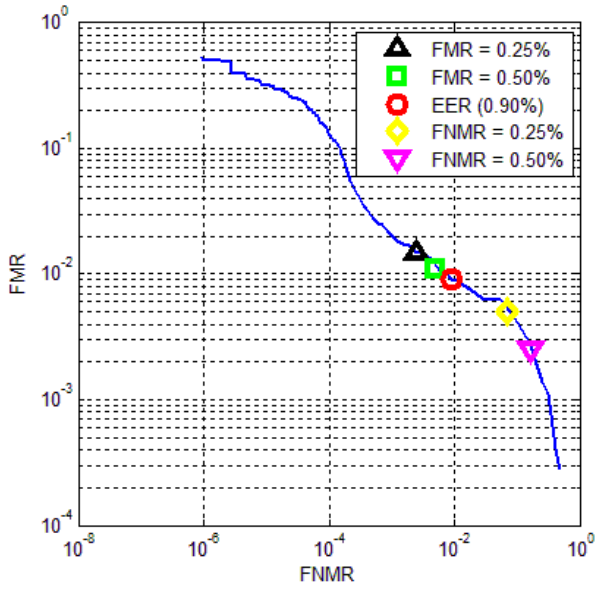

Figure 6.15: DET curve obtained by the researched multimodal approach based on multiple two-dimensional samples on Dataset C3d. The marked points represent the error values reported in Table 6.12.

ples on the images captured by the two views of the considered acquisition setup. This technique can be considered as a multimodal system based on multiple snapshots, which performs the fusion at the matching score level [321]. We evaluated different fusion functions, but we did not considered data normalization techniques because the matching values are obtained using the same recognition algorithm on similar data. Considering the matching scores $m_A(i,j)$ and $m_B(i,j)$, the strategies adopted for the computation of the final matching score $m_s(i,j)$ are:

1. $m_s(i,j) = \text{mean}\left(m_A(i,j), m_B(i,j)\right)$;
2. $m_s(i,j) = \min\left(m_A(i,j), m_B(i,j)\right)$;
3. $m_s(i,j) = \max\left(m_A(i,j), m_B(i,j)\right)$;

The best obtained results are related to the mean fusion function, and obtained an EER equal to 0.90%. The DET curve of the multimodal technique on Dataset C3d is shown in Fig. 6.15, while FMR and FNMR at different points of the DET curve are reported in Table 6.12.

Table 6.12: FMR and FNMR obtained by the researched multimodal approach based on multiple two-dimensional samples on Dataset C3d.

EER %	FNMR @FMR=0.25%	FNMR @FMR=0.50%	FMR @FNMR=0.25%	FMR @FNMR=0.50%
0.900	1.470	1.099	16.524	6.872

Table 6.13: FMR and FNMR obtained by using recognition techniques designed for contact-based recognition systems on contact-equivalenet images computed using the researched 3D Method C and the studied unwrapping technique on Dataset C3d.

EER %	FNMR @FMR=0.05%	FNMR @FMR=0.10%	FNMR @FMR =0.25%	FMR @FNMR=0.25%
0.309	0.453	0.398	0.343	1.521

It is possible to observe that the presented multimodal technique effectively increased the recognition accuracy with respect to the technique based on single contactless acquisitions. Moreover, the obtained results are comparable with contact-based fingerprint recognition systems in the literature. Table 6.12 also shows that the system is able to obtain good results with thresholds of the matching scores that obtain small numbers of false matches. However, the performances decrease drastically with threshold values that obtain small numbers of false non-matches.

6.4.3.2 Accuracy of the approach based on three-dimensional samples

The accuracy obtained by applying the matching algorithm NIST BOZORTH3 [199] to the contact-equivalent images obtained by applying the 3D Method C on Dataset C3d has been evaluated. Fig. 6.16 shows an example of three-dimensional fingerprint model and the corresponding contact-equivalent image.

Fig. 6.17 shows the DET curve obtained by performing 1080560 identity comparisons on Dataset C3d, and Table 6.13 depicts the obtained FMR and FNMR in different points of the DET curve.

The obtained results indicate that the researched approach is able to obtain accurate biometric recognitions. The obtained EER, in fact, is equal to 0.31%. Moreover, the

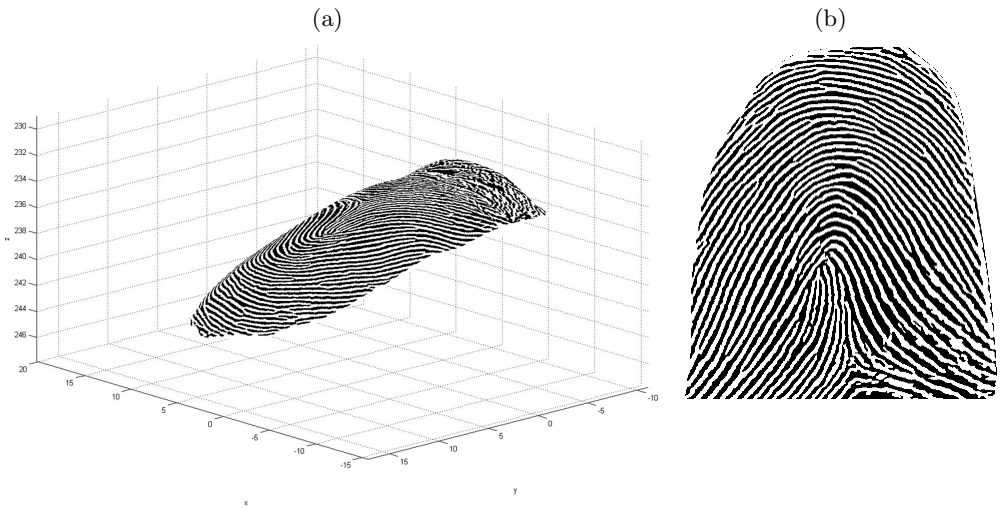

Figure 6.16: Examples of results obtained by the 3D Method C: (a) three-dimensional fingerprint model; (b) corresponding contact-equivalent image.

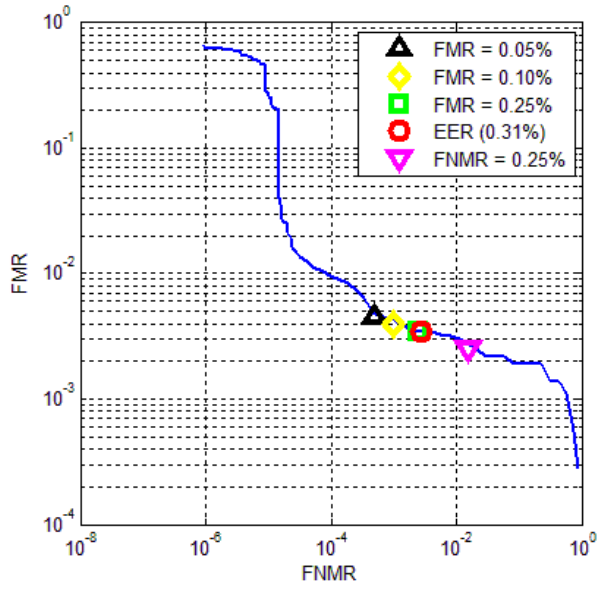

Figure 6.17: DET curve obtained by a minutiae matching technique designed for contact-based recognition systems on contact-equivalent images computed using the 3D Method C and the studied unwrapping technique on Dataset C3d. The marked points represent the error values reported in Table 6.13.

Table 6.14: FMR and FNMR obtained by different recognition technologies in the performed scenario evaluation: approach based on the unwrapping of three-dimensional models; contact-based recognition system; multimodal system based on two-dimensional samples.

Method	EER %	FNMR @ FMR=0.05%	FNMR @FM=0.25%	FMR @FNMR=0.25%
Contact-equivalent 3D	0.309	0.453	0.343	1.521
Contact-based	0.323	0.522	0.385	0.351
2D multimodal	0.900	2.555	1.470	16.524

approach obtained good performances with thresholds of the matching scores that permit to obtain a small number of false matches. This characteristic can permit the use of the approach in high security applications. Differently, with thresholds corresponding to small numbers of false non-matches, the recognition accuracy is less satisfactory. This fact can be caused by poor quality three-dimensional reconstructions due to the presence of motion blur in the captured contactless images.

6.4.3.3 Comparison between different technologies

The best results obtained by the studied contactless approaches on Dataset C3d have been compared with the ones obtained by the algorithm NIST BOZHORT3 [199] on the contact-based images of Dataset Ct. The methods compared with the evaluated recognition system based on contactless acquisitions consist in the unwrapping of three-dimensional samples obtained applying the 3D Method C, and the multimodal technique based on two-dimensional samples.

Fig. 6.18 shows the DET curves obtained by the analyzed biometric recognition systems. The results obtained by these methods in different points of the DET curve are summarized in Table 6.14. The results reported in Table 6.14 are ranked considering the EER values. The best EER was obtained by the researched approach based on three-dimensional samples.

With respect to the compared methods, the approach based on three-dimensional fingerprint samples permits to obtain a greater accuracy in the operative regions characterized by a low number of false acceptances. This fact suggests that fingerprint recognition systems based on contactless multiple view acquisitions should effectively

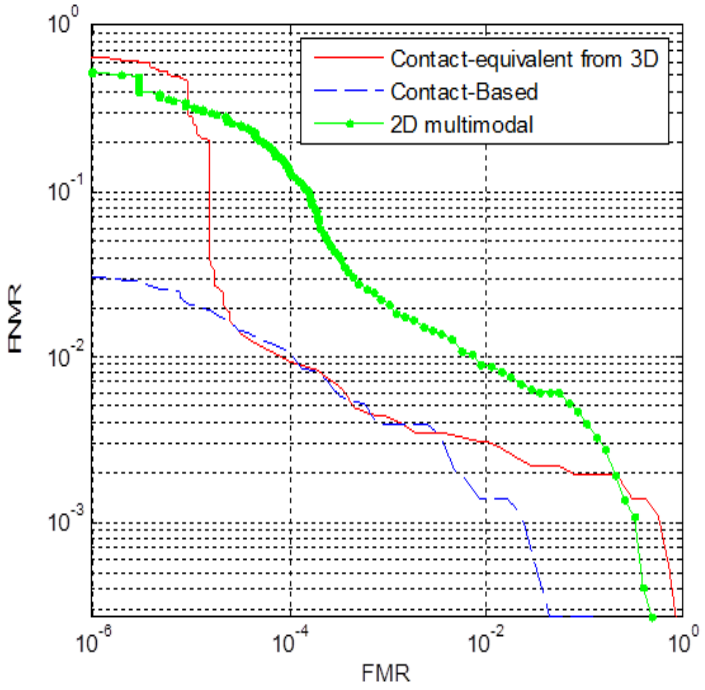

Figure 6.18: DET curves obtained by different recognition technologies in the performed scenario evaluation: approach based on the unwrapping of three-dimensional models; contact-based recognition system; multimodal system based on two-dimensional samples.

be adopted in high security applications. The evaluated contact-based system, however, achieved better performances in other regions of the DET curve.

In order to better evaluate the applicability of the contactless approaches in real applicative contexts, we estimated the confidence limits of the studied method that obtained the most accurate results by using two well-known techniques in the literature. The first technique assumes a normal distribution of the obtained data; while the second technique is based on a bootstrap approach. These techniques are described in Section 2.4.4.

The performed tests were conducted on the results of the studied approach based on contact-equivalent images obtained by the 3D Method C on Dataset C3d. All the obtained results are related to a confidence level equal to 90%. As suggested in [47], the bootstrap technique was applied for 1000 iterations.

Fig. 6.19 shows the obtained DET curves, while Table 6.15 shows the estimated confidence boundaries of the EER point.

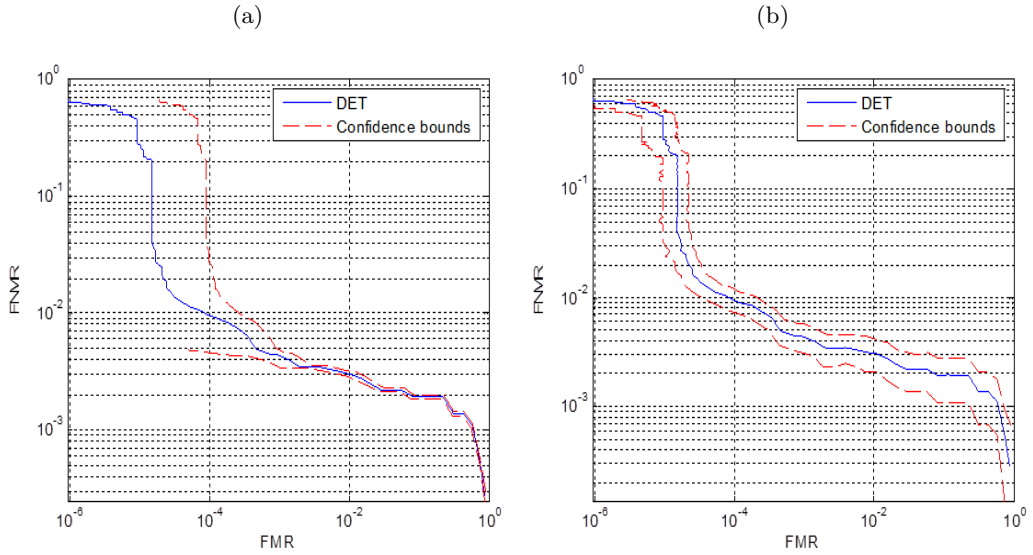

Figure 6.19: Confidence limits of the DET curve obtained by the researched approach based on the unwrapping of three-dimensional models on Dataset C3d: (a) confidence estimated assuming a Normal distribution; (a) confidence estimated assuming the bootstrap technique.

Table 6.15: Confidence limits of the EER obtained by the researched approach based on the unwrapping of three-dimensional models on Dataset C3d.

Confidence estimation	EER	min FMR	max FMR	min FNMR	max FNMR
Normal distribution	0.309	0.208	0.410	0.300	0.3185
Bootstrap	0.309	0.300	0.317	0.200	0.420

Fig. 6.19 and Table 6.15 show that the figures of merit computed for the evaluation of the biometric approach can describe the system accuracy with small confidence boundaries. For this reason, it is possible to think that the researched approach should obtain satisfactory results also on bigger biometric datasets.

6.4.4 Speed

The studied approaches for contactless fingerprint recognition based on two-dimensional and three-dimensional samples have been compared with contact based biometric systems in terms of computational time.

All the methods have been written in Matlab language (R2011b 64 bit) on Intel Xeon 3.30 Ghz working with Windows 7 Professional 64 bit. The considered implementations are not optimized in terms of computational complexity and they do not use parallel computing strategies.

The evaluated contactless techniques first compute contact-equivalent fingerprint images, and then apply the same feature extraction and matching algorithms used for contact-equivalent images. With respect to biometric recognitions performed using contact-based systems, the recognitions based on contactless samples therefore require an additional time t_e for the computation of contactless-equivalent images. In the case of systems based on two dimensional samples, t_e is about 2.70 s. Considering systems based on three-dimensional data, the time interval t_e can be divided into the time t_s needed to perform the three-dimensional reconstruction of the finger surface, and the time t_u needed by the unwrapping step. The values of t_s and t_u are about 28.47 s and 8.25 s, respectively. About 27.35% of the time needed by the implemented three-dimensional reconstruction technique is required for the estimation of the corresponding pairs of points in the images related to the different views of the acquisition setup.

Moreover, the researched techniques are designed to be easily parallelizable. For example, a parallel implementation of these methods based on CUDA techniques [14] can drastically decrease the required computational time. With high probability, a parallel implementation can permit to use the studied techniques based on three-dimensional samples in real-time live biometric applications.

6.4.5 Cost

Contact-based biometric sensors for fingerprint recognition systems have different prices. For example, swipe sensors integrated in mobile devices or personal computers can cost around 10 $, and optical area scan sensors can cost more than 1000 $. The price of the sensor is determined by the acquisition technology, provided accuracy, and number of fingerprints that can be captured at the same time.

The contact-based sensor used to perform the scenario evaluation is a CrossMatch Verifier V300 [319], which is an area scan sensor based on optical technologies, and costs about 700 $.

The realized contactless acquisition systems are based on different hardware setups, which have different costs. These systems, in fact, use one or two cameras and different illumination techniques. We used SX90CR CCD cameras with 25 mm Tamron lenses, which cost about 1500 $. The price of the used led illuminators is less than 100 $.

The final cost of the realized hardware setups is higher with respect of many contact-based fingerprint sensors. Anyway, the reported prices are related to prototypal hardware configurations. Commercial versions of the studied contactless recognition systems should be based on less expansive cameras.

Similarly to contact-based recognition systems, contactless sensors can also use low-cost hardware configurations. The system described in [270], for example, is based on a single webcam. It is also possible to use cameras integrated in mobile devices [271], removing the hardware costs of the cameras.

6.4.6 Scalability

Contact-based fingerprint recognition systems are characterized by high scalability. The biggest biometric datasets in the literature, in fact, are composed by fingerprint samples. Moreover, the existing AFIS are able to perform the recognition of millions of templates [24].

The studied contactless fingerprint techniques that compute contact-equivalent images can use many modules of traditional recognition systems based contact fingerprint acquisitions: feature extraction techniques, matching methods, databases, and network infrastructures. Moreover, they can perform acquisitions based on webcams or cameras integrated in mobile devices, increasing the possible diffusion of fingerprint recognition systems. Contactless techniques can therefore improve the scalability of fingerprint recognition systems.

Table 6.16: Mean matching score between genuine samples captured using contactless and contact-based techniques.

Comparison	Mean matching score between genuines
Contactless - Contactless	133.625
Contact - Contact	157.163
Contact - Contactless	62.288
Contactless - Contact	62.349

6.4.7 Interoperability

An important goal of the studies on contactless fingerprint recognition systems is to guarantee the interoperability with the existing AFIS. This property allows AFIS systems to effectively work with fingerprints acquired and processed with different sensors and techniques (e.g., live and latent fingerprints).

In order to evaluate the compatibility of contact-equivalent fingerprint images obtained by the studied approach based on three-dimensional models with existing AFIS, we evaluated the performance of a well-known recognition technique on a dataset composed both by contact-equivalent images and contact-based images. The used dataset is composed by the contact-equivalent images of Dataset C3d, and the contact-based images appertaining to Dataset Ct. The adopted matching algorithm is NIST BOZORTH3 [199].

Fig. 6.20 shows the achieved DET curve. The reported results are related to 4324320 identity comparisons. The obtained EER is equal to 1.654%. It is possible to observe that the performed test obtained less accurate results with respect to the ones achieved by the used matching method on the single datasets separately.

Considering that contact-equivalent images obtained from three-dimensional models do not present non-linear distortions due to different pressures of the finger on the sensor platen, and they can present artifacts introduced by the three-dimensional reconstruction and unwrapping process, we evaluated the matching scores between genuine samples obtained by the considered acquisition techniques. Fig. 6.21 shows the functions describing the matching scores between genuine samples acquired using contactless and contact-based sensors, and Table 6.16 reports the mean matching scores.

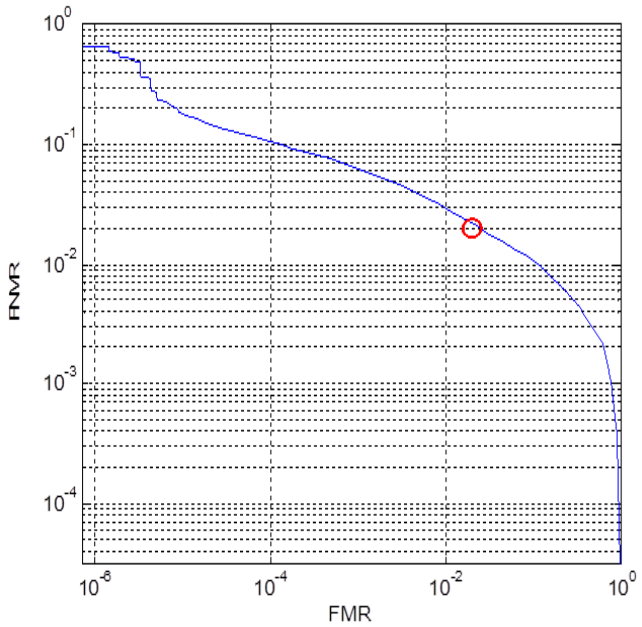

Figure 6.20: DET curve obtained by the method NIST BOZORTH3 [199] on a dataset composed by contact-equivalent and contact-based images. The Equal Error Rate position is marked as a circle in the plot (EER = 1.654%).

It is possible to observe that matching scores between genuine samples acquired using different sensors are around a half of the matching scores achieved by samples acquired with the same technique. Contact-equivalent images and contact-based fingerprint images can therefore be considered as partially compatible. In order to increase the interoperability between contactless and contact-based technologies, future studies should model the distortions present in the considered kinds of fingerprint images.

6.4.8 Usability

Similarly to the study reported in [39], we performed a preliminary usability evaluation according to ISO 9241-11 [322]. Usability is defined as "the extent to which a product can be used by specified users to achieve specified goals with effectiveness, efficiency and satisfaction in a specified context of use". This standard considers three areas of measurement: efficiency, effectiveness, and user satisfaction.

1. The efficiency quantifies the resources expended in relation to the accuracy and completeness. The efficiency is usually measured in terms of time.

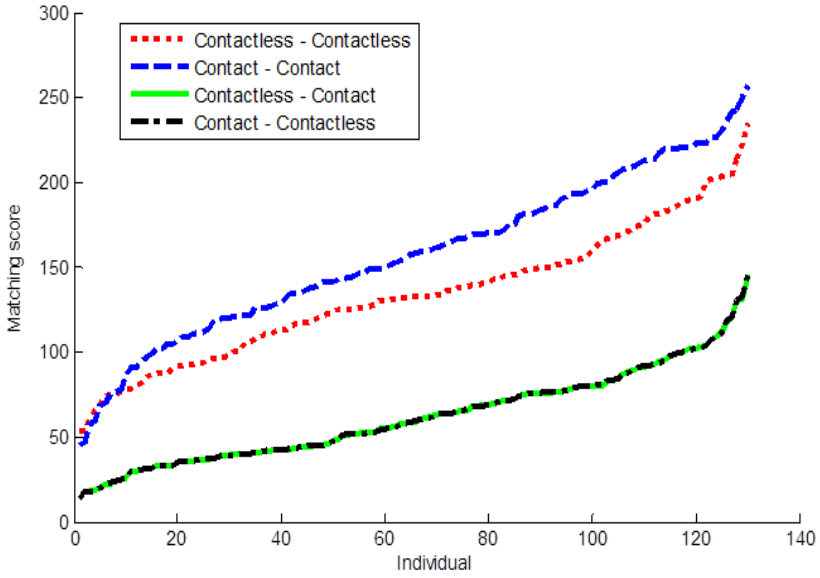

Figure 6.21: Matching scores between genuine samples captured using contactless and contact-based techniques.

2. The effectiveness measures the accuracy and completeness with which users achieve specified goals. Important evaluated aspects are the completion rate and number of errors.

3. The user satisfaction is subjective and is the degree in which the considered technology meets the users' expectations. The evaluation of the user satisfaction should consider the ease of use, and usefulness of the technology.

The usability evaluation was performed on the 13 volunteers during the creation of Dataset C3d and Dataset Ct, which are related to a scenario evaluation regarding the access control in a laboratory. This test aims to compare the usability of the 3D Method C and a biometric system that use a contact-based acquisition sensor CrossMatch V300 [319].

The creation of Dataset C3d was performed without using techniques that permit to automatically capture sufficient quality frames during the live acquisitions, and the best quality frames representing the captured fingerprints were selected by a skilled operator during every acquisition. This is due to the fact that our implementation of the studied technique for the search of the best quality frames in frames sequences

describing contactless fingerprint acquisitions (Section 5.2) cannot actually work in real-time since it consists in prototypal software developed in Matlab [323]. In order to obtain comparable data, also the images appertaining to Dataset C3t ware captured without using automatic quality evaluation methods. An industrial implementation of the quality assessment technique for contactless fingerprint images, anyway, should permit to adopt the quality assessment method in real-time acquisition systems.

Considering the variability introduced by the human operator in every biometric acquisition, we propose a preliminary qualitative evaluation of efficiency aspects focused on quantitative measurements on the time need for every biometric acquisition. As in [39, 324], the first considered aspect is the time needed for a proper placement of the finger on the acquisition sensor, which is very similar for the evaluated contactless and contact-based fingerprint recognition technologies. The training time is also evaluated measuring the time needed to teach the users in a verbal manner. Contactless acquisition techniques required to describe the finger placement needed to prevent out-of focus problems. Contact-based acquisitions required a description of the proper pressure that should be applied to the sensor platen. Results show similar times for the contactless and contact-based sensors. Anyway, the training for using the considered contact-based fingerprint sensor was not necessary for 5 volunteers, since they previously tried traditional fingerprint recognition systems. These cases are not considered in the evaluation of the mean training time needed by the contact-based fingerprint recognition system.

Similarly to [39], the evaluation of the effectiveness is performed by analyzing the quality of the captured images. In order to obtain comparable results, we applied the quality evaluation method NIST NFIQ [233] on the contact-based samples appertaining to Dataset Ct, contact-equivalent images obtained by applying the 3D Method C on Dataset C3d, and contact-equivalent images obtained using the studied approach for the processing of single contactless images on Dataset C3d-1 and Dataset C3d-2. The method returns five quality levels: (5) “poor”, (4) “fair”, (3) “good”, (2) “very good”, and (1) “excellent”. Table 6.17 reports the number of images appertaining to the evaluated datasets with quality level equal or greater than 2. In the performed experiment, contactless acquisition techniques obtained less low-quality images with respect to contact-based acquisition systems. It is possible to observe that all the contact-equivalent images obtained from Dataset C3d are characterized by good and

Table 6.17: Effectiveness comparison of contactless and contact-based systems based on the software NIST NFIQ.

Dataset	Percentage of images with quality ≥ 2
Dataset C3d	100.000
Dataset C3t	95.000
Dataset C3d-1	99.423
Dataset C3d-2	99.231

very good quality levels. Moreover, the number of contact-equivalent images appertaining to Datasets C3d-1 and Datasets C3d-2 with quality equal to (2) very good or (1) excellent is higher with respect to the contact-based Datasets Ct.

In order to evaluate the user satisfaction, each volunteer was asked to perform a satisfaction survey after completing the biometric acquisitions. The questions included in the form are the follows:

- **Q1** - Is the acquisition procedure comfortable?
- **Q2** - What do you think about the time needed for every acquisition?

The possible responses are: (1) very poor; (1) poor; (3) sufficient; (4) good; (5) excellent. The questions are related to the used systems and to two new envisioned technologies:

a) tested contact-based acquisition sensor;

b) tested two-view acquisition technique of the 3D Method C;

c) proposed contactless acquisition system similar to the hardware setup used by the 3D Method C, but with inverted finger placement (rotated of 180°);

d) proposed contactless acquisition system based on active cameras.

The envisioned acquisition system based on active cameras consists in a calibrated multiple-view setup which can be moved in the three-dimensional space by stepper motors. The cameras are fixed on a support which is dynamically moved by the motors according to the finger position. The movements are performed evaluating the camera

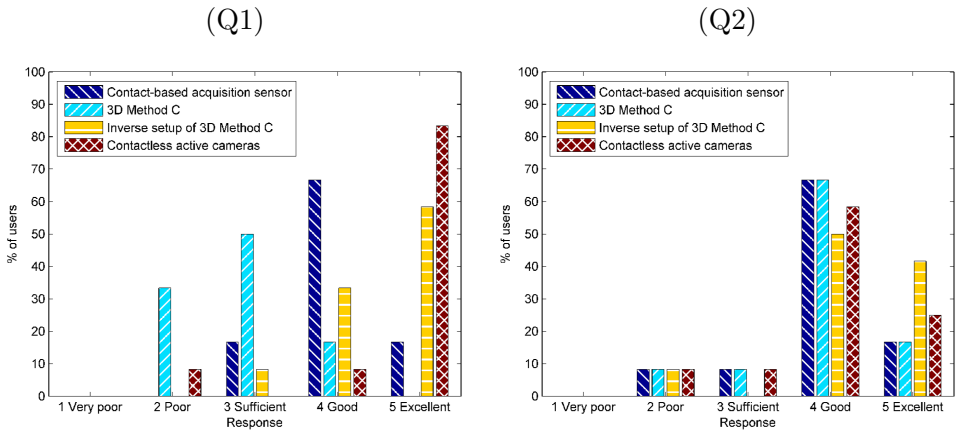

Figure 6.22: Usability comparison of different technologies. A set of volunteers responded to the questions: (Q1) "Is the acquisition procedure comfortable?"; (Q2) "What do you think about the time needed for every acquisition?".

focus in the captured images. In order to obtain metric three-dimensional reconstructions of the finger surface based on hardware calibrations performed offline, the zoom and relative distances between the cameras are constant. The finger would be placed in front to the cameras at an approximate distance of 20 cm.

Fig. 6.22 shows the responses to the questionnaire on the different acquisition technologies.

The mean values of the obtained votes related to the question Q1 are: (I) 4.00, (II) 2.83, (III) 4.50, (IV) 4.67. The best results were obtained by the envisioned system based on the 3D Method C with inverse finger placement. A two samples t-test assuming unequal variances was then conducted to compare the votes obtained by the envisioned system based on the 3D Method C with inverse finger placement with the ones obtained by the used contact-based acquisition systems. In this case, the null hypothesis assumes that the two samples used to process the mean values belong to the same distribution, hence there is no difference in the user opinion about the two tested systems. This result is significant at the 0.044 level and beyond, indicating that the null hypotheses can be rejected with confidence.

The mean values of the obtained votes related to the question Q2 are: (I) 3.92, (II) 3.92, (III) 4.25, (IV) 4.00. The best results were obtained by the envisioned system based on the 3D Method C with inverse finger placement. A two samples t-test

assuming unequal variances was then conducted to compare the votes obtained by the envisioned system based on the 3D Method C with inverse finger placement with the ones obtained by the used contact-based acquisition systems. In this case, the null hypothesis assumes that the two samples used to process the mean values belong to the same distribution, hence there is no difference in the user opinion about the two tested systems. There was a difference in the scores for the two conditions equal to $P = 0.336$. This result suggests that it should be useful to collect more samples in order to properly analyze this aspect.

The performed usability evaluation obtained satisfactory results. The efficiency of the researched contactless approach, in fact, is comparable to the one of contact-based biometric systems. The effectiveness obtained by the contactless recognition technique based on three-dimensional samples outperformed the one of the evaluated contact-based biometric system. Moreover, it is possible to expect that the use of active cameras can permit to obtain more user satisfaction with respect to contact-based systems.

6.4.9 Social acceptance

Similarly to other studies in the literature [40], we compare the social acceptability of different biometric techniques by analyzing the answers to specific sets of questions.

After the acquisition of the Dataset C3d and Dataset Ct, the volunteers were asked to respond to a first set of questions focused on the analysis of the feelings about different aspects of contactless and contact-based fingerprint recognition systems, and to a second set of questions that aim to evaluate the final opinion of the users about contactless technologies.

The first set of questions includes:

- **Q3** - Are you worried about hygiene issues?
- **Q4** - Are you worried about possible security lacks due to latent fingerprints?
- **Q5** - Do you think that biometric data could be improperly used for police investigations?
- **Q6** - Do you feel the system attack your privacy?

Table 6.18: Comparison of social acceptance aspects of different technologies.

		Mean vote	
Question		**Contact-based**	**Contactless**
Q3	Are you worried about hygiene issues?	2.500	4.667
Q4	Are you worried about possible security lacks due to latent fingerprints?	2.500	4.417
Q5	Do you consider the system a hygienic solution?	2.917	2.917
Q6	Do you feel the system attack your privacy?	3.250	3.417

Notes. The possible responses are: (1) very worried; (2) worried; (3) normal; (4) not worried; (5) high trust.

The possible responses are: (1) very worried; (2) worried; (3) normal; (4) not worried; (5) high trust.

For each question, the mean of the obtained votes was computed. The obtained results are shown in Table 6.18. It is possible to observe that the volunteers perceive contactless techniques as more hygienic than contact-based methods. Moreover, they are less worried about possible security lacks due to the release of latent fingerprints in the case of contact-less acquisitions. Differently, the evaluated techniques obtained similar results on the questions regarding the privacy invasiveness, and worries on possible improperly uses of biometric data for police investigations.

We then conducted a two samples t-test assuming unequal variances to compare the results obtained by contactless and contact-based systems on the question Q3. In this case, the null hypothesis assumes that the two samples used to process the mean values belongs to the same distribution, hence there is no difference in the user opinion about the two tested sistems. This result is significant at the $2.142E-07$ level and beyond, indicating that the null hypotheses can be rejected with confidence.

Similarly, we conducted a two samples t-test assuming unequal variances to compare the results obtained by contactless and contact-based systems on the question Q4. In this case, the null hypothesis assumes that the two samples used to process the mean values belongs to the same distribution, hence there is no difference in the user opinion about the two tested sistems. This result is significant at the $6.115E-06$ level and beyond, indicating that the null hypotheses can be rejected with confidence.

Fig. 6.23 shows the histograms of the obtained results.

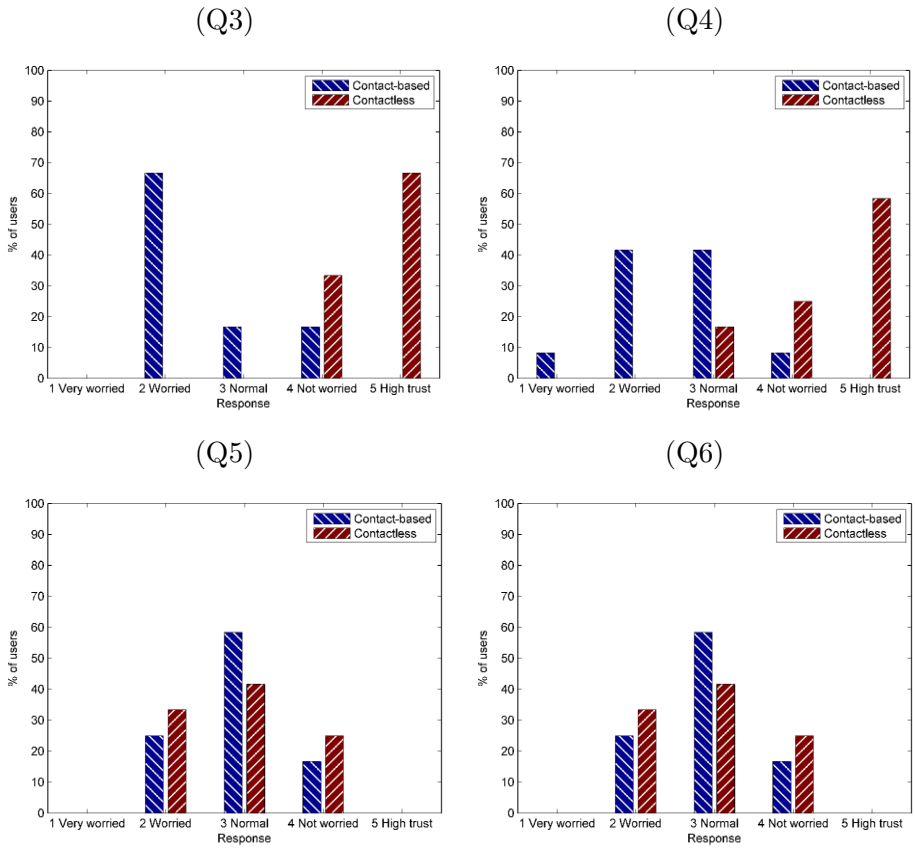

Figure 6.23: Social acceptance comparison of different technologies. A set of volunteers responded to the questions: (Q3) "Are you worried about hygiene issues?"; (Q4) "Are you worried about possible security lacks due to latent fingerprints?"; (Q5) "Do you think that biometric data could be improperly used for police investigations?"; (Q6) "Do you feel the system attack your privacy?".

The second set of questions includes:

- **Q7** Would you be willing to use the contactless fingerprint biometric system daily?
- **Q8** Do you prefer contactless systems against contact-based systems?

All the volunteers responded that they are favorevole to use the contactless fingerprint biometric system daily, and prefer contactless systems.

The obtained results suggest that contactless fingerprint recognition systems can obtain greater social acceptance with respect to contact-based methods.

6.4.10 Security

With respect to contact-based fingerprint recognition systems, contactless techniques do not present security lacks due to the release of latent fingerprints during the acquisition step. The studied biometric recognition methods, however, do not include a vitality detection module. Anyway, it is possible to integrate techniques in the literature based on infrared illumination methods [294].

6.4.11 Privacy

The level of privacy compliancy of contact-equivalent recognition techniques is very similar to the one of contact-based biometric systems. Specific strategies for the privacy protection, in fact, have to be adopted considering the applicative scenario. Moreover, privacy protection methods in the literature designed for contact-based fingerprint recognition systems (like the one presented in Chapter 8) would be applied to the studied contactless fingerprint recognition techniques in order to obtain privacy compliant systems.

6.4.12 Final results

The results obtained by the studied contactless fingerprint recognition techniques in the performed scenario evaluation are summarized.

1. **Accuracy**: the studied method based on two-dimensional samples can obtain satisfactory results and should effectively be used in different applicative contexts. The researched approach based on two-dimensional templates extracted from three-dimensional samples can obtain a comparable or enhanced accuracy with respect to contact-based fingerprint recognition systems.

2. **Speed**: the implemented contactless recognition techniques require more computational time with respect to contact-based methods. In particular, the performance of the used three-dimensional reconstruction technique should be improved by using parallel computing strategies. With high probability, an industrial implementation of the studied approaches should be usable in real-time live applications.

3. **Cost**: the realized contactless acquisition techniques are prototypals based on industrial cameras, which should be substituted by less expensive devices in order to obtain costs inferior to the ones of contact-based acquisition sensors.

4. **Scalability**: contactless fingerprint recognition systems can provide a greater scalability with respect to contact-based methods since they can work using hardware devices already adopted for different applications (e.g. cameras integrated in mobile devices and webcams).

5. **Interoperability**: the studied contactless fingerprint recognition methods are partially compatible with the existing AFIS. Studies on the skin deformation due the contact with the sensor platen should improve the interoperability between contactless and contact-based techniques.

6. **Usability**: the studied contactless acquisition technique for the computation of three-dimensional samples obtains better effectiveness with respect to the evaluated contact-based method. The efficiency of the two techniques is comparable. Differently, the user satisfaction obtained using the realized acquisition setup is lower than the one achieved using contact-based sensors. Anyway, the envisioned systems based the 3D Method C with inverted finger orientation and the envisioned systems based on active cameras obtained better results with respect to contact-based techniques.

7. **Social acceptance**: the use of contactless acquisition techniques can permit to increase the user acceptance of fingerprint recognition systems. In particular, users appreciate the absence of latent fingerprints, and hygienic improvements.

8. **Security**: contactless acquisitions can increase the security of fingerprint recognition systems since no latent fingerprints are released on the sensor surface.

9. **Privacy**: the privacy compliance of contactless and contact-based fingerprint recognition systems is comparable. Privacy protection techniques should be applied in all the systems by considering the applicative context.

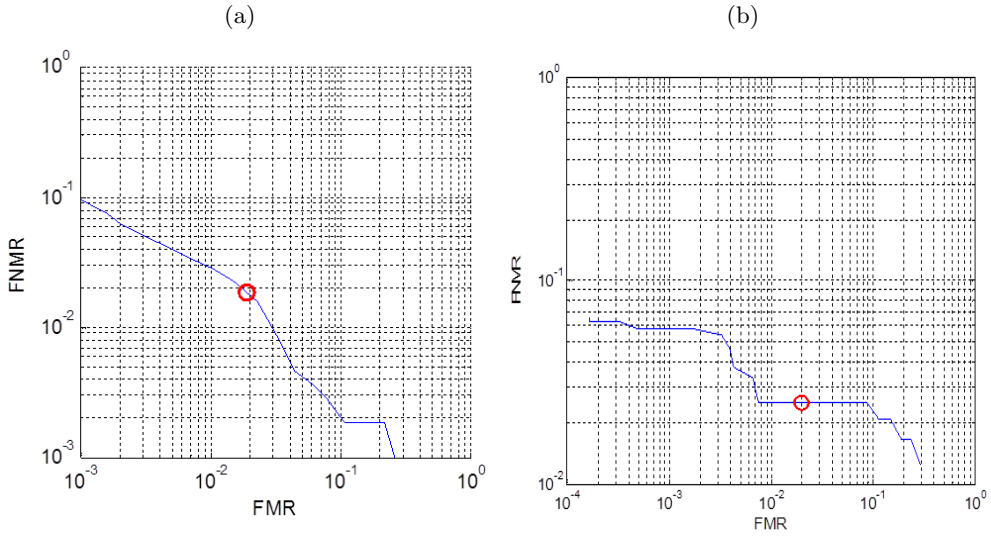

Figure 6.24: DET curve obtained by the studied three-dimensional matching technique: (a) Dataset 3D-1 (EER = 1.86%); Dataset 3D-2 (EER = 2.53%). The Equal Error Rate positions are marked as circles in the plots.

6.5 Preliminar results of the studied three-dimensional matcher

In this subsection, the preliminary results obtained by evaluating the studied biometric recognition technique based on the evaluation of the three-dimensional coordinates of minutia points (Section 5.3.3) are presented. The method was evaluated using two datasets: Dataset 3D-1 is composed by 120 three-dimensional fingerprint samples obtained by randomly selecting a 10 samples from 12 individuals appertaining to Dataset A3d. Dataset 3D-2 is composed by 80 three-dimensional fingerprint samples obtained by randomly selecting 4 samples from 20 individuals appertaining to Dataset C3d. These three-dimensional models present more differences in the finger placement with respect to the ones appertaining to Dataset 3D-1.

The comparisons are performed by using empirically estimated threshold values: $s_D = 0.7\,\text{mm}$ for the distance between minutiae, $s_\vartheta = 5°$ for the minimum angular difference, and $s_D = 0.3\,\text{mm}$, and $s_O = 15°$ for the matching of the Delaunay triangles. In order to overcome problems related to differences in the finger placement during the acquisition process, a preliminary rigid registration task was performed on the three-

dimensional templates appertaining on Dataset 3D-2. Considering two templates T_A and T_B, this step performs a rigid transformation of the template T_B by using the iterative closest point (ICIP) technique [325].

The obtained DET curves are shown in Fig. 6.24. The obtained EER on Dataset 3D-1 is equal to 1.86%, while the EER on Dataset 3D-2 is equal to 2.53%.

It should be noted that the limited dimensions of the tested population does not yet allow for generalizing the results concerning FMR, and FNMR. The obtained results, however, are encouraging and show that matching techniques based on three-dimensional coordinates of minutia points are feasible.

The evaluated method, however, obtained less accurate results with respect to well-known techniques in the literature based on two-dimensional features. The main observed problem is related to the rigid registration of three-dimensional templates obtained from samples captured with different finger placements. This is due to the fact that well-known techniques designed for the alignment of three-dimensional models, like ICIP, can obtain poor results on three-dimensional minutia templates. These templates, in fact, are composed by small sets of points, can present false and missed minutiae, and are composed by points estimated with small errors. For this reason, it would be necessary to design more robust template alignment strategies.

6.6 Computation of synthetic three-dimensional models

In order to evaluate the researched method for the computation of synthetic three-dimensional fingerprint models (Section 5.4), we acquired samples from 10 fingers. We captured 5 images for each fingerprint using a Crossmatch V300 contact-based sensor [318, 319], and 5 images for each fingerprint with a Sony XCD-SX90CR camera, using an acquisition setup similar to the one presented in Section 5.3.2. The size of each contactless fingerprint image is 1280×960 pixel. We applied the described approach on the contact-based fingerprint images, and compared the results with the corresponding contactless fingerprint images.

The parameters used in these experiments are: $t_b = 0.1$, $\Delta_r = 0.2$, $n_n = 3$, $\Delta_n = 0.2$, $t_w = 60$, $b_{min} = 1$, $b_{max} = 3$, $m = 30$, $v_s = 0.0001$, $\sigma_p = 0.7$.

The schema of the used evaluation method is shown in Fig. 6.25. We considered the parameters of the light illuminating the finger in the acquisition of the images, in

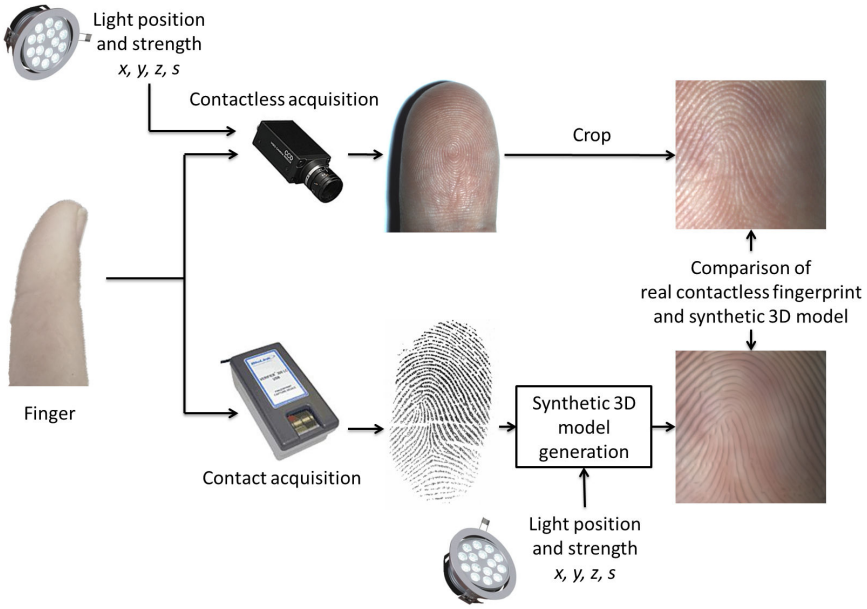

Figure 6.25: Schema of the used method for the evaluation of synthetic fingerprint models.

particular the position and strength of the light, and simulate the same parameters in the computation of the synthetic fingerprint models by moving the light source across a reference Cartesian system centered on the three-dimensional model. The strength of the light source is also experimentally chosen in order to match the illumination used during the contactless acquisitions.

Examples of contactless fingerprint acquisitions and the corresponding synthetic three-dimensional models are shown in Fig. 6.26. In order to better evaluate the results, the corresponding central regions of the fingerprint images were cropped. From the images shown in Fig. 5, it is possible to observe that the studied method achieves a realistic three-dimensional simulation of fingerprints, which resemble the corresponding contactless images. However, some regions of the obtained fingerprint models (in particular the external regions) present small differences compared to the corresponding contactless images. These differences are due to the fact that the studied method estimates the height and focus blur of the model by assuming a cylindrical approximating shape for the finger. This assumption is reasonable in most of the cases, but can produce some small differences with respect to real contactless fingerprint images. Better results should be obtained by applying more complex models of the finger shape.

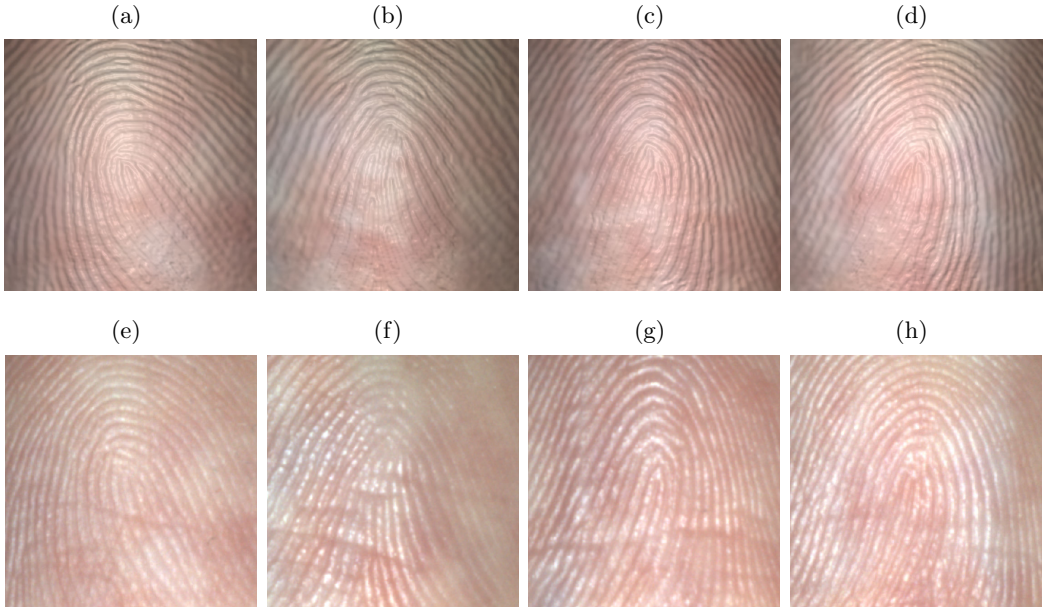

Figure 6.26: Examples of the results of the researched approach for the computation synthetic fingerprint models: (a-e) synthetic models computed using the studied approach; (e-h) corresponding contactless images.

In order to evaluate the realism of the light source simulation, we also collected a set of contactless fingerprints under different illumination conditions and used the implemented method to compute realistic synthetic models. The results obtained by simulating the light conditions shown in Fig. 4.20 are depicted in Fig. 6.27. In particular, we compared the synthetic models with real contactless images captured with an illumination from the left side (Fig. 6.27 d), from the right side (Fig. 6.27 e), and from the top side (Fig. 6.27 f). It is possible to observe that the simulated fingerprint models are very similar to the corresponding contactless images.

We also tested the capability of the method of simulating fingerprint models obtained using different kinds of cameras. As an example, Fig. 6.28 shows a comparison of the results obtained by simulating a fingerprint captured by a Sony XCD-SX90CR camera (Fig. 6.28a) and a VGA webcam (Fig. 6.28b). In order to compute the model shown in Fig. 6.28b, we used different parameters for the simulation of the lens focus ($b_{min} = 3$, $b_{max} = 5$) and color pattern ($v_s = 0.001$). It can be observed that the fingerprint model depicted in Fig. 6.28b presents typical characteristics of the images captured using webcams, such as blur, out of focus regions, and noise.

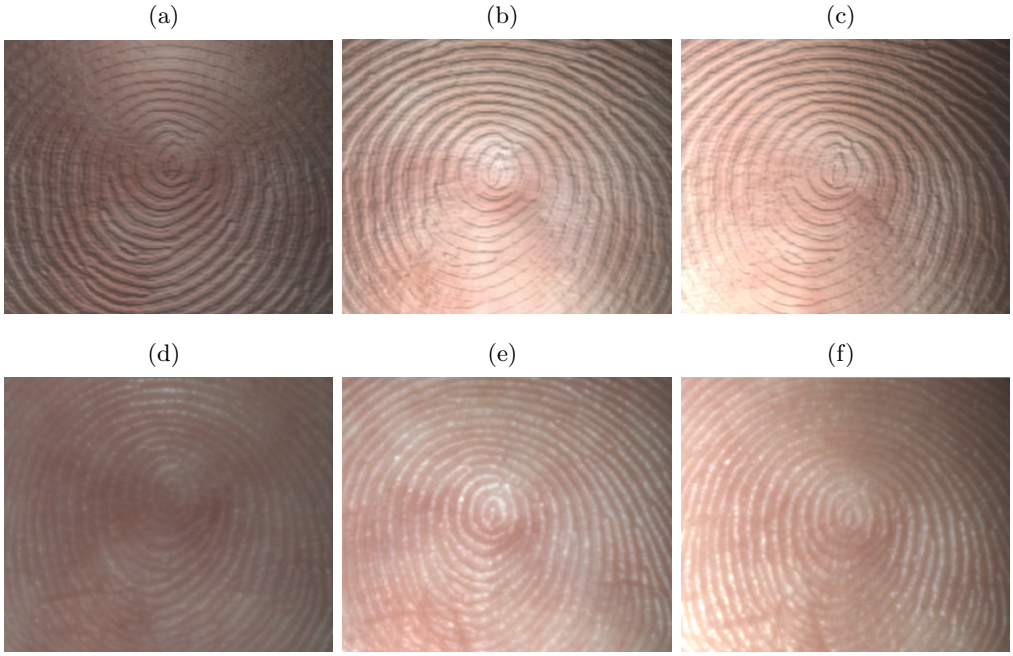

Figure 6.27: Examples of results obtained by the studied approach for the simulation of different illumination conditions: (a-c) synthetic models obtained using our approach; (d-f) corresponding contactless images. The images (a, d) are related to an illumination from the left side; (b, e) from the right side; (c, f) from the top side.

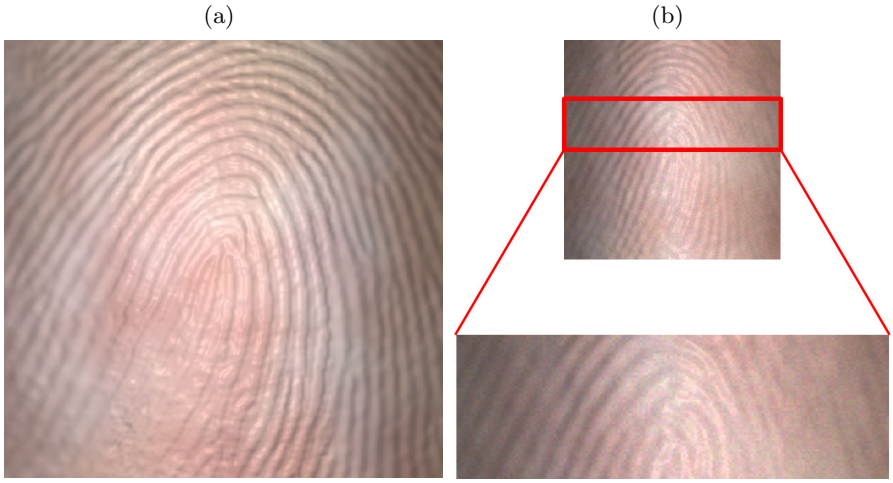

Figure 6.28: Examples of results obtained by simulating a fingerprint captured by a Sony XCD-SX90CR camera (a) and a VGA webcam (b).

6.7 Summary

This chapter has described the experiments performed on the researched approaches for contactless fingerprint recognition systems. The accuracy evaluation of the studied techniques for contactless systems based on two-dimensional samples has first been detailed. The experiments have been performed on datasets of contactless fingerprint images captured in our laboratory with different hardware setups. The evaluated techniques are the methods for the quality assessment of contactless fingerprint images, and the approach for the estimation of the core point in contactless images. The methods for the quality assessment of contactless images have showed good performances and experiments have proved that they can be effectively used to search the best quality frames in frame sequences captured in unconstrained scenarios. Also the core detection approach has obtained satisfactory results on contactless and contact-based images.

The researched approaches based on three-dimensional fingerprint samples have then been analyzed. The results obtained by different three-dimensional reconstruction strategies have been compared, obtaining encouraging results with all the researched techniques. The quality of the contact-based images obtained by unwrapping three-dimensional models have then been analyzed. In this context, the studied method for the quality assessment of contact-equivalent images has provided more accurate results with respect to methods in the literature designed for contact-based techniques.

A comparison between recognition techniques based on contactless samples and traditional contact-based systems has then been described. This comparison include different aspects of biometric technologies: I accuracy; II speed; III cost; IV scalability; V interoperability; VI usability; VII social acceptance; VIII security; IX privacy. The performed accuracy evaluation has showed that the researched method based on two dimensional templates obtained from of three-dimensional models has obtained a comparable or enhanced accuracy with respect to contact-based recognition techniques. Also systems based on contactless two-dimensional samples have obtained satisfactory accuracy. The compatibility between contact-equivalent and contact-based fingerprint images has then been analyzed. Results are encouraging, but they have only proved a partial compatibility between contact-equivalent images and the existing AFIS. Moreover, the studied approaches have obtained improvements in the scalability, usability, social acceptance, and security with respect to traditional techniques.

Results obtained by preliminary tests on recognition methods based on templates describing three-dimensional characteristics of minutia points have then been analyzed. The results have showed that the matching of three-dimensional minutia features is feasible, but more robust template registration strategies should improve the obtained accuracy.

Finally, the results obtained by the researched technique for the computation of synthetic contactless samples have been evaluated. The performed tests have showed that this method permits to simulate realistic data.

Chapter 7

Contactless Three-Dimensional Reconstruction of Ancient Fingerprints

The previous chapters have described the researched acquisition techniques and software methods designed to perform live biometric recognitions. These approaches can also be used to improve the accuracy and usability of other biometric applications based on the fingerprint trait.

This chapter describes a study on the use of contactless three-dimensional techniques for the authentication of clay artworks [326].

7.1 Authentication of ancient fingerprints

Clay artworks are often used by artists to build a preliminary sketch of the sculptures. These artifacts are very important and valuable since they show the artistic path of the authors to the creation of the final artworks.

The authentication of clay artifacts is performed in order to distinguish the original artworks from the numerous forgeries often present in the market in the case of famous sculptors. This process can be made by using different techniques, like the microscope analysis and carbon 14 dating. The authentication is usually performed by art historians in cooperation with forensic scientists. In this context, the analysis of latent fingerprints present on the artifacts is an important recognition technique. In order to

prove the authenticity of a sculpture, the fingerprints present on the artifact can be compared with other latent fingerprints attributed to a specific artist.

This analysis is performed by forensic experts, and there are no automatic methods able to perform a complete authentication. In the literature, there are examples of the use of fingerprints for the authentication of works attributed to important artists, such as Leonardo Da Vinci (Italy, 1452–1519) [327, 328].

In particular, the authentication of statues using latent fingerprints is a complex process because they can present irregular shapes and different levels of degradation. The work described in [329] divides the ancient fingerprints into two-dimensional and three-dimensional impressions. The first class of fingerprints is usually present on hard materials and is due to the chemical substances on the epidermal ridge surfaces. The second class is more present in soft materials, like ceramics or clay, and is related to the imprint of the epidermal ridges into the material. In both cases, the visibility of the ridge pattern can be reduced by different factors, like the humidity and the aging of the artwork.

Classical forensic techniques for the acquisition of latent fingerprints, involving the use of films, molds, or dusts, are often impossible to be applied to ancient artworks because of their value and fragility. Another important problem consists in the position of the latent fingerprints, which can be placed on a surface patch that is difficult to reach. For these reasons, contactless acquisition techniques and classical photographic techniques have been used. In the literature, there are many studies on automatic and semi-automatic methods for the enhancement and segmentation of the ridge pattern in latent fingerprint images [330, 331, 332].

An important problem that affects the acquisition of latent fingerprint images in clay artworks is that the perspective distortion present in the captured images can be very high, due to the irregular shape of the object. Moreover, the aging of the artifacts can modify the color of the material, reducing the visibility of the ridge pattern. In order to overcome these problems, multiple view acquisition systems and three-dimensional reconstruction techniques can be used to compute three-dimensional models of the artifact and fingerprints. In the literature, there are different three-dimensional reconstruction techniques that can be used for capturing small details of a statue [333]. Contactless techniques should be preferred for precious artworks in order

not to damage them. Multiple view techniques [292] are one of the most suitable methods in this applicative context. In fact, other three-dimensional reconstruction methods (e.g. techniques based on structured light, or profilometers [334]) require more complex hardware setups, are more difficult to transport, and can be problematic to use for capturing small details of complex surfaces like statues.

The reconstructed models can then be used to perform the authentication by applying algorithms based on two-dimensional or three-dimensional data. In order to compare the fingerprint models with traditional fingerprint images, different unwrapping techniques can be used to obtain the corresponding two-dimensional representation of the fingerprint model [284, 310]. The ridge pattern should then be enhanced by using techniques for the latent fingerprint analysis [330, 331, 332] or systems specifically designed for contactless fingerprint data [44, 284, 303, 307, 310].

In this context, a novel three-dimensional acquisition system has been studied. The studied approach consists in a low-cost, contactless, two-view acquisition technique able to acquire the latent fingerprints left on a clay artwork, and to perform a three-dimensional metric reconstruction of the captured area. In this way, it is possible to obtain a less-distorted reconstruction of the fingerprints with respect to traditional methods. The metric reconstruction permits to determine the size of the fingerprint models in a view-independent manner. In particular, the focus of this study is on the application of the acquisition method on a specific clay artwork, attributed by experts to the Italian sculptor Antonio Canova (Italy, 1757–1822), which is probably a sketch of the well-known statue "Ninfa Dormiente" ("Sleeping Nymph") shown at the Victoria and Albert Museum, London.

This chapter is organized as follow. First, Section 7.2 describes the realized acquisition setup and three-dimensional reconstruction technique. Finally, Section 7.3 reports the results obtained in the considered case study.

7.2 The researched approach

A contactless and low-cost two-view acquisition system and a three-dimensional reconstruction method have been researched in order to capture the areas of the clay artwork containing latent fingerprints, and to compute the corresponding metric three-dimensional models. The resulting models are less-distorted than single-view acquisi-

tions, and represent a view-independent, metric reconstruction of the considered regions, which allow determining the size of the latent fingerprints. Moreover, they can be processed using unwrapping algorithms and enhancement techniques.

The studied method is based on image processing techniques and processes pairs of images captured using two synchronized color CCD cameras. First, a correlation-based matching technique is used in order to determine a series of corresponding points in the two images. The points are then triangulated and the three-dimensional model is finally completed with the wrapping of the interpolated texture computed from the original pair of images.

The method can be divided in the following steps:

1. calibration of the cameras and image acquisition;
2. image preprocessing and extraction of the reference points;
3. point matching and triangulation;
4. surface estimation and texture mapping.

7.2.1 Calibration of the cameras and image acquisition

The calibration of the cameras is computed off-line, by acquiring multiple views of a chessboard, which are processed using a corner detector algorithm. The intrinsic and extrinsic parameters of the cameras are then computed using the calibration algorithms described in [311, 312]. The homography matrix is computed using a DLT algorithm described in [292]. A RANSAC algorithm is used to estimate the fundamental matrix [313].

The image acquisition is based on two synchronized CCD color cameras (Fig. 7.1).

7.2.2 Image preprocessing and extraction of the reference points

In order to enhance the details of the captured images, an adaptive histogram equalization technique [195] is applied.

Considering the images I_A and I_B (related to the cameras A and B, respectively), the three-dimensional reconstruction process requires the search of the points of I_B that correspond to a set of points of I_A. A set of reference points is then selected from the image I_A by downsampling the image with a step of s_d pixel.

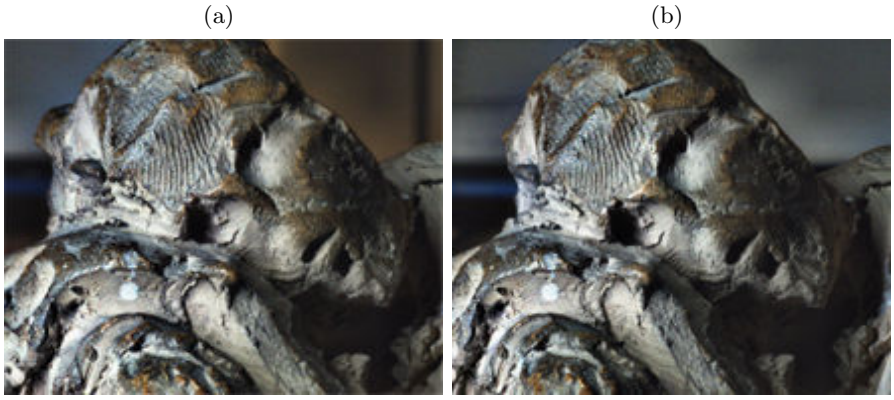

Figure 7.1: Example of a two-view acquisition of the considered artwork: (a) image A; (b) image B.

7.2.3 Point matching and triangulation

In the literature, there are approaches specifically designed for the purpose of matching the corresponding pairs of points in two-view acquisition systems, which consider the differences in the orientations of the cameras and illumination conditions [335, 336]. The realized setup, anyway, is specifically designed in order to have limited differences in the orientations of the cameras, and the same illumination conditions in the captured images. For this reason, it is not necessary to apply particularly complex constraints during the matching step. In the literature, there are also approaches designed in order to match the minutiae in contactless fingerprint acquisitions [308]. These approaches, however, cannot be applied in the considered case study because the material presents many irregularities. The studied matching algorithm is based on the methods described in [310, 337] and uses a correlation technique.

As a first step, a preliminary matching is computed. For each point x_A appertaining to I_A, the search for the matching point in the second image is performed by using the homography matrix:

$$X'_B = HX_A \ , \tag{7.1}$$

where H represents the 3×3 homography matrix, X_A is the point x_A converted in homogeneous coordinates, and X'_B is the preliminary matching point, expressed in homogeneous coordinates:

$$X'_B = \begin{bmatrix} X \\ Y \\ W \end{bmatrix} \ . \tag{7.2}$$

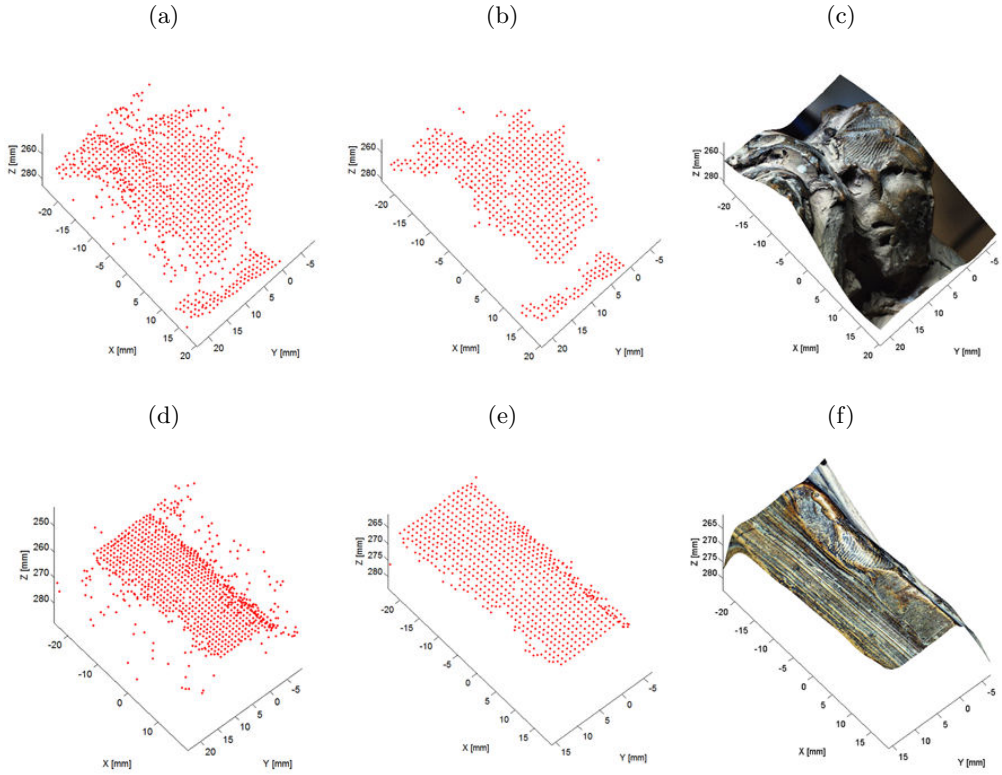

Figure 7.2: Examples of reconstructed point clouds obtained from two artwork acquisitions, and the relative texture mappings: (a, d) unfiltered point clouds; (b, e) filtered point clouds; (c, f) mapped textures.

A Cartesian representation of the point X'_B is then computed as:

$$x'_B = \begin{bmatrix} \frac{X}{W} \\ \frac{Y}{W} \end{bmatrix} . \tag{7.3}$$

A series of possible matching points adjacent to x'_B are extracted in a rectangular region centered in x'_B. The possible matching points are considered if:

$$\begin{aligned} d_x(x^i_B, x'_B) &< \Delta_x \\ d_y(x^i_B, x'_B) &< \Delta_y \ , \end{aligned} \tag{7.4}$$

where x^i_B is the i-th adjacent point, d_x and d_y represent the distances in the x and y directions, and Δ_x and Δ_y are the dimensions of the rectangular area.

The distance from the corresponding epipolar line is computed for each possible matching point x_B^i:

$$d_{ep}^i = \frac{(X_B^i)^T F X_A}{\sqrt{(l_1)^2 + (l_2)^2}} \ , \tag{7.5}$$

where d_{ep}^i is the epipolar distance, X_B^i is the i-th adjacent point expressed in homogeneous coordinates, F is the fundamental matrix, and l_1, l_2 are the first two components of the epipolar line l, which is computed using the equation:

$$l = F X_A \ . \tag{7.6}$$

The possible matching points must have an epipolar distance inferior to a threshold t_{ep}:

$$d_{ep}^i < t_{ep} \ . \tag{7.7}$$

The Canny edge detector is applied to the images I_A and I_B, and used as a check for the consistency of the possible matching points. Only the candidate matching points with corresponding values in the binary edge images are considered:

$$C_A(x_A) = C_B(x_B^i) \ , \tag{7.8}$$

where C_A, C_B are the images resulting from the application of Canny edge detector to I_A and I_B.

The set of possible matching points x_B^i are inserted in the list V_B of the valid points to be checked using the normalized cross-correlation:

$$x_B^i \in V_B \text{ if } \begin{cases} d_{ep}^i < t_{ep} \ , \\ d_x(x_B^i, x_B') < \Delta_x \ , \\ d_y(x_B^i, x_B') < \Delta_y \ , \\ C_A(x_A) = C_B(x_B^i) \end{cases} \ . \tag{7.9}$$

The matching point is then computed by performing the cross-correlation of $l \times l$ windows, one centered in x_A, and the others centered in every valid point of V_B. The cross-correlation between the windows is performed on the Y, R, G, B channels separately, and is computed as:

$$r = \frac{\sum_m \sum_n (A_{mn} - \bar{A})(B_{mn} - \bar{B})}{\sqrt{(\sum_m \sum_n (A_{mn} - \bar{A})^2)(\sum_m \sum_n (B_{mn} - \bar{B})^2)}} \ , \\ 1 < m < l, \ \ 1 < n < l \ , \tag{7.10}$$

where A and B are the two windows of size $l \times l$. The final matching point x_B is chosen as the one which produces the highest cross-correlation coefficient.

The pairs of matched points are then rectified using the calibration data. Then, the z coordinates of each pair of points are computed using the triangulation equation (5.20).

Since the points are obtained using a downsampling method with a constant step s_d, and the surface is sufficiently smooth, the three-dimensional point cloud of the reconstructed model should then present a regular distribution of the points.

A check for outliers is then performed by removing the three-dimensional points that are not close to any other point of the point cloud. The distance from each point and the points appertaining to its 4-neighborhood must be inferior to a threshold t_d:

$$d((x_i, y_i, z_i), (x_{i+j}, y_{i+j}, z_{i+j})) < t_d \ ; \ 1 \leq j \leq 4 \ , \tag{7.11}$$

where (x_i, y_i, z_i) is the i-th three-dimensional point, $(x_{i+j}, y_{i+j}, z_{i+j})$ are the points appertaining to its 4-neighborhood, and d represents the Euclidean distance.

The threshold t_d is computed as the double of the minimum distance between adjacent three-dimensional points:

$$t_d = 2 \min_{i=1...N} (d((x_i, y_i, z_i), (x_{i+1}, y_{i+1}, z_{i+1}))) \ , \tag{7.12}$$

where N is the number of three-dimensional points.

7.2.4 Surface estimation and texture mapping

The reconstructed points are merged in a single point cloud (X, Y, Z) and the intensity values of the original image I_A are stored in the vector C. From the vectors X, Y, the maps S_x and S_y are computed as a mesh with a constant step s_{interp}. The surface map S_z and the intensity map S_c are then obtained by applying a bilinear interpolation to the vectors Z and C at the coordinates described by the meshed maps S_x and S_y. Examples of reconstructed point clouds with the relative estimated surfaces and wrapped textures are shown in Fig. 7.2.

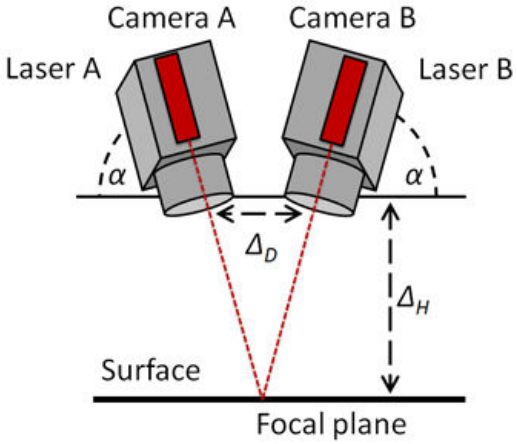

Figure 7.3: Schema of the acquisition setup used by the studied technique for the three-dimensional reconstruction of latent fingerprints.

7.3 Experimental Results

Two Sony XCD-SX90CR CCD color cameras synchronized using a trigger mechanism have been used to capture the images of the artwork. The angle of the cameras with respect of the horizontal support is $\alpha = 85°$, and the baseline distance between the cameras is $\Delta_D = 45$ mm (considering the centers of the CCDs). The distance from the cameras to the surface of the statue is about $\Delta_H = 205$ mm, chosen according to the focal planes of the two cameras. The intersection of the focal planes of the two cameras was guaranteed by mounting on the cameras two lasers that projected two vertical lines during the mounting step of the setup. The intersection of the vertical lines was set in order to correspond to the region of the acquisition volume with the best optical focus. Fig. 7.3 shows the schema of the used acquisition setup.

We used 15 pairs of chessboard acquisitions to calibrate the cameras. The chessboard is composed by 12×9 squares of 2.8×2.8 mm. We used these images also to estimate a calibration error, computed by reconstructing the point clouds of the chessboard and interpolating a plane through the three-dimensional points. The error measure is defined as the standard deviation of the distances of the reconstructed points from the interpolating plane [320], and is equal to 0.04 mm. In order to measure the accuracy of the studied method, we captured also a semi-sphere with radius of 20 mm, and reconstructed the corresponding three-dimensional model. Then, we computed the

difference between the radius of the sphere fitted using the three-dimensional reconstructed points and the actual radius. The resulting reconstruction error is equal to 0.5 mm.

We captured a total of 275 pairs of images with different points of view and illumination conditions. We used a led illumination only to enhance the visibility of the particular area of the surface. Anyway, no specific illumination system is needed. The captured images represent all the ancient fingerprints present on the clay artwork.

The majority of the captured images describe impressions that cannot be used to perform an identification since they represent very small regions of the finger or are affected by problems related to deformations and aging of the statue. In some acquisitions, the reconstructed samples can probably be sufficient to try an authentication procedure with different clay artworks of the same author, even if the matching can be done only on fragments and not by using complete fingerprints.

We applied these method on the captured two-view images and reconstructed the corresponding metric three-dimensional models. Fig. 7.4, shows some examples of the reconstructed models of the regions containing latent fingerprints. It is possible to observe that three-dimensional models of the fingerprint area permit to obtain a view-independent, metric reconstruction of the fingerprint, and to compensate problems related to distortions and different camera orientations.

The fingerprint can then be analyzed using a more suitable point of view. Fig. 7.5 shows an example of captured pairs of images and the corresponding three-dimensional models. It is possible to observe how the three-dimensional models help in creating less-distorted acquisitions of the fingerprints. In order to compute the same viewpoint, the models were registered using an Iterative Closest Point algorithm [325], which computes the rotation and translation of a model, with respect to another point cloud. The computed transformations were applied on one of the reconstructed point clouds, using the equation:

$$P_i' = RP_i + T \ , \tag{7.13}$$

where $P_i = (x_i, y_i, z_i)$, R is the 3×3 rotation matrix, and T is the 3×1 translation vector. It is possible to observe that the three-dimensional models obtained by the researched method are effectively less distorted and independent by the acquisition view point.

Another example of registered three-dimensional models obtained by using the researched method is shown in Fig. 7.6. Despite, Fig. 7.6 depicts three-dimensional models representing only a partial fingerprint, Fig. 7.6 e and Fig. 7.6 f are clear examples of the capability of the researched method to obtain aligned, view-independent portions of clay artifacts.

Metric fingerprint samples independent by the view point can also be obtained by using other acquisition techniques based on single images. These techniques, however, require complex hardware setups and are difficult to apply in the evaluated context.

The three-dimensional models obtained by the studied method can then be used in order to perform biometric recognitions. For example, it is possible to apply matching techniques based on traditional two-dimensional images three-dimensional data [284]. Matching techniques based on two-dimensional templates can guarantee the compatibility of the fingerprint models with fingerprint images captured using touch-based sensors or traditional forensic techniques. However, they require the estimation of an equivalent two-dimensional representation of the fingerprint from the three-dimensional model. The computation of this fingerprint representation should be performed by considering the shape of the surface in which the latent fingerprint is present. Considering flat surfaces with two-dimensional impressions, in fact, it can be sufficient to extract the texture of the three-dimensional model. More complex surfaces require the use of unwrapping techniques.

7.4 Summary

This chapter has described a contactless and low-cost two-view acquisition method, and a three-dimensional reconstruction technique able to capture pairs of images of latent fingerprints left on a clay artworks and to estimate three-dimensional metric models of the captured areas. The researched method permits to obtain a less-distorted representation of the fingerprints, with respect to single-view acquisitions achieved by classical photographic techniques. The computed models have the advantages of allowing a view-independent and metric reconstruction, which is difficult to obtain using single-view acquisition setups.

The method uses an algorithm based on the normalized cross-correlation to perform the search of corresponding pairs of points in the images obtained by multiple view

acquisitions. The three-dimensional coordinates of the matched pairs of points are then computed, and an outlier removal algorithm is applied. The resulting model is completed by applying a surface interpolation technique and performing a texture mapping procedure.

The accuracy of the method has been evaluated by using objects with known shapes. Then, the quality of the three-dimensional models computed using the researched method has been inspected by a visual analysis and compared with the images captured using a single-view system. The obtained results have showed that the approach is able to compute less-distorted, metric and view-independent representations of the latent fingerprints left on the artwork, using a contactless low-cost acquisition setup.

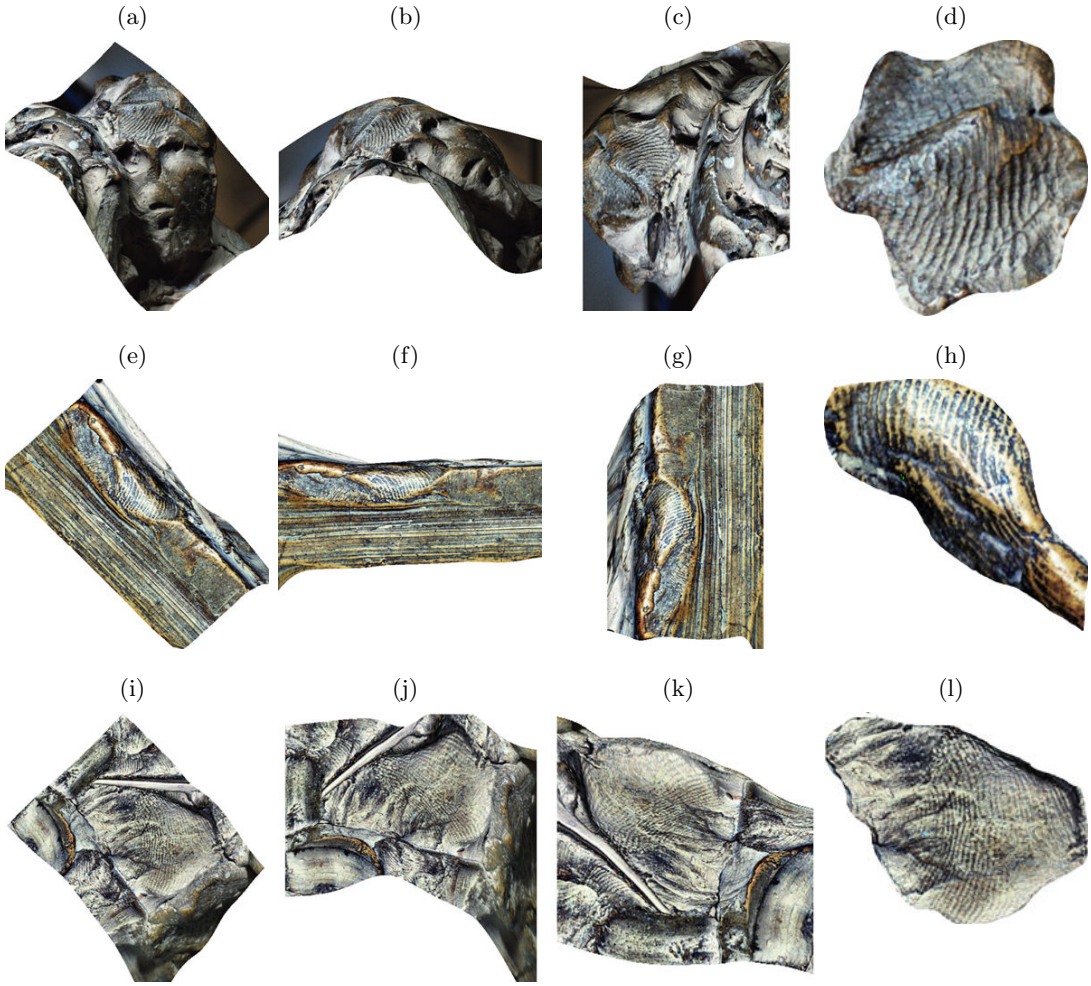

Figure 7.4: Examples of reconstructed three-dimensional models of regions appertaining to the considered artwork: (a,e,i) models seen from the first view point; (b, f, j) models seen from a second view point; (c, g, k) models seen from a third view point; (d, h, l) particulars of the reconstructed latent fingerprints.

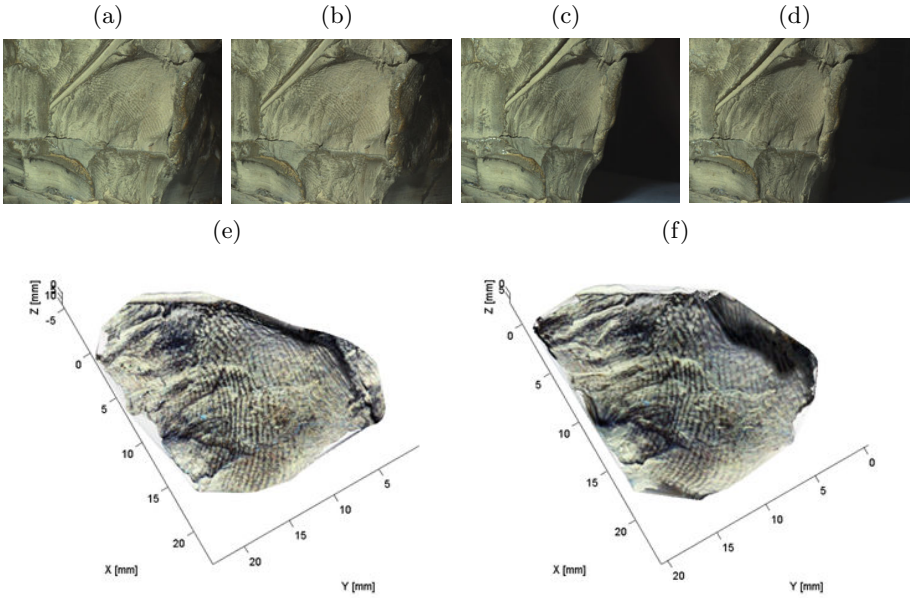

Figure 7.5: Examples of pairs of images and corresponding three-dimensional models related to the considered clay artwork: pair of images 1 (a, b), pair of images 2 (c, d), three-dimensional model 1 (e), three-dimensional model 2 (f). It is possible to observe that the use of three-dimensional models reduces perspective problems related to different view points and provides a robust metric reconstruction of the fingerprint.

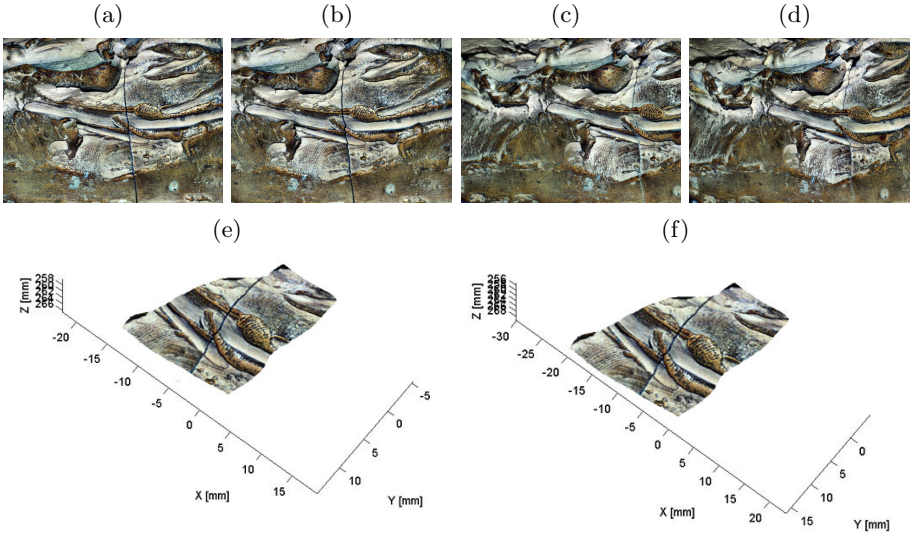

Figure 7.6: Examples of pairs of images and corresponding three-dimensional models related to the considered clay artwork: pair of images 1 (a, b), pair of images 2 (c, d), three-dimensional model 1 (e), three-dimensional model 2 (f). It is possible to observe that the three-dimensional models are independent from the view points.

Chapter 8

Fingerprint Privacy Protection

The privacy protection of the biometric data is an important research topic, especially in the case of distributed biometric systems. In this scenario, it is very important to guarantee that biometric data cannot be steeled by anyone, and that the biometric clients are unable to gather any information different from the single user verification/identification. In a biometric system with high level of privacy compliance, also the server that processes the biometric matching should not learn anything on the database and it should be impossible for the server to exploit the resulting matching values in order to extract any knowledge about the user presence or behavior.

A novel privacy protection approach based on the fingerprint trait has been researched. This approach is based on a distributed biometric system that is capable to protect the privacy of the individuals by exploiting cryptosystems. The researched system computes the matching task in the encrypted domain by exploiting homomorphic encryption and using Fingercode templates. The studied approach has been fully implemented and tested in real applicative conditions.

8.1 Introduction

The privacy protection of biometric data is particularly critical in the case of distributed biometric systems since the biometric data are transmitted through a network infrastructure and hence it is greatly reduced the direct user control about her/his biometric information. In a distributed biometric system with a high level of privacy compliance, also the server that processes the biometric matching should not learn anything on the

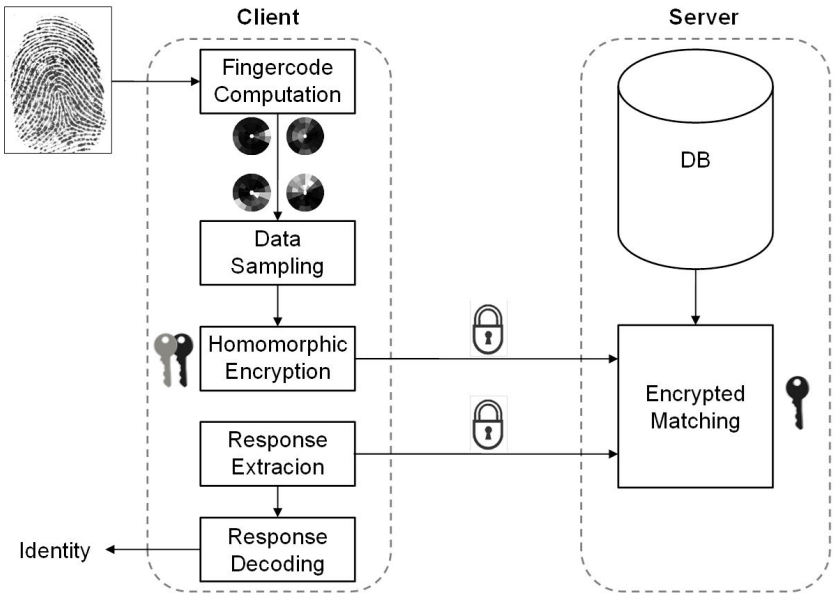

Figure 8.1: Schema of the researched approach for the privacy protection of fingerprint templates.

database and it should be impossible for the server to exploit the resulting matching values in order to extract any knowledge about the user presence or behavior.

In this chapter, we refer to the general application where a biometric client checks if the "fresh" captured fingerprint belongs to the database of authorized entities managed by a biometric server. In order to preserve the user's privacy, we require that the biometric client trusts the server to correctly perform the matching algorithm for the fingerprint recognition and it also should not learn anything about the fingerprint templates stored in the server with the exception of the resulting matching process. On the server side, we want to guarantee that it is not possible to get any information about the requested biometry and even also the resulting matching value. This working hypothesis is very important since it allows avoiding any tracking and logging activity of the user presence and behavior on the server side.

Within this conceptual framework, an approach capable to deal with distributed biometric systems protecting the privacy of the individuals by exploiting cryptosystems has been researched. Different aspects of the approach are presented in [103, 338, 339].

The system computes the matching task in the encrypted domain, by exploiting homomorphic encryption and using the template Fingercode [3].

In this approach, the biometric client captures the user fingerprint trait and it processes the obtained sample in order to produce the related Fingercode template (Fig. 8.1). The underling cryptographic protocol accepts in input only integer values, hence a data sampling operation is needed in order to suitably convert the floating point elements of the Fingercode template in integer values. The quantized biometric template is then sent to the biometric server in the encrypted format and the server returns the identity information in the encrypted format as well (or just a Boolean outcome for the authentication request). Hence, on the server side (the right subplot in Figure 8.1), it is not possible to extract or determine any personal information on the biometric data of the users during all the phases of the verification / identification procedures.

The chapter is structured as follows. Section 8.2 details the steps of the researched approach, and Section 8.3 describes the implementation of the described system, its accuracy and performance evaluation in different applicative conditions, and the obtained results.

8.2 The researched approach

The researched approach can be applied in distributed biometric systems in verification/identification tasks. Without any lack of generality, in this section we describe a technique for the identification procedure. On the client side (left subplot, Figure 8.1), the biometric sample is captured and then computed in order to obtain the related Fingercode template [193] (Template Creation step). Then, the floating point elements of the Fingercode template are sampled and converted to integers in order to allow the adoption of the following encryption method (Template Quantization step). The important effects on the final accuracy and bandwidth of this step will be further discussed in the following subsections. The reduced template is now encrypted using the public-key of the client and the biometric matching is processed on the server side (right subplot, Figure 8.1) by a homomorphic cryptosystems (Encrypted Matching step). The matching algorithms do not transform the data in the plain domain. All computation steps of the matching method (evaluation of the matching value, thresholding and extraction of the best candidates) are processed directly in the encrypted domain. Let us now detail all the design steps of the studied approach.

8.2.1 Encrypted matching of Fingercode templates

The computation of the biometric template in the plain domain is based on a method that uses the Fingercode template. This method starts with the estimation of the reference point, defines the ROI as a ring with fixed size, divides the ROI in n_R rings and n_A arcs, applies n_F Gabor filters with different directions to the fingerprint image, and finally computes the AAD of each filtered sector. The obtained feature vector is therefore composed by $n_V = n_S \times n_F$ values (for example, in [193], n_V ranges from 640 to 896 according to the used fingerprint dataset). In order to compensate possible rotations of the samples, n_θ rotations of the biometric template are computed. A more detailed description of the Fingercode computation algorithm is l in Section 4.5.4.3.

It is well known in the literature that the estimation of the reference point for the Fingercode template is a critical task with respect to the final accuracy of the system (an incorrect estimation of this point implies a different ROI evaluation, causing an increasing of the identification errors). We manually selected the reference point for each image in order to create a supervised point dataset as reference, and then we applied different methods present in the literature in order to study this effect and to reduce its impact. First of all, we tested the identification of the reference point by selecting the candidate points in the image with the highest Poincaré index [3], then we tested the different methods creating a single Fingercode template for each candidate point. In any case, if a fingerprint image does not present any singular point, we consider the point with the maximum Poincaré index as the reference point. Since a complete discussion of the effect of the reference point on the accuracy is outside the scope of this chapter, in the following we refer to the first described method.

8.2.2 Template quantization

In order to limit the complexity of the Fingercode matching in the encrypted domain, we investigated the possibility of reducing the number of features of the Fingercode templates and the number of bits used for the physical representation of each value of the template. The effects of the reduction of the number of features have been studied by appropriately decimating the tesselation of the region of interest. We tested different configurations of the algorithm: h, n_R, n_A, n_F. We preferred to use a fixed reduction strategy, instead of methods that minimize the correlation among different features,

like the principal component analysis, since the latter should be optimized for each database and their application in the encrypted domain would not be convenient. The quantization effects have been studied by converting each value of the template into an integer number representable with b bits, according to a uniform quantization criterion. The performances of the different configurations have been compared by evaluating the empirical distribution of the distances of genuines and impostors after feature reduction and quantization, from which we can compute ROC curves and EER values.

We presented more details about the template quantization strategy in [103].

8.2.3 The encryption method

The cryptographic protocol strongly relies on the notion of (additively) homomorphic encryption. A public-key encryption scheme is said to be additively homomorphic if, given the encryptions of two messages a and b, the ciphertext of $a + b$ can be easily computed (for example, by multiplication) from the two original ciphertexts without the knowledge of the secret key. As a consequence, it is also possible to compute the multiplication of the encryption of a for any constant c by iterations of the homomorphic addition.

The studied solution makes use of two specific encryption schemes: the Paillier's encryption scheme [340] and a known-variant of the ElGamal encryption scheme [341] but ported on Elliptic Curves. The latter scheme is widely used in order to save further bandwidth.

We detailed the used encryption method in [339].

8.2.4 The matching method in the encrypted domain

The protocol may be subdivided into three main steps to be accomplished by the two parties (the client with the biometric measure to authenticate and the server with an in-clear database with all the features of the enrolled persons).

- **Vector extraction**: on a first stage the target biometry (i.e. the information acquired by the biometric device) is "converted" by the client in a quantized characteristic feature vector; this preliminary work is performed in clear and only the resulting feature vector is encrypted and sent to the server.

- **Distances computation**: the distances (more specifically the square of the Euclidean distance) between the target vector and the vectors in the database are computed in the ciphertext domain: this is done by the server exploiting the homomorphic properties of the adopted cryptosystems. The outcome of this phase consists of the encryption of the required distances that still remain unknown to the server. Differently from the original Fingercode matching method, we decided to compute the squared distance between two templates in order to reduce the computational complexity.

- **Selection of the matching identities**: in this final step the server interacts with the client in order to select, in the ciphertext domain, the enrolled identities with the related distances that are below a known threshold. This is accomplished through several internal sub-protocols nevertheless keeping a constant round complexity. The final outcome is kept secret to the server and is only revealed to the client: it can consist of more than one identity (if this is the case) where the previous works [104, 105] just report the identity with the minimum distance. A simple variant allows the use of a Boolean outcome: authenticated/rejected.

Such solution has been formally proven to be secure against an *honest-but-curious* adversary, where we assume that he follows the protocol but may try to learn additional information from the protocol trace beyond what can be derived from the inputs and outputs of the algorithm when used as a black-box.

More details on the protocol are available in [339].

8.2.5 Individual Threshold

In many biometric systems, the use of individual threshold values can produce a better final accuracy than a single threshold value used for all the enrolled individuals. This is related to the fact that different training levels of the users and skin conditions can be present in the dataset. Considering a dataset D composed by n samples of m individuals, for each individual i is assigned a different threshold value t_i that is used in the identity verification step of the biometric recognition process. For each individual i, the distributions of False Match (FM_i) and False Non Match (FNM_i) are computed (with the corresponding individual EER_i) considering only the set of user templates X_i as the genuine template set. All other samples of the dataset are considered as the

Figure 8.2: Examples of fingerprint images used to evaluate the studied privacy protection approach.

set of the impostor $I_i = D \supset X_i$. In the performed experiments, we set the value t_i as the threshold corresponding to the individual Equal Error Rate (EER_i). Differently, it is possible to set the individual threshold value as the threshold that corresponds to the Zero FMR or Zero FNMR. This important method can be applied to the studied approach.

8.3 Implementation and experimental results

The researched approach has been tested by using a well-known public fingerprint dataset composed by 408 grayscale fingerprint images acquired by a CrossMatch Verifier 300 sensor [319, 342]. The dataset contains 8 images for each individual with a resolution equal to 500 dpi and the dimension of 512×480 pixel. Figure 8.2 shows two examples of images of the test database.

The application of the Individual Threshold method described in Section 8.2.5 is shown in Fig. 8.3 where different figures of merits are reported with $n_V = 640$. The overall accuracy has been enhanced by reducing the initial EER (equals to 0.065) of a factor close to 0.5. In particular, we obtained a ZeroFM rate with FMR=0.1653 and a ZeroFNM rate with FMR=0.0512. This method can typically produce relevant enhancement in overall accuracy when the samples belonging to the considered dataset have not the same quality level. This is the case of the used test dataset.

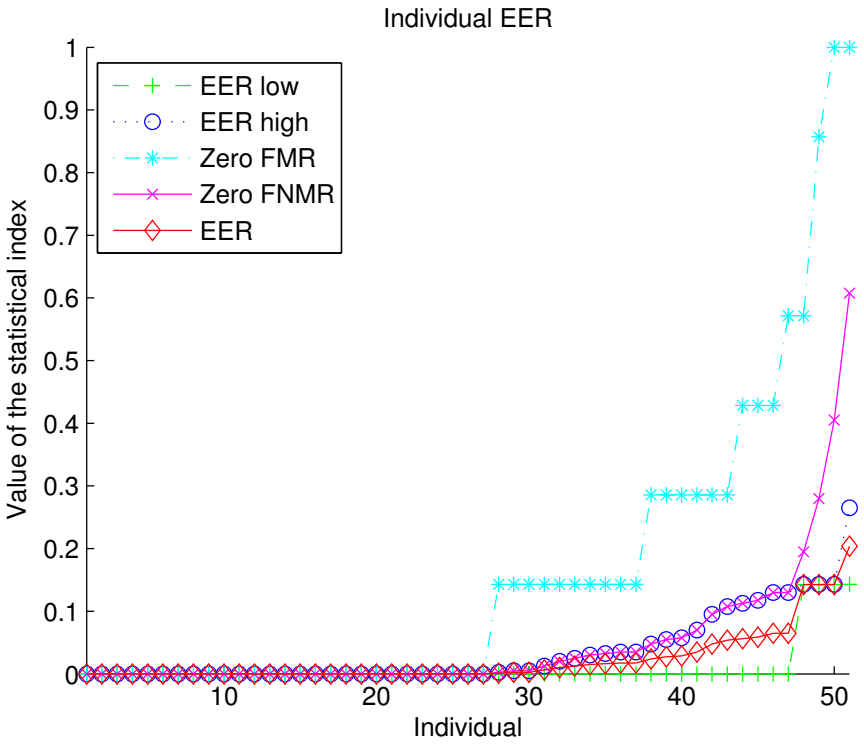

Figure 8.3: Accuracy obtained by computing the method Individual Threshold in the researched privacy protection technique.

As a second step, in order to test the effect of the number of features in the Fingercode template, we generated a total of eight different configurations, corresponding to eight sets of Fingercode vectors with length ranging from 640 features (the original configuration) to 8 features. The parameters of the reduced tesselations for each configuration are detailed in Table 8.1.

In order to investigate the effects of the Template Quantization, each configuration had been normalized and quantized using a different number of bits, ranging from eight bits to a single bit, producing a total of $5 \times 8 = 40$ quantized configurations. The behavior of the EER for the testing dataset is shown in Fig.8.4. From the above figure, it is evident that the performance of the system is practically unaffected by the feature size reduction when the number of features is above 96 and the number of bit is above 2. This suggested considering for further testing only the configurations C and D, both quantized with 4 and 2 bits.

Table 8.1: Tested configurations for the feature size reduction performed by the researched privacy protection technique.

Configuration	n_V	n_F	n_R	h (pixel)	n_A
A	640	8	5	20	16
B	384	8	4	25	12
C	192	8	3	20	8
D	96	4	3	33	8
E	48	4	3	33	4
F	32	4	2	50	4
G	16	4	2	50	2
H	8	2	2	50	2

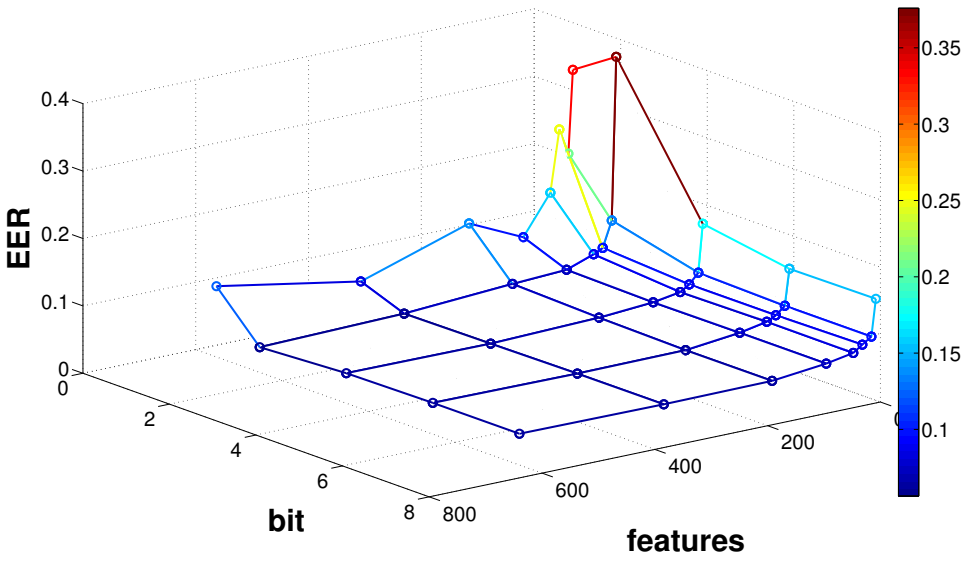

Figure 8.4: Equal Error Rate obtained by different configurations of the researched privacy protection technique.

Table 8.2: Performance of the researched privacy protection method with a database of 408 entries (3672 feature vectors).

Parameters				
Configuration	Quantization	Security	EER	Bandwidth (bit)
C	2	80	0.0758	6568792
		112		10824021
		128		14374232
C	4	80	0.0732	7802584
		112		12527832
		128		16313048
D	2	80	0.0715	6902008
		112		11299320
		128		14932856
D	4	80	0.0673	8135800
		112		13003128
		128		16871672

To evaluate the performances in bandwidth and computational complexity we implemented a client-server prototype version of our construction written in C++, using the GMP Library (version 5.0.1) and the PBC Library (version 0.5.8). The experimental results were run on 2.4 GHz with 4 GB of RAM PCs. The experimental results show that the studied method based on Fingercode templates and homomorphic cryptosystem is feasible in the cases when the privacy of the data is more important than the accuracy of the system, and the obtained performances on accuracy measured as EER are comparable to the original method. Table 8.2 shows the obtained accuracy, the computational time, and the bandwidth required by the configurations C and D.

We estimated the time required for the identification in the encrypted domain on a dataset composed by 100 enrolled individuals using an 80 bits security key. Table 8.3 reports the obtained results. The time complexity of the underling protocol is linear in the number of enrolled identities.

As shown in Table 8.2 and Table 8.3, different performances can be obtained varying the number of features of the template and the number of bits used for representing each value. On the other hand, the best computational performances can be obtained

Table 8.3: Required time for the identification in the encrypted domain using a dataset composed by 100 enrolled entries using a 80 bits security key.

Configuration	Quantization	Time (s)
C	2	44.43
	4	53.66
D	2	37.43
	4	45.58

with a small number of features and bits.

Fig. 8.5 plots the ROC curves of the configurations that we consider as a good trade off. The performances of the different configurations are very close each other, the effects of both feature reduction and quantization being very limited on the accuracy of the system. It is worth noting that the original configuration, i.e., 640 features with floating point implementation, reported an EER of 0.065 on the testing dataset, which is comparable with the performance of the tested configurations.

The obtained final results of the system (in term of ERR and ROC curves) show that the studied method is only slightly worse than the results of the original Fingercode technique applied on the same dataset, and that the realized privacy protection implementation can be feasible in the cases when the privacy of the data is more important than the accuracy of the system. Unfortunately, the simplicity of the matching function used in the Fingercode is suitable for the processing in the encrypted domain, but it limits the final accuracy of the system. In fact, much more accurate methods capable to work with the same fingerprint dataset are available in the literature, but their complexity excludes their adoption in the realized approach.

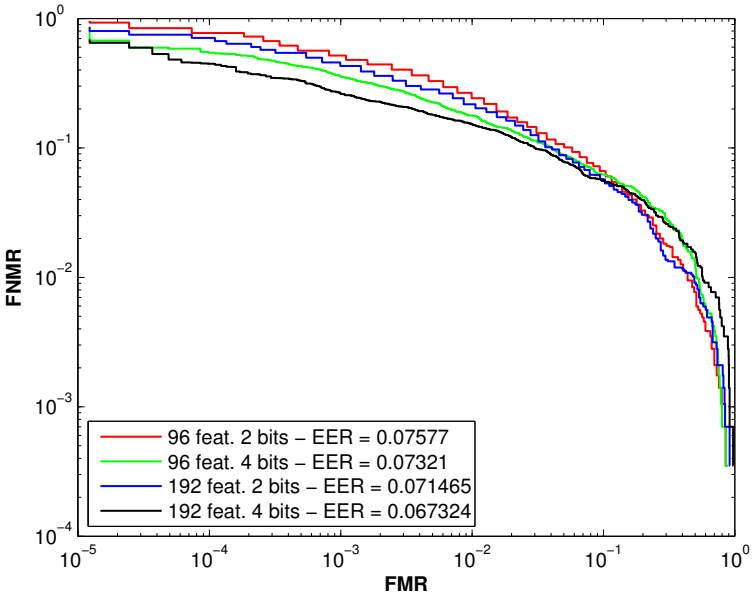

Figure 8.5: ROC curves related to different configurations of the studied privacy protection method. The reported configurations are the ones that we consider as the best suitable in real applicative conditions.

8.4 Summary

The chapter has described an approach to protect the privacy of the biometric data in distributed biometric systems based on fingerprints. In this approach, on the client side, the biometric data are captured and then an encrypted representation of the template Fingercode is computed. We have reduced the data contained in the template for obtaining a smaller representation of the encrypted template that should be shared with the server. The encryption matching algorithm is based on the homomorphic cryptosystems.

Experimental results show that the researched approach has an equivalent accuracy with respect the original Fingercode method.

Improvements of the security model will be considered in the future work by applying encryption methods also on the biometric templates stored in the database. This new security model is stronger than the model described in this chapter, but it is also more difficult to realize. The obtained computational time permits the use of the realized system in real applications.

The main drawback of this approach consists in the low accuracy of the recognition method based on the Fingercode template that permit the use of this system only in a limited subset of security applications with respect to methods based on minutiae featueres.

The studied approach has been evaluated on contact-based fingerprint samples. This approach, however, can also be applied to contactless fingerprint images. The application of this privacy protection technique should be studied in future work.

Chapter 9

Conclusion and Future Works

9.1 Conclusion

The objective of this thesis has been the research of innovative approaches able to increase the usability and social acceptance of biometric systems by performing less-constrained and highly accurate biometric recognitions in a privacy compliant manner.

In particular, the main contribution of this work consists in the realization of novel biometric systems based on contactless fingerprint acquisitions. In this contest, different techniques for every step of the recognition process based on two-dimensional and three-dimensional samples have been researched. Moreover, techniques for the privacy protection of fingerprint data have been designed.

The researched approaches are multidisciplinary since their design and realization have involved optical acquisition systems, multiple view geometry, image processing, pattern recognition, computational intelligence, statistics, and cryptography.

The studied approaches encompass all the aspects of contactless biometric recognition systems based on two-dimensional and three-dimensional fingerprint samples, including methods for the acquisition, processing, and privacy protection of biometric data. In particular, all the modules of the biometric systems have been studied and implemented: hardware setups, acquisition techniques, quality assessment of biometric samples, three-dimensional reconstruction of fingerprint models, computation of contact-equivalent images, feature extraction, matching, and template protection. A method for the computation of synthetic contactless fingerprint samples has also

been developed, and the use of contact-less techniques in forensic applications based on latent and ancient fingerprints has been studied.

The evaluation of the implemented approaches has been performed on datasets composed by contactless biometric samples captured in different applicative contexts, obtaining satisfactory results that prove the applicability of contactless fingerprint recognition systems in different applicative scenarios.

Moreover, the realized contactless biometric systems have been compared with traditional contact-based fingerprint recognition systems in a scenario evaluation that regarded different aspects of the biometric technologies: accuracy, speed, cost, scalability, interoperability, usability, social acceptance, security, and privacy. Results prove that contactless biometric systems based on three-dimensional samples can obtain a comparable or enhanced accuracy with respect to traditional fingerprint recognition techniques. For example, the realized system based on the analysis of two-dimensional minutiae templates extracted from three-dimensional samples has obtained an equal error rate of 0.309% on a dataset of 1040 samples, and the one obtained by the considered contact-based system on a dataset composed by the same number of samples captured from the same individuals is 0.323%. Satisfactory results have also been achieved by the implemented system based on contactless two-dimensional samples, which has obtained sufficient accuracy to be used in many low-cost applications (e.g. in mobile devices), with an equal error rate of 1.320%. During the performed scenario evaluation, the compatibility of contact-equivalent images obtained from three-dimensional models with existing biometric databases has also been analyzed, obtaining encouraging results. Furthermore, the researched approaches have obtained improvements in terms of scalability, usability, social acceptance, and security with respect to traditional techniques.

The performances of the implemented feature extraction and matching techniques based on three-dimensional templates have also been analyzed, obtaining encouraging results. The obtained performances, however, should be improved by using more accurate strategies for the template alignment.

Furthermore, the researched techniques based on three-dimensional samples have been evaluated on latent and ancient fingerprints, achieving satisfactory results.

Finally, results have proved that the implemented method for the privacy protection of fingerprint recognition systems can effectively be applied in client-server applications

without decreasing the recognition accuracy, also obtaining satisfactory results in terms of security, computational time, bandwidth, and memory usage.

The performed tests therefore prove that contactless fingerprint recognition methods should be effectively used in the different applicative scenarios in which live contact-based techniques are adopted, obtaining great advantages.

9.2 Future Works

One of the goals of the approaches researched in this thesis is to increase the usability and acceptability of biometric systems. As shown by the experimental results and the notes collected in the volunteer forms, it is very likely that the usability of the realized approaches should be further improved by using acquisition setups based on active cameras. The envisioned setup is composed by a multiple view acquisition system placed on a support dynamically moved by stepper motors according to the finger coordinates and camera focus. This setup should permit to perform acquisitions in a more comfortable manner with respect to the existing fingerprint recognition technologies.

Optical techniques able to increase the distance of the finger from the cameras should also be studied in order reduce the needed level of cooperation during the biometric acquisitions.

Moreover, further studies on autofocus methods should permit to search the acquisition scenarios that permit to obtain the best results in terms of recognition accuracy.

The compatibility of the implemented techniques with the existing AFIS should also be improved in order to permit their diffusion in governmental and investigative applications. For this reason, future studies will regard new techniques for the computation of contact-equivalent images able to simulate the skin distortion caused by the pressure of the finger on the sensor.

In order to increase the accuracy of contactless fingerprint recognition systems, further studies should also be performed on feature extraction and matching methods based on three-dimensional feature sets, for example exploiting the additional information related to finger volume, and focusing on the creation of new distinctive features.

Three-dimensional reconstruction techniques more robust to noisy data should also be studied in order to apply the researched approaches based on three-dimensional models in a wider set of applicative contexts, and to increase the obtained accuracy.

Moreover, new datasets should be collected with the aim of proving the applicability of the proposed approaches in different scenarios and environmental conditions.

In this context, the researched biometric recognition techniques should also be evaluated on relevant numbers of simulated contactless samples obtained from public datasets of contact-based images. This kind of tests should require the study of new techniques for the simulation of three-dimensional finger models. The realized approach, in fact, only permits to simulate models describing a limited area of the ridge pattern centered in the core region of the fingerprint.

An industrial implementation of the researched approaches should also drastically reduce the computational time needed by the implement techniques. With high probability, the use of parallel computing techniques based on graphic processing units (GPU) should also permit the use of the researched approaches in real-time live applications.

In order to increase the user acceptance of the realized biometric recognition systems, future studies will also regard privacy protection methods. The performances of the implemented privacy protection technique should be evaluated on different datasets of contact-based and contactless samples, and privacy protection techniques based on homomorphic cryptosystems should also be studied for applications based on more accurate feature extraction and matching algorithms.

This work is focused on the fingerprint biometric trait since it is one of the most used and studied traits in the literature. The researched approaches, anyway, are general and should also be extended to other biometric traits. For example, it is possible to use contactless acquisition techniques to perform less-constrained biometric recognitions in systems based on the hand characteristics. The use of three-dimensional reconstruction methods based on multiple view techniques, moreover, should permit to obtain high accuracy biometric systems able to work in unconstrained scenarios.

References

[1] International Organization for Standards, "ISO/IEC JTC1 SC37 Standing Document 2, version 8, Harmonized Biometric Vocabulary ," August 1997. 1

[2] A. Jain, A. Ross, and S. Prabhakar, "An introduction to biometric recognition," *IEEE Transactions on Circuits and Systems for Video Technology*, vol. 14, no. 1, pp. 4 – 20, January 2004. 10

[3] D. Maltoni, D. Maio, A. K. Jain, and S. Prabhakar, *Handbook of Fingerprint Recognition*, 2nd ed. Springer Publishing Company, Incorporated, 2009. 11, 16, 25, 26, 27, 34, 62, 63, 66, 68, 77, 80, 242, 244

[4] R. Donida Labati and F. Scotti, "Fingerprint," in *Encyclopedia of Cryptography and Security (2nd ed.)*, H. van Tilborg and S. Jajodia, Eds. Springer, 2011, pp. 460 – 465. 11

[5] Y.-H. Li and M. Savvides, "Iris recognition, overview," in *Encyclopedia of Biometrics*, S. Z. Li and A. K. Jain, Eds., 2009, pp. 810 – 819. 11

[6] J. Daugman, "How iris recognition works," in *Proceedings of the International Conference on Image Processing*, vol. 1, 2002, pp. 33 – 36. 11, 16, 41

[7] R. Gross, "Face databases," in *Handbook of Face Recognition*, A. S.Li, Ed. New York: Springer, February 2005. 12, 16

[8] N. Duta, "A survey of biometric technology based on hand shape," *Pattern Recognition*, vol. 42, no. 11, pp. 2797 – 2806, 2009. 12, 16, 55, 56

[9] A. Kong, D. Zhang, and M. Kamel, "A survey of palmprint recognition," *Pattern Recognition*, vol. 42, pp. 1408 – 1418, July 2009. 12, 16, 55

[10] D. Zhang, Z. Guo, G. Lu, L. Zhang, Y. Liu, and W. Zuo, "Online joint palmprint and palmvein verification," *Expert Systems with Applications*, vol. 38, no. 3, pp. 2621 – 2631, 2011. 12, 16, 55

[11] B. Bhanu and H. Chen, *Human Ear Recognition by Computer (Advances in Pattern Recognition)*, 1st ed. Springer Publishing Company, Incorporated, 2008. 12, 55

[12] J. Benesty, M. M. Sondhi, and Y. A. Huang, *Springer Handbook of Speech Processing*. Secaucus, NJ, USA: Springer-Verlag New York, Inc., 2007. 12, 17

[13] D. Impedovo and G. Pirlo, "Automatic signature verification: The state of the art," *IEEE Transactions on Systems, Man, and Cybernetics, Part C: Applications and Reviews*, vol. 38, no. 5, pp. 609 – 635, September 2008. 12, 17

[14] R. Chellappa, A. Veeraraghavan, and N. Ramanathan, "Gait biometrics, overview," in *Encyclopedia of Biometrics*, 2009, pp. 628 – 633. 12, 17, 55

[15] D. Shanmugapriya and G. Padmavathi, "A survey of biometric keystroke dynamics: approaches, security and challenges," *Proceedings of the International Journal of Computer Science and Information Security*, pp. 115 – 119, 2009. 12, 17

[16] A. K. Jain, S. C. Dass, K. Nandakumar, and K. N, "Soft biometric traits for personal recognition systems," in *Proceedings of the International Conference on Biometric Authentication*, 2004, pp. 731 – 738. 12, 17, 54

[17] S. Denman, A. Bialkowski, C. Fookes, and S. Sridharan, "Determining operational measures from multi-camera surveillance systems using soft biometrics," in *Proceedings of the IEEE International Conference on Advanced Video and Signal-Based Surveillance*, 2011, pp. 462–467. 12, 54

[18] R. Donida Labati, A. Genovese, V. Piuri, and F. Scotti, "Weight estimation from frame sequences using computational intelligence techniques," in *Proceedings of the IEEE International Conference on Computational Intelligence for Measurement Systems and Applications*, July 2012, pp. 29 – 34. 12, 55

[19] S. Denman, C. Fookes, A. Bialkowski, and S. Sridharan, "Soft-biometrics: unconstrained authentication in a surveillance environment," in *Proceedings of the 2009 Digital Image Computing: Techniques and Applications*, 2009, pp. 196–203. 12, 54

[20] M. Demirkus, K. Garg, and S. Guler, "Automated person categorization for video surveillance using soft biometrics," in *Biometric Technology for Human Identification VII*, 2010. 12, 54

[21] A. Dantcheva, N. Erdogmus, and J.-L. Dugelay, "On the reliability of eye color as a soft biometric trait," in *Proceedings of the IEEE Workshop on Applications of Computer Vision*, January 2011, pp. 227 –231. 12

[22] RNCOS, Ed., *Electronics Security: Global Biometric Forecast to 2012*, 2010. 15

[23] International Biometric Group, "Biometrics market and industry report, BMIR 2009-2014," http://www.ibgweb.com/. 15, 63, 104

[24] P. Komarinski, *Automated Fingerprint Identification Systems (AFIS)*. Elsevier Academic Press, 2005. 16, 63, 208

[25] W. Zhao, R. Chellappa, A. Rosenfeld, and P. J. Phillips, "Face Recognition: A Literature Survey," *ACM Computing Surveys*, pp. 399 – 458, 2003. 16

[26] Y. Du, E. Arslanturk, Z. Zhou, and C. Belcher, "Video-based non-cooperative iris image segmentation," *IEEE Transactions on Systems, Man, and Cybernetics, part B: Cybernetics*, vol. 41, no. 1, pp. 64 – 74, February 2011. 16

[27] R. Donida Labati and F. Scotti, "Noisy iris segmentation with boundary regularization and reflections removal," *Image Vision and Computing*, vol. 28, no. 2, pp. 270 – 277, February 2010. 16, 41, 53

[28] T. Hicks and R. Coquoz, "Forensic dna evidence," in *Encyclopedia of Biometrics*, 2009, pp. 573 – 579. 16

[29] D. J. Hurley, B. Arbab-zavar, and M. S. Nixon, "The ear as a biometric," in *Handbook of Biometrics*, 2007. 16

[30] A. A. Ross, K. Nandakumar, and A. K. Jain, *Handbook of Multibiometrics (International Series on Biometrics)*. Secaucus, NJ, USA: Springer-Verlag New York, Inc., 2006. 17, 41, 54

[31] A. Azzini, S. Marrara, R. Sassi, and F. Scotti, "A fuzzy approach to multimodal biometric continuous authentication," *Fuzzy Optimization and Decision Making*, vol. 7, no. 3, pp. 243 – 256, September 2008. 17, 41

[32] S. Cimato, M. Gamassi, V. Piuri, D. Sana, R. Sassi, and F. Scotti, "Personal identification and verification using multimodal biometric data," in *Proceedings of the 2006 IEEE International Conference on Computational Intelligence for Homeland Security and Personal Safety*, October 2006, pp. 41 – 45. 17

[33] M. Gamassi, V. Piuri, D. Sana, O. Scotti, and F. Scotti, "A multi-modal multi-paradigm agent-based approach to design scalable distributed biometric systems," in *Proceedings of the 2005 IEEE International Conference on Computational Intelligence for Homeland Security and Personal Safety*, April 2005, pp. 65 – 70. 17

[34] M. Gamassi, V. Piuri, D. Sana, and F. Scotti, "A high-level optimum design methodology for multimodal biometric systems," in *Proceedings of the IEEE International Conference on Computational Intelligence for Homeland Security and Personal Safety*, July 2004, pp. 117 – 124. 17

[35] NSTC Subcommittee on Biometrics, "Biometric testing and statistics," 2006, http://www.biometrics.gov/documents/biotestingandstats.pdf. 18

[36] "FVC-onGoing: on-line evaluation of fingerprint recognition algorithms," https://biolab.csr.unibo.it/FVCOnGoing/UI/Form/Home.aspx. 18

[37] T. Mansfield, G. Kelly, D. Chandler, and J. Kane, "Biometric Product Testing Final Report V1.0," *Contract*, vol. 92, 2001. 18

[38] R. Ryan, "The importance of biometric standards," *Biometric Technology Today*, vol. 2009, no. 7, pp. 7 – 10, 2009. 20

[39] M. Theofanos, B. Stanton, C. Sheppard, R. Micheals, N. Zhang, W. Wydler, L. Nadel, and R. Rubin, "Usability testing of height and angles of ten-print fingerprint capture," NISTIR, June 2008. 20, 42, 210, 212

[40] M. El-Abed, R. Giot, B. Hemery, and C. Rosenberger, "A study of users' acceptance and satisfaction of biometric systems," in *Proceedings of the IEEE International Carnahan Conference on Security Technology*, October 2010, pp. 170 –178. 21, 42, 215

[41] International Bureau of Weights and Measures, ISO, IEC, OIML, IFCC, IUPAC, and IUPAP, "International vocabulary of basic and general terms in metrology," 2003. 21

[42] A. K. Jain, R. M. Bolle, and S. Pankanti, *Biometrics: Personal Identification in Networked Society*. Springer, October 2005. 22

[43] M. Gamassi, M. Lazzaroni, M. Misino, V. Piuri, D. Sana, and F. Scotti, "Quality assessment of biometric systems: a comprehensive perspective based on accuracy and performance measurement," *IEEE Transactions on Instrumentation and Measurement*, vol. 54, no. 4, pp. 1489–1496, August 2005. 22, 75

[44] R. Donida Labati, A. Genovese, V. Piuri, and F. Scotti, "Quality measurement of unwrapped three-dimensional fingerprints: a neural networks approach," in *Proceedings of the 2012 International Joint Conference on Neural Networks (IJCNN)*, June 2012. 25, 154, 229

[45] L. Masek and P. Kovesi, *MATLAB Source Code for a Biometric Identification System Based on Iris Patterns*. The School of Computer Science and Software Engineering, The University of Western Australia, 2003. 26

[46] C.B.S.R., Center for Biometrics and Security Research, CASIA Iris Dataset, http://www.cbsr.ia.ac.cn. 26

[47] A. J. Mansfield, J. L. Wayman, A. Dr, D. Rayner, and J. L. Wayman, "Best practices in testing and reporting performance," 2002. 27, 28, 205

[48] T. A. Louis, "Confidence intervals for a binomial parameter after observing no successes," *The American Statistician*, vol. 35, no. 3, pp. 154 – 154, 1981. 27

[49] B. D. Jovanovic and P. S. Levy, "A look at the rule of three," *The American Statistician*, vol. 51, no. 2, pp. 137 – 139, 1997. 27

[50] G. R. Doddington, M. A. Przybocki, A. F. Martin, and D. A. Reynolds, "The NIST speaker recognition evaluation - overview, methodology, systems, results, perspective," *Speech Communication*, vol. 31, no. 2 - 3, pp. 225 – 254, 2000. 27

[51] G. W. Snedecor and W. G. Cochran, *Statistical Methods, Seventh Edition*. Iowa State University, 1980. 28

[52] R. Bolle, N. Ratha, and S. Pankanti, "Confidence interval measurement in performance analysis of biometrics systems using the bootstrap," in *Proceedings of the IEEE Workshop on Empirical Evaluation Methods in Computer Vision*, 2001. 28

[53] N. Poh and S. Bengio, "Estimating the confidence interval of expected performance curve in biometric authentication using joint bootstrap," in *Proceedings of the IEEE International Conference on Acoustics, Speech and Signal Processing*, vol. 2, April 2007, pp. 137 – 140. 28

[54] R. M. Bolle, N. K. Ratha, and S. Pankanti, "Error analysis of pattern recognition systems - the subsets bootstrap," *Computer Vision and Image Understanding*, vol. 93, no. 1, pp. 1 – 33, 2004. 28

[55] R. Li, D. Tang, W. Li, and D. Zhang, "Second-level partition for estimating FAR confidence intervals in biometric systems," in *Computer Analysis of Images and Patterns*, ser. Lecture Notes in Computer Science, X. Jiang and N. Petkov, Eds. Springer Berlin Heidelberg, 2009, vol. 5702, pp. 58 – 65. 29

[56] R. Li, B. Huang, R. Li, and W. Li, "Test sample size determination for biometric systems based on confidence elasticity," in *Proceedings of the International Joint Conference on Neural Networks (IJCNN)*, June 2012, pp. 1 – 7. 29

[57] S. Dass, Y. Zhu, and A. Jain, "Validating a biometric authentication system: Sample size requirements," *IEEE Transactions on Pattern Analysis and Machine Intelligence*, vol. 28, no. 12, pp. 1902 – 1319, December 2006. 29

[58] N. Poh, A. Martin, and S. Bengio, "Performance generalization in biometric authentication using joint user-specific and sample bootstraps," *IEEE Transactions on Pattern Analysis and Machine Intelligence*, vol. 29, no. 3, pp. 492 – 498, March 2007. 29

[59] S. Cimato, R. Sassi, and F. Scotti, "Biometrics and privacy," *Recent Patents on Computer Science*, vol. 1, pp. 98 –109, June 2008. 29

[60] S. Cimato, M. Gamassi, V. Piuri, R. Sassi, and F. Scotti, *Privacy in biometrics*, ser. IEEE Press Series on Computational Intelligence, N. Boulgouris, K. Plataniotis, and E. Micheli-Tzanakou, Eds. Wiley-IEEE Press, 2009. 29

[61] S. Cimato, M. Gamassi, V. Piuri, R. Sassi, and F. Scotti, *Privacy Issues in Biometric Identification*, ser. Touch Briefings. Business Briefings LtD, 2006. 29

[62] S. Cimato, R. Sassi, and F. Scotti, "Biometric privacy," in *Encyclopedia of Cryptography and Security (2nd ed.)*, H. van Tilborg and S. Jajodia, Eds. Springer, 2011, pp. 101 – 104. 29

[63] M. Faundez-Zanuy, "On the vulnerability of biometric security systems," *IEEE Aerospace and Electronic Systems Magazine*, vol. 19, no. 6, pp. 3 – 8, June 2004. 30

[64] N. K. Ratha, J. H. Connell, and R. M. Bolle, "An analysis of minutiae matching strength," in *Proceedings of the Third International Conference on Audio- and Video-Based Biometric Person Authentication (AVBPA)*, 2001, pp. 223 – 228. 30

[65] F. Sabena, A. Dehghantanha, and A. Seddon, "A review of vulnerabilities in identity management using biometrics," *Proceedings of the Second International Conference on Future Networks (CFN)*, pp. 42 – 49, January 2010. 30

[66] A. K. Jain, K. Nandakumar, and A. Nagar, "Biometric template security," *EURASIP Journal on Advances in Signal Processing*, vol. 2008, pp. 1–17, 2008. 30, 34, 37

[67] International Biometric Group, "Bioprivacy initiative," 2003, http://www.bioprivacy.org/. 31, 32, 33

[68] C. Rathgeb and A. Uhl, "A survey on biometric cryptosystems and cancelable biometrics," *EURASIP Journal on Information Security*, no. 1, 2011. 34

[69] A. Cavoukian and A. Stoianov, "Biometric encryption," in *Encyclopedia of Cryptography and Security (2nd Ed.)*, 2011, pp. 90 – 98. 34

[70] N. K. Ratha, J. H. Connell, and R. M. Bolle, "Enhancing security and privacy in biometrics-based authentication systems," *IBM Systems Journal*, vol. 40, no. 3, pp. 614 – 634, 2001. 35, 36

[71] A. B. J. Teoh, Y. W. Kuan, and S. Lee, "Cancellable biometrics and annotations on biohash," *Pattern Recognition*, vol. 41, no. 6, pp. 2034 – 2044, June 2008. 35, 36

[72] C. S. Chin, A. T. B. Jin, and D. N. C. Ling, "High security iris verification system based on random secret integration," *Computer Vision and Image Understanding*, vol. 102, pp. 169 –177, May 2006. 35, 36

[73] A. Teoh, A. Goh, and D. Ngo, "Random multispace quantization as an analytic mechanism for biohashing of biometric and random identity inputs," *IEEE Transactions on Pattern Analysis and Machine Intelligence*, vol. 28, no. 12, pp. 1892 – 1901, December 2006. 35, 36

[74] A. Teoh, B. Jin, T. Connie, D. Ngo, and C. Ling, "Remarks on biohash and its mathematical foundation," *Information Processing Letters*, vol. 100, pp. 145 – 150, November 2006. 36

[75] L. Nanni and A. Lumini, "Empirical tests on biohashing," *Neurocomputing*, vol. 69, pp. 2390 – 2395, 2006. 36

[76] A. T. B. Jin, D. N. C. Ling, and A. Goh, "Biohashing: two factor authentication featuring fingerprint data and tokenised random number," *Pattern Recognition*, vol. 37, no. 11, pp. 2245 – 2255, 2004. 36

[77] M. Savvides, B. Vijaya Kumar, and P. Khosla, "Cancelable biometric filters for face recognition," in *Proceedings of the International Conference on Pattern Recognition*, vol. 3, August 2004, pp. 922 – 925. 36

[78] A. Makrushin, T. Scheidat, and C. Vielhauer, "Towards robust biohash generation for dynamic handwriting using feature selection," in *Proceedings of the International Conference on Digital Signal Processing*, July 2011, pp. 1 – 6. 36

[79] A. Nagar and A. Jain, "On the security of non-invertible fingerprint template transforms," in *Proceedings of the First IEEE International Workshop on Information Forensics and Security (WIFS)*, 2009, pp. 81 – 85. 36

[80] Z. Jin, A. Teoh, T. S. Ong, and C. Tee, "Generating revocable fingerprint template using minutiae pair representation," in *Proceedings of the International Conference on Education Technology and Computer*, vol. 5, June 2010. 36

[81] Y. Wang and K. N. Plataniotis, "An analysis of random projection for changeable and privacy-preserving biometric verification," *IEEE Transaction on Systems, Man and Cybernetic, Part B: Cybernetics*, vol. 40, pp. 1280 – 1293, October 2010. 36

[82] Y. Wang and D. Hatzinakos, "On random transformations for changeable face verification," *IEEE Transaction on Systems, Man and Cybernetic, Part B: Cybernetics*, vol. 41, no. 3, pp. 840 – 854, June 2011. 36

[83] E. Maiorana, P. Campisi, J. Fierrez, J. Ortega-Garcia, and A. Neri, "Cancelable templates for sequence-based biometrics with application to on-line signature recognition," *IEEE Transaction on Systems, Man and Cybernetic, Part A: Systems and Humans*, vol. 40, no. 3, pp. 525 – 538, May 2010. 36

[84] N. K. Ratha, S. Chikkerur, J. H. Connell, and R. M. Bolle, "Generating cancelable fingerprint templates," *IEEE Transaction on Pattern Analysis and Machine Intelligence*, vol. 29, no. 4, pp. 561 – 572, 2007. 37

[85] T. Boult, "Robust distance measures for face-recognition supporting revocable biometric tokens," in *Proceedings of the International Conference on Automatic Face and Gesture Recognition*, April 2006, pp. 560 – 566. 37

[86] T. Boult, W. Schdrer, and R. Woodworth, "Revocable fingerprint biotokens: Accuracy and security analysis," in *Proceedings of the IEEE Conference on Computer Vision and Pattern Recognition (CVPR)*, June 2007, pp. 1 – 8. 37

[87] R. K. Nichols, *Icsa Guide to Cryptography*. McGraw-Hill Professional, 1998. 38

[88] A. Juels and M. Wattenberg, "A fuzzy commitment scheme," in *Proceedings of the Sixth ACM Conference on Computer and Communications Security*, 1999, pp. 28 – 36. 38

[89] A. Juels and M. Sudan, "A fuzzy vault scheme," in *Proceedings of the IEEE International Symposium on Information Theory*, 2002, p. 408. 38

[90] L. Huixian, W. Man, P. Liaojun, and Z. Weidong, "Key binding based on biometric shielding functions," in *Proceedings of the International Conference on Information Assurance and Security*, vol. 1, August 2009, pp. 19 – 22. 38

[91] S. Draper, A. Khisti, E. Martinian, A. Vetro, and J. Yedidia, "Using distributed source coding to secure fingerprint biometrics," in *Proceedings of the IEEE International Conference on Acoustics, Speech and Signal Processing*, vol. 2, April 2007, pp. 29 –132. 38

[92] T. Ignatenko and F. Willems, "Information leakage in fuzzy commitment schemes," *IEEE Transactions on Information Forensics and Security*, vol. 5, no. 2, pp. 337 – 348, June 2010. 38

[93] K. Nandakumar, A. Jain, and S. Pankanti, "Fingerprint-based fuzzy vault: Implementation and performance," *IEEE Transactions on Information Forensics and Security*, vol. 2, no. 4, pp. 744 – 757, December 2007. 38

[94] Y. J. Lee, K. R. Park, S. J. Lee, K. Bae, and J. Kim, "A new method for generating an invariant iris private key based on the fuzzy vault system," *IEEE Transactions on Systems, Man, and Cybernetics, Part B: Cybernetics*, vol. 38, no. 5, pp. 1302 – 1313, October 2008. 38

[95] E. Maiorana and P. Campisi, "Fuzzy commitment for function based signature template protection," *IEEE Signal Processing Letters*, vol. 17, no. 3, pp. 249 – 252, March 2010. 38, 40

[96] T. Ignatenko and F. Willems, "Information leakage in fuzzy commitment schemes," *IEEE Transactions on Information Forensics and Security*, vol. 5, no. 2, pp. 337 – 348, June 2010. 39

[97] J. Bringer, H. Chabanne, G. Cohen, B. Kindarji, and G. Zemor, "Theoretical and practical boundaries of binary secure sketches," *IEEE Transactions on Information Forensics and Security*, vol. 3, no. 4, pp. 673 – 683, December 2008. 39

[98] Y. Dodis, R. Ostrovsky, L. Reyzin, and A. Smith, "Fuzzy extractors: How to generate strong keys from biometrics and other noisy data," *SIAM Journal on Computing*, vol. 38, no. 1, pp. 97 – 139, 2008. 39

[99] S. Cimato, M. Gamassi, V. Piuri, R. Sassi, F. S. Cimato, and F. Scotti, "A biometric verification system addressing privacy concerns," in *Proceedings of the International Conference on Computational Intelligence and Security*, December 2007, pp. 594 – 598. 40

[100] Y. Sutcu, Q. Li, and N. Memon, "Protecting biometric templates with sketch: Theory and practice," *IEEE Transactions on Information Forensics and Security*, vol. 2, no. 3, pp. 503 – 512, September 2007. 40

[101] S. Cimato, M. Gamassi, V. Piuri, R. Sassi, and F. Scotti, "Privacy-aware biometrics: Design and implementation of a multimodal verification system," in *Proceedings of the Annual Computer Security Applications Conference*, December 2008, pp. 130 –139. 40

[102] C. Fontaine and F. Galand, "A survey of homomorphic encryption for nonspecialists," *EURASIP Journal on Information Security*, pp. 1 – 15, 2007. 40

[103] T. Bianchi, R. Donida Labati, V. Piuri, A. Piva, F. Scotti, and S. Turchi, "Implementing fingercode-based identity matching in the encrypted domain," in *Proceedings of the IEEE Workshop on Biometric Measurements and Systems for Security and Medical Applications (BIOMS)*, September 2010, pp. 15–21. 40, 242, 245

[104] Z. Erkin, M. Franz, J. Guajardo, S. Katzenbeisser, I. Lagendijk, and T. Toft, "Privacy-preserving face recognition," in *Proceedings of the 9th International Symposium on Privacy Enhancing Technologies (PETS)*, 2009, pp. 235 – 253. 41, 246

[105] A. Sadeghi, T. Schneider, and I. Wehrenberg, "Efficient privacy-preserving face recognition," in *Proceedings of the 12th Annual International Conference on Information Security and Cryptology*, ser. LNCS, vol. 5984. Springer-Verlag, December 2009, pp. 235 – 253. 41, 246

[106] A. Stoianov, "Cryptographically secure biometrics," in *Biometric Technology for Human Identification VII*, B. V. K. V. Kumar, S. Prabhakar, and A. A. Ross, Eds., vol. 7667, no. 1. SPIE, 2010, p. 76670C. 41

[107] J. Bringer, H. Chabanne, M. Izabachène, D. Pointcheval, Q. Tang, and S. Zimmer, "An application of the Goldwasser-Micali cryptosystem to biometric authentication," in *Proceedings of the 12th Australasian conference on Information security and privacy (ACISP)*, 2007, pp. 96 – 106. 41

[108] J. Bringer and H. Chabanne, "An authentication protocol with encrypted biometric data," in *Proceedings of the Cryptology in Africa 1st international conference on Progress in cryptology (AFRICACRYPT)*, 2008, pp. 109 – 124. 41

[109] B. Schoenmakers and P. Tuyls, *Computationally Secure Authentication with Noisy Data*. Berlin, Heidelberg: Springer-Verlag, 2007, pp. 141 – 149. 41

[110] R. Donida Labati, V. Piuri, and F. Scotti, "Agent-based image iris segmentation and multiple views boundary refining," in *Proceedings of the IEEE Third International Conference on Biometrics: Theory, Applications and Systems*, November 2009, pp. 1 – 7. 41

[111] R. Donida Labati, V. Piuri, and F. Scotti, "Neural-based iterative approach for iris detection in iris recognition systems," in *Proceedings of the IEEE Symposium on Computational Intelligence for Security and Defence Applications*, December 2009, pp. 1 – 6. 41

[112] K. W. Bowyer, "The results of the NICE.II iris biometrics competition," *Pattern Recognition Letters*, vol. 33, no. 8, pp. 965 – 969, June 2012. 41, 54

[113] B. Kamgar-Parsi, W. Lawson, and B. Kamgar-Parsi, "Toward development of a face recognition system for watchlist surveillance," *IEEE Transactions on Pattern Analysis and Machine Intelligence*, vol. 33, no. 10, pp. 1925 –1937, October 2011. 41, 48, 49

[114] J. Matey, O. Naroditsky, K. Hanna, R. Kolczynski, D. LoIacono, S. Mangru, M. Tinker, T. Zappia, and W. Zhao, "Iris on the move: Acquisition of images for iris recognition in less constrained environments," *Proceedings of the IEEE*, vol. 94, no. 11, pp. 1936 – 1947, November 2006. 42, 53

[115] K. Bowyer, K. Chang, and P. Flynn, "A survey of approaches to three-dimensional face recognition," in *Proceedings of the 17th International Conference on Pattern Recognition*, vol. 1, August 2004, pp. 358 – 361. 42

[116] K. Plataniotis, D. Hatzinakos, and J. Lee, "ECG biometric recognition without fiducial detection," in *Proceedings of the Biometrics Symposium: Special Session on Research at the Biometric Consortium Conference*, August 2006, pp. 1 – 6. 42

[117] F. Wheeler, R. Weiss, and P. Tu, "Face recognition at a distance system for surveillance applications," in *Proceedings of the Fourth IEEE International Conference on Biometrics: Theory Applications and Systems*, September 2010, pp. 1 – 8. 48

[118] B. Chen, J. Shen, and H. Sun, "A fast face recognition system on mobile phone," in *Proceedings of the International Conference on Systems and Informatics*, May 2012, pp. 1783 –1786. 48, 49

[119] A. Pentland and T. Choudhury, "Face recognition for smart environments," *Computer*, vol. 33, no. 2, pp. 50 – 55, February 2000. 49

[120] T. Leyvand, C. Meekhof, Y.-C. Wei, J. Sun, and B. Guo, "Kinect identity: Technology and experience," *Computer*, vol. 44, no. 4, pp. 94 – 96, April 2011. 49

[121] J. Y. Choi, W. De Neve, and Y. M. Ro, "Towards an automatic face indexing system for actor-based video services in an iptv environment," *IEEE Transactions on Consumer Electronics*, vol. 56, no. 1, pp. 147 – 155, February 2010. 49

[122] S. K. Zhou, R. Chellappa, and W. Zhao, *Unconstrained Face Recognition*, ser. International Series on Biometrics. Boston, MA: Springer US, 2006. 49, 50

[123] M. Turk and A. Pentland, "Eigenfaces for recognition," *Journal of Cognitive Neuroscience*, vol. 3, no. 1, pp. 71 – 86, January 1991. 50

[124] R. Basri and D. Jacobs, "Lambertian reflectance and linear subspaces," *IEEE Transactions on Pattern Analysis and Machine Intelligence*, vol. 25, no. 2, pp. 218 – 233, February 2003. 50

[125] J. J. Atick, P. A. Griffin, and A. N. Redlich, "Statistical approach to shape from shading: Reconstruction of three-dimensional face surfaces from single two-dimensional images," *Neural Computation*, vol. 8, no. 6, pp. 1321 – 1340, August 1996. 50

[126] V. Blanz and T. Vetter, "Face recognition based on fitting a 3d morphable model," *IEEE Transactions on Pattern Analysis and Machine Intelligence*, vol. 25, no. 9, pp. 1063 – 1074, September 2003. 50

[127] X. Zhang and Y. Gao, "Face recognition across pose: A review," *Pattern Recognition*, vol. 42, no. 11, pp. 2876 – 2896, 2009. 50

[128] U. Park, Y. Tong, and A. Jain, "Age-invariant face recognition," *IEEE Transactions on Pattern Analysis and Machine Intelligence*, vol. 32, no. 5, pp. 947 – 954, May 2010. 50

[129] H. Ling, S. Soatto, N. Ramanathan, and D. Jacobs, "Face verification across age progression using discriminative methods," *IEEE Transactions on Information Forensics and Security*, vol. 5, no. 1, pp. 82 – 91, March 2010. 50

[130] S. Zhou, V. Krueger, and R. Chellappa, "Probabilistic recognition of human faces from video," *Computer Vision and Image Understanding*, vol. 91, no. 1 - 2, pp. 214 – 245, 2003. 50

[131] A. Scheenstra, A. Ruifrok, and R. C. Veltkamp, "A survey of 3d face recognition methods," in *Lecture Notes in Computer Science*. SpringerVerlag, 2005, pp. 891 – 899. 50

[132] C. L. Fancourt, L. Bogoni, K. J. Hanna, Y. Guo, R. P. Wildes, N. Takahashi, and U. Jain, "Iris recognition at a distance," in *Proceedings of Audio and Video Based Person Authentication*, 2005, pp. 1 –13. 51, 52

[133] Z. Sun, W. Dong, and T. Tan, "Technology roadmap for smart iris recognition," in *Proceedings of the International Conference on Computer Graphics & Vision*, 2008, pp. 12 – 19. 52

[134] W. Dong, Z. Sun, T. Tan, and X. Qiu, "Self-adaptive iris image acquisition system," in *Proceedings of SPIE*, 2008. 52

[135] W. Dong, Z. Sun, and T. Tan, "A design of iris recognition system at a distance," in *Proceedings of the Chinese Conference on Pattern Recognition*, November 2009, pp. 1 – 5. 53

[136] R. Donida Labati, A. Genovese, V. Piuri, and F. Scotti, *Iris segmentation: state of the art and innovative methods*, ser. Intelligent Systems Reference Library, C. Liu and V. Mago, Eds. Springer, 2012, vol. 37. 53

[137] H. Proença, "Iris recognition: On the segmentation of degraded images acquired in the visible wavelength," *IEEE Transaction on Pattern Analysis and Machine Intelligence*, vol. 32, no. 8, pp. 1502 – 1516, August 2010. 53

[138] S. Shah and A. Ross, "Iris segmentation using geodesic active contours," *IEEE Transaction on Information Forensics Security*, vol. 4, no. 4, pp. 824 – 836, December 2009. 53

[139] F. Scotti and V. Piuri, "Adaptive reflection detection and location in iris biometric images by using computational intelligence techniques," *IEEE Transactions of Instrumentation and Measurement*, vol. 59, no. 7, pp. 1825 – 1833, July 2010. 53

[140] F. Scotti, "Computational intelligence techniques for reflections identification in iris biometric images," in *Proceedings of the IEEE International Conference on Computational Intelligence for Measurement Systems and Applications*, June 2007, pp. 84 – 88. 53

[141] K. Nguyen, C. Fookes, S. Sridharan, and S. Denman, "Quality-driven super-resolution for less constrained iris recognition at a distance and on the move," *IEEE Transactions on Information Forensics and Security*, vol. 6, no. 4, pp. 1248 – 1258, December 2011. 54

[142] S. Schuckers, N. Schmid, A. Abhyankar, V. Dorairaj, C. Boyce, and L. Hornak, "On techniques for angle compensation in nonideal iris recognition," *IEEE Transactions on Systems, Man, and Cybernetics, Part B: Cybernetics*, vol. 37, no. 5, pp. 1176 – 1190, October 2007. 54

[143] C.-T. Chou, S.-W. Shih, W.-S. Chen, V. Cheng, and D.-Y. Chen, "Non-orthogonal view iris recognition system," *IEEE Transactions on Circuits and Systems for Video Technology*, vol. 20, no. 3, pp. 417 – 430, March 2010. 54

[144] K. Niinuma, U. Park, and A. Jain, "Soft biometric traits for continuous user authentication," *IEEE Transactions on Information Forensics and Security*, vol. 5, no. 4, pp. 771–780, December 2010. 54

[145] Y. Ran, G. Rosenbush, and Q. Zheng, "Computational approaches for real-time extraction of soft biometrics," in *Proceedings of the 19th International Conference on Pattern Recognition*, 2008, pp. 1–4. 55

[146] J. Zhang, Y. Cheng, and C. Chen, "Low resolution gait recognition with high frequency super resolution," in *PRICAI 2008: Trends in Artificial Intelligence*, ser. Lecture Notes in Computer Science, T.-B. Ho and Z.-H. Zhou, Eds. Springer Berlin / Heidelberg, 2008, vol. 5351, pp. 533–543. 55

[147] J. Bustard and M. Nixon, "Toward unconstrained ear recognition from two-dimensional images," *IEEE Transactions on Systems, Man and Cybernetics, Part A: Systems and Humans*, vol. 40, no. 3, pp. 486 – 494, May 2010. 55

[148] R. Raposo, E. Hoyle, A. Peixinho, and H. Proenca, "Ubear: A dataset of ear images captured on-the-move in uncontrolled conditions," in *Proceedings of the IEEE Workshop on Computational Intelligence in Biometrics and Identity Management*, April 2011, pp. 84 – 90. 55

[149] M. Ramalho, P. Correia, and L. Soares, "Hand-based multimodal identification system with secure biometric template storage," *IET Computer Vision*, vol. 6, no. 3, pp. 165 – 173, May 2012. 55

[150] V. Kanhangad, A. Kumar, and D. Zhang, "Contactless and pose invariant biometric identification using hand surface," *IEEE Transactions on Image Processing*, vol. 20, no. 5, pp. 1415 – 1424, May 2011. 55, 56

[151] D. L. Woodard and P. J. Flynn, "Finger surface as a biometric identifier," *Computer Vision and Image Understanding*, vol. 100, no. 3, pp. 357 – 384, December 2005. 56

[152] S. Ribaric and I. Fratric, "A biometric identification system based on eigenpalm and eigenfinger features," *IEEE Transactions on Pattern Analysis and Machine Intelligence*, vol. 27, no. 11, pp. 1698 – 1709, November 2005. 56

[153] A. Kumar, "Incorporating cohort information for reliable palmprint authentication," in *Proceedings of the Sixth Indian Conference on Computer Vision, Graphics Image Processing*, December 2008, pp. 583 – 590. 56

[154] R.-X. Hu, W. Jia, D. Zhang, J. Gui, and L.-T. Song, "Hand shape recognition based on coherent distance shape contexts," *Pattern Recognition*, vol. 45, no. 9, pp. 3348 – 3359, 2012. 56

[155] A. Kumar and D. Zhang, "Personal recognition using hand shape and texture," *IEEE Transactions on Image Processing*, vol. 15, no. 8, pp. 2454 –2461, August 2006. 56

[156] J. Doublet, O. Lepetit, and M. Revenu, "Contactless hand recognition based on distribution estimation," in *Proceedings of the Biometrics Symposium*, September 2007, pp. 1 – 6. 56

[157] A. de Santos Sierra, J. Casanova, C. Avila, and V. Vera, "Silhouette-based hand recognition on mobile devices," in *Proceedings of the 43rd Annual 2009 International Carnahan Conference on Security Technology*, October 2009, pp. 160 – 166. 56

[158] "PolyU 3D Palmprint Database," http://www4.comp.polyu.edu.hk/. 56

[159] "CASIA Palmprint Image Database," http://www.idealtest.org. 56

[160] P. T. H. John D. Woodward (Jr.), Nicholas M. Orlans, *Biometrics*. McGraw-Hill/Osborne, 2003. 60

[161] A. Jain, A. Ross, and S. Pankanti, "Biometrics: a tool for information security," *IEEE Transactions on Information Forensics and Security*, vol. 1, no. 2, pp. 125 – 143, June 2006. 61

[162] W. Babler, "Embryologic development of epidermal ridges and their configurations," *Birth Defects Original Article Series*, vol. 27, no. 2, pp. 95 – 112, 1991. 61

[163] A. K. Jain, S. Prabhakar, and S. Pankanti, "On the similarity of identical twin fingerprints," *Pattern Recognition*, vol. 35, no. 11, pp. 2653 – 2663, 2002. 61

[164] X. Tao, X. Chen, X. Yang, and J. Tian, "Fingerprint recognition with identical twin fingerprints," *PLoS ONE*, vol. 7, no. 4, April 2012. 61, 62

[165] S. Pankanti, S. Prabhakar, and A. Jain, "On the individuality of fingerprints," *IEEE Transactions on Pattern Analysis and Machine Intelligence*, vol. 24, no. 8, pp. 1010 – 1025, August 2002. 62

[166] K. Kryszczuk, P. Morier, and A. Drygajlo, "Study of the distinctiveness of level 2 and level 3 features in fragmentary fingerprint comparison," in *Biometric Authentication*, ser. Lecture Notes in Computer Science, D. Maltoni and A. Jain, Eds. Springer Berlin / Heidelberg, 2004, vol. 3087, pp. 124 – 133. 62

[167] M. Puertas, D. Ramos, J. Fierrez, J. Ortega-Garcia, and N. Exposito, "Towards a better understanding of the performance of latent fingerprint recognition in realistic forensic conditions," in *Proceedings of the 20th International Conference on Pattern Recognition*, 2010, pp. 1638 – 1641. 62

[168] N. K. Ratha and R. Bolle, *Automatic Fingerprint Recognition Systems*. SpringerVerlag, 2003. 63

[169] T.-T. Truong, M.-T. Tran, and A.-D. Duong, "Robust mobile device integration of a fingerprint biometric remote authentication scheme," in *Proceedings of the IEEE 26th International Conference on Advanced Information Networking and Applications (AINA)*, March 2012, pp. 678 – 685. 63

[170] S. B. Pan, D. Moon, Y. Gil, D. Ahn, and Y. Chung, "An ultra-low memory fingerprint matching algorithm and its implementation on a 32-bit smart card," *IEEE Transactions on Consumer Electronics*, vol. 49, no. 2, pp. 453 – 459, May 2003. 63

[171] Z. Hou, W.-Y. Yau, and Y. Wang, "A review on fingerprint orientation estimation," *Security and Communication Networks*, June 2009. 64

[172] A. Grasselli, *Methodologies of Pattern Recognition*. New York: Academic, 1969, ch. On the automatic classification of fingerprints. 64

[173] A. Bazen and S. Gerez, "Systematic methods for the computation of the directional fields and singular points of fingerprints," *IEEE Transactions on Pattern Analysis and Machine Intelligence*, vol. 24, no. 7, pp. 905 – 919, July 2002. 64

[174] Y. Mei, G. Cao, H. Sun, and R. Hou, "A systematic gradient-based method for the computation of fingerprint's orientation field," *Computers & Electrical Engineering*, 2011. 64

[175] L. Ji and Z. Yi, "Fingerprint orientation field estimation using ridge projection," *Pattern Recognition*, vol. 41, no. 5, pp. 1491 – 1503, 2008. 64

[176] T. Kamei, "Image filter design for fingerprint enhancement," in *Automatic Fingerprint Recognition Systems*, N. Ratha and R. Bolle, Eds. Springer New York, 2004, pp. 113–126. 64

[177] S. Chikkerur, A. N. Cartwright, and V. Govindaraju, "Fingerprint enhancement using stft analysis," *Pattern Recognition*, vol. 40, no. 1, pp. 198 – 211, January 2007. 64, 65, 78, 93

[178] M. Oliveira and N. Leite, "A multiscale directional operator and morphological tools for reconnecting broken ridges in fingerprint images," *Pattern Recognition*, vol. 41, no. 1, pp. 367 – 377, 2008. 64

[179] L. min Liu and T.-S. Dai, "A reliable fingerprint orientation estimation algorithm," *Journal of Information Science and Engineering*, vol. 27, no. 1, pp. 353 – 368, 2011. 64

[180] B. Sherlock and D. Monro, "A model for interpreting fingerprint topology," *Pattern Recognition*, vol. 26, no. 7, pp. 1047 – 1055, 1993. 64

[181] L. Hong, Y. Wan, and A. Jain, "Fingerprint image enhancement: algorithm and performance evaluation," *IEEE Transactions on Pattern Analysis and Machine*

Intelligence, vol. 20, no. 8, pp. 777–789, August 1998. 65, 77, 78, 93, 100, 123, 124, 153, 161

[182] X. Jiang, "Fingerprint image ridge frequency estimation by higher order spectrum," in *Proceedings of the International Conference on Image Processing*, vol. 1, 2000, pp. 462 – 465. 65

[183] A. Almansa and T. Lindeberg, "Fingerprint enhancement by shape adaptation of scale-space operators with automatic scale selection," *IEEE Transactions on Image Processing*, vol. 9, no. 12, pp. 2027 – 2042, December 2000. 65

[184] C. Gottschlich, "Curved-region-based ridge frequency estimation and curved gabor filters for fingerprint image enhancement," *IEEE Transactions on Image Processing*, vol. 21, no. 4, pp. 2220 – 2227, April 2012. 65

[185] M. Kawagoe and A. Tojo, "Fingerprint pattern classification," *Pattern Recognition*, vol. 17, no. 3, pp. 295 – 303, June 1984. 66, 125, 128

[186] L. Fan, S. Wang, H. Wang, and T. Guo, "Singular points detection based on zero-pole model in fingerprint images," *IEEE Transactions on Pattern Analysis and Machine Intelligence*, vol. 30, pp. 929–940, 2008. 66

[187] J. Zhou, J. Gu, and D. Zhang, "Singular points analysis in fingerprints based on topological structure and orientation field," in *Proceedings of the International Conference of Biometrics*, 2007, pp. 261 – 270. 66

[188] H. Kekre and V. Bharadi, "Fingerprint's core point detection using orientation field," in *Proceedings of the International Conference on Advances in Computing, Control, Telecommunication Technologies*, December 2009, pp. 150 – 152. 66

[189] T. Liu, C. Zhang, and P. Hao, "Fingerprint reference point detection based on local axial symmetry," in *Proceedings of the '18th International Conference on Pattern Recognition*. Washington, DC, USA: IEEE Computer Society, 2006, pp. 1050 – 1053. 66

[190] J. L. A. Samatelo and E. O. T. Salles, "Determination of the reference point of a fingerprint based on multiple levels of representation," in *Proceedings of the 2009*

XXII Brazilian Symposium on Computer Graphics and Image Processing, 2009, pp. 209 – 215. 66

[191] H. Lam, Z. Hou, W. Yau, T. Chen, J. Li, and K. Sim, "Reference point detection for arch type fingerprints," in *'Proceedings of the Third International Conference on Advances in Biometrics*, 2009, pp. 666 – 674. 66

[192] W.-C. Lin and R. C. Dubes, "A review of ridge counting in dermatoglyphics," *Pattern Recognition*, vol. 16, no. 1, pp. 1–8, 1983. 67

[193] A. Jain, S. Prabhakar, L. Hong, and S. Pankanti, "Filterbank-based fingerprint matching," *IEEE Transactions on Image Processing*, vol. 9, no. 5, pp. 846–859, May 2000. 67, 83, 97, 135, 243, 244

[194] R. Bansal, P. Sehgal, and P. Bedi, "Minutiae extraction from fingerprint images - a review," *IJCSI International Journal of Computer Science Issues*, vol. 8, no. 5, pp. 929–940, November 2012. 67, 68

[195] R. C. Gonzalez and R. E. Woods, *Digital Image Processing (3rd Edition)*. Upper Saddle River, NJ, USA: Prentice-Hall, Inc., 2006. 69, 77, 79, 144, 230

[196] R. M. Stock, "Automatic fingerprint reading," in *Proceedings of the Carnahan Conference on Electronic Crime Countermeasure*, 1972. 69

[197] M. Verma, A. Majumdar, and B. Chatterjee, "Edge detection in fingerprints," *Pattern Recognition*, vol. 20, no. 5, pp. 513 – 523, 1987. 69

[198] J. Bartunek, M. Nilsson, J. Nordberg, and I. Claesson, "Adaptive fingerprint binarization by frequency domain analysis," in *Proceedings of the Fortieth Asilomar Conference on Signals, Systems and Computers*, November 2006, pp. 598 – 602. 69

[199] C. I. Watson, M. D. Garris, E. Tabassi, C. L. Wilson, R. M. Mccabe, S. Janet, and K. Ko, "User's guide to NIST biometric image software (NBIS)," 2007. 69, 70, 71, 76, 81, 125, 127, 130, 132, 150, 157, 189, 193, 195, 202, 204, 209, 210

[200] V. Espinosa-Duro, "Fingerprints thinning algorithm," *IEEE Aerospace and Electronic Systems Magazine*, vol. 18, no. 9, pp. 28 – 30, September 2003. 69

[201] L. Ji, Z. Yi, L. Shang, and X. Pu, "Binary fingerprint image thinning using template-based pcnns," *IEEE Transactions on Systems, Man, and Cybernetics, Part B: Cybernetics*, vol. 37, no. 5, pp. 1407 –1413, October 2007. 69

[202] B. Fang, H. Wen, R.-Z. Liu, and Y.-Y. Tang, "A new fingerprint thinning algorithm," in *Proceedings of the Chinese Conference on Pattern Recognition*, October 2010, pp. 1 – 4. 69

[203] C. Arcelli and G. S. Di Baja, "A width-independent fast thinning algorithm," *IEEE Transactions on Pattern Analysis and Machine Intelligence*, vol. 7, no. 4, pp. 463 – 474, July 1985. 70

[204] R. Bansal, P. Sehgal, and p. Bedi, "Effective morphological extraction of true fingerprint minutiae based on the hit or miss transform," *International Journal of Biometrics and Bioinformatics*, vol. 4, pp. 471 – 85, 2010. 70

[205] F. Zhao and X. Tang, "Preprocessing and postprocessing for skeleton-based fingerprint minutiae extraction," *Pattern Recognition*, vol. 40, no. 4, pp. 1270 – 1281, April 2007. 70

[206] D. Maio and D. Maltoni, "Neural network based minutiae filtering in fingerprints," in *Proceedings of the Fourteenth International Conference on Pattern Recognition*, vol. 2, August 1998, pp. 1654 – 1658. 70

[207] M. Gamassi, V. Piuri, and F. Scotti, "Fingerprint local analysis for high-performance minutiae extraction," in *Proceedings of the IEEE International Conference on Image Processing*, vol. 3, September 2005, pp. 265 – 8. 70

[208] S. Di Zenzo, L. Cinque, and S. Levialdi, "Run-based algorithms for binary image analysis and processing," *IEEE Transactions on Pattern Analysis and Machine Intelligence*, vol. 18, no. 1, pp. 83 – 89, January 1996. 70

[209] Z. Shi and V. Govindaraju, "A chaincode based scheme for fingerprint feature extraction," *Pattern Recognition Letters*, vol. 27, no. 5, pp. 462 – 468, April 2006. 70

[210] D. Maio and D. Maltoni, "Direct gray-scale minutiae detection in fingerprints," *IEEE Transaction o Pattern Analysis and Machine Intelligence*, vol. 19, pp. 27–40, January 1997. 71

[211] J. Liu, Z. Huang, and K. L. Chan, "Direct minutiae extraction from gray-level fingerprint image by relationship examination," in *Proceedings of the International Conference on Image Processing*, vol. 2, September 2000, pp. 427 – 430. 71

[212] N. Canyellas, E. Cantó, G. Forte, and M. López, "Hardware-software codesign of a fingerprint identification algorithm," in *Audio- and Video-Based Biometric Person Authentication*, ser. Lecture Notes in Computer Science, T. Kanade, A. Jain, and N. Ratha, Eds. Springer Berlin / Heidelberg, 2005, vol. 3546, pp. 165 – 200. 71

[213] M.-T. Leung, W. Engeler, and P. Frank, "Fingerprint image processing using neural networks," in *Proceedings of the IEEE Region 10 Conference on Computer and Communication Systems*, vol. 2, September 1990, pp. 582 – 586. 71

[214] V. Sagai and A. Koh Jit Beng, "Fingerprint feature extraction by fuzzy logic and neural networks," in *Proceedings of the International Conference on Neural Information Processing*, vol. 3, 1999, pp. 1138 – 1142. 71

[215] K. Nilsson and J. Bigun, "Using linear symmetry features as a pre-processing step for fingerprint images," in *Proceedings of the Audio and Video based Person Authentication - AVBPA 2001*. Springer, 2001, pp. 247 – 252. 71

[216] J. D. Stoszlisa and A. Alyea, "Automated system for fingerprint authentication using pores and ridge structure," in *Proceedings of SPIE (Automatic Systems for the Identification and Inspection of Humans)*, vol. 2277, 1994, pp. 210 – 223. 71

[217] A. K. Jain, Y. Chen, and M. Demirkus, "Pores and ridges: High-resolution fingerprint matching using level 3 features," *IEEE Transactions on Pattern Analysis and Machine Intelligence*, vol. 29, pp. 15 –27, 2007. 71, 84

[218] G. Marcialis, F. Roli, and A. Tidu, "Analysis of fingerprint pores for vitality detection," in *Proceedings of the 20th International Conference on Pattern Recognition*, August 2010, pp. 1289 – 1292. 71

[219] FBI, "The Science of Fingerprints. Classification and Uses," U.S. Department of Justice, FBI. Superintendent of Documents, U.S. Government Printing Office, Washington, D.C., 2006. 73

[220] J. Berry and D. Stoney, *Advances in Fingerprint Technology*. Boca Raton, FL, USA: CRC Press, Inc., 2001, ch. The history and development of fingerprinting, pp. 1 – 40. 73

[221] S. Memon, M. Sepasian, and W. Balachandran, "Review of finger print sensing technologies," in *Proceedings of the IEEE International Multitopic Conference*, December 2008, pp. 226 – 231. 74

[222] U.S. Dept. of Justice, Federal Bureau of Investigation, Criminal Justice Information Services Division, Washington, D.C., "Electronic fingerprint transmission specification," 1999, http://nla.gov.au/nla.cat-vn4185009. 74

[223] "The FBI Federal Bureau of Investigation, U.S.A." http://www.fbi.gov. 74

[224] J. N. Bradley, C. M. Brislawn, and T. Hopper, "FBI wavelet/scalar quantization standard for gray-scale fingerprint image compression," *Visual Information Processing II*, vol. 1961, no. 1, pp. 293 – 304, 1993. 75, 92

[225] A. Skodras, C. Christopoulos, and T. Ebrahimi, "The jpeg 2000 still image compression standard," *Signal Processing Magazine, IEEE*, vol. 18, no. 5, pp. 36 – 58, September 2001. 75

[226] N. M. Allinson, "Fingerprint compression," in *Encyclopedia of Biometrics*, S. Z. Li and A. K. Jain, Eds., 2009, pp. 447 – 452. 75

[227] F. Alonso-Fernandez, J. Fierrez, J. Ortega-Garcia, J. Gonzalez-Rodriguez, H. Fronthaler, K. Kollreider, and J. Bigun, "A comparative study of fingerprint image-quality estimation methods," *IEEE Transactions on Information Forensics and Security*, vol. 2, no. 4, pp. 734–743, December 2007. 75

[228] S. Lee, H. seung Choi, K. Choi, and J. Kim, "Fingerprint-quality index using gradient components," *IEEE Transactions on Information Forensics and Security*, vol. 3, no. 4, pp. 792 – 800, 2008. 75

[229] L. Shen, A. C. Kot, and W. M. Koo, "Quality measures of fingerprint images," in *Proceedings of the Third International Conference on Audio and Video Based Biometric Person Authentication*, 2001, pp. 266 – 271. 75, 116, 189

[230] N.Ratha and R.Bolle, "Fingerprint image quality estimation," IBM Computer Science Research, Report RC21622, 1999. 76

[231] D. Yu, L. Ma, H. Lu, and Z. Chen, "Fusion method of fingerprint quality evaluation: from the local gabor feature to the global spatial-frequency structures," in *Proceedings of the 8th international conference on Advanced Concepts For Intelligent Vision Systems*, 2006, pp. 776 – 785. 76

[232] X. kun Yang and Y. Luo, "A classification method of fingerprint quality based on neural network," in *Proceedings of the International Conference on Multimedia Technology (ICMT)*, July 2011, pp. 20 – 23. 76

[233] E. Tabassi, C. Wilson, and C. Watson, "Fingerprint image quality," National Institute of Standards and Technology (NIST), Technical Report NISTIR 7151, August 2004. 76, 116, 122, 129, 193, 212

[234] S. Greenberg, M. Aladjem, D. Kogan, and I. Dimitrov, "Fingerprint image enhancement using filtering techniques," in *Proceedings of the International Conference on Pattern Recognition*, vol. 3, 2000, pp. 322 – 325. 77

[235] L. O'Gorman and J. V. Nickerson, "An approach to fingerprint filter design," *Pattern Recognition*, vol. 22, no. 1, pp. 29 – 38, January 1989. 78

[236] W. Wang, J. Li, F. Huang, and H. Feng, "Design and implementation of Log-Gabor filter in fingerprint image enhancement," *Pattern Recognition Letters*, vol. 29, no. 3, pp. 301 – 308, 2008. 78

[237] H. Fronthaler, K. Kollreider, and J. Bigun, "Local features for enhancement and minutiae extraction in fingerprints," *IEEE Transactions on Image Processing*, vol. 17, no. 3, pp. 354 – 363, March 2008. 78

[238] J. Zhou, F. Chen, N. Wu, and C. Wu, "Crease detection from fingerprint images and its applications in elderly people," *Pattern Recognition*, vol. 42, no. 5, pp. 896 – 906, 2009. 78

[239] T. Hatano, T. Adachi, S. Shigematsu, H. Morimura, S. Onishi, Y. Okazaki, and H. Kyuragi, "A fingerprint verification algorithm using the differential matching rate," in *Proceedings of the International Conference on Pattern Recognition*, vol. 3, 2002, pp. 799 – 802. 79

[240] K. Nandakumar and A. K. Jain, "Local correlation-based fingerprint matching," in *Proceedings of the Indian Conference on Computer Vision, Graphics and Image Processing*, 2004, pp. 503 – 508. 79

[241] N. Yager and A. Amin, "Fingerprint verification based on minutiae features: a review," *Pattern Analysis & Applications*, vol. 7, pp. 94–113, 2004. 79

[242] A. Bishnu, S. Das, S. C. Nandy, and B. B. Bhattacharya, "Simple algorithms for partial point set pattern matching under rigid motion," *Pattern Recognition*, vol. 39, no. 9, pp. 1662 – 1671, September 2006. 80

[243] N. Ratha, K. Karu, S. Chen, and A. Jain, "A real-time matching system for large fingerprint databases," *IEEE Transactions on Pattern Analysis and Machine Intelligence*, vol. 18, no. 8, pp. 799 – 813, August 1996. 80

[244] S. Ranade and A. Rosenfeld, "Point pattern matching by relaxation," *Pattern Recognition*, vol. 12, no. 4, pp. 269–75, 1980. 80

[245] W. Sheng, G. Howells, M. Fairhurst, and F. Deravi, "A memetic fingerprint matching algorithm," *IEEE Transactions on Information Forensics and Security*, vol. 2, no. 3, pp. 402 – 412, September 2007. 80

[246] H. Lam, W. Yau, T. Chen, Z. Hou, and H. Wang, "Fingerprint pre-alignment for hybrid match-on-card system," in *Proceedings of the 6th International Conference on Information, Communications Signal Processing*, December 2007, pp. 1 – 4. 80

[247] X. Jiang and W.-Y. Yau, "Fingerprint minutiae matching based on the local and global structures," in *Proceedings of the 5th International Conference on Pattern Recognition*, vol. 2, 2000, pp. 1038 – 1041. 81

[248] N. Ratha, R. Bolle, V. Pandit, and V. Vaish, "Robust fingerprint authentication using local structural similarity," in *Proceedings of the Workshop on Applications of Computer Vision*, January 2000, pp. 29 – 34. 81

[249] G. Bebis, T. Deaconu, and M. Georgiopoulos, "Fingerprint identification using delaunay triangulation," in *Proceedings of the IEEE International Conference on Intelligence, Information, and Systems*, 1999, pp. 452 – 459. 82

[250] G. Parziale and A. Niel, "Fingerprint matching using minutiae triangulation," in *Proceedings of the International Conference on Biometric Authentication*, vol. 3072, July 2004, pp. 241–248. 82

[251] X. Liang, A. Bishnu, and T. Asano, "A robust fingerprint indexing scheme using minutia neighborhood structure and low-order delaunay triangles," *IEEE Transactions on Information Forensics and Security*, vol. 2, no. 4, pp. 721 – 733, December 2007. 82, 85

[252] X. Tong, S. Liu, J. Huang, and X. Tang, "Local relative location error descriptor-based fingerprint minutiae matching," *Pattern Recognition Letters*, vol. 29, no. 3, pp. 286 – 294, February 2008. 82

[253] L. Sha, F. Zhao, and X. Tang, "Minutiae-based fingerprint matching using subset combination," in *Proceedings of the International Conference on Pattern Recognition*, vol. 4, 2006, pp. 566 –569. 82

[254] A. Ross and R. Nadgir, "A thin-plate spline calibration model for fingerprint sensor interoperability," *IEEE Transactions on Knowledge and Data Engineering*, vol. 20, no. 8, pp. 1097 – 1110, August 2008. 82, 148

[255] R. Cappelli, D. Maio, and D. Maltoni, "Modelling plastic distortion in fingerprint images," in *Advances in Pattern Recognition*, 2001, vol. 2013, pp. 371–378. 82

[256] L. Coetzee and E. C. Botha, "Fingerprint recognition in low quality images," *Pattern Recognition*, vol. 26, no. 10, pp. 1441 – 1460, 1993. 84

[257] R. Zhou, S. Sin, D. Li, T. Isshiki, and H. Kunieda, "Adaptive sift-based algorithm for specific fingerprint verification," in *Proceedings of the International Conference on Hand-Based Biometrics*, November 2011, pp. 1 – 6. 84

[258] J. Feng and A. Cai, "Fingerprint representation and matching in ridge coordinate system," in *Proceedings of the International Conference on Pattern Recognition*, vol. 4, 2006, pp. 485 – 488. 84

[259] Q. Zhao, L. Zhang, D. Zhang, and N. Luo, "Direct pore matching for fingerprint recognition," in *Proceedings of the Third International Conference on Advances in Biometrics*, 2009, pp. 597 – 606. 84

[260] A. Jain, Y. Chen, and M. Demirkus, "Pores and ridges: Fingerprint matching using level 3 features," in *Proceedings of the International Conference on Pattern Recognition*, vol. 4, 2006, pp. 477 – 480. 84

[261] R. Cappelli and D. Maio, "The state of the art in fingerprint classification," in *Automatic Fingerprint Recognition Systems*, N. Ratha and R. Bolle, Eds. Springer New York, 2004, pp. 183–205. 85

[262] G. A. Drets and H. G. Liljenström, *Intelligent biometric techniques in fingerprint and face recognition*. Boca Raton, FL, USA: CRC Press, Inc., 1999, ch. Fingerprint sub-classification: a neural network approach, pp. 107–134. 85

[263] J. Araque, M. Baena, B. Chalela, D. Navarro, and P. Vizcaya, "Synthesis of fingerprint images," in *Proceedings of the 16th International Conference on Pattern Recognition*, vol. 2, 2002, pp. 422–425. 85

[264] M. Kücken and A. C. Newell, "A model for fingerprint formation," *EPL (Europhysics Letters)*, vol. 68, no. 1, p. 141, 2004. 86

[265] M. Kücken, "Models for fingerprint pattern formation," *Forensic Science International*, vol. 171, no. 2-3, pp. 85–96, 2007. 86

[266] U.-K. Cho, J.-H. Hong, and S.-B. Cho, "Automatic fingerprints image generation using evolutionary algorithm," in *Proceedings of the 20th international conference on Industrial, engineering, and other applications of applied intelligent systems*, ser. IEA/AIE'07. Berlin, Heidelberg: Springer-Verlag, 2007, pp. 444–453. 86

[267] R. Cappelli, "Synthetic fingerprint generation," in *Handbook of Fingerprint Recognition*, 2nd ed., A. J. D. Maltoni, D. Maio and S. Prabhakar, Eds. Springer London, 2009, pp. 271–301. 86

[268] J. Xue, S. Xing, Y. Guo, and Z. Liu, "Fingerprint generation method based on gabor filter," in *Proceedings of the 2010 International Conference on Computer Application and System Modeling (ICCASM)*, vol. 8, October 2010, pp. 115–119. 86

[269] G. Parziale, "Touchless fingerprinting technology," in *Advances in Biometrics*, N. K. Ratha and V. Govindaraju, Eds. Springer London, 2008, pp. 25 – 48. 87, 91, 92, 94, 96

[270] V. Piuri and F. Scotti, "Fingerprint biometrics via low-cost sensors and webcams," in *Proceedings of the 2nd IEEE International Conference on Biometrics: Theory, Applications and Systems*, October 2008, pp. 1 – 6. 90, 93, 94, 96, 208

[271] M. O. Derawi, B. Yang, and C. Busch, "Fingerprint recognition with embedded cameras on mobile phone," in *MobiSec*, ser. Lecture Notes of the Institute for Computer Sciences, Social Informatics and Telecommunications Engineering, R. Prasad, K. Farkas, A. U. Schmidt, A. Lioy, G. Russello, and F. L. Luccio, Eds., vol. 94. Springer, 2011, pp. 136 – 147. 90, 208

[272] F. Han, J. Hu, M. Alkhathami, and K. Xi, "Compatibility of photographed images with touch-based fingerprint verification software," in *Proceedings of the IEEE Conference on Industrial Electronics and Applications*, June 2011, pp. 1034 – 1039. 90, 92, 102, 103

[273] B. Hiew, A. Teoh, and D. Ngo, "Automatic digital camera based fingerprint image preprocessing," in *Proceedings of the International Conference on Computer Graphics, Imaging and Visualisation*, July 2006, pp. 182 – 189. 90, 93

[274] B. Hiew, B. Andrew, and Y. Pang, "Digital camera based fingerprint recognition," in *Proceedings of the IEEE International Conference on Telecommunications and Malaysia International Conference on Communications*, May 2007, pp. 676 – 681. 90, 93

[275] B. Hiew, A. Teoh, and D. Ngo, "Preprocessing of fingerprint images captured with a digital camera," in *Proceedings of the International Conference on Control, Automation, Robotics and Vision*, December 2006, pp. 1 – 6. 90, 93

[276] Y. Song, C. Lee, and J. Kim, "A new scheme for touchless fingerprint recognition system," in *Proceedings of 2004 International Symposium on Intelligent Signal Processing and Communication Systems*, November 2004, pp. 524 – 527. 91, 92, 94

[277] L. Wang, R. H. A. El-Maksoud, J. M. Sasian, and V. S. Valencia, "Illumination scheme for high-contrast, contactless fingerprint images," in *Novel Optical Systems Design and Optimization XII*, R. J. Koshel and G. G. Gregory, Eds., vol. 7429, no. 1. SPIE, 2009. 91

[278] C. Lee, S. Lee, and J. Kim, "A study of touchless fingerprint recognition system," in *Structural, Syntactic, and Statistical Pattern Recognition*, ser. Lecture Notes in Computer Science, D.-Y. Yeung, J. Kwok, A. Fred, F. Roli, and D. de Ridder, Eds. Springer Berlin / Heidelberg, 2006, vol. 4109, pp. 358 – 365. 91

[279] L. Wang, R. H. A. El-Maksoud, J. M. Sasian, W. P. Kuhn, K. Gee, and V. S. Valencia, "A novel contactless aliveness-testing (CAT) fingerprint sensor," in *Novel Optical Systems Design and Optimization XII*, R. J. Koshel and G. G. Gregory, Eds., vol. 7429, no. 1. SPIE, 2009. 91, 92, 97

[280] E. Sano, T. Maeda, T. Nakamura, M. Shikai, K. Sakata, M. Matsushita, and K. Sasakawa, "Fingerprint authentication device based on optical characteristics inside a finger," in *Proceedings of the Conference on Computer Vision and Pattern Recognition Workshop*, June 2006, pp. 27 – 32. 91

[281] H. Choi, K. Choi, and J. Kim, "Mosaicing touchless and mirror-reflected fingerprint images," *IEEE Transactions on Information Forensics and Security*, vol. 5, no. 1, pp. 52 – 61, March 2010. 91, 92, 94, 95, 96

[282] N. Francisco, A. Zaghetto, B. Macchiavello, E. da Silva, M. Lima-Marques, N. Rodrigues, and S. de Faria, "Compression of touchless multiview fingerprints," in *Proceedings of the IEEE Workshop on Biometric Measurements and Systems for Security and Medical Applications*, September 2011, pp. 1 – 5. 92

[283] C. Lee, S. Lee, J. Kim, and S.-J. Kim, "Preprocessing of a fingerprint image captured with a mobile camera," in *Advances in Biometrics*, ser. Lecture Notes

in Computer Science, D. Zhang and A. Jain, Eds. Springer Berlin / Heidelberg, 2005, vol. 3832, pp. 348 – 355. 93, 94

[284] G. Parziale and Y. Chen, "Advanced technologies for touchless fingerprint recognition," in *Handbook of Remote Biometrics*, ser. Advances in Pattern Recognition, M. Tistarelli, S. Z. Li, and R. Chellappa, Eds. Springer London, 2009, pp. 83–109. 95, 96, 97, 99, 100, 103, 229, 237

[285] B. Y. Hiew, A. B. J. Teoh, and O. S. Yin, "A secure digital camera based fingerprint verification system," *Journal of Visual Communication and Image Representation*, vol. 21, no. 3, pp. 219 – 231, 2010. 97

[286] A. Kumar and Y. Zhou, "Contactless fingerprint identification using level zero features," in *Proceedings of the IEEE Computer Society Conference on Computer Vision and Pattern Recognition Workshops*, June 2011, pp. 114 – 119. 97

[287] S. Mil'shtein, M. Baier, C. Granz, and P. Bustos, "Mobile system for fingerprinting and mapping of blood - vessels across a finger," in *Proceedings of the IEEE Conference on Technologies for Homeland Security*, May 2009, pp. 30 – 34. 97

[288] G. Parziale, E. Diaz-Santana, and R. Hauke, "The surround imager: A multi-camera touchless device to acquire 3D rolled-equivalent fingerprints." in *Proceedings of the International Conference of Biometrics ICB'06*, 2006, pp. 244–250. 97, 99, 103

[289] Y. Wang, L. Hassebrook, and D. Lau, "Data acquisition and processing of 3-D fingerprints," *IEEE Transactions on Information Forensics and Security*, vol. 5, no. 4, pp. 750–760, December 2010. 98, 100, 101, 102, 153

[290] Y. Wang, L. G. Hassebrook, and D. L. Lau, "Noncontact, depth-detailed 3D fingerprinting," *SPIE Newsroom*, November 2009. 98, 100

[291] G. Paar, M. d. Perucha, A. Bauer, and B. Nauschnegg, "Photogrammetric fingerprint unwrapping," *Journal of Applied Geodesy*, vol. 2, pp. 13 – 20, 2008. 99

[292] R. I. Hartley and A. Zisserman, *Multiple View Geometry in Computer Vision*, 2nd ed. Cambridge University Press, 2004. 99, 101, 136, 137, 229, 230

[293] M. J. Brooks, *Shape from shading*, B. K. P. Horn, Ed. Cambridge, MA, USA: MIT Press, 1989. 100

[294] D. Koller, L. Walchshäusl, G. Eggers, F. Neudel, U. Kursawe, P. Kühmstedt, M. Heinze, R. Ramm, C. Bräuer-Burchardt, G. Notni, R. Kafka, R. Neubert, H. Seibert, M. C. Neves, and A. Nouak, "3D capturing of fingerprints - on the way to a contactless certified sensor," in *BIOSIG*, 2011, pp. 33 – 44. 100, 103, 218

[295] Y. Wang, D. L. Lau, and L. G. Hassebrook, "Fit-sphere unwrapping and performance analysis of 3d fingerprints," *Applied Optics*, vol. 49, no. 4, pp. 592 – 600, February 2010. 103

[296] S. Shafaei, T. Inanc, and L. Hassebrook, "A new approach to unwrap a 3-d fingerprint to a 2-d rolled equivalent fingerprint," in *Proceedings of the IEEE 3rd International Conference on Biometrics: Theory, Applications, and Systems*, September 2009, pp. 1 – 5. 103

[297] Q. Zhao, A. Jain, and G. Abramovich, "3D to 2D fingerprints: Unrolling and distortion correction," in *Proceedings of the 2011 International Joint Conference on Biometrics*, October 2011, pp. 1 – 8. 103

[298] Touchless Biometric Systems, TBS, http://www.tbs-biometrics.com/. 104

[299] Touchless Sensor Technology, TST, http://www.tst-biometrics.com/en/. 104

[300] Safran Morpho, http://www.morpho.com/. 104

[301] Mitsubishi Electric, http://www.mitsubishielectric.com/. 104

[302] S. Milshtein, A. Pillai, V. O. Kunnil, M. Baier, and P. Bustos, *Recent Application in Biometrics*. InTech, 2011, ch. Applications of Contactless Fingerprinting, pp. 107–134. 105

[303] R. Donida Labati, V. Piuri, and F. Scotti, "Neural-based quality measurement of fingerprint images in contactless biometric systems," in *Proceedings of the 2010 International Joint Conference on Neural Networks (IJCNN)*, July 2010, pp. 1–8. 115, 229

[304] R. Kohavi and G. H. John, "Wrappers for feature subset selection," *Artificial Intelligence*, vol. 97, no. 1 - 2, pp. 273 – 324, 1997. 121

[305] I. Guyon and A. Elisseeff, "An introduction to variable and feature selection," *Journal of Machine Learning Research*, vol. 3, pp. 1157 – 1182, 2003. 121

[306] C. Alippi, P. Braione, V. Piuri, and F. Scotti, "A methodological approach to multisensor classification for innovative laser material processing units," in *Proceedings of the 18th IEEE Instrumentation and Measurement Technology Conference*, vol. 3, 2001, pp. 1762 – 1767. 121

[307] R. Donida Labati, A. Genovese, V. Piuri, and F. Scotti, "Measurement of the principal singular point in contact and contactless fingerprint images by using computational intelligence techniques," in *Proceedings of the IEEE International Conference on Computational Intelligence for Measurement Systems and Applications*, September 2010, pp. 18 – 23. 125, 229

[308] R. Donida Labati, V. Piuri, and F. Scotti, "A neural-based minutiae pair identification method for touchless fingeprint images," in *Proceedings of the IEEE Workshop on Computational Intelligence in Biometrics and Identity Management*, April 2011. 131, 231

[309] D. G. Lowe, "Distinctive image features from scale-invariant keypoints," *Proceedings of the International Joint Conference on Computer Vision*, vol. 60, pp. 91–110, November 2004. 135, 157

[310] R. Donida Labati, A. Genovese, V. Piuri, and F. Scotti, "Fast 3-D fingertip reconstruction using a single two-view structured light acquisition," in *Proceedings of the 2011 IEEE Workshop on Biometric Measurements and Systems for Security and Medical Applications (BIOMS)*, September 2011, pp. 1–8. 137, 229, 231

[311] Z. Zhang, "A flexible new technique for camera calibration," *IEEE Transactions on Pattern Analysis and Machine Intelligence*, vol. 22, no. 11, pp. 1330 – 1334, 2000. 137, 189, 198, 230

[312] J. Heikkila and O. Silvén, "A four-step camera calibration procedure with implicit image correction," *Proceedings of the IEEE Computer Society Conference*

on Computer Vision and Pattern Recognition (CVPR'97), pp. 1106 – 1112, 1997. 137, 189, 198, 230

[313] P. D. Kovesi, "MATLAB and Octave functions for computer vision and image processing," Centre for Exploration Targeting, School of Earth and Environment, The University of Western Australia, available from: http://www.csse.uwa.edu.au/∼pk/research/matlabfns/. 147, 230

[314] R. Donida Labati, A. Genovese, V. Piuri, and F. Scotti, "Virtual environment for 3-d synthetic fingerprints," in *Proceedings of the 2012 IEEE International Conference on Virtual Environments, Human-Computer Interfaces and Measurement Systems*, July 2012, pp. 48 – 53. 158

[315] Blender, http://www.blender.org/. 164

[316] A. K. Jain, R. P. Duin, and J. Mao, "Statistical pattern recognition: A review," *IEEE Transactions on Pattern Analysis and Machine Intelligence*, vol. 22, pp. 4 – 37, 2000. 172

[317] R. O. Duda, P. E. Hart, and D. G. Stork, *Pattern Classification (2nd Edition)*, 2nd ed. Wiley-Interscience, November 2000. 173, 179, 181, 193

[318] Neurotechnology, http://www.neurotechnology.com. 177, 198, 221

[319] CROSSMATCH Technologies, Verifier 300, http://www.neurotechnology.com. 177, 198, 208, 211, 221, 247

[320] R. Guerchouche and F. Coldefy, "Camera calibration methods evaluation procedure for images rectification and 3D reconstruction," *Orange Labs, France Telecom R & D*, 2008. 185, 235

[321] A. Ross and A. K. Jain, "Multimodal Biometrics: an overview," in *Proceedings of 12th European Signal Processing Conference*, 2004, pp. 1221 – 1224. 201

[322] International Organization for Standards, "ISO 9241-11 Ergonomic requirements for office work with visual display terminals (VDTs) - Part 11: guidance on usability ," 1998. 210

[323] MathWorks, Matlab, http://www.mathworks.it/products/matlab. 212

[324] M. Theofanos, B. Stanton, C. Sheppard, R. Micheals, and N. Zhang, "Usability testing of ten-print fingerprint capture," NISTIR, Tech. Rep., 2007. 212

[325] P. Besl and H. McKay, "A method for registration of 3-D shapes," *IEEE Transactions on Pattern Analysis and Machine Intelligence*, vol. 14, no. 2, pp. 239 – 256, February 1992. 221, 236

[326] R. Donida Labati, A. Genovese, V. Piuri, and F. Scotti, "Two-view contactless fingerprint acquisition systems: a case study for clay artworks," in *Proceedings of the IEEE Workshop on Biometric Measurements and Systems for Security and Medical Applications*, September 2012. 227

[327] J. Daab, "Forensic science and fine art authentication, la bella principessa," Fine art registry, http://www.fineartregistry.com/. 228

[328] D. Grann, "The mark of a masterpiece," The New Yorker, http://www.newyorker.com/, 2010. 228

[329] M. Králík, "Fingerprints on artifacts and historical items: examples and comments," *Journal of Ancient Fingerprints*, 2007. 228

[330] S. Yoon, J. Feng, and A. K. Jain, "On latent fingerprint enhancement," *Biometric Technology for Human Identification VII*, vol. 7667, no. 1, 2010. 228, 229

[331] S. Yoon, J. Feng, and A. K. Jain, "Latent fingerprint enhancement via robust orientation field estimation," *Proceedings of the International Joint Conference on Biometrics (IJCB)*, pp. 1–8, 2011. 228, 229

[332] F. Chen, J. Feng, A. Jain, J. Zhou, and J. Zhang, "Separating overlapped fingerprints," *IEEE Transactions on Information Forensics and Security*, vol. 6, no. 2, pp. 346–359, June 2011. 228, 229

[333] C. Nitschke, *3D Reconstruction - Real-time Volumetric Scene Reconstruction from Multiple Views*. VDM Verlag Dr. Muller, April 2007. 228

[334] B. Curless, "From range scans to 3D models," *SIGGRAPH Computer Graphics*, vol. 33, no. 4, pp. 38–41, November 1999. 229

[335] Y. S. Heo, K. M. Lee, and S. U. Lee, "Robust stereo matching using adaptive normalized cross-correlation," *IEEE Transactions on Pattern Analysis and Machine Intelligence*, vol. 33, no. 4, pp. 807–822, April 2011. 231

[336] J. Sarvaiya, S. Patnaik, and S. Bombaywala, "Image registration by template matching using normalized cross-correlation," in *Proceedings of the International Conference on Advances in Computing, Control, and Telecommunication Technologies*, December 2009, pp. 819–822. 231

[337] R. Donida Labati, A. Genovese, V. Piuri, and F. Scotti, "Low-cost volume estimation by two-view acquisitions: A computational intelligence approach," in *Proceedings of the 2012 International Joint Conference on Neural Networks (IJCNN)*, June 2012. 231

[338] M. Barni, T. Bianchi, D. Catalano, M. Di Raimondo, R. Donida Labati, P. Failla, D. Fiore, R. Lazzeretti, V. Piuri, A. Piva, and F. Scotti, "A privacy-compliant fingerprint recognition system based on homomorphic encryption and fingercode templates," in *Proceedings of the Fourth IEEE International Conference on Biometrics: Theory Applications and Systems (BTAS)*, September 2010, pp. 1–7. 242

[339] M. Barni, T. Bianchi, D. Catalano, M. D. Raimondo, R. Donida Labati, P. Failla, D. Fiore, R. Lazzeretti, V. Piuri, F. Scotti, and A. Piva, "Privacy-preserving fingercode authentication," in *Proceedings of the 12th ACM workshop on Multimedia and security*. New York, NY, USA: ACM, September 2010, pp. 231–240. 242, 245, 246

[340] P. Paillier, "Public-key cryptosystems based on composite degree residuosity classes," in *Proceedings of the 17th international conference on Theory and application of cryptographic techniques*, 1999, pp. 223 – 238. 245

[341] T. El Gamal, "A public key cryptosystem and a signature scheme based on discrete logarithms," in *Proceedings of CRYPTO 84 on Advances in cryptology*, 1985, pp. 10 – 18. 245

[342] Neurotechnology, dataset Cross Match Verifier 300, http://www.neurotechnology.com. 247